LIGHT ELEMENTS IN OCEANIC AND OPHIOLITIC SERPENTINITES

Thèse présentée à la Faculté des Sciences
Institut de Géologie et d'Hydrogéologie
Université de Neuchâtel
pour l'obtention du grade de
Docteur ès sciences par

Flurin Andri Vils

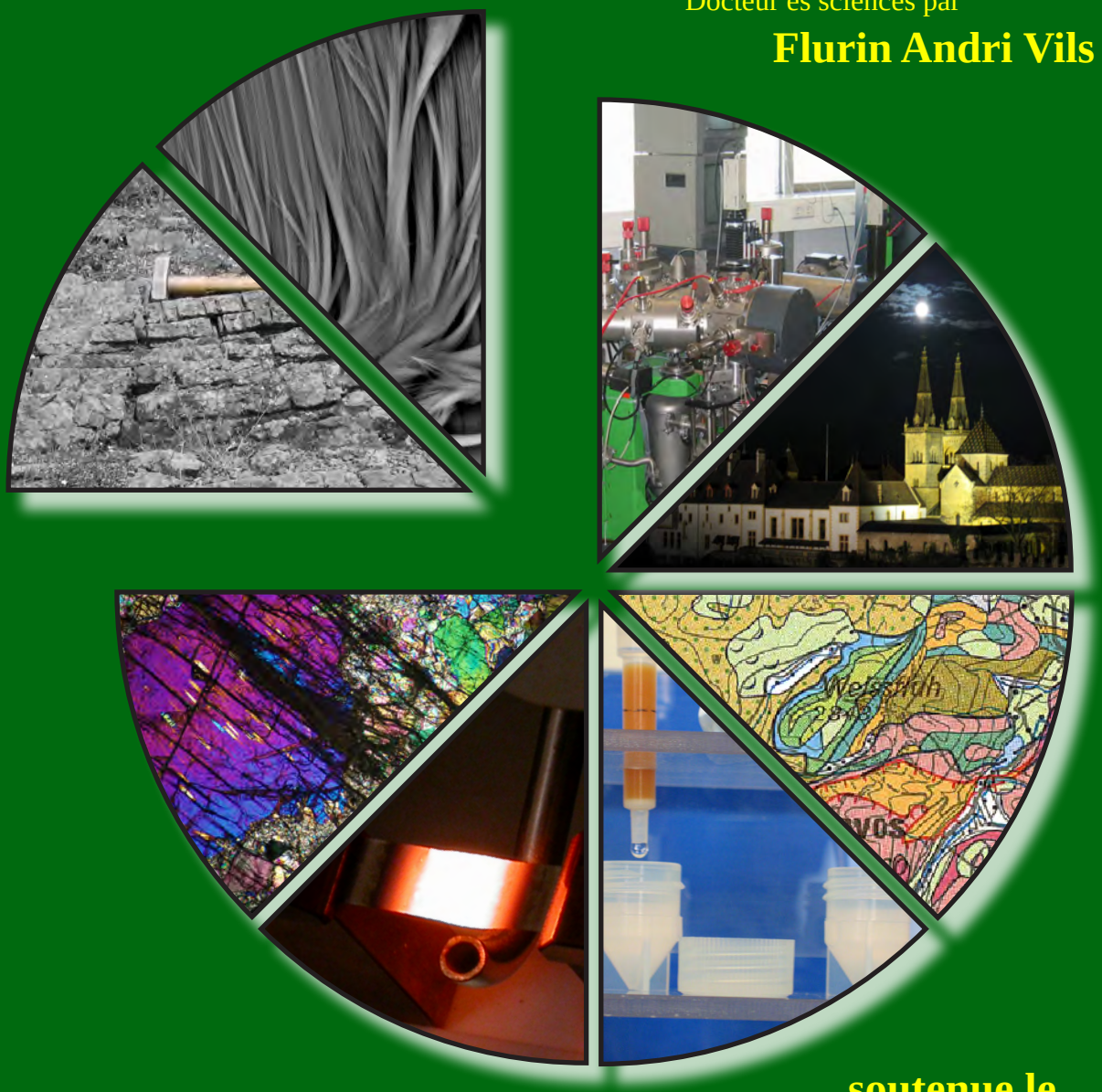

soutenue le
21 JANVIER 2008

Les membres du jury:
Prof. Dr. Angelika Kalt (Neuchâtel, CH, directrice de thèse)
Prof. Dr. Othmar Müntener (Lausanne, CH)
Dr. Tim Elliott (Bristol, UK)
Dr. Sonia Tonarini (Pisa, I)
Dr. Arjan Dijkstra (Neuchâtel, CH)

Université de Neuchâtel

Université de Neuchâtel

FACULTE DES SCIENCES
Secrétariat-Décanat de la faculté
- Rue Emile-Argand 11
- CP 158
- CH-2009 Neuchâtel

IMPRIMATUR POUR LA THESE

Light elements in oceanic and ophiolitic serpentinites

Flurin VILS

UNIVERSITE DE NEUCHATEL

FACULTE DES SCIENCES

La Faculté des sciences de l'Université de Neuchâtel,
sur le rapport des membres du jury

Mmes A. Kalt (directrice thèse), S. Tonarini (Pise I),
MM. O. Müntener (Lausanne), A. Dijkstra et T. Elliott (Bristol UK)

autorise l'impression de la présente thèse.

Neuchâtel, le 20 février 2009

Le doyen :
F. Kessler

UNIVERSITE DE NEUCHATEL
FACULTE DES SCIENCES
Secrétariat - décanat de la faculté
Rue Emile-Argand 11 - CP 158
CH-2009 Neuchâtel
Felix Kessler

In memoria

ut duos valde
Alpine fieldgeologists

Volkmar Trommsdorff (1936-2005)

and

Martin Burkhard (1957-2006)

Contents

Chapter IV

Chapter V

Chapter VI

Appendix

Acknowledgements

During my PhD I have visited many Universities and conferences and worked together with a lot of people. First of all I would like to thank all of you for the time you invested in my PhD-project, for motivating me, discussing light elements with me and supporting me; everybody in the way she or he could.

From the beginning of my thesis I was given freedom to head on with the project at my own pace. As soon as I had difficult decisions to take, problems to solve or was in need of a packet of motivation, my PhD advisor (Prof. ***Angelika Kalt***) had an ear and time for me. I appreciated this very much.

Struggling over different problems in mantle petrology, I was sure to find an advice by calling, e-mailing or seeing Prof. ***Othmar Müntener***, my second advisor. I always appreciated the business-like way he treated my demands and needs, so in short time I could make big steps forward.

Just knowing each other from one funny coffee break, ***Laure Pelletier*** and I were heading for a month of fieldwork to the Pindos mountain (Greece) at the very beginning of my PhD. It was a great experience and we learned to understand each other. During the PhD-years that followed, I have learned to appreciate the structured way Laure worked and had somebody to discuss all the questions popping up during work. Thank you very much for the friendship and the time we spent together somewhere at the other end of the world or in the freezer in Heidelberg.

I highly appreciated the **technical support** I got from the machines of Massoud Dadras (Neuchâtel), Julien Allaz (Bern), Edwin Gnos (Bern), Alfons Berger (Bern), Eric Reussert (Zürich), Hiltrud Müller-Sigmund (Freiburg), Hans Meier (Heidelberg), Thomas Ludwig (Heidelberg) and Bernard Grobéty (Fribourg). High quality thin-sections were the basis for good analytical work and have been prepared by Iona Fin (Heidelberg), Oliver Wieland (Heidelberg) and André Villard (Neuchâtel).

For the isotopic part of my PhD, I was glad to have the chance to visit two top laboratories. Starting during the World Cup 2006 in the Mineralogisches Institut of Frankfurt (D) and finishing in the same year in the CNR in Pisa (I). Both supervisors (***Hans-Michael Seitz*** and ***Sonia Tonarini***) guided me with a passion I highly appreciated.

I would also like to thank the many **reviewers** for their effort to improve the quality of the manuscript; Laureline Scherler, Anne-Lise Jourdan, Geoffrey Ruiz, Dunja Minder, François Negro and my co-authors of the different papers/chapters. I highly appreciated the comments and suggestions by the **jury members** and thank them for accepting being my examiners (Angelika Kalt, Othmar Müntener, Tim Elliott, Sonia Tonarini and Arjan Dijkstra).

Coffee break was always an important place to switch off the brain and overrule the problems that occurred during my work. Without the endless discussion about life, science, daily business or just nonsense I might never have found the power to continue or finish my PhD. Thanks to ***all the members of the Institut de Géologie et Hydrogéologie*** for the nice time together. It was just awesome!!!!

From the back row, I was always sure to have the support of ***my family*** and ***my friends***. I would not have survived the last 4 years without the chance to recharge my batteries with you. I enjoyed seeing my two god children growing and smiling during the last year, a special thank to them.

Last, but not least I would like to thank ***Laureline Scherler*** who have spent nearly all my PhD-time with me, taking me away from the University at weekends and evenings to enjoy life. *Merci mille fois pour ton soutien et pour ta compréhension pendant les derniers mois.*

Flurin Andri Vils
Neuchâtel
beginning of 2009

ABSTRACT

Keywords: lithium, beryllium, boron, oceanic serpentinites, $\delta^{7}Li$, $\delta^{11}B$, $^{87}Sr/^{86}Sr$, Iridium-strip heater, water-rock interaction, hydrothermal fluids

Mot-clé: lithium, béryllium, bore, serpentinites océanique, $\delta^{7}Li$, $\delta^{11}B$, $^{87}Sr/^{86}Sr$, Iridium-strip heater, interaction eau-roches, fluides hydrothérmeaux

Despite the key importance of altered oceanic mantle as a repository and carrier of light elements (B, Li, and Be) to depth, its inventory of these elements has hardly been explored and quantified. In previous studies about the input of light elements into subduction zones, serpentinites were largely neglected, as only rare data have been available. In order to constrain the systematics and budgets of these elements in the oceanic lithosphere, this thesis has studied samples of highly serpentinized peridotites from the mid-Atlantic ridge (ODP Leg 209) and progressively metamorphosed alpine ophiolites (Totalp, Platta and Malenco, Swiss-Italian Alps). Light element concentrations in minerals and whole rock samples within serpentinized peridotites were thus acquired to understand these processes. Moreover the isotopic ratios ($\delta^{7}Li$, $\delta^{11}B$ and $^{87}Sr/^{86}Sr$) of whole rock samples of oceanic serpentinites have been determined.

Different in-situ analytical methods (electron microprobe analysis, secondary ion mass spectrometry) were used to determine major and light element compositions of primary and secondary minerals. B and Cl concentrations of whole rock samples were determined with prompt-gamma activation analysis (PGAA). B-isotopes were analysed with TIMS, while Li concentration and isotopes were measured with MC-ICPMS. As imaging techniques, the backscattered electron (BSE) device of a scanning electron microscope (SEM) was used, while images on the nm scale were obtained from transmission electron microscopy (TEM).

With the aim of developing a new analytical protocol to analyse efficiently Li, Be and B whole rock data, we combined fusion of sample powders using an Iridium-strip heater with in-situ Li, Be and B measurements on SIMS. To assure that no light element loss or gain occurs during heating on the Ir-strip, experiments were conducted at different heating times and temperatures. In general, all light elements show volatile behaviour as loss is reported compared to reference values. Li and Be concentrations however are within analytical uncertainties. B, on the contrary, is highly volatile on the Ir-strip and high loss occurs at 1800°C. Additionally, one samples showed that light element loss is probably also related to initial water content, as nearly no B loss was measured in a nearly water free sample.

During exhumation of the mantle, late stage melt impregnation can influence the light element whole rock signal. Once exposed or emplaced near the ocean floor, alteration is the major process influencing the primary light element mantle signature of the oceanic mantle. At ODP Leg 209, late-stage clinopyroxenes have distinctly higher Li concentrations than depleted mantle, thus the latter dominates Li in whole rock sample. B, on the contrary, is enriched in serpentine and the latter hence controls the B content of the serpentinized mantle. Calculation of the B and Li budget of an idealized oceanic plate showed that at slow and fast spreading ridges, B content is controlled by serpentinites, while the oceanic crust controls the Li budget. Thus, serpentinization of the oceanic plate is an important process in the understanding of the element recycling within the subduction zone factory.

Isotope measurements on whole rock samples from ODP Leg 209 revealed the highest $\delta^{11}B$ (+40.66‰) and the lowest $\delta^{7}Li$ (-28.46‰) reported so far for oceanic serpentinites. Serpentinization is the major process enriching B and leaching Li out of the rock. Hence, also the isotopic signal must

be related to serpentinization. Moderate water-rock interaction, as calculated on the basis of $^{87}Sr/^{86}Sr$ ratios, very likely produced the $\delta^{7}Li$ and $\delta^{11}B$ values found at ODP Leg 209. Seawater alteration would lead to an isotopic signal of $\delta^{11}B$ +21‰ in serpentinized peridotite, which is not in line with our data set. Therefore, a different process must have led to such high $\delta^{11}B$ values, if equilibrium conditions are assumed. Our modelling results, based on the isotopic signature of a batch of fluid interacting with rocks during penetration into the oceanic plate, show that with increasing volume passed continuously evolution occurs. Such an evolved fluid could account for the high $\delta^{11}B$ and low $\delta^{7}Li$ signal reported at ODP Leg 209.

The Totalp-Platta-Malenco transect shows prograde alpine metamorphism from prehnite-pumpellyite to epidote-amphibolite facies from north to south. In the Malenco massif (epidote-amphibolite facies), the Be concentrations within primary mantle phases and metamorphic minerals are similar. Thus, Be mobility during prograde metamorphism is very low or Be is immobile. B and Li, on the contrary, show a mobile behaviour. The polymorphic change between chrysotile and antigorite expels B, while Li concentration stays in the same range, but decreases slightly. Further on, chlorites behave similar to serpentine with respect to B and Li loss with increasing metamorphism. As serpentine and chlorite are phyllosilicates, an explanation for the observed B and Li change might be the internal structural order, as internal order increases with increasing P-T. Nevertheless, the loss of B during antigorite formation shows that during chrysotile breakdown, a B-rich fluid should be expelled from the rocks and influence the overlying mantle wedge.

Chapter I

Introduction

Since at least a decade, light elements, their behaviour and cycle through the Earth have become an important topic for geochemists. But actually, what are "light elements"? The term roots in the very low atomic mass of these elements, which are hydrogen (H), helium (He), lithium (Li), beryllium (Be) and boron (B). In general, geochemists referring to light elements include only Li, Be and B in their definition and tend to exclude H and He. In the periodic system, the light elements are situated just next to each other and show an electron configuration of He ($1s^2$) plus one, two or three electrons. They are monovalent (Li^+), divalent (Be^{2+}) and trivalent (B^{3+}). The interest of geochemists in Li, Be and B is due to two fundamental characteristics of these elements. First, Li and B are fluid-mobile. Second, each has two major isotopes with a large mass difference, and therefore a large fractionation in nature. Be, on the contrary is mostly of low abundance and rather fluid-immobile. Light elements and their isotopes can hence be used to monitor many geological processes (e.g. $\delta^{11}B$ in foraminifers as a paleo-pH-meter of the ocean; Spivack et al., 1993, or dating surface exposure time in carbonate rocks; Merchel et al., 2008). Also, recent increase of precision on diverse methods and machines leads to more and more studies of rocks with low light element abundances (e.g. mantle, meteorites).

Lithium sits on position 3 within the periodic system of the elements and has an atomic mass of 6.94u. Melting point of pure lithium is 180.5°C. Lithium belongs to the alkali metals and has two stable isotopes, ^6Li and ^7Li, with a natural abundance of 7.59% and 92.41%, respectively. The relatively large isotopic fractionation occurring in nature (up to 60‰) is a result of the large mass difference between the two isotopes. The atomic radius of Li^+ in 6-fold coordination is 0.76Å, similar to that of octahedrally coordinated Mg^{2+} (0.72Å) and Fe^{2+} (0.76Å). Radioactive isotopes of Li have half-lives of <1s and therefore no geological application. Major Li-bearing mineral phases are lepidolite (Li mica), spodumene (Li pyroxene) and lithium carbonates.

Beryllium, an alkaline metal, has an atomic number of 4 and an atomic mass of 9.01u. Beryllium has a melting point of T= 1287°C. The atomic radius of Be^{2+} (0.26Å) is similar to that of Si^{4+} (0.27Å), but direct substitution is rare due to the high difference in charge. Although twelve isotopes of beryllium exist, only one isotope (^9Be) is stable. The short-lived isotopes ^6Be, ^8Be, ^{11}Be and ^{12}Be decay within a fraction of a second. Cosmic ray spallation of oxygen and nitrogen in the atmosphere produces cosmogenic ^{10}Be. As the half-life time of ^{10}Be is 1.51 million years, the analysis of $^{10}Be/^9Be$ ratios in natural surfaces allows determination of exposure ages. Beryl is the most abundant Be-containing mineral.

Boron is a non-metallic element with an atomic mass of 10.81u. The melting point of boron is at 2300°C. The atomic radius of B^{3+} is 0.11Å in tetrahedral coordination and 0.01Å in trigonal coordination. As B is mostly bound to O [forming $B(OH)_3$ or $B(OH)_4$], substitution in silicates is limited to Si^{4+} and Al^{3+} on tetrahedral sites, creating a distortion of the TO_4 units. Boron has thirteen known isotopes, with ^7B as the most unstable one (half-life of $3.265x10^{-22}$ s). The half-lives of all radioactive isotopes (^8B and ^{12}B to ^{19}B) are below 1 second and have therefore no geological application. ^{10}B and ^{11}B are the two stable isotopes with natural abundances of 18.8% and 80.2% respectively. During alteration processes, ^{11}B may be enriched or depleted in fluids compared to the residue. The wide range of natural fractionation (~60‰) of B isotopes is a result of this geochemical behaviour. Major boron-containing minerals are boron silicates (e.g. tourmaline) and evaporite minerals (e.g. probertite, rivadavite, borax).

1.1 Aims & scope of the thesis

Despite the potential key importance of the oceanic mantle as a repository of light elements, its inventory of these elements was only poorly constrained. Rare measurements indicated that Li and B are enriched in serpentinites (Bonatti et al., 1984; Decitre et al., 2002), but a detailed in-situ and whole rock study on these elements in serpentinites was missing. Studies on arc-volcanoes revealed that light element concentrations and isotopic ratios changed with increasing depth to the slab and / or distance from the subduction zone (see Fig. 1.1 for detailed data and references). It is therefore important to understand the processes in the oceanic plate, which control the potential input of B and Li into subduction zones. Alteration has been identified to be the most important process for enriching B in the oceanic crust (e.g. Seyfried et al., 1984). Furthermore, the ocean Li and B budget is controlled by the alteration of the oceanic plate (Seyfried et al., 1984; Spivack and Edmond, 1987; Chan et al., 1992;). To constrain the importance of lithium, beryllium and boron in mantle rocks in the global geochemical cycle, the SNF-project "The oceanic mantle as an important repository for the light elements Li, Be and B" was defined.

This project gave rise to two PhD projects (Laure Pelletier and Flurin Vils). Together, we studied the abundance of light elements, their mobility and partitioning and their isotope systematic in rock-forming minerals and whole rock samples of hydrothermally altered oceanic mantle. To understand the behaviour of the light elements within the subduction zone factory as well as during emplacement into the continental crust, samples from different geodynamic environments have been studied during this project: ocean floor serpentinite (ODP Leg 209; mid Atlantic ridge), non-subducted ophiolites (Pindos and Vourinos ophiolites; Greece), non-metamorphic ophiolite in crustal environment (Geisspfad; Alps) and metamorphic ophiolites in crustal environment (Totalp, Platta, Malenco and Cima di Gagnone; Alps). My thesis focused mainly on serpentinized spinel harzburgites from a) ODP Leg 209 Site 1272A & 1274A and b) Alpine ophiolites (Totalp, Platta and Malenco).

Our detailed study of the different ophiolites is the first systematic high quality dataset on the concentrations of light elements of serpentinites. This dataset will considerably influence the general understanding of the light elements behaviour, e.g. behaviour of light elements during polymorphic change from chrysotile to antigorite (Totalp-Platta-Malenco profile) or during alteration of the oceanic mantle. Further on, potential contribution of serpentinites to the light element input into subduction zones can be affirmed, shedding light on processes occurring in the subduction zone factory.

1.2 Isotopes and water/rock ratios

Isotopes of an element (same number of electrons and protons) have different numbers of neutrons and thus different masses (e.g. ^{6}Li and ^{7}Li). Some isotopes decay within seconds, days or years (e.g. ^{7}B half-life of 3.265 x 10^{-22} s) and others are stable. Stable isotopes with large mass differences show a distinct behaviour. During incorporation of elements in minerals, certain isotopes are preferred, which leads to a disequilibrium in favour of one isotope, called fractionation. Fractionation refers to the isotopic composition of mineral-fluid or mineral-mineral in equilibrium, but with different isotopic signatures. The fractionation factor between two isotopes (expressed as "alpha") is calculated using EQ 1.1.

$$\alpha_{A-B} = \frac{\delta^{x}A_{phase\_A}}{\delta^{x}A_{phase\_B}} \qquad \text{(EQ 1.1)}$$

To express the ratio of isotopic abundance in a two-isotope system, the delta notation is used (e.g. δ^{11}B). It reflects the isotope ratio in a sample relative to the same ratio in a standard, in permil (EQ 1.2).

$$\delta^{x}A = \left(\frac{(^{x}A/^{y}A)_{sample}}{(^{x}A/^{y}A)_{standard}} - 1\right) * 1000 \qquad \text{(EQ 1.2)}$$

where A is the element, and x and y the mass number of the heavier and the lighter isotope, respectively (e.g. ^{7}Li/^{6}Li). Different standards are used for different isotope systems. Li isotope ratios are expressed relative to those of NIST L-SVEC (Li_2CO_3), B isotope ratios are given relative to those of NIST-SRM 951 (H_3BO_3).

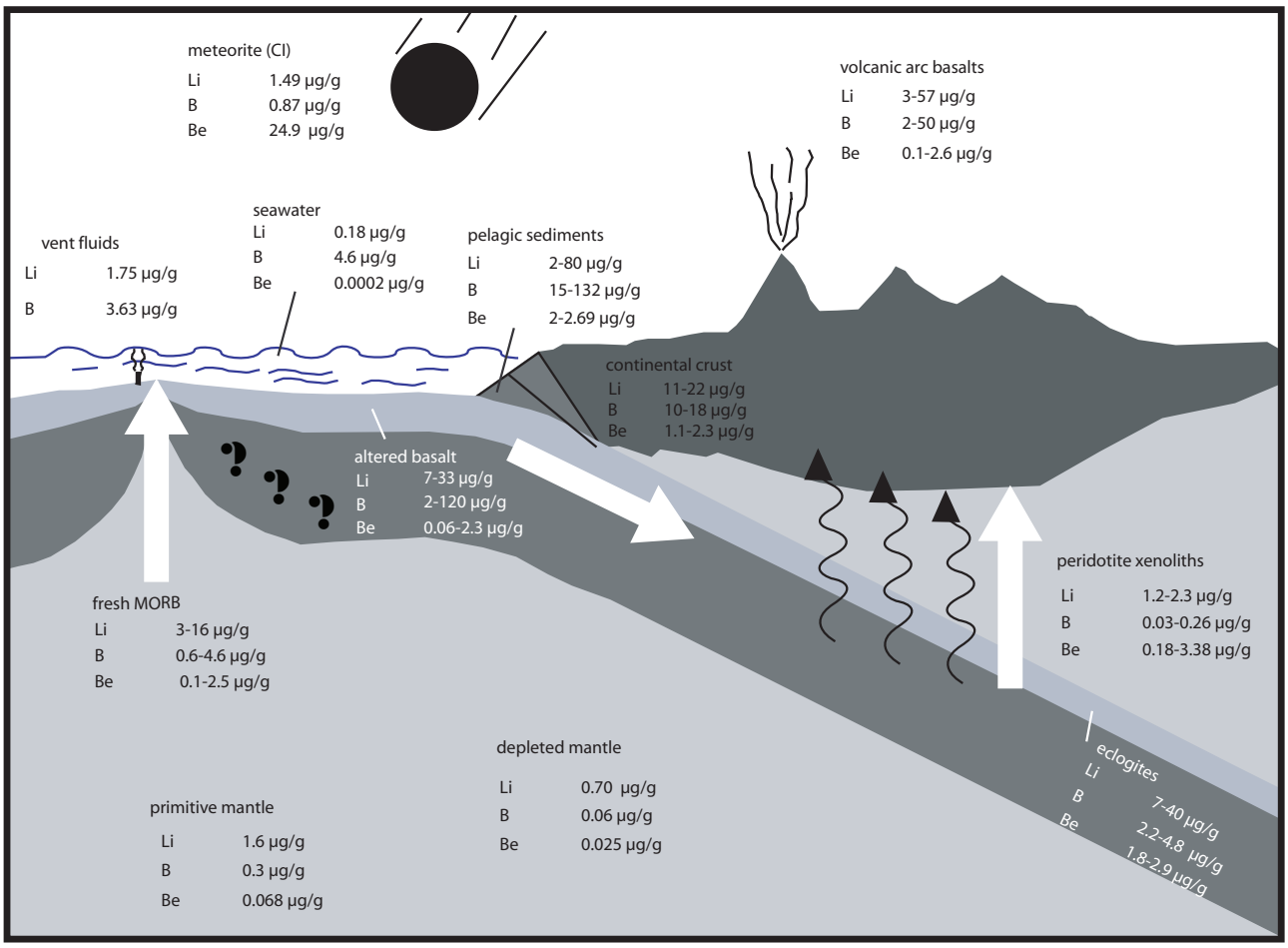

Fig. 1.1. Illustration showing the Li, Be and B cycle of the oceanic plate (primitive mantle: McDonough and Sun, 1995; depleted mantle: Salters and Stracke, 2004; MORB: Ryan and Langmuir, 1987; Chan et al., 1992; Ryan and Langmuir, 1993; seawater: Quinby-Hunt and Turekian, 1983; Douville et al., 2002; chondrite: Anders and Grevesse, 1989; continental crust: Gao et al., 1998; Rudnick and Gao, 2004; eclogites: Zack et al., 2003; Marschall et al., 2007; pelagic sediments: Ishikawa and Nakamura, 1993; volcanic arc basalts: Ryan et al., 1995; Moriguti and Nakamura, 1998; Tomascak et al., 2002; vent fluids: Schmidt et al., 2007; xenoliths: Ottolini et al., 2004; Pearson et al., 2004).

While studying alteration of the ocean floor, it is also important to be able to quantify the water-rock interactions. Taylor (1977) and McCulloch et al. (1980) showed that water/rock ratios (N) can be calculated using EQ 1.3.

$$N = \left(\frac{\delta_r^f - \delta_r^i}{\delta_w^i - \delta_w^f}\right) \times \frac{c_r^i}{c_w^i} \qquad \text{(EQ 1.3)}$$

where r corresponds to rock, w to water or fluid, f to final, i to initial, and c to concentration. As strontium isotopes show no fractionation ($\alpha = 1$) and as we are interested in the final isotopic composition of the fluid, EQ 1.3 can be transformed into EQ1.4, if $\delta_r^f = \delta_w^f - \Delta$ is assumed.

$$\delta_w^f = \frac{N * \delta_w^i + \frac{C_r}{C_w} * (\delta_r^i + \Delta_{w-r})}{N + C_r / C_w} \qquad \text{(EQ 1.4)}$$

Fractionation of isotopes is not only dependent on water-rock interaction but also controlled by pH, temperature and pressure. For example, B is trigonally coordinated at low pH, but tetragonal coordination is dominant at high pH (Spivack and Edmond, 1987; Boschi et al., 2008). The change in coordination also modifies the possibility of incorporation in minerals, e.g. trigonally coordinated B is incorporated in calcite, tetrahedrally coordinated B in aragonite, but not vice versa. In melts, B is also trigonally or tetragonally coordinated. Li isotope fractionation is not pH-dependent, but P- and T-dependent (Wunder et al., 2006; Vigier et al., 2008).

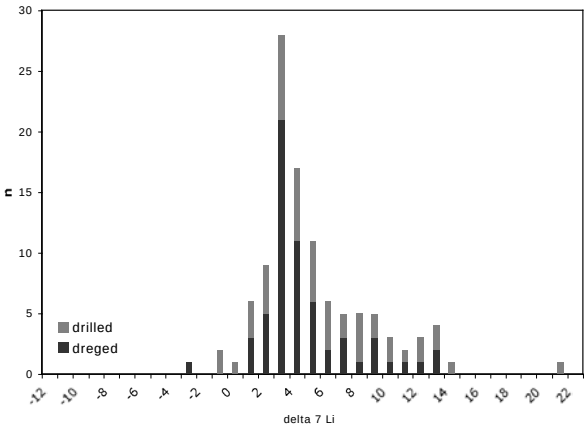

Fig. 1.2. δ^7Li histogram of a compilation on MORB showing the average concentration of the mantle (values are from Chan et al., 1992; Chan et al., 2002; Bouman et al., 2004; Elliott et al., 2006; Tomascak et al., 2008).

1.3 Light elements in the Earth

1.3.1 Light elements in the mantle

Based on element partition coefficients, the light element content of the primitive mantle is estimated to be 1.6 µg/g Li, 0.054-0.068 µg/g Be and 0.17-0.3 µg/g B (McDonough and Sun, 1995; Lyubetskaya and Korenaga, 2007). Depleted mantle as the residue after extraction of modern basalt is estimated to contain 0.7 µg/g Li, 0.025 µg/g Be and 0.06 µg/g B (Salters and Stracke, 2004). CI meteorites have an average of 1.49 µg/g Li, 0.0249 µg/g Be and 0.69 µg/g B (Palme and Beer, 1993). They show similarity in Li content but enrichment in Be and B compared to primitive mantle.

Estimates for Li and B isotope ratios of primitive or depleted mantle do not exist. As no fractionation between source material and magma occurs, mid-ocean ridge basalt (MORB) values should represent the values of the underlying mantle. A compilation of δ^7Li data from MORB (Fig. 1.2) suggests that the δ^7Li value of the depleted mantle is around +4 ‰ , although lower and higher values have also been measured. Average δ^{11}B of N-MORB is -3 ‰ (Hart et al., 1999; Fig. 1.3).

Slightly serpentinized to fresh harzburgites from Pindos (Greece) have low Li (0.5 to 1.1 µg/g) and low B contents (0.1 to 1.1 µg/g B) (Pelletier et al., 2008). Highly serpentinized peridotites dredged on the Atlantic ocean floor show high B content varying from 20 to 100 µg/g (Thompson and Melson, 1970; Bonatti et al., 1984). Dredged abyssal peridotites (world wide) show Li and Be contents of 0.6-13.7 µg/g and 0.001-0.212 µg/g, respectively (Niu, 2004).

Additional information about the upper mantle composition can be obtained from studies on mantle xenoliths. Recent publications revealed that B and Li isotope ratios vary and may not always represent the upper mantle composition (e.g. Jeffcoate et al., 2007; Rudnick and Ionov, 2007;

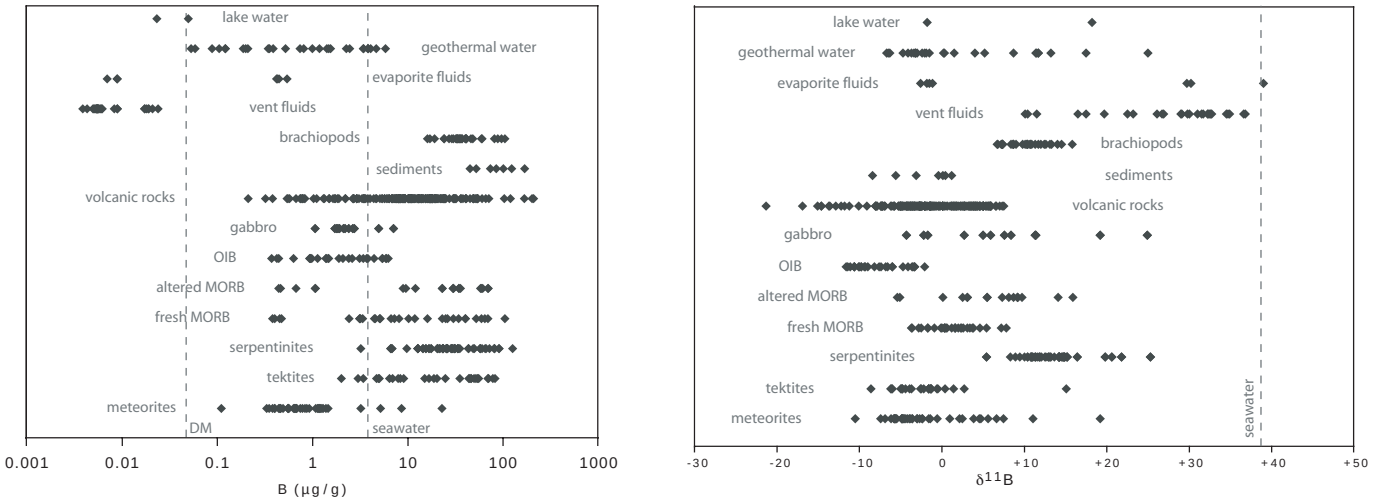

Fig. 1.3. Compilation of published B and δ^{11}B data (Spivack and Edmond, 1987; Palmer, 1991; Chaussidon and Koeberle, 1995; Chaussidon and Marty, 1995; Smith et al., 1995; Zhai et al., 1996; Ishikawa and Tera, 1997; Smith et al., 1997; Moriguti and Nakamura, 1998; Hart et al., 1999; Aggarwal et al., 2000; Benton et al., 2001; Ishikawa et al., 2001; Rose et al., 2001; Tonarini et al., 2001; Rosner et al., 2003; Kobayashi et al., 2004; Leeman et al., 2004; Moriguti et al., 2004; Joachimski et al., 2005; Tonarini et al., 2005; Krolikowska-Ciaglo et al., 2007; Turner et al., 2007; Boschi et al., 2008).

Ionov and Seitz, 2008). Metasomatism, host magma - xenolith interaction and high-temperature fractionation probably modified the initial isotope ratios in these cases. Further on, in-situ Li isotope measurements on one orthopyroxene grain revealed 40 ‰ fractionation within a single zoning profile, corresponding to the entire spread in δ^7Li observed on Earth (Fig. 1.4). This isotopic disequilibrium might be explained with rapid diffusion in the magma chamber (Jeffcoate et al., 2007).

1.3.2 Light element cycle in the oceanic plate

Accurate studies of light elements may help to understand the processes and interactions between the large geochemical reservoirs of the Earth. Therefore, constraining the composition of the primitive and modern depleted mantle is also important for understanding the behaviour of the light elements during cycling through a subduction zone. Figure 1.1 indicates the different values for the three elements related to processes and reservoirs. Melts emerging at the MOR from the underlying mantle are low in Li, Be and B content compared to continental crust, although they are enriched in these elements compared to primitive mantle (Fig. 1.1). Interaction of MORB with the seawater leads to altered basalts with high Li and B contents. These enrichment processes are in line with the Li and B contents of fluids from hydrothermal vent sites. Recent discoveries of hydrothermal vent sites reflecting serpentinization processes (e.g. Lost City; Kelley et al., 2001) may help to understand the evolution of altered peridotites. Up to date, no isotopic data of such fluids are published and light element concentration data are rare (Logatchev: Douville et al., 2002; Schmidt et al., 2007). Serpentinites tend to show two characteristics: high-temperature fluids, such as those found in Hess Deep (Decitre et al., 2002) induce high Li contents and heavy δ^7Li in the altered rock, while low-temperature serpentinization leads to low Li contents and light δ^7Li compared to the depleted mantle. When an oceanic plate enters a subduction zone, dehydration reactions occur and deplete the altered MORB in light elements. However, eclogites (high-pressure MORB) can still contain much Li (up to 72.3 µg/g) and B (up to 2.48 µg/g; Marschall, 2005). Intense studies of back-arc volcanoes showed that there seems to be a decrease in Li and B with increasing slab depth (e.g. Ryan et al., 1995). The authors concluded that this might

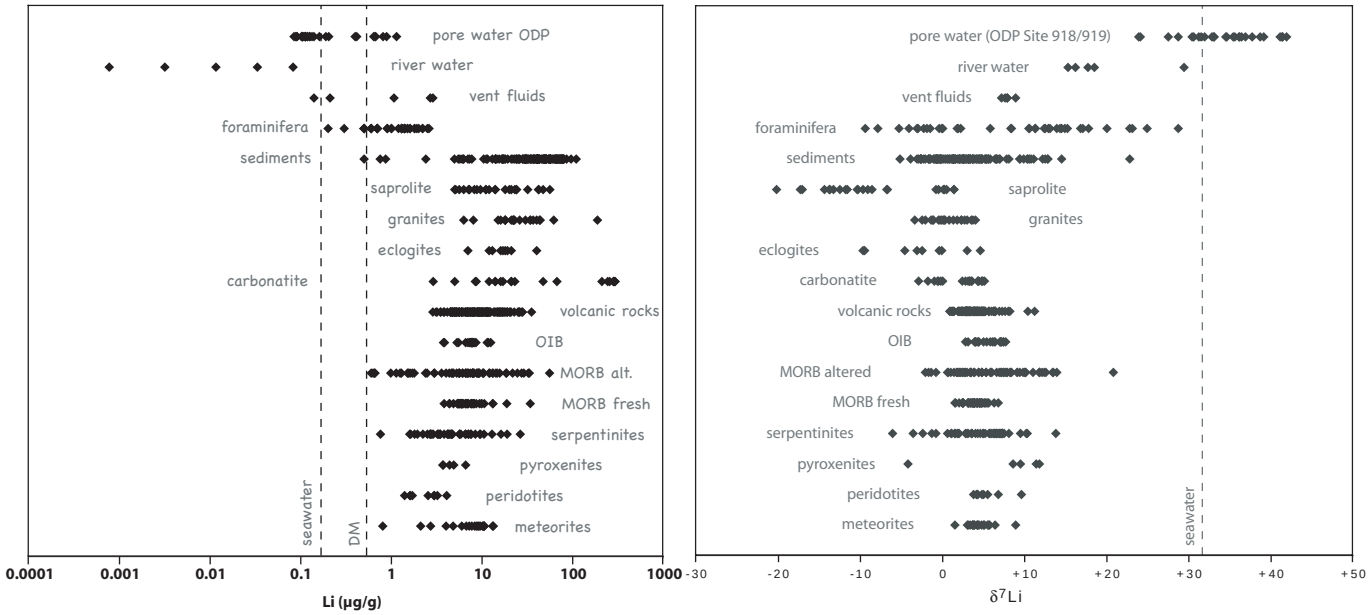

Fig. 1.4. Compilation of published Li and δ^7Li data (Chan et al., 1992; Hoefs and Sywall, 1997; Moriguti and Nakamura, 1998; Zhang et al., 1998; Chan and Kastner, 2000; Tomascak et al., 2000; Chan et al., 2002; Decitre et al., 2002; Tomascak et al., 2002; Zack et al., 2003; Benton et al., 2004; Brooker et al., 2004; Kobayashi et al., 2004; Leeman et al., 2004; Nishio et al., 2004; Rudnick and Gao, 2004; Ryan and Kyle, 2004; Teng et al., 2004; Chan et al., 2006; Elliott et al., 2006; Magna et al., 2006a; Magna et al., 2006b; Halama et al., 2007; Tomascak et al., 2008).

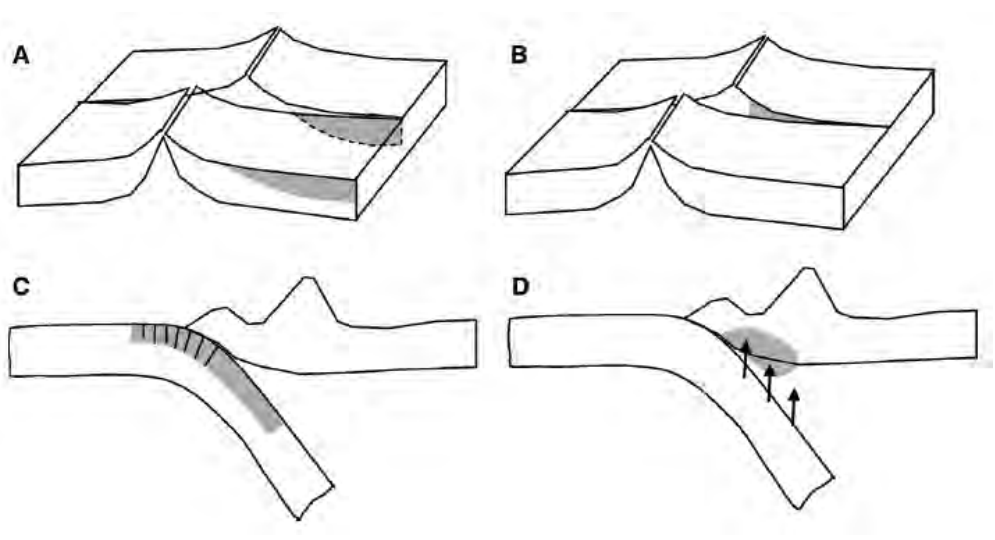

Fig. 1.5. Illustration after Li and Lee (2006), showing the different geotectonic settings in which serpentinization may occur. A: infiltration of seawater via transform faults; B: marine weathering due to exposure on the ocean floor; C: seawater infiltration during bending of the subducting slab; D: serpentinization of the forearc mantle wedge by fluids from the dehydrating slab.

be a hint of decreasing water release from the subducted slab. Further on, B/Be ratios are used to understand such processes, as Be is an immobile element and B tends to migrate with the fluid phase (Bebout et al., 1993; Bouvier et al., 2008).

1.3.3 B and Li isotopes

Li and B concentrations within rocks of the Earth vary over several orders of magnitude (e.g. 0.004 to 209 µg/g for B; Fig. 1.3). As enrichment and depletion are related to dehydration, alteration, erosion, or melting, light element isotope ratios of rocks may contain signals of older events and can thus be used as fingerprints of the geodynamic history of the studied rocks (Fig. 1.3, 1.4). Transformation of granites to saprolites leads to a decrease in Li and to lighter δ^7Li (up to -25 ‰ ; Rudnick et al., 2004). Alteration of the continental crust leads to an enrichment of river water in ^{7}Li (e.g. +29.4 ‰ δ^7Li, Amazone; Chan et al., 1992). As measured and assumed in- and outputs of the ocean do not match and as seawater (+32.3 ‰ δ^7Li) shows a steady state (Chan et al., 1992), a missing phase was proposed with a δ^7Li fractionation factor (α) between 0.981 and 0.973 (Chan et al., 1992). Recent low-temperature experiments on δ^7Li fractionation of clay minerals showed lower α (0.899 at 25°C), and new calculations of the ocean budget suggested that the missing phase should have a fractionation factor of α= 0.979 (Vigier et al., 2008).

Contrary to Li, B is pH-dependent, as B forms trigonal and tetragonal complexes in water (Spivack and Edmond, 1987). Therefore, in addition to mineral-fluid fractionation, a fractionation within the fluid phase has to be considered. As silicates prefer incorporation of tetragonal bound B, the abundance or absence of the two complex species leads to the wide δ^{11}B variety observed in nature (Fig. 1.3). E.g. alteration of MORB leads in average to heavier δ^{11}B whole rock composition. Similar enrichment of ^{11}B during alteration can be observed in serpentinites. Mariana fore-arc serpentinites are enriched in ^{11}B (δ^{11}B of up to +25.3 ‰ ; Benton et al., 2001) compared to mantle (-3 ‰ , Hart et al., 1999).

1.4 Geological setting

The main focus of this study are hydrothermally altered ultramafic rocks (serpentinites), composed mostly of serpentine. This phyllosilicate occurs as three polymorphs: chrysotile, antigorite and lizardite. Antigorite is the high-temperature polymorph and is normally less abundant in rocks altered at low temperatures, while chrysotile and lizardite are the low-temperature mineral phases. Serpentine is the alteration product formed after olivine, orthopyroxene and clinopyroxene. The mineralogical structure of serpentine favours the incorporation of water and small cations (like B^{3+}). Some key reaction paths are: Mg_2SiO_2 (forsterite) + SiO_2(aq) + H_2O => $Mg_3Si_2O_5(OH)_4$ (serpentine) or chrysotile + talc => antigorite.

Serpentinization of peridotites is thought to occur in four different geological settings: at transform faults at MOR, seafloor weathering, plate bending and hydration of the mantle wedge (Fig. 1.5). Additionally, serpentinization might also occur during metamorphism. Penetration depth of serpentinization within the oceanic plate is still under discussion in

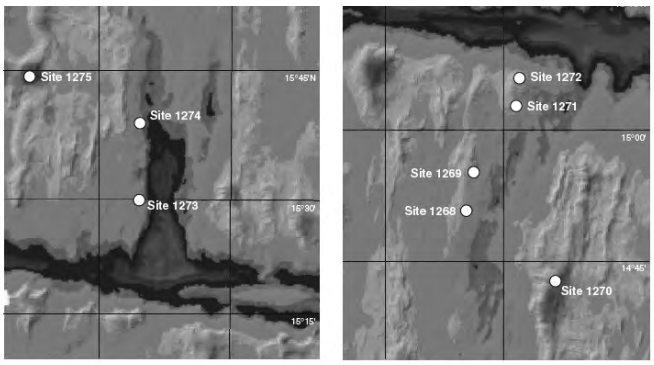

Fig. 1.6. Bathymetric map of the 15°20'-fracture zone, illustrating the ODP Leg 209 drillholes (from Kelemen et al., 2004).

the scientific community. Estimates range from some hundreds of meters up to 40 km depth (e.g. Macdonald and Fyfe, 1985; Li and Lee, 2006). As the serpentinized layer can drag an important amount of trace elements into a subduction zone, antigorite breakdown can liberate these elements to the mantle wedge and bring it into the arc volcano cycle (see also Fig. 1.1; Ulmer and Trommsdorff, 1995; Schmidt and Poli, 1998). It is therefore important to study these elements in serpentinites to understand the recycling of the latter in the subduction zone factory.

To study the light element content of serpentinized oceanic mantle, several places were chosen in order to cover the most abundant types of oceanic mantle exposed on the Earth today. The areas I studied during my thesis are a part of the mid-Atlantic ridge (ODP Leg 209 Sites 1272A & 1274A), Totalp and Platta (Swiss Alps) and Malenco ophiloites (Italian Alps).

1.4.1 ODP Leg 209

Situated at the mid-Atlantic ridge (MAR), ODP Leg 209 was drilled to recover mantle material and compared it with models of mantle flow underneath a slow-spreading ridge with a natural example. From the 8 drilling sites, we obtained samples from Site 1272A and 1274A drilled north and south of the Fifteen-Twenty-Fracture zone (Fig. 1.6). Full spreading rate at that part of the MAR is 25 mm/y (Fujiwara et al., 2003), corresponding to a slow-spreading ridge. Mostly ultrabasic rocks crop out in this area, covered only by a thin sediment layer (Kelemen et al., 2004; Kelemen et al., 2007).

In 2004, Bach et al. showed the down-hole distribution of minerals (mainly serpentine, olivine, clinopyroxene, spinel and magnetite). ODP Leg 209 Site 1272A is characterized by a higher degree of serpentinization and by the presence of iowaite compared to Site 1274A. The latter is characterized by the presence of talc and by higher calcite/brucite ratios. Recent studies consider the early evolution of the peridotites at the two drilling sites (1272A and 1274A) to be different (Seyler et al., 2007; Godard et al., 2008). Site 1272A has less abundant clinopyroxene than Site 1274A and seems to reflect partial melting and melt extraction, while Site 1274A records in addition pervasive melt-rock interaction (Seyler et al., 2007; Godard et al., 2008).

Just south of Site 1272A, a hydrothermal field named Logatchev is localized. Found in the 90ies by a Russian expedition, the long-term fluid evolution is controlled each year by German expeditions. The Logatchev fluids display a chemical signal resulting from interaction with ultramafic rocks (Douville et al., 2002; Schmidt et al., 2007). Pillow basalts, gabbros (diabase) and serpentinites are present in the surroundings (e.g. Kuhn et al., 2004).

1.4.2 Totalp – Malenco

The Eastern Central Alps contain parts of the Mesozoic-Alpine Tethys ocean (the Liguria-Piemonte segment). These ophiolite bodies belong to the Penninic nappes and can be traced along a ~60 km N-S section from Davos (CH) to the Valmalenco (I) region at the boundary with the overlying Austroalpine nappes (Fig. 1.7). Representing the southern part of the Alpine Tethys and the continental margin of the Adria (micro) continent, they are generally interpreted as an ocean-continent transition zone similar to the "active" Iberian margin (Desmurs et al., 2002; Manatschal and Müntener, 2008). During my study I focused on three ophiolite bodies which are from north to south: Totalp, Platta and Malenco (Fig. 1.7). Detailed petrographic studies on this transect showed that from north to south, alpine regional metamorphism increases from prehnite-pumpellyite to amphibolte-facies conditions (Trommsdorff, 1983; Ulmer and Trommsdorff, 1999). In the prehnite-pumpellyite facies, chrysotile/lizardite occurs with relictic olivine and orthopyroxene. Increasing metamorphic degree leads to increasing serpentinization of olivine and orthopyroxene to the south

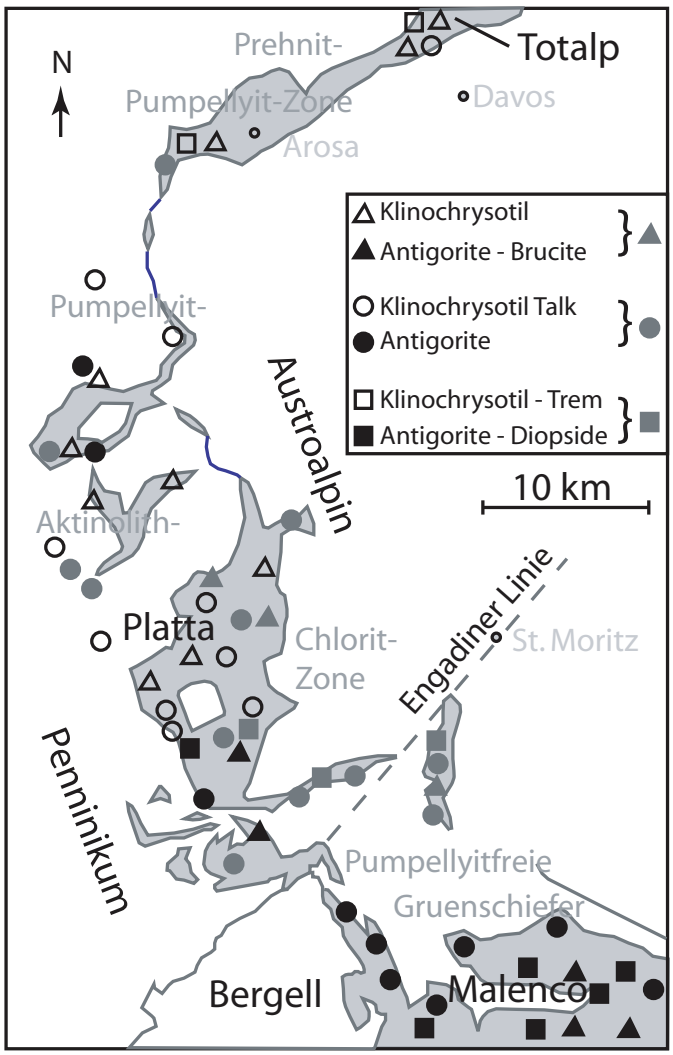

Fig. 1.7. Simplified geological map of the Totalp-Malenco area (from Trommsdorff, 1983).

(Burkhard, 1987). Clinopyroxene on the contrary can be found throughout these ophiolite bodies (Burkhard, 1987).

The Totalp massif (TO) consists of serpentine, pyroxenite (rare garnet-pyroxenite), diabase, ophicarbonates, and pelagic sediments (Peters, 1963). The Platta massif consists of basalts, gabbros, serpentinized mantle, sediments, and extensional allochthons of continental basement rocks, and their pre- and synrift sedimentary cover locally overlies the exhumed mantle rocks (Dietrich, 1970; Manatschal and Nievergelt, 1997). The Malenco ophiolite body (MAL) is composed of gabbros, dunites, spinel-peridotites, pyroxenites, rodingites (mafic dikes), and ophicarbonates (Trommsdorff et al., 2005 and references therein). Further detailed maps and stratigraphic descriptions of the three ophiolite bodies can be found in Dietrich (1970), Montrasio et al. (2005), Peters (1963) and Trommsdorff et al. (2005).

1.5 Thesis outline

The thesis is structured in six chapters, apart from the introduction (this chapter) and the conclusions (chapter VI), each chapter represent a published or potential paper. Contents of chapters II to V are summarized below:

In the **second chapter,** whole rock and in-situ mineral analyses of major and **light element** contents of samples drilled from the MAR (**ODP Leg 209**) are presented. The data set shows nicely the enrichment of B and the Li depletion of peridotite through the formation of serpentine. This signal is also reflected in the whole rock analyses and leads to the calculation of the possible light element composition of the altered oceanic plate before subduction. This chapter has already been published (*Geochimica et Cosmochimica Acta 2008, 72, p. 5475-5504*).

In the **third** chapter I present the **Li, B and Sr isotopic** composition of the same samples (**ODP Leg 209**), combining the mineral and whole rock light element contents with the isotope ratios. The light element isotope data contain the highest ($\delta^{11}B$) and lowest ($\delta^{7}Li$) values measured so far in serpentinized peridotites. The reacting fluid during serpentinization could be identified as evolved seawater and we modelled the fluid/rock evolution with increasing interaction. This chapter has been submitted to *Earth and Planetary Science Letters*.

The **fourth** chapter contains the results of an in-situ **light elemen**t study on **Totalp, Platta and Malenco** ophiolites, which represents a transect of increasing metamorphic grade. The data from Malenco show that transformation of mantle to secondary phases (e.g. serpentinization) does not modify the initial Be contents. This means that Be is relatively immobile and, contrary to Li and B, is not very fluid-mobile. With increasing metamorphism the change from chrysotile to antigorite leads to a sharp change of Li and B element concentration related to antigorite formation. Serpentine polymorphs have therefore a different Li-, Be- and B-signal. This chapter will be submitted to *Geochimica et Cosmochimica Acta*.

The **fifth** chapter sums up the experiments conducted to test the potential loss of **light elements** during direct flux-free fusion at 1500-1800°C and for 30-240s.

Combining **Iridium-strip heater** direct fusion with SIMS measurements would allow contamination-free measurements of Li, Be and B concentrations in whole rock samples. Loss of the three elements occurred during the experiments. As Li and Be loss was within methodological error, these elements can be analyzed after fusion of samples with the strip heater. B, on the other side, shows highly volatile behaviour and is almost completely lost at 1800°C. This chapter will be submitted to G*eochemical Standards Newsletter.*

The **appendix** contains several data not discussed in one of the chapters, which have been collected during this thesis. Li, Be and B-data from Vourinos ophiolite and the Cima di Gagnone peridotite are reported, as well as in-situ $\delta^{11}B$ data of two ODP Leg 209 samples measured by ion probe. These data are included in the final summary (Chapter VI).

1.6 Authorship

Laure Pelletier and I worked in the joint SNF project "The oceanic mantle as an important repository for the light elements Li, Be and B". We studied the light element contents of oceanic mantle in various settings, with the intention to create a large database on oceanic mantle, from the modern ocean to ophiolites. Laure Pelletier focussed more on non-metamorphic ophiolites (Greece) while I concentrated on samples from the MAR and from metamorphic ophiolites of the Alps. In order to make the study more efficient, we split up much of the analytical work. Laure Pelletier used mainly techniques for in-situ mineral analysis (EMPA, SIMS, micro-Raman, LA-ICP MS) and XRF for whole-rock analysis. Besides EMPA and SIMS, I used mainly TIMS and MC ICP MS for isotope analysis. Through this partitioning of tasks, each of us has made considerable contributions to the thesis of the other. Therefore, Table 1.1 details the contributions of all persons involved in the project to the chapters of this thesis (see also Table 1.1 in thesis of Laure Pelletier; 2008).

CO-AUTHORS

Angelika Kalt[a]
Laure Pelletier[a]
Othmar Müntener[b]
Thomas Ludwig[c]
Hans-Michael Seitz[e]
Arjan Dijkstra[a]
Sonia Tonarini[d]

Addresses

a Institut de Géologie et d'Hydrogéologie, Université de Neuchâtel, Rue Emile-Argand 11, CP 158, 2009 Neuchâtel, Switzerland
b Institut de Minéralogie et Géochimie, Université de Lausanne, Anthropole, 1015 Lausanne, Switzerland
c Mineralogisches Institut, Ruprecht-Karls-Universität Heidelberg, Im Neuenheimer Feld 236, 69120 Heidelberg, Germany
d CNR, Istituto di Geoscienze e Georisorse Via Moruzzi 1, 56124 Pisa, Italy
e Wolfgang Goethe Universität, Altenhöferallee 1, 60438 Frankfurt am Main, Germany

Table 1.1 Contribution of the co-authors and collaborators to the different chapters

		Chapters						Appendix				Ad. Papers	
Collaborator	University	I	II	III	IV	V	VI	A	B	C	D	1	2
Analytics													
Vils Flurin	University of Neuchâtel	-	60%	50%	95%	95%	-	95%	60%	90%	50%	10%	35%
Pelletier Laure	University of Neuchâtel	-	30%	-	-	-	-	-	-	-	-	80%	50%
Ludwig Thomas	University of Heidelberg (D)	-	5%	-	5%	5%	-	5%	-	-	-	-	-
Tonarini Sonja	CNR Pisa (I)	-	-	25%	-	-	-	-	-	-	-	-	-
Seitz Hans-Michael	University of Frankfurt	-	-	25%	-	-	-	-	-	-	-	-	-
Pabst Sonja	University of Heidelberg (D)	-	-	-	-	-	-	-	40%	-	-	-	-
Grobéty Bernard	University of Fribourg (Ch)	-	-	-	-	-	-	-	-	-	25%	-	-
Others		-	5%	-	-	-	-	-	-	10%	25%	10%	15%
Writing													
Vils Flurin	University of Neuchâtel	90%	70%	70%	80%	90%	90%	-	-	-	-		
Kalt Angelika	University of Neuchâtel	10%	25%	20%	-	-	10%	-	-	-	-	20%	10%
Müntener Othmar	University of Lausanne	-	5%	-	20%	-	-	-	-	-	-	-	10%
Dijkstra Arjan	University of Neuchâtel	-	-	-	-	10%	-	-	-	-	-	-	-
Others		-	-	10%	-	-	-	-	-	-	-	80%	80%
Interpretations of the Results													
Vils Flurin	University of Neuchâtel	-	70%	65%	70%	70%	-	-	-	-	-		
Kalt Angelika	University of Neuchâtel	-	25%	10%	-	-	-	-	-	-	-	50%	40%
Müntener Othmar	University of Lausanne	-	5%	-	30%	-	-	-	-	-	-	-	-
Tonarini Sonja	CNR Pisa (I)	-	-	25%	-	-	-	-	-	-	-	-	-
Dijkstra Arjan	University of Neuchâtel	-	-	-	-	30%	-	-	-	-	-	-	-
Others		-	-	-	-	-	-	-	-	-	-	50%	60%

Additional papers 1 and 2 correspond to chapter 1 and 5 in the thesis of Laure Pelletier (2008, University of Neuchâtel). Paper 1 published 2008 in Journal of Petrology (**49**, p. 2043-2080). Paper 2 submitted to European Journal of Mineralogy.

REFERENCES

Aggarwal, J. K., Palmer, M. R., Bullen, T., Arnorsson, S., and Ragnarsdottir, K. V., 2000. The boron isotope systematics of Icelandic geothermal waters: 1. Meteoric water charged systems. Geochimica et Cosmochimica Acta 64, 579-585.

Anders, E. and Grevesse, N., 1989. Abundance of the elements: meteoritic and solar. Geochimica et Cosmochimica Acta 53, 197-214.

Bach, W., Garrido, C. J., Paulick, H., Harvey, J., and Rosner, M., 2004. Seawater-peridotite interactions: First insights from ODP Leg 209, MAR 15°N. Geochemistry Geophysics Geosystems 5, 1-22.

Bebout, G. E., Ryan, J. G., and Leeman, W. P., 1993. B-Be systemtics in subduction-related metamorphic rocks: Characterization of the subducted component. Geochimica et Cosmochimica Acta 57, 2227-2237.

Benton, L. D., Ryan, J. G., and Savov, I. P., 2004. Lithium abundance and isotopic systematics of forarc serpentinites, Conical Seamount, Mariana forearc: Insights into the mechanics of slab-mantle exchange during subduction. Geochemistry Geophysics Geosystems 5, 1-14.

Benton, L. D., Ryan, J. G., and Tera, F., 2001. Boron isotope systematics of slab fluids as inferred from a serpentine seamount, Mariana forearc. Earth and Planetary Science Letters 187, 273-282.

Bonatti, E., Lawrence, J., and Morandi, N., 1984. Serpentinization of oceanic peridotites: temperature dependence of mineralogy and boron content. Earth and Planetary Science Letters 70, 88-94.

Boschi, C., Dini, A., Früh-Green, G., and Kelley, D. S., 2008. Isotopic and element exchange during serpentinization and metasomatism at the Atlantis Massif (MAR 30°N): Insights from B and Sr isotope data. Geochimica et Cosmochimica Acta 72, 1801-1823.

Bouman, C., Elliott, T., and Vroon, P. Z., 2004. Lithium inputs to subduction zones. Chemical Geology 212, 59-79.

Bouvier, A.-S., Métrich, N., and Deloule, E., 2008. Slab-derived fluids in the magma sources of St. Vincent (Lesser Antilles Arc): Volatile and light element imprints. Journal of Petrology 49, 1427-1448.

Brooker, R. A., James, R. H., and Blundy, J. D., 2004. Trace elements and Li isotope systematics in Zabargad peridotites: evidence of ancient subduction processes in the Red Sea mantle. Chemical Geology 212, 179-204.

Burkhard, D. J. M., 1987. Ore minerals and geochemistry in the serpentitnites of the Estern Central Alps (Davos to the Val Malenco) compared to occurrences in the Klamath Mountains (California and Oregon). Ph.D. thesis, Ruprecht-Karls-Universität Heidelberg.

Chan, L. H., Alt, J. C., and Teagle, D. A. H., 2002. Lithium and lithium isotope profiles through the upper oceanic crust: A study of seawater-basalt exchange at ODP Sites 504B and 896A. Earth and Planetary Science Letters 201, 187-201.

Chan, L. H., Edmond, J., Thompson, G., and Gillis, K. M., 1992. Lithium isotopic composition of submarine basalts: Implications for the lithium cycle in the oceans. Earth and Planetary Science Letters 108, 151-160.

Chan, L. H. and Kastner, M., 2000. Lithium isotopic compositions of pore fluids and sediments in the Costa Rica subduction zone: implications for fluid processes and sediment contribution to the arc volcanoes. Earth and Planetary Science Letters 183, 275-290.

Chan, L. H., Leeman, W. P., and Plank, T., 2006. Lithium isotopic composition of marine sediments. Geochemistry Geophysics Geosystems 7.

Chaussidon, M. and Koeberle, C., 1995. Boron content and isotopic composition of tektites and impact glasses: Constraints on source regions. Geochimica et Cosmochimica Acta 59, 613-624.

Chaussidon, M. and Marty, B., 1995. Primitive boron isotope composition of the mantle. Science 269, 383-386.

Decitre, S., Buatier, M., and James, R., 2004. Li and Li isotopic composition of hydrothermally alteres sediments at Middle Valley, Juan De Fuca. Chemical Geology 211, 363-373.

Decitre, S., Deloule, E., Reisberg, L., James, R., Agrinier, P., and Mével, C., 2002. Behavior of Li and its isotopes during serpentinization of oceanic peridotites. Geochemistry Geophysics Geosystems 3.

Desmurs, L., Müntener, O., and Manatschal, G., 2002. Onset of magmatic accretion within a magma-poor rifted margin: A case study from the Platta ocean-continent transition, eastern Switzerland. Contributions to Mineralogy and Petrology 144, 365-382.

Dietrich, V., 1970. Die Stratigraphie der Platta-Decke. Eclogae Geologica Helvetia 633, 631-671.

Douville, E., Charlou, J. L., Oelkers, E. H., Bienvenu, P., Jove Colon, C. F., Donval, J. P., Fouquet, Y., Prieur, D., and Appriou, P., 2002. The rainbow vent fluids (36°14′N, MAR): The influence of ultramafic rocks and phase separation on trace metal content in mid-atlantic ridge hydrothermal fluids. Chemical Geology 184, 37-48.

Elliott, T., Thomas, A., Jeffcoate, A., and Niu, Y., 2006. Lithium isotope evidence for subduction-enriched mantle in the source of mid-ocean-ridge basalts. Nature 443, 565-568.

Fujiwara, T., Lin, J., Matsumoto, T., Kelemen, P. B., Tucholke, B. E., and Casey, J. F., 2003. Crustal evolution of the mid-atlantic ridge near the Fifteen-Twenty Fracture zone in the last 5 Ma. Geochemistry Geophysics Geosystems 4, 1-25.

Gao, S., Luo, T.-C., Zhang, B.-R., Zhang, H.-F., Han, Y.-W., Zhao, Z.-D., and Hu, Y.-K., 1998. Chemical composition of the continental crust as revealed by studies in East China. Geochimica et Cosmochimica Acta 62, 1959-1975.

Godard, M., Lagabrielle, Y., Alard, O., and Harvey, J., 2008. Geochemistry of the highly depleted peridotites drilled at ODP Sites 1272 and 1274 (Fiffteen-Twenty Fracture Zone, Mid-Atlantic Ridge): Implications for mantle dynamics beneath a slow spreading ridge. Earth and Planetary Science Letters 267, 410-425.

Halama, R., McDonough, W. F., Rudnick, R. L., Keller, J., and Klaudius, J., 2007. The Li isotopic composition of Oldoinyo Lengai: Nature of the mantle sources and lack of isotopic fractionation during carbonatite petrogenesis. Earth and Planetary Science Letters 254, 77-89.

Hart, S. R., Blusztajn, J., Dick, H. J. B., Meyer, P. S., and Muehlenbachs, K., 1999. The fingerprint of seawater circulation in a 500-meter section of ocean crust gabbros. Geochimica et Cosmochimica Acta 63, 4059-4080.

Hoefs, J. and Sywall, M., 1997. Lithium isotope composition of quaternary and tertiary biogene carbonates and a global lithium isotope balance. Geochimica et Cosmochimica Acta 61, 2679-2690.

Ionov, D. and Seitz, H.-M., 2008. Lithium abundances and isotopic compositions in mantle xenolith from subduction and intra-plate settings: mantle sources vs. eruption histories. Earth and Planetary Science Letters 266, 316-331.

Ishikawa, T. and Nakamura, E., 1993. Boron isotope systematics of marine sediments. Earth and Planetary Science Letters 117, 567-580.

Ishikawa, T. and Tera, F., 1997. Source, composition and distribution of the fluid in the Kurile mantle wedge: Constraints from across-arc variations of B/Nb and B isotopes. Earth and Planetary Science Letters 152, 123-138.

Ishikawa, T., Tera, F., and Nakazawa, T., 2001. Boron isotope and trace element systematics of the three volcanic zones in the Kamchatka arc. Geochimica et Cosmochimica Acta 65, 4523-4537.

Jeffcoate, A., Elliott, T., Kasemann, S. A., Ionov, D., Cooper, K., and Brooker, R. A., 2007. Li isotope fractionation in peridotites and mafic melts. Geochimica et Cosmochimica Acta 71, 22-218.

Joachimski, M. M., Simon, L., van Geldern, R., and Lècuyer, C., 2005. Boron isotope geochemistry of Paleozoic brachiopod calcite: Implications for a secular change in the boron isotope geochemistry of seawater over the Phanerozoic. Geochimica et Cosmochimica Acta 69, 4035-4044.

Kelemen, P. B., Kikawa, E., and Miller, D. J., 2004. Proceedings of the Ocean Drilling Programm. Preliminary Report Leg 209.

Kelemen, P. B., Kikawa, E., and Miller, D. J., 2007. Proc. ODP, Sci. Results, College Station, TX (Ocean Drilling Program).

Kelley, D. S., Karson, J. A., Blackman, D. K., Früh-Green, G., Butterfield, D. A., Lilley, M. D., Olson, E. J., Schrenk, M. O., Roe, K., Lebon, G. T., and Rivizzigno, P., 2001. An off-axis hydrothermal field near the mid-atlantic ridge at 30°N. Nature 412, 145-149.

Kobayashi, K., Tanaka, R., Moriguti, T., Shimizu, K., and Nakamura, E., 2004. Lithium, boron, and lead isotope systematics of glass inclusions in olivines from Hawaiian lavas: Evidence for recycled components in the Hawaiian plume. Chemical Geology 212, 143-161.

Krolikowska-Ciaglo, S., Deyhle, A., Hauff, F., and Hoernle, K., 2007. Boron isotope geochemistry and U-Pb systematics of altered MORB from the Australian Antarctic Discordance (ODP Leg 187). Chemical Geology 242, 458-472.

Kuhn, et, and al, 2004. The Logatchev hydrothermal field - revisited: preliminary results of the R/V Meteor cruise hydromar I (M60/3). Interridge News 13, 1-4.

Leeman, W. P., Tonarini, S., Chan, L. H., and Borg, L. E., 2004. Boron and lithium isotopic variations in a hot subduction zone - the southern Washington Cascades. Chemical Geology 212, 101-124.

Li, Z.-X. A. and Lee, C.-T. A., 2006. Geochemical investigation of serpentinized oceanic lithospheric mantle in the Feather River Ophiolite, California: Implications for the recycling rate of water by subduction. Chemical Geology 235, 161-185.

Lyubetskaya, T. and Korenaga, J., 2007. Chemical composition of Earth's primitive mantle and its variance: 1. Method and results. Journal of Geophysical Research 112.

MacDonald, A. H. and Fyfe, W. S., 1985. Rate of serpentinization in seafloor environments. Tectonophysics 116, 123-135.

Magna, T., Wiechert, U., Grove, T. L., and Halliday, A. N., 2006a. Lithium isotope fractionation in the southern Cascadia subduction zone. Earth and Planetary Science Letters 250, 428-443.

Magna, T., Wiechert, U., and Halliday, A. N., 2006b. New constraints on the lithium isotope compositions of the Moon and terrestrial planets. Earth and Planetary Science Letters 243, 336-353.

Manatschal, G. and Müntener, O., 2008. A type sequence across an ancient magma-poor ocean-continent transition: the example of the

western Alpine Tethys ophiolites. Tectonophysics 458, 1-8.

Manatschal, G. and Nievergelt, P., 1997. A continent ocean transition recorded in the Err and Platta nappes (eastern Switzerland). Eclogae Geologica Helvetia 90, 3-27.

Marschall, H., Pogge von Strandmann, P. A. E., Seitz, H.-M., Elliott, T., and Niu, Y., 2007. The lithium composition of orogenic eclogites and deep subducted slabs. Earth and Planetary Science Letters.

Marschall, H. R., 2005. Lithium, beryllium and boron in high-pressure metamorphic rocks from Syros (Greece). Ph. D. thesis, Ruprecht-Karls Universität.

McCulloch, M., Gregory, R. T., Wasserburg, G. J., and Taylor, H. P. J., 1980. A neodymium, strontium and oxygen isotopic study of the cretaceous samail ophiolite and implications for the petrogenesis and seawater-hydrothermal alteration of oceanic crust. Earth and Planetary Science Letters 46, 201-211.

McDonough, W. F. and Sun, S.-S., 1995. The composition of the Earth. Chemical Geology 120, 223-253.

Merchel, S., Braucher, R., Benedetti, L., Grauby, O., and Bourlès, D., 2008. Dating carbonate rocks with in-situ produced cosmogenic ^{10}Be: Why it often fails. Quaternary Geochronology 3, 299-307.

Montrasio, A., Trommsdorff, V., Hermann, J., Müntener, O., and Spillmann, P., 2005. Carta Geologica della Valmalenco. Supplement to Schweizerische Mineralogische und Petrographische Mitteilungen 85.

Moriguti, T. and Nakamura, E., 1998. Across-arc variation of lithium isotopes in lavas and implications for crust/mantle recycling at subduction zones. Earth and Planetary Science Letters 163, 167-174.

Moriguti, T., Shibata, T., and Nakamura, E., 2004. Lithium, boron and lead isotope and trace element systematics of Quaternary basaltic volcanic rocks in northeastern Japan: Mineralogical controls on slab-derived fluid composition. Chemical Geology 212, 81-100.

Nishio, Y., Nakai, S. i., Yamamoto, J., Sumino, H., Matsumoto, T., Prikhod'ko, V. S., and Arai, S., 2004. Lithium isotopic systematics of the mantle-derived ultranafic xenoliths: Implications for EM1 origin. Earth and Planetary Science Letters 217, 245-261.

Niu, Y., 2004. Bulk-rock major and trace element compositions of abyssal peridotites: Implications for mantle melting, melt extraction and post-melting processes beneath mid-ocean ridges. Journal of Petrology 45, 2423-2458.

Ottolini, L., Le Fèvre, B., and Vannucci, R., 2004. Direct assessment of mantle boron and lithium contents and distribution by SIMS analyses of peridotite minerals. Earth and Planetary Science Letters 228, 19-36.

Palme, H. and Beer, H., 1993. Abundances of the elements in the solar system, Instruments, Methods, Solar System. Springer Verlang, Berlin.

Palmer, M. R., 1991. Boron isotope systematics of hydrothermal fluids and tourmalines: A synthesis. Chemical Geology 94, 111-121.

Pearson, D. G., Canil, D., and Shirey, S. B., 2004. Mantle Samples Included in Volcanic Rocks: Xenoliths and Diamonds. In: Holland, H. D. and Turrekian, K. K. Eds.), Treatis on geochemistry. Elsevier, Amsterdam.

Pelletier, L., 2008. The oceanic mantle as an important repository for the light elements Li, Be and B, PhD-thesis at the University of Neuchâtel.

Pelletier, L. Vils, F., Kalt, A., and Gméling, K., 2008. Li, B and Be contents of harzburgites from the Dramala Complex (Pinods ophiolite, Greece): Evidence for a MOR-type mantle in a supra-subduction zone environment. Journal of Petrology 49, 2043-2080.

Peters, T., 1963. Mineralogie und Petrographie des Totalpserpentins bei Davos. Schweizerische Mineralogische und Petrographische Mitteilungen 43, 529-684.

Quinby-Hunt, M. S. and Turekian, K. K., 1983. Distribution of elements in sea water. EOS 64, 130-132.

Rose, E. F., Shimizu, N., Layne, G. D., and Grove, T. L., 2001. Melt production beneath Mt. Shasta from boron data in primitive melt inclusions. Science 293, 281-283.

Rosner, M., Erzinger, J., Franz, G., and Trumbull, R. B., 2003. Slab-derived boron isotope signatures in arc volcanic rocks from the Central Andes and evidence for boron isotope fractionation during progressive slab dehydration. Geochemistry Geophysics Geosystems 4, 1-25.

Rudnick, R. L. and Gao, S., 2004. Composition of the continental crust. In: Holland, H. D. and Turekian, K. K. Eds.), Treatise on Geochemistry. Elsevier, Amsterdam, 1-64.

Rudnick, R. L. and Ionov, D., 2007. Lithium elemental and isotopic disequilibrium in minerals from peridotite xenolith form far-east Russia: Product of recent melt/fluid-rock reaction. Earth and Planetary Science Letters 256, 278-293.

Rudnick, R. L., Tomascak, P. B., Njo, H. B., and Gardner, R. l., 2004. Extreme lithium isotopic fractionation during continental weathering revealed in saprolites from South Carolina. Chemical Geology 212, 45-57.

Ryan, J. and Kyle, P. R., 2004. Lithium abundance and lithium isotope variations in mantle sources: Insights from intraplate volcanic rocks from Ross Island and Marie Byrd Land (Antarctica) and other oceanic islands. Chemical Geology 212, 125-142.

Ryan, J. G. and Langmuir, C. H., 1987. The systematics of lithium abundances in young volcanic rock. Geochimica et Cosmochimica Acta 51, 1727-1741.

Ryan, J. G. and Langmuir, C. H., 1993. The systematics of boron abundances in young volcanic rocks. Geochimica et Cosmochimica Acta 57, 1489-1498.

Ryan, J. G., Morris, J., Tera, F., Leeman, W. P., and Tsvetkov, A., 1995. Cross-Arc geochemical variations in the Kurile Arc as a function of slab. Science 270, 625-627.

Salters, V. J. M. and Stracke, A., 2004. Composition of the depleted mantle. Geochemistry Geophysics Geosystems 5, 1-27.

Schmidt, K., Koschinsky, A., Garbe-Schönberg, D., de Carvalho, L. M., and Seifert, R., 2007. Geochemistry of hydrothermal fluids from the ultramafic-hosted Logatchev hydrothermal field, 15°N on the mid-atlantic ridge: Temporal and spatial investigation. Chemical Geology 242, 1-21.

Schmidt, M. and Poli, S., 1998. Experimentally based water budgets for dehydrating slabs and consequences for arc magma generation. Earth and Planetary Science Letters 163, 361-379.

Seyfried, W. E., Janecky, D. R., and Mottl, M. J., 1984. Alteration of the oceanic crust: Implications for geochemical cycles of lithium and boron. Geochimica et Cosmochimica Acta 48, 557-569.

Seyler, M., Lorand, J.-P., Dick, H. J. B., and Drouin, M., 2007. Pervasive melt percolation reactions in ultra-depleted refractory harzburgites at the mid-atlantic ridge, 15°20'N: ODP Hole 1274A. Contributions to Mineralogy and Petrology 153, 303-319.

Smith, H. J., Leeman, W. P., Davidson, J., and Spivack, A. J., 1997. The B isotopic composition of arc lavas from Martinique, Lesser Antilles. Earth and Planetary Science Letters 146, 303-314.

Smith, H. J., Spivack, A. J., Staudigel, H., and Hart, S. R., 1995. The boron isotopic composition of altered oceanic crust. Chemical Geology 126, 119-135.

Spivack, A. J. and Edmond, J., 1987. Boron isotope exchange between seawater and oceanic crust. Geochimica et Cosmochimica Acta 51, 1033-1043.

Spivack, A. J., You, C. F., and Smith, H. J., 1993. Foraminiferal boron isotope ratios as a proxy for surface ocean pH over the past 21 Myr. Nature 363, 149-151..

Taylor, H. P. J., 1977. Water/rock interactions and the origin of H20 in granitic batholiths. Journal of the Geological Society, London 133, 509-558.

Teng, F. Z., McDonough, W. F., Rudnick, R. L., Dalpé, C., Tomascak, P. B., Chappell, B. W., and Gao, S., 2004. Lithium isotopic composition and concentration of the upper continental crust. Geochimica et Cosmochimica Acta 68, 4167-4178.

Thompson, G. and Melson, W. G., 1970. Boron contents of serpentinites and metabasalts in the oceanic crust: implications for the boron cycle in the oceans. Earth and Planetary Science Letters 8, 61-65.

Tomascak, P. B., Langmuir, C. H., and Le Roux, P. J., 2008. Lithium isotopes in global mid-ocean ridge basalts. Geochimica et Cosmochimica Acta 72, 1626-1637.

Tomascak, P. B., Ryan, J. G., and Defan, M. J., 2000. Lithium isotope evidence for light element decoupling in the Panama subarc mantle. Geology 28, 507-510.

Tomascak, P. B., Widom, E., Benton, L. D., Goldstein, S. L., and Ryan, J. G., 2002. The control of lithium budgets in island arcs. Earth and Planetary Science Letters 196, 227-238.

Tonarini, S., Agostini, S., Innocenti, F., and Manetti, P., 2005. $\delta^{11}B$ as tracer of slab dehydration and mantle evolution in Western Anatolia Cenozoic Magmatism. Terra nova 17, 259-264.

Tonarini, S., Armienti, P., D'Orazio, M., and Innocenti, F., 2001. Subduction-like fluids in the genesis of Mt. Etna magmas: Evidence from boron isotopes and fluid mobile elements. Earth and Planetary Science Letters 192, 471-483.

Trommsdorff, V., 1983. Metamorphose magnesiumreicher Gesteine: Kritischer Vergleich von Natur, Experiment und thermodynamischer Datenbasis. Fortschritte der Mineralogie 61, 238-308.

Trommsdorff, V., Montrasio, A., Hermann, J., Müntener, O., Spillmann, P., and Gieré, R., 2005. The geological map of Valmalenco. Schweizerische Mineralogische und Petrographische Mitteilungen 85, 1-13.

Turner, S., Tonarini, S., Bindeman, I., Leeman, W. P., and Schaefer, B. F., 2007. Boron and oxygen isotope evidence for recycling of subducted components over the past 2.5Gyr. Nature 447, 702-705.

Ulmer, P. and Trommsdorff, V., 1995. Serpentine stability to mantle depths and subduction-related magmatism. Science 268, 858-861.

Ulmer, P. and Trommsdorff, V., 1999. Phase relations of hydrous mantle subducting to 300 km, Mantle petrology: Field observations and high pressure experimentation. The Geochemical Society, 259-281.

Vigier, N., Decarreau, A., Millot, R., Carignan, J., Petit, S., and France-Lanord, C., 2008. Quantifying Li isotope fractionation during smectite formation and implications for the Li cycle. Geochimica et Cosmochimica Acta 72, 780-792.

Wunder, B., Meixner, A., Romer, R. L., and Heinrich, W., 2006. Temperature-dependent isotopic

fractionation of lithium between clinopyroxene and high-pressure hydrous fluids. Contributions to Mineralogy and Petrology 151, 112-120.

Zack, T., Tomascak, P. B., Rudnick, R. L., Dalpé, C., and McDonough, W. F., 2003. Extremely light Li in orogenic eclogites. The role of isotope fractionation during dehydration in subducted oceanic crust. Earth and Planetary Science Letters 208, 279-290.

Zhai, M., Nakamura, E., Shaw, D. M., and Nakano, T., 1996. Boron isotope ratios in meteorites and lunar rocks. Geochimica et Cosmochimica Acta 60, 4877-4881.

Zhang, L., Chan, L. H., and Gieskes, J. M., 1998. Lithium isotope geochemistry of pore waters from Ocean Drilling Programm Sites 918 and 919, Irminger Basin. Geochimica et Cosmochimica Acta 62, 2437-2450.

Chapter II

The lithium, boron and beryllium content of serpentinized peridotites from ODP Leg 209 (Sites 1272A and 1274A): Implications for lithium and boron budgets of oceanic lithosphere

Published in 2008 in Geochimica and Cosmochimca Acta Vol 72, pages 5475-5504

ABSTRACT

Despite the key importance of altered oceanic mantle as a repository and carrier of light elements (B, Li, and Be) to depth, its inventory of these elements has hardly been explored and quantified. In order to constrain the systematics and budget of these elements we have studied samples of highly serpentinized (>50%) spinel harzburgite drilled at the mid-Atlantic ridge (Fifteen–Twenty Fracture zone, ODP Leg 209, Sites 1272A and 1274A). In-situ analysis by secondary ion mass spectrometry reveals that the B, Li and Be contents of mantle minerals (olivine, orthopyroxene, and clinopyroxene) remain unchanged during serpentinization. B and Li abundances largely correspond to those of unaltered mantle minerals whereas Be is close to the detection limit. The Li contents of clinopyroxene are slightly higher (0.44–2.8 µg/g) compared to unaltered mantle clinopyroxene, and olivine and clinopyroxene show an inverse Li partitioning compared to literature data. These findings along with textural observations and major element composition obtained from microprobe analysis suggest reaction of the peridotites with a mafic silicate melt before serpentinization. Serpentine minerals are enriched in B (most values between 10 and 100 µg/g), depleted in Li (most values below 1 µg/g) compared to the primary phases, with considerable variation within and between samples. Be is at the detection limit. Analysis of whole rock samples by prompt gamma activation shows that serpentinization tends to increase B (10.4–65.0 µg/g), H_2O and Cl contents and to lower Li contents (0.07–3.37 µg/g) of peridotites, implying that - contrary to alteration of oceanic crust - B is fractionated from Li and that the B and Li inventory should depend essentially on rock–water ratios. Based on our results and on literature data, we calculate the inventory of B and Li contained in the oceanic lithosphere, and its partitioning between crust and mantle as a function of plate characteristics. We model four cases, an ODP Leg 209-type lithosphere with almost no igneous crust, and a Semail-type lithosphere with a thick igneous crust, both at 1 and 75 Ma, respectively. The results show that the Li contents of the oceanic lithosphere are highly variable (17–307 kg in a column of 1 m 1 m thickness of the lithosphere (kg/col)). They are controlled by the primary mantle phases and by altered crust, whereas the B contents (25–904 kg/col) depend entirely on serpentinization. In all cases, large quantities of B reside in the uppermost part of the plate and could hence be easily liberated during slab dehydration. The most prominent input of Li into subduction zones is to be expected from Semail-type lithosphere because most of the Li is stored at shallow levels in the plate. Subducting an ODP Leg 209-type lithosphere would mean only very little Li contribution from the slab. Serpentinized mantle thus plays an important role in B recycling in subduction zones, but it is of lesser importance for Li.

2.1. Introduction

At mid-ocean ridges, plates spread and new oceanic lithosphere is produced. At slow spreading-ridges, the magmatic section is often reduced and the oceanic mantle is exhumed at the ocean floor (e.g. Cannat, 1993; Michael et al., 2003; Escartin et al., 2003). The two currently debated models to explain mantle exhumation in slow-spreading environments invoke either spreading, and focused magmatism at the center of a ridge segment (Cannat, 1993; Ghose et al., 1996 and Dijkstra et al., 2001) or detachment faulting (Tucholke et al., 1998; Escartin et al., 2003; Boschi et al., 2006; Ildefonse et al., 2007). In both cases, hydrothermal fluids transform olivine, orthopyroxene and clinopyroxene into serpentine, chlorite, tremolite, brucite or magnetite (e.g. Bach et al., 2004), depending on temperature and pressure conditions (e.g. Ulmer and Trommsdorff, 1995).

In the last years, the systematics of the light elements Li, B, and Be have been used to chemically trace low-temperature alteration processes in different geological environments (e.g. James and Palmer, 2000; Chan et al., 2002; Pistiner and Henderson, 2003; Rudnick et al., 2004; Kisakürek et al., 2004). Studies on fresh mid-ocean ridge basalts (MORB; Ryan and Langmuir, 1987; Ryan and Langmuir, 1993) and on altered MORB (e.g. Thompson and Melson, 1970; Bouman et al., 2004; Elliott et al., 2006) showed that during alteration Li and B may be enriched by a factor of 2 and 30, respectively.

A similar reasoning can be applied to the underlying mantle lithosphere. Estimates of the light element content of the primitive mantle (McDonough and Sun, 1995; Lyubetskaya and Korenaga, 2007) and of the depleted mantle (Salters and Stracke, 2004) imply very low light element abundances in whole rock samples and major mantle phases (around 1 µg/g for Li and B). These whole rock data are consistent with C1 chondrite concentrations (Anders and Grevesse, 1989; Lyubetskaya and Korenaga, 2007). In contrast, elevated Li (up to 13.7 µg/g, Decitre et al., 2002; Niu, 2004) and high B whole rock contents (up to 85 µg/g, Bonatti et al., 1984; Spivack and Edmond, 1987) were found in dredged abyssal peridotites. High Li (<19.5 µg/g, Decitre et al., 2002) and B abundances (47 µg/g, Scambelluri et al., 2004) were found in serpentine minerals.

In addition, high but variable whole rock B (0.4–79.0 µg/g; Benton et al., 2001; Savov et al., 2005; Wei et al., 2005) and Li concentrations (0.5–18.9 µg/g; Parkinson and Pearce, 1998; Benton et al., 2004; Savov et al., 2005; Zanetti et al., 2006; Savov et al., 2007) were measured in serpentinized peridotites from forearc settings.

Beryllium (Be) data are scarce, and concentrations are extremely low in primitive mantle (0.054 µg/g or 0.068 µg/g; McDonough and Sun, 1995; Lyubetskaya and Korenaga, 2007) and in depleted mantle (0.025 µg/g; Salters and Stracke, 2004), highly variable in dredged abyssal peridotites (0.001–0.212 µg/g, Niu, 2004), and elevated in forearc peridotites (0.07–0.16 µg/g, Zanetti et al., 2006).

Experimentally determined mineral/melt and mineral/fluid partition coefficients are in line with these observations and show that B, Li and Be are incompatible in mantle minerals (e.g. Brenan et al., 1998; Taura et al., 1998). However, there are only a few experiments concerning the light element contents of hydrothermally precipitated minerals. Seyfried and Dibble (1980) performed seawater–peridotites experiments at 300°C and 500 bar. During the experiment, the B content in the solution (pH <5) remained constant, but during quenching the B content decreased from 4.01 to 1.75 µg/g. It was proposed that B is incorporated into serpentinized peridotite at low temperatures (<300°C).Bonatti et al. (1984) suggested that the maximum B uptake in peridotite is related to temperature and to the serpentine polymorph, and measured a maximum value of 110 µg/g B in serpentine minerals (orthochrysotile, clinochrysotile and lizardite). Reversing the alteration process by heating up altered basalt to 350°C at 500 bar showed that Li and B are incorporated in low-temperature alteration phases and are liberated into the fluid phase upon heating (Seyfried et al., 1998).

The light element content of the oceanic mantle is important in the context of recycling of these elements in subduction zones. Previous studies have shown that the magmatic and sedimentary oceanic crust can be a major host for Li and B. Oceanic sediments are enriched in B (up to 100.2 µg/g, Leeman et al., 2004) and Li (up to 74.3 µg/g, Bouman et al., 2004; Leeman et al., 2004).

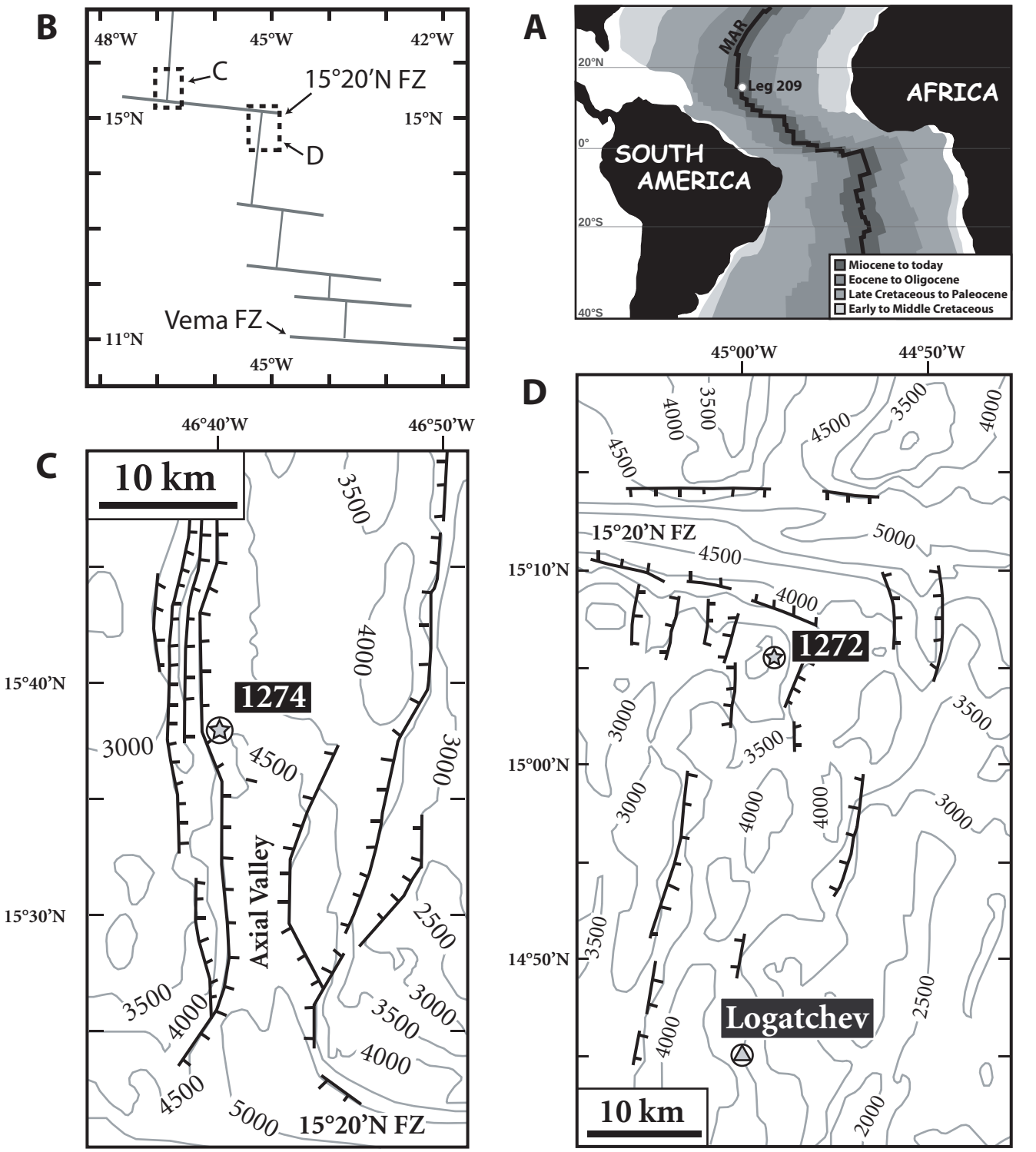

Fig. 2.1. (A) Isochrone map illustrating the age of the Atlantic ocean (modified after Scotese et al., 1988) and displaying ODP Leg 209 on the mid-Atlantic ridge (MAR). (B) Details of drill sites of the Northern and the Southern areas of ODP Leg 209. (C and D) Bathymetric map (after Lagabrielle et al., 1998) showing the location of ODP Sites 1272A and 1274A (stars; modified after Paulick et al., 2006). The Logachev active hydrothermal field is also shown (triangle).

Even after metamorphism at high pressure and moderate temperature (400°C) in a subduction zone, they retain up to 66.7 µg/g Li, 2.32 µg/g Be, and 93.9 µg/g B (Marschall et al., 2006). Altered oceanic basalt may contain up to 36.5 µg/g Li (Bouman et al., 2004). Subducted oceanic crust, nowadays eclogites, was found to contain up to 37.4 µg/g Li (Zack et al., 2002; Marschall et al., 2006), and up to 4.77 µg/g B (Marschall et al., 2006). However, the crustal section of a subducting oceanic lithosphere is thin compared to the mantle part and magmatic crust can be largely absent in lithosphere produced at slow-spreading ridges. Therefore, serpentinized mantle should play a key role

in light element recycling. Experiments on serpentinite breakdown (simulation of a subducting plate) by Tenthorey and Hermann (2004) suggest that serpentinized mantle should be the major sink of B in subduction zones. The extreme enrichment in B of the Mariana forearc mantle wedge supports this theory (Savov et al., 2007).

In this study, we investigated serpentinized oceanic peridotites drilled from near the mid-Atlantic ridge (MAR, ODP Leg 209, Sites 1272A and 1274A). We analyzed minerals and whole rock samples for major elements, Li, Be and B contents. Our aims were to identify the host minerals of the light elements, to understand light element systematics, to establish a mass balance and to discuss the calculations in the framework of light element recycling at subduction zones.

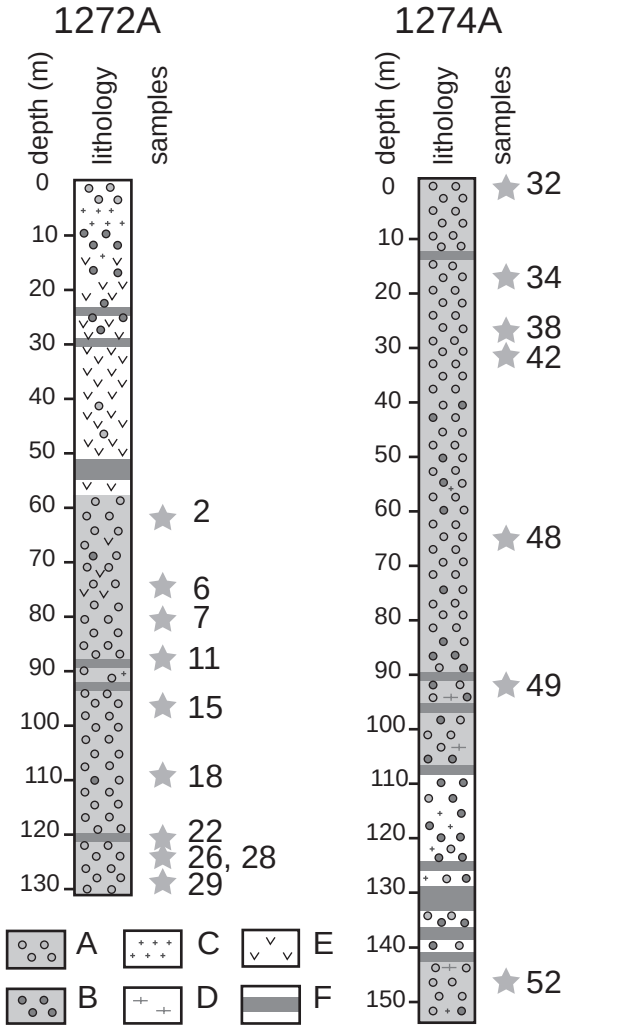

Fig. 2.2. Core description and sample location for ODP Leg 209, modified after Bach et al. (2004). (A) Harzburgite, (B) dunite, (C) gabbro, (D) magmatic dikelets, (E) basalt and diabase, (F) fracture zone. Numbers correspond to sample numbers (e.g. 26= OD 26).

2.2. Geological setting

ODP Leg 209 was drilled at the MAR, north and south of the Fifteen–Twenty Fracture zone (Fig. 2.1, Kelemen et al., 2004a; Paulick et al., 2006; Kelemen et al., 2007). A full spreading rate of 25 mm/year was determined (Fujiwara et al., 2003), corresponding to a slow-spreading ridge. The half-spreading rates (E and W) show little long-term asymmetry. This inspired Fujiwara et al. (2003) and later Escartin et al. (2003) to propose a model of shallow detachment faults to explain the geomorphologic and geologic situation around the Fifteen–Twenty Fracture zone. The major difference with respect to previously proposed models (amagmatic extension or melt-assisted extension; e.g. Tucholke et al., 1998; Dick et al., 2003) is the rooting of detachment faults in the shallow lithosphere, probably coinciding with the rheological boundary between the alteration (serpentinization) front and the unaltered lithosphere. Mostly ultrabasic rocks crop out in this area, covered by a thin sediment layer (Kelemen et al., 2004a; Kelemen et al., 2007). The mineralogical composition and evolution of the peridotites at the two drilling sites (1272A and 1274A) is considered to be different (Seyler et al., 2007; Godard et al., 2008). Site 1272A has less abundant clinopyroxene than Site 1274A and seems to reflect partial melting and melt extraction, while Site 1274A records in addition pervasive melt–rock interaction (Seyler et al., 2007; Godard et al., 2008).

35 miles south of the Fifteen–Twenty Fracture zone (44 580N 14 450W, Sudarikov and Roumiantsev, 2000), the Logatchev hydrothermal field is located on the rift flank. It was discovered during several Russian expeditions in the 90s. It is situated within steeply faulted blocks of ultramafic rocks, which experienced variable degrees of serpentinization (Sharapov and Simonov, 1991). Basalts and gabbros are commonly exposed around the vent sites (Escartin and Cannat, 1999; Kuhn et al., 2004; Schmidt et al., 2007). Recent expeditions studied the hydrothermal fluids in more detail. The latter contain 1.75 µg/g Li and 3.63 µg/g B at a temperature of 353°C and a pH of 3.3 (Douville et al., 2002; Schmidt et al., 2007).

Table 1
ODP sample names and modes

Working no.	Sample depth [m.b.s.f.]	ODP sample no.	Modes (%)					Modes serp min. (%)			
			Cpx	Opx	Ol	Spl	Serp	Ba	Pi	Cy	Aom
Leg 1272A											
OD 2	61.75	209-1272A-13R-1, 103.5-106.5	0	0	3	3	94	30	–	2	62
OD 6	76.53	209-1272A-16R-2, 6-8	0	0	1	2	97	40	7	3	47
OD 7	80.18	209-1272A-17R-1, 57-60	0	0	0	4	96	40	3	1	52
OD 11	89.92	209-1272A-19R-1, 60-64	0	0	0	1	99	55	4	2	38
OD 15	99.85	209-1272A-21R-1, 102-108	0	0	0	3	97	30	2	2	63
OD 18	110.19	209-1272A-23R-2, 22-25	0	0	0	1	99	39	2	2	56
OD 22	120.05	209-1272A-25R-2, 67-71	0	0	0	2	98	32	1	2	63
OD 26	125.08	209-1272A-26R-2, 66-72	0	18	10	2	70	40	–	5	25
OD 28	127.30	209-1272A-27R-1, 28-31.5	1	15	10	1	73	25	2	4	42
OD 29	129.42	209-1272A-27R-2, 90-95	0.5	10	18	1.5	70	30	2	1	37
Leg 1274A											
OD 32	0.89	209-1274A-1R-1, 88-92	3	27	13	5	52	35	–	2	15
OD 34	17.27	209-1274A-3R-1, 35-38	1	23	15	2	59	25	–	4	30
OD 38	27.54	209-1274A-5R-1, 123-125	1	25	14	2	58	30	–	3	25
OD 42	32.14	209-1274A-6R-2, 68-70	1	10	15	2	72	20	17	5	30
OD 48	69.79	209-1274A-14R-1, 76-82	1	30	15	3	51	25	–	3	23
OD 49	94.11	209-1274A-18R-1, 80-83	0	0	0	3	97	20	–	10	67
OD 52	146.69	209-1274A-27R-1, 56-61	1	15	15	5	64	26	–	3	35

Cpx, clinopyroxene; opx, orthopyroxene; ol, olivine; spl, spinel; serp, serpentine; ba, bastite; pi, picrolite; cy, chrysotile; and aom, after ol and matrix.

2.3. Site and sample characteristics

2.3.1. Site 1272A

Site 1272A was drilled at a water depth of 2560 m at the ridge (Fig. 2.1). The drilled material consists of ~55 m diabase in the upper part, and 75 m of harzburgite containing rare dunite in the lower part (Fig. 2.2; Kelemen et al., 2004a). The major mineral phase in the mantle rocks is lizardite, and a downhole decrease in serpentinization can be observed (Kelemen et al., 2004a). Modal mineralogy and petrographic features of the analyzed spinel harzburgites are summarized in Table 1 and Fig. 2.2.

The studied samples were collected from the lower part of the drill core, at depths between 61.75 and 129.42 m.b.s.f. (meters below sea floor) and are serpentinized spinel harzburgites (Fig. 2.2). Macroscopically, the samples have a dark green to whitish green color. Some white veins can be observed and a dark vein occurs in sample OD 11. In most samples, porphyroclastic orthopyroxene forms large (<1 cm) grains, which are surrounded by dark green serpentine. They are distributed irregularly in a homogeneous matrix of serpentine minerals.

The degree of serpentinization ranges from 70% to 99% and tends to decrease with increasing depth. Apart from serpentine minerals and orthopyroxene, the samples may contain variable proportions of olivine, clinopyroxene, spinel and magnetite (Table 1). Olivine, pyroxenes and spinel are 'primary' minerals related to mantle processes, while serpentine and magnetite are of secondary origin, related to serpentinization. Olivine forms isolated, large fragments within serpentine (Fig. 2.3.C). Orthopyroxene grains may show exsolution lamellae of clinopyroxene (Fig. 2.3.B). Clinopyroxene occurs as interstitial phase at orthopyroxene grain boundaries (Fig. 2.3.A). Magnetite forms euhedral grains and symplectites with spinel (Fig. 2.3.D).

The terminology of Wicks and Whittaker (1977) is used to describe the serpentine textures of the studied samples. We observe pseudomorphic textures after olivine and orthopyroxene, vein textures, as well as non-pseudomorphic textures. Bastite after orthopyroxene (in the following termed bastite; Fig. 2.3.A) is the most common type of pseudomorphic serpentine texture in the studies rocks. Often, pseudomorphs of clinopyroxene exsolution lamellae are preserved within bastite, as described by Viti et al. (2005). Serpentine pseudomorphing olivine in mesh and hourglass textures (O'Hanley, 1996) is also abundant (Fig. 2.3.C). The inner parts of mesh rims are often reddish brown to black. In bastite, the reddish-brown colors are attributed to the presence of brucite (Wicks and Whittaker, 1977). All samples

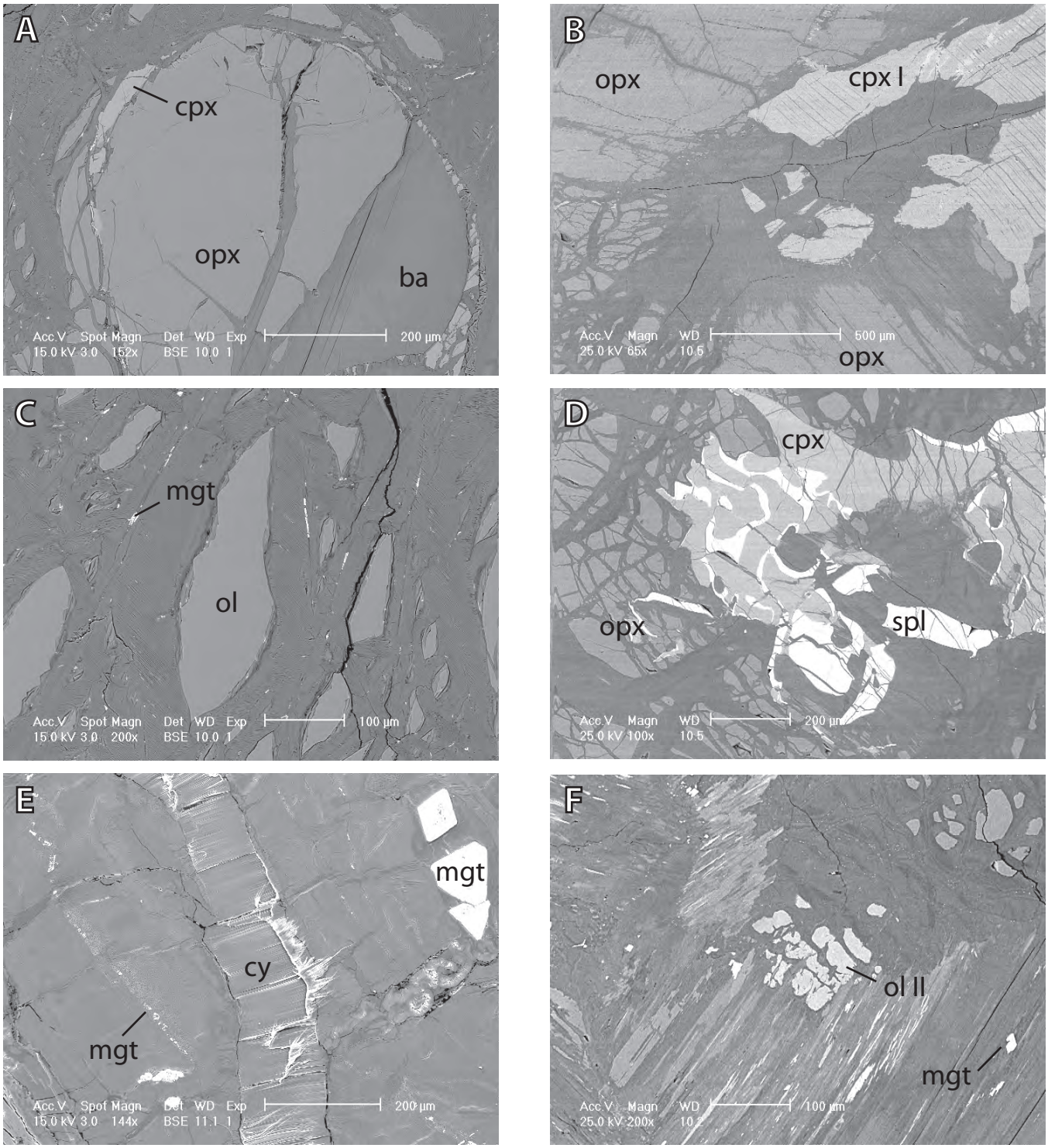

Fig. 2.3. Backscattered images of the different mineral phases from the ODP Sites 1272A (A, C, and D) and 1274A (B, D, and F); scale bars on the image. (A) Primary orthopyroxene (opx) with interstitial clinopyroxene (cpx) and bastite after opx (sample OD 29). (B) Primary clinopyroxene with exsolution lamellae of opx, now serpentinized (sample OD 32). (C) Relicts of primary olivine surrounded by serpentine in mesh textures. Magnetite (mgt) can be found in small picolite veins (sample OD 29). (D) Spinel (spl) with clinopyroxene (cpx) overgrowing orthopyroxene (sample OD 32). (E) Chrysotile vein (cy) in a completely serpentinized harzburgite (sample OD 2). (F) Cluster of magmatic olivine (ol II) in a serpentine matrix (sample OD 42).

display picrolite vein textures (lizardite according to Bach et al., 2004) and chrysotile asbestos cross-fiber veins (Fig. 2.3.E, F). While chrysotile veins crosscut bastites and are distributed randomly within the samples, lizardite picrolites are preferably found along mineral boundaries and natural weak zones (e.g. OD 28). Iowaite, as described by Bach et al. (2004), and brucite could not be identified directly using SEM or EMP. We found some magnetite strings (Fig. 2.3.E) in samples OD 2, OD 22 and OD 29.

2.3.2. Site 1274A

The drill hole is located on the western flank of a seamount at a water depth of 3940 m, in a weathered area north of the Fifteen–Twenty fracture zone (Fig. 2.1). Beneath 2 m of sediment, a total of 155.8 m of mantle rocks was drilled (Fig. 2.2). The site was divided into 3 units (Kelemen et al., 2004a). Unit I (top) and III (bottom) are serpentinized harzburgites, whereas unit II (middle) is interpreted as a 50-m fault gouge (mostly peridotite clasts within a mud matrix, all brecciated; Kelemen et al., 2004a).

The studied samples are from unit I, except OD 52 (unit III). They are all serpentinized spinel harzburgites. In unit I, serpentinization increases from the top to the base (Table 1). Macroscopically, the samples are all dark green with orthopyroxene blasts of up to 1 cm size. Rarely, whitish veins can be found. Samples OD 34 and OD 42 are crosscut by a large serpentine vein (up to 0.4 cm wide). The brownish color of some veins under the optical microscope could be related to brucite (Wicks and Whittaker, 1977).

The primary phases are olivine, orthopyroxene and clinopyroxene, all with the same textural characteristics as at Site 1272A. In addition, one large grain of primary clinopyroxene with exsolution lamellae of (serpentinized) orthopyroxene is preserved (sample OD 32, Fig. 2.3.B). Also, sample OD 42 contains a cluster of small olivine grains (Fig. 2.3.F) associated with chlorite and phlogopite. This assemblage most likely represents a micro-gabbroic pocket and is probably related to the magmatic vein crosscutting the drillcore between 31.95 and 32.45 m.b.s.f. (Kelemen et al., 2004b, core description). Such small gabbroic pockets were also identified in the MARK area (Niida, 1997). In the following, this olivine will be termed 'magmatic'. Spinel forms symplectites with clinopyroxene (Fig. 2.3.D), growing into orthopyroxene. This process preferably starts at boundaries between orthopyroxene grains and between orthopyroxene and olivine.

Serpentine mineral textures and vein types correspond to those described for Site 1272A. Magnetite is more abundant in the picrolite veins than within mesh structures. In bastite, relicts of orthopyroxene show serrate boundaries indicating ongoing serpentinization (Wicks and Whittaker, 1977). In OD 48 and OD 49, magnetite forms thick ribbons (Fig. 2.3.F), crosscutting through the entire thin section. They are interpreted as ancient picrolite veins. Sample OD 34 contains Ni-bearing sulfides. Rare iowaite ($Mg_4(OH)_8FeOCl_2 \cdot nH_2O$ [n= 1–4]) could be identified in sample OD 34, but was too small to be quantitatively analyzed.

The size of mineral grains in both sites is 50–500 µm for olivine, 50–1000 µm for orthopyroxene and 30–80 µm for clinopyroxene. Serpentine mineral grain size is much lower than the resolution of SEM, except for chrysotile veins (Fig. 2.3.E), where asbestos fibers are visible at SEM scale. They probably form late-stage fracture filling (Prichard, 1979).

2.4. Analytical techniques

The major element compositions of olivine, clinopyroxene, orthopyroxene, spinel, magnetite and serpentine minerals were determined by electron microprobe analysis (EPMA) using a JEOL JXA-8200 (University of Bern, and ETH Zürich, Switzerland), a Cameca SX-51 (University of Heidelberg, Germany) and a SX-100 (University of Freiburg, Germany), all equipped with wavelengthdispersive systems. An accelerating potential of 15 kV, a beam current of 20 nA and counting times of 30s for Si, Al, Mg and Na and 20s for the other elements were used. Minerals and synthetic glasses were used as standards. Samples were analyzed with a spot size of approximately 1 µm. For serpentine minerals, analyses with a 1 µm and a 15 µm spot size provided identical results within the analytical error of the microprobe (Table 2). Therefore, a 1 µm spot size was chosen to obtain a better spatial resolution.

Li, B and Be were analyzed in-situ on

Table 2
Results of electron microprobe analysis of serpentine with different spot size, all Fe considered as Fe^{2+}

OD32	sela	selb	se9a	se9b
SiO_2	40.51	41.49	39.26	39.37
TiO_2	0.02	0.00	0.00	0.00
Cr_2O_3	0.95	0.94	1.45	1.39
Al_2O_3	2.79	2.58	0.03	0.00
FeO	4.47	4.72	6.78	6.68
MnO	0.07	0.12	0.18	0.12
MgO	36.72	37.10	36.37	36.47
CaO	0.10	0.13	0.17	0.14
Na_2O	0.04	0.04	0.04	0.02
K_2O	0.02	0.02	0.01	0.00
H_2O	12.45	12.66	12.07	12.07
Cl	0.17	0.15	0.16	0.17
Total	98.30	99.96	96.51	96.44
F,Cl=O	0.04	0.03	0.04	0.04
Total	98.26	99.93	96.48	96.40
Cat	4.959	4.954	5.015	5.012
Spot size	1 μm	15 μm	1 μm	15 μm

Cat, total cations.

polished thin sections by Secondary Ion Mass Spectrometry (SIMS) using a modified Cameca IMS 3f ion microprobe at the Mineralogical Institute of Heidelberg, Germany. A 14.5 keV/20 nA ^{16}O primary beam with 30 μm diameter and acceleration to a nominal energy of 4.5 keV for the positive secondary ions was used. Secondary ^{7}Li, ^{9}Be, ^{11}B and ^{30}Si ions were collected applying the energy filtering method using an offset of 75 eV at a mass resolution of 1030 (m/Dm, 10%) and a nominal imaged field of 25 mm. Secondary ion intensities were normalized to the count rates of ^{30}Si and calibrated against the NIST SRM610 glass reference material using the concentrations (preferred averages) reported in Pearce et al. (1997); the accuracy is estimated to be <20% for Li and <10% for Be and B (Ottolini et al., 1993). Li, B and Be concentrations were quantified using the SiO_2 values of the corresponding EPMA analysis. One single analysis comprised 10 cycles for each isotope with integration times of 8s/cycle for Li, 16s/cycle for Be and B, and 2s/cycle for Si. The mass spectrometer's and the counting system's background of 0.02 ions/s where determined independently ('well known background'). The setup chosen and the background lead to a detection limit (critical value) of 1.4 ng/g (Li), 1.0 ng/g (Be) and 2.6 ng/g (B) (Currie, 1968; Marschall and Ludwig, 2004).

Due to the generally low concentration levels of Li, Be and B in mantle rocks, contamination during sample preparation and handling is always problematic, particularly for B (Shaw et al., 1988). Careful sample preparation is thus a necessary prerequisite for accurate analyses. The standard protocol established by Marschall and Ludwig (2004) was used to prepare the thin sections for this study at the Mineralogical Institute of Heidelberg. Carbon-coated samples were used for BSE investigation (textures) and electron microprobe analyses (major element composition of minerals; see further on). At the beginning of each SIMS analysis, a presputtering of 400s was applied to eliminate the potential rest of surface contamination. Additionally, the imaged field was set smaller than the primary beam diameter (applying field aperture #2, d= 750 μm) to suppress contaminating secondary ions from the crater edges (Benninghoven et al., 1987). Following the procedure described by Marschall and Ludwig (2004), the B contamination level is <2 ng/g. Li contamination is typically ~50 times less than for B, and Be does not show any sign of contamination. The area analyzed by SIMS has a diameter of ~12 μm (determined by the field aperture and the nominal imaged field), but all serpentine minerals have smaller grain size (<0.5 μm; Fig. 2.3). This means that one SIMS analysis corresponds to several grains of serpentine and in some cases to mixtures of serpentine and other minerals such as magnetite, brucite or small fluid inclusions. However, the fraction of non-serpentine minerals included

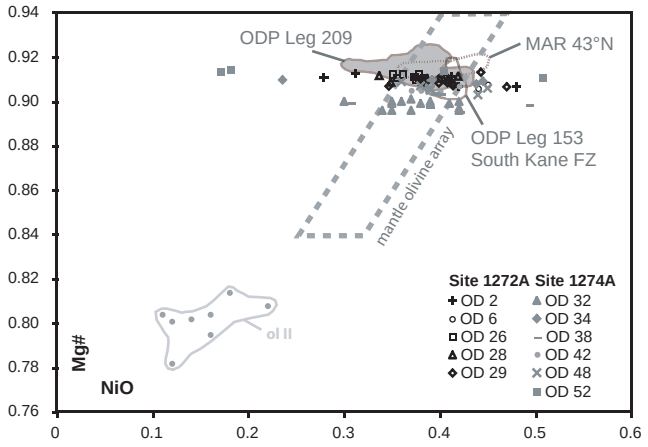

Fig. 2.4. NiO versus Mg#-diagram showing olivine compositions from ODP Leg 209 Sites 1272A and 1274A. Mantle olivine array after Takahashi et al. (1987). MAR 43°N after Shibata and Thompson (1986). ODP Leg 153 data after Ross and Elthon (1997); ODP Leg 209 data after Moll et al. (2007).

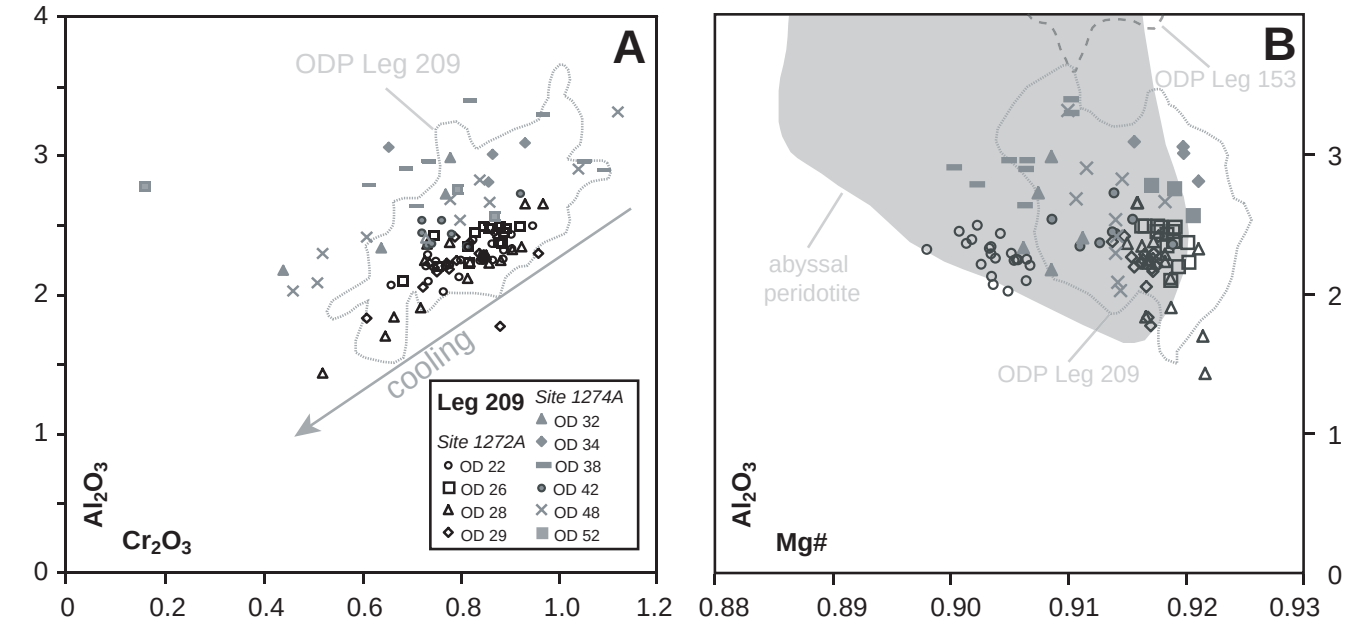

Fig. 2.5. (A) Al_2O_3 versus Cr_2O_3 diagram of orthopyroxene from ODP Leg 209, Sites 1272A and 1274A. (B) Mg# versus Al_2O_3 diagram. Abyssal peridotite field and ODP Leg 153 data after Ross and Elthon (1997). ODP Leg 209 data field after Seyler et al. (2007) and Moll et al. (2007).

in a SIMS analysis was small as can be depicted from the major element composition (Table 3). Whole rock concentrations of major elements and their oxides and some trace elements (H, B, and Cl) of 14 samples were determined using the prompt gamma activation analysis (PGAA) facility at the Budapest Research Reactor (Hungary). PGAA is especially useful for analyzing whole rock boron, chlorine and hydrogen concentrations. In contrast to other geoanalytical methods, sample preparation procedures are not needed, and hence contamination problems are eliminated (Anderson and Kasztovszky, 2004). Accuracy of trace element analyses by PGAA was checked by measurements of geological reference materials (Gméling et al., 2005) and of natural samples (Marschall et al., 2005). The spectra were evaluated with Hypermet-PC software; the element identification was performed using a prompt-gamma library (Révay et al., 2001). The H_2O content of the sample is determined by stoichiometry. Each sample (0.3–4.5 g) was hot-sealed in a fluorinated ethylene propylene (FEP) film (about 20 30 mm), which produces a negligible background. The analytical setup was described by Molnar (2004). All of the samples were thinner than 5 mm; thus the selfabsorption of neutrons and c-photons was negligible. The measurement time for each individual sample varied between 4500 and 10,000s (OD 26: 55'000s).

2.5. Results

2.5.1. Major and light element contents of minerals

Concentrations of major and light elements are given in Tables 3 and 4, respectively. Primary olivine is homogeneous with an average Mg# of 0.91 (Mg#= 100 Mg/ [Mg + Fe_{tot}], all iron assumed as divalent), and NiO contents of 0.4 wt% (Fig. 2.4). Magmatic olivine in sample OD 42 (Fig. 2.3.F) has a Mg# of 0.80 and NiO contents of 0.1–0.2 wt%. Average light element contents of primary olivine are 1.04 µg/g for Li, 0.022 µg/g for B, and below the critical value for Be. They are higher in magmatic olivine of sample OD 42 (Li 8.29 µg/g, B 0.54 µg/g and Be 9.8 ng/g). There is no core-to-rim variation in major and light elements for primary olivine; magmatic olivine is too small to detect zoning.

2.5.1.1. Pyroxenes

Orthopyroxene is homogeneous and not zoned, with an average Mg# of 0.91 (Table 3c). The Al_2O_3 and Cr_2O_3 contents are quite variable (1.4–2.3 wt% Al_2O_3 and 0.1– 1.1 wt% Cr_2O_3) and positively correlated (Fig. 2.5.A), with the exception of sample OD 52. Average light element contents of orthopyroxene are 0.7 µg/g Li, 0.011 µg/g B and below the critical value for Be. There is no core-torim variation in major and light elements for orthopyroxene

(profile in Table 4, OD22C3opp1–1 to 1–6, rim to core). Primary clinopyroxene in sample OD 32 is zoned. The rim is enriched in Mg and Si, depleted in Al and Cr compared to the core (Fig. 2.6). The rim composition of the primary clinopyroxene is similar to the composition of interstitial clinopyroxene (Fig. 2.6). The light element contents show no difference between rim and core. The average values are 1.5 µg/g for Li, 0.07 µg/g for B, and below critical value for Be. Interstitial clinopyroxene has Mg# between 0.91 and 0.95, CaO is 20–25 wt%, Na_2O 0.2 wt% and TiO_2 0.2wt%. Interstitial clinopyroxene has average light element contents of 2.05 µg/g Li, 0.89 µg/g B and 8.6 ng/g Be, higher than those of primary clinopyroxene.

2.5.1.2. Serpentine minerals

There is no systematic difference in the major and light element composition of serpentine minerals from different textures (see section 'Site and sample characteristics'). Serpentine minerals have SiO_2 between 39.1 and 42.0 wt% and an average FeO content of 4.3 wt%. NiO is below 0.44 wt%. Cr_2O_3 is below 0.81 wt%. Analyses within serpentine matrix give lower oxide totals than analyses of other serpentine textures, but calculated cations normalized to nine oxygens are conform with serpentine stoichiometry. The light element content of the serpentine minerals is highly variable, ranging from 0.002 to 9.37 µg/g Li, and from 0.09 to 138 µg/g B. The results of micro-Raman analyses performed on some of the spots analyzed for light element concentrations by SIMS showed that in cases where Li concentrations exceed 1 µg/g, serpentine (lizardite) is mixed with orthopyroxene (Pelletier, 2008). The average light element abundances in serpentine of our samples are 0.67 µg/g Li, 48.29 µg/g B, and 4.5 ng/g Be (Table 4).

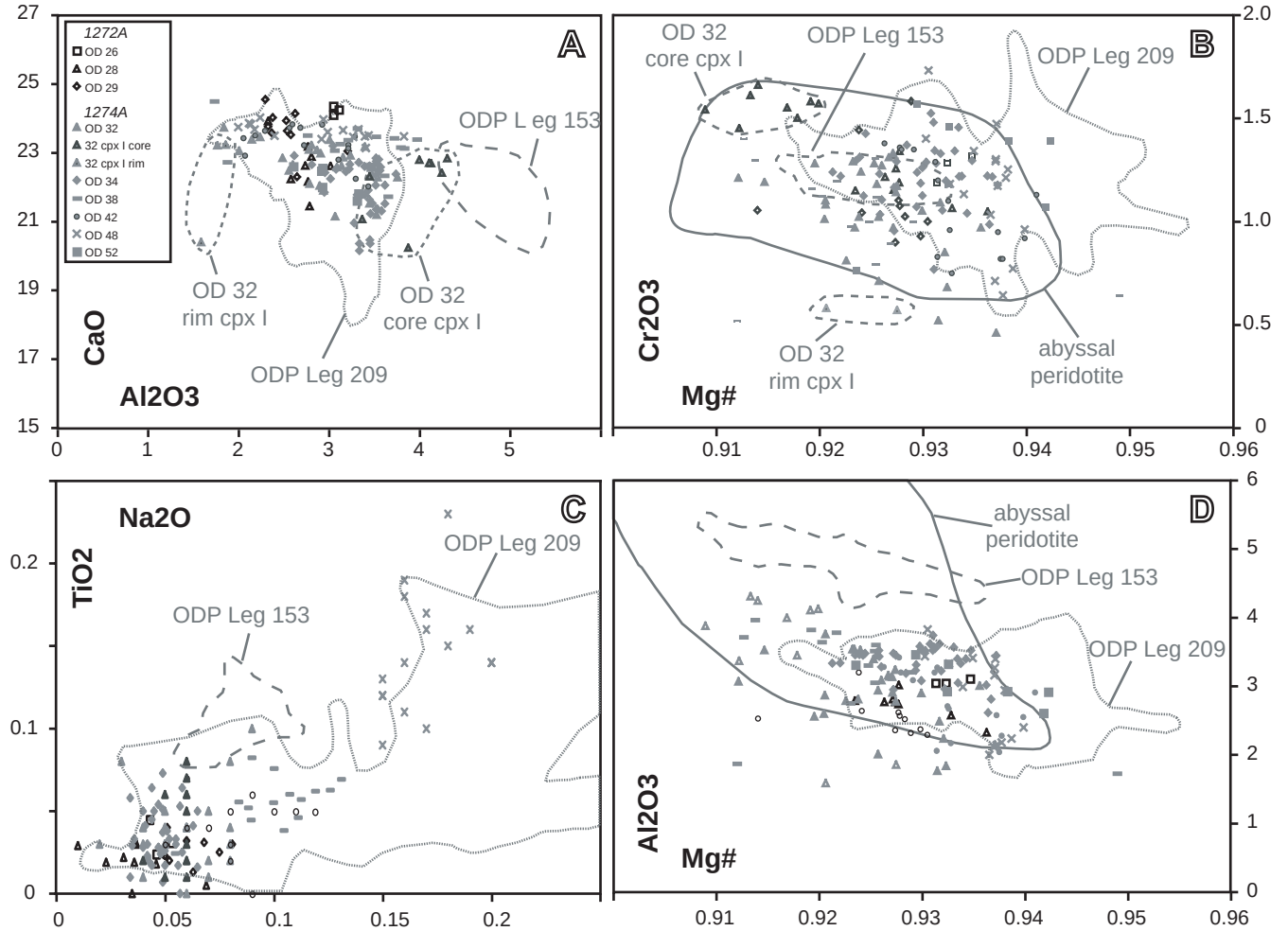

Fig. 2.6. Major element composition of clinopyroxene, core and rim of primary clinopyroxene (cpxI) are indicated as fields delimited by dashed lines. (A) Al_2O_3 versus CaO diagram, with data from ODP Leg 153 for comparison (MARK area). (B) Cr2O3 versus Mg# diagram. (C) TiO_2 versus Na_2O diagram. (D) Al_2O_3 versus Mg# diagram. Abyssal peridotites field after Ross and Elthon (1997), and references therein. ODP Leg 209 field after Seyler et al. (2007) and Moll et al. (2007).

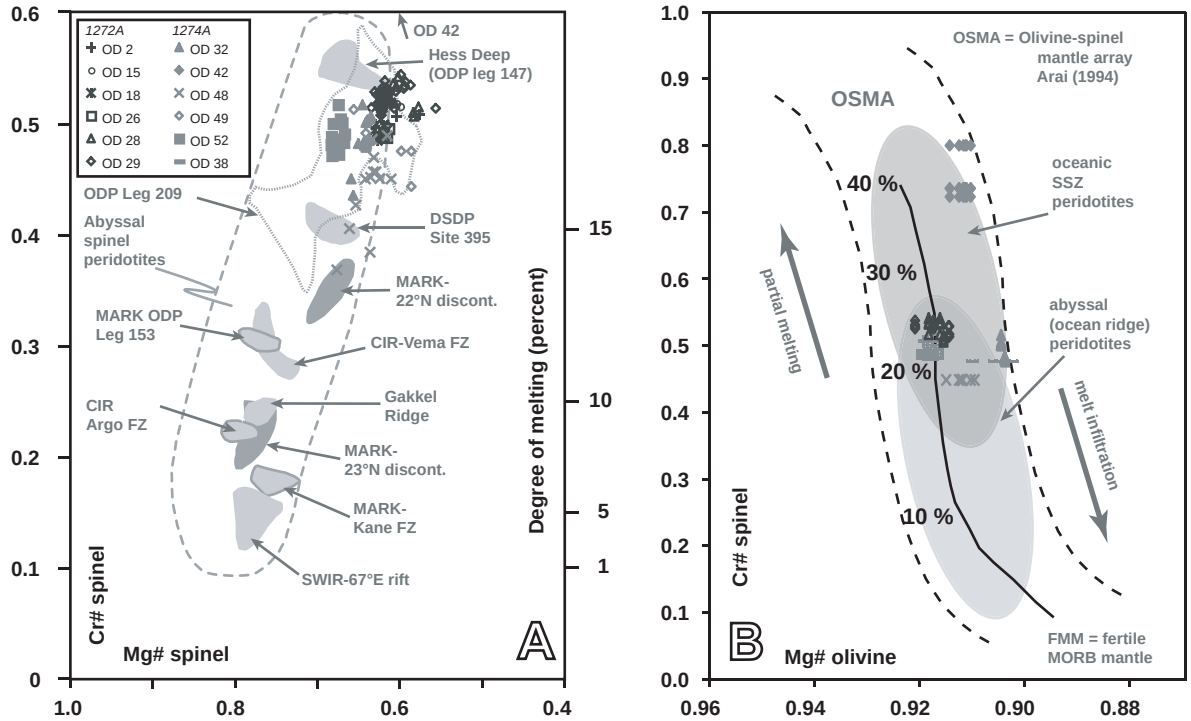

Fig. 2.7. (A) Cr# (=Cr/Cr + Al) versus Mg# (=Mg/(Mg + Fe^{2+}_{tot}) diagram for spinel, modified after Hellebrand et al. (2002), showing the relative depletion of the mantle at ODP Leg 209. ODP Leg 209 field after Seyler et al. (2007) and Moll et al. (2007). (B) Cr# in spinel versus Mg# in olivine diagram, modified after Pelletier (2008) and references therein. OSMA, Olivine–spinel mantle array (after Arai, 1994); FMM, fertile MORB mantle (after Arai, 1994); and SSZ, supra subduction zone.

2.5.1.3. Accessory minerals

Spinel has Cr# (Cr#= Cr/[Cr + Al]) between 0.37 and 0.54 and Mg# from 0.55 to 0.68 (Fig. 2.7). In sample OD 42, spinel has higher Cr# (0.70) and lower Mg# (0.29). TiO2 values are below 0.2 wt%. Fe2O3 in magnetite varies from 61.2 to 67.9 wt%. Small grain size led to some SiO2 contamination. Chlorite has Mg# 0.92 and Cr2O3 contents of <1.2 wt%. The light element contents of the two mineral grains analyzed are 0.40 µg/g and 0.53 µg/g for Li, 44.9 ng/g and 61.3 ng/g for Be and 0.97 µg/g and 0.85 µg/g for B. The mica (coexisting with magmatic olivine) in OD 42 is a phlogopite with Mg# of 0.91. 5.2. Light element, H_2O and Cl contents of whole rock samples

As only little material was available, only limited whole rock analysis for B, H and Cl by PGAA could be performed (Table 5, Fig. 2.8). Li concentrations in some samples are available from isotope dilution (data from Vils et al., 2008). PGAA measures of B whole rock contents range from 50.3 µg/g to 65 µg/g at Site 1272A and from 10.4 µg/g to 38.5 µg/g at Site 1274A. H_2O contents of whole rock samples determined by PGAA vary between 13.0 and 16.4wt% at Site 1272A, and from 10.9 to 15.0wt% at Site 1274A. Cl whole rock contents determined by PGAA range from 6032 to 10,114 µg/g at Site 1272A and from 1061 to 3566 µg/g at Site 1274A (Table 5). Li content of whole rock determined by isotope dilution varies between 0.07 and 0.81 µg/g at Site 1272A, and between 0.28 and 3.37 µg/g at Site 1274A (data from Vils et al., 2008).

Calculated Li and B contents of whole rock samples based on mineral modes, in-situ measurements on minerals (this study) and spinel data from Ottolini et al. (2004; 0.51 µg/g for Li and 0.0035 µg/g for B), show no systematic deviation from measured values towards higher or lower values. Seventy percent of all analyzed samples are within an error of 20% (B) and 50% for Li, respectively. The low abundance of Li-bearing phases in ODP Leg 209 (only clinopyroxene) leads to a large uncertainty when calculating whole rock Li content. Whole rock samples were not analyzed for Be. Due to the low abundance of this element found during the in-situ mineral analyses, we conclude that there is negligible Be in the serpentinized oceanic mantle. The down-hole variation of B, Li, Cl and H_2O is illustrated in Fig. 2.8. At Site 1274, B, Cl and H_2O contents are generally higher at depth, although there is no clear correlation. The Li content remains more or less constant with

Table 3
Representative analyses of major phases

3a																	
Mineral	Olivine (normalized to four oxygens)																
Sample	OD 2 o2c6ol3	OD 6 o6c2sp4	OD 26 o26c3ol4c	OD 28 o28c3ol2r	OD 29 o29c5ol3c	OD 38 dp38ol1	OD 32 dp32ol1	OD 32 dp32ol4	OD 34 OD34ol3	OD 34 OD34ol5	OD 42 42ol1	OD 42 42ol4	OD 48 48ol4	OD 48 48ol5	OD 52 oD52ol2	OD 52 OD52ol3	OD 52 odp52ol4
SiO_2	41.15	41.60	39.99	40.83	40.68	41.47	41.14	41.16	41.15	40.91	40.66	40.74	40.72	40.75	41.06	40.61	40.73
TiO_2	<0.01	0.01	<0.01	<0.01	0.01	<0.01	<0.01	<0.01	<0.01	0.01	<0.01	<0.01	0.01	0.02	<0.01	<0.01	<0.01
Cr_2O_3	0.07	0.02	0.01	<0.01	0.01	0.03	0.05	0.03	<0.01	0.02	<0.01	0.01	<0.01	<0.01	<0.01	<0.01	0.04
Al_2O_3	0.03	0.04	<0.01	0.01	<0.01	0.01	0.02	0.02	<0.01	0.02	0.04	<0.01	<0.01	0.02	0.02	<0.01	0.01
FeO	8.21	8.59	8.34	8.958	8.33	8.93	9.30	9.40	8.44	8.33	8.75	8.78	8.95	8.44	8.06	7.92	8.14
MnO	0.10	0.17	0.12	0.10	0.12	0.11	0.21	0.09	0.13	0.11	0.14	0.14	0.11	0.13	0.09	0.15	0.03
NiO	0.28	0.4	0.36	0.35	0.41	0.39	0.35	0.39	0.44	0.45	0.40	0.37	0.39	0.36	0.18	0.40	0.51
MgO	50.59	50.55	51.95	50.26	49.63	50.26	50.82	50.88	50.15	50.46	50.38	50.18	50.66	50.61	50.30	50.56	50.26
CaO	0.10	0.06	0.04	0.05	0.05	0.08	0.08	0.10	0.06	0.05	0.03	0.03	0.02	0.05	0.03	0.03	0.04
Total	100.54	101.49	100.83	100.57	99.28	101.29	101.97	102.06	100.37	100.36	100.45	100.26	100.87	100.37	99.73	99.68	99.76
Si	0.997	1.000	0.970	0.991	0.999	1.000	0.989	0.988	1.000	0.994	0.990	0.993	0.988	0.991	1.001	0.992	0.995
Ti	0.000	0.000	0.000	0.000	0.000	0.000	0.000	0.000	0.000	0.000	0.000	0.000	0.000	0.000	0.000	0.000	0.000
Cr	0.001	0.000	0.000	0.000	0.000	0.001	0.001	0.001	0.000	0.000	0.000	0.000	0.000	0.000	0.000	0.000	0.001
Al	0.001	0.001	0.000	0.000	0.000	0.000	0.001	0.001	0.000	0.000	0.001	0.000	0.000	0.001	0.001	0.000	0.000
Fe	0.166	0.173	0.169	0.174	0.171	0.180	0.187	0.189	0.171	0.169	0.178	0.179	0.182	0.172	0.164	0.162	0.166
Mn	0.002	0.003	0.003	0.002	0.002	0.002	0.004	0.002	0.003	0.002	0.003	0.003	0.002	0.003	0.002	0.003	0.001
Ni	0.005	0.009	0.007	0.007	0.008	0.008	0.007	0.008	0.009	0.009	0.008	0.007	0.008	0.007	0.004	0.008	0.010
Mg	1.827	1.811	1.879	1.833	1.817	1.806	1.820	1.821	1.816	1.828	1.828	1.823	1.832	1.834	1.827	1.841	1.830
Ca	0.003	0.002	0.001	0.001	0.001	0.002	0.002	0.003	0.001	0.001	0.001	0.001	0.001	0.001	0.001	0.001	0.001
Cat	3.002	2.999	3.030	3.009	3.000	3.000	3.011	3.011	3.000	3.005	3.011	3.007	3.012	3.009	2.999	3.008	3.005
Mg#	0.917	0.913	0.917	0.913	0.914	0.909	0.907	0.906	0.914	0.915	0.911	0.911	0.910	0.914	0.918	0.919	0.917

Table 3 continued at the end of chapter 2

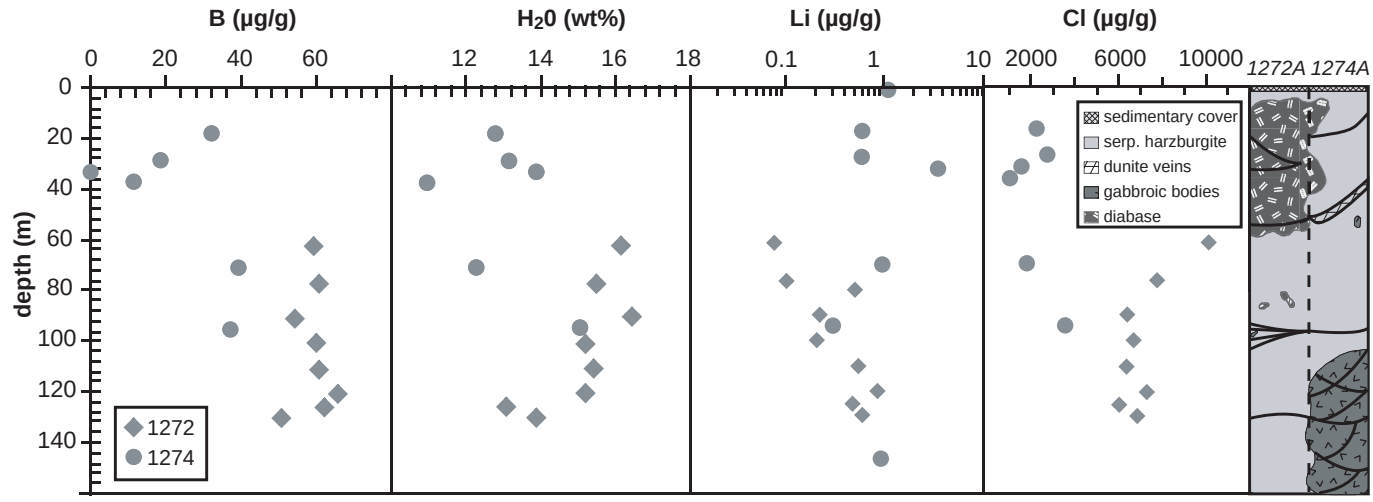

Fig. 2.8. Down hole distribution of B, Li, H_2O, Cl contents of whole rock analyzes and a simplified stratigraphic log (modified after Bach et al., 2004). Black lines in the log: deformation zones. ODP Leg 209 Site 1272A (grey diamonds) and Site 1274A (grey dots). B, H_2O and Cl data are listed in Table 5, Li data from isotope dilution (Vils et al., 2008).

depth. At Site 1272A, H_2O tends to lower values with depth, B may display a similar trend, while Li contents clearly increase with depth. The Cl whole rock content seems to decrease with depth from 10'000 to 6'000 µg/g and then remains roughly constant.

2.6. Discussion

In the following, we will discuss the nature of the protoliths, including chemical and textural evidence of melt infiltration. Then, we will examine the impact of serpentinization on the B and Li contents of whole rock samples and present a model of the light element budget of the oceanic lithosphere.

2.6.1. Light element contents of primary minerals

Primary olivine of both ODP Sites shows Mg# between 0.90 and 0.92 (except sample OD 42), which is within the range of mantle olivine. This variation does not correlate with NiO contents, the latter varying at any given Mg. The Cr–Al systematics of orthopyroxene (Fig. 2.5.B) and the Ca–Al–Cr systematics of clinopyroxene (Fig. 2.5.A) are in line with those of other abyssal peridotites (e.g. Shibata and Thompson, 1986; Ross and Elthon, 1997). Spinel compositions are also concordant with values for abyssal peridotites (Fig. 2.7), except for a weak shift towards lower Mg#. This trend could be explained by partial diffusive re-equilibration to magnetite formed during serpentinization or upon cooling after melt infiltration (see section 'Protoliths and melt refertilization'). Light element contents of olivine and orthopyroxene (Table 4, Fig. 2.9) are close to the depleted mantle values reported by Salters and Stracke (2004). There is no trend for Li and B towards or away from seawater composition (4.6 µg/g B, 0.18 µg/g Li; Quinby-Hunt and Turekian, 1983; Jean-Baptise et al., 1991; Schmidt et al., 2007). The B and Li contents obtained in this study are also similar to those of olivine and orthopyroxene from the Pindos ophiolite, Greece (Pelletier, 2008). In contrast, B and Li in clinopyroxene show a wider range of values that trend towards the MORB field (Fig. 2.9, Ryan and Langmuir, 1987; Ryan and Langmuir, 1993), confirming that clinopyroxene probably crystallized later than primary olivine, orthopyroxene and spinel (see below). In summary, major, minor and light element composition of pyroxenes, spinel and the Mg# of olivine were not changed by serpentinization and can be used to constrain the peridotitic protolith of the serpentinites.

2.6.2. Protoliths and melt refertilization

It is commonly accepted that the spectrum of mantle rock samples at mid-ocean ridges has been produced by partial melting of the upper mantle at spinel-facies conditions, followed by removal of basaltic melt (e.g. Hamlyn and Bonatti, 1980; Dick and Bullen, 1984). The degree of partial melting can be deduced from the Cr# of spinel (Hellebrand et al., 2001), and spinel compositions from mantle rocks along the MAR suggest partial melting between 7% and 20% (Fig. 2.7.A).

Table 4
Representative light element contents of minerals from the two drill sites

Site 1272A	Li		Be		B	
	µg g^{-1}	1σ	ng g^{-1}	1σ	µg g^{-1}	1σ
Olivine						
OD29Cloll	0.98	0.05	0.000	0.62	0.00	0.00
OD29Clol2	0.90	0.05	b.d.l.	—	0.00	0.01
OD26C3ol2	0.67	0.05	0.75	1.31	0.00	0.01
OD26C3ol3	0.68	0.08	0.75	1.31	0.01	0.01
OD28Cloll	0.52	0.06	0.56	0.91	0.00	0.01
OD28C3ol3	0.61	0.04	2.54	5.35	0.01	0.01
OD6C2oll	1.04	0.04	b.d.l.	—	0.01	0.01
OD2Cloll	0.89	0.05	0.98	2.08	0.03	0.02
Orthopyroxene						
OD22C4op2	0.67	0.03	0.22	0.23	0.02	0.01
OD22C3oppl-l	0.72	0.07	0.80	1.42	0.00	0.01
OD22C3opp1-2	0.69	0.13	1.03	1.33	0.01	0.01
OD22C3opp1-3	0.56	0.06	0.64	1.25	0.01	0.01
OD22C3opp1-4	0.80	0.37	1.93	4.00	0.01	0.01
OD22C3opp1-5	0.54	0.05	0.63	0.90	0.00	0.00
OD22C3opp1-6	0.78	0.16	0.13	0.42	0.00	0.00
OD29C5op1	0.76	0.04	1.19	1.17	0.02	0.01
OD26C4op2	0.95	0.03	0.16	0.49	0.01	0.01
OD26C3op3	0.72	0.04	0.16	0.50	0.00	0.00
OD26C3op2	0.80	0.07	0.50	0.81	0.00	0.01
OD28C2op6	0.61	0.03	0.99	1.39	0.01	0.01
OD28C1op3	1.00	0.04	0.50	0.81	0.16	0.02
Clinopyroxene						
OD29C2cp4	5.41	0.23	0.16	0.50	0.93	0.13
OD29C2cp5	4.39	0.20	0.67	1.17	2.39	0.19
OD29C2cp1	2.69	0.04	0.22	0.29	0.74	0.7
OD28C2cp2	1.56	0.07	0.91	1.17	0.041	0.01
OD28Clcp5	2.14	0.10	b.d.l.	—	0.04	0.01
Serpentine minerals						
OD7C9srlO	0.05	0.01	0.25	0.53	39.29	0.55
OD7C5sr11	0.11	0.01	0.70	1.22	14.79	0.29
OD26C3sr2	0.44	0.02	1.29	1.52	58.10	2.90
OD28C2sr15	2.09	0.03	0.30	0.70	71.38	2.33
OD28C1sr8	1.80	0.06	0.49	0.79	138.20	3.16
OD11C5sr11	0.07	0.01	0.27	0.57	37.94	0.02
OD6C1sr4	0.01	0.01	0.70	1.23	38.94	1.13
OD7C3sr8	0.22	0.2	0.27	0.57	84.57	2.16
OD11C2sr5	0.19	0.02	0.16	0.52	52.77	1.95
OD6C3sr4	0.00	0.00	0.38	0.62	31.56	0.56
OD7C1sr14	0.02	0.01	0.22	0.46	24.14	0.52
OD7C3sr1	0.22	0.03	0.13	0.42	80.50	2.31
OD11C5sr9	0.03	0.01	0.39	0.63	12.92	0.34
OD22C3srl	0.01	0.00	0.43	0.95	20.0	1.03
OD2C2srl0	0.03	0.01	0.77	0.95	37.08	0.76
OD2C2sr31	0.39	0.04	0.38	0.76	72.42	3.41
OD2C3sr7	0.07	0.02	0.53	0.81	13.76	0.53
OD2C5srll	0.06	0.01	b.d.l.	—	65.10	0.95
OD15C2sr7	0.19	0.01	0.34	0.67	76.13	0.84
OD15C1sr6	0.00	0.00	0.18	0.55	35.00	0.68
OD15C1sr10	0.27	0.04	0.20	0.61	92.51	1.17
OD15C3sr4	0.18	0.03	0.20	0.59	27.72	0.31
OD15C3srll	1.61	0.09	b.d.l.	—	101.53	2.09
OD18C2sr8	1.50	0.16	b.d.l.	—	83.73	1.59
ODP18C2sr5	0.62	0.04	0.87	1.06	88.89	2.84
OD6C1sr1	0.03	0.27	0.32	2.11	37.58	0.034
OD6C1sr5	0.21	0.6	0.54	4.1	74.1	0.045
OD6C1sr6	0.07	0.16	0.31	2.11	33.54	0.016

Table 4 (*continued*)

Site 1274A	Li		Be		B	
	µg g^{-1}	1σ	ng g^{-1}	1σ	µg g^{-1}	1σ
Olivine						
OD32oli-1	0.86	0.03	0.42	0.83	0.00	0.00
OD34oli2	0.81	0.04	0.49	0.62	0.01	0.00
OD34oli3	1.15	0.04	0.00	0.00	0.02	0.01
OD38ol-1	0.85	0.04	0.22	0.44	0.01	0.00
OD38ol-4	1.02	0.04	0.22	0.43	0.02	0.01
OD42oli-1	1.30	0.04	0.48	0.49	0.00	0.00
OD42oli-4	1.04	0.02	0.61	0.68	0.01	0.00
OLII-42oli-5	8.29	0.09	9.87	2.92	0.55	0.04
OD48oli-2	0.94	0.02	0.60	0.92	0.04	0.02
OD52ol1	0.88	0.03	0.56	0.71	0.00	0.00
OD52olb1	0.76	0.03	0.29	0.55	0.01	0.00
Orthopyroxene						
OD52opxb2	0.61	0.02	3.64	1.57	0.08	0.02
OD52opxb3	0.65	0.03	2.76	1.43	0.01	0.00
OD34opxb1	0.60	0.01	0.43	0.54	0.01	0.00
OD34opxb2	0.48	0.03	0.90	0.95	0.01	0.01
OD34opxc1	0.67	0.04	0.42	0.53	0.01	0.00
OD38opx-1	0.83	0.03	0.94	0.84	0.01	0.01
OD48opx-3	0.39	0.02	0.25	0.34	0.01	0.00
OD32opxI-1	0.61	0.02	0.55	0.56	0.01	0.00
Clinopyroxene						
OD32cpxI-l	1.56	0.05	0.50	0.71	0.05	0.01
OD32cpxI-2	1.42	0.07	0.22	0.44	0.10	0.02
OD34cpxcl	2.80	0.08	1.30	1.51	0.01	0.01
OD34cpxc3	0.45	0.02	0.83	0.65	0.01	0.01
OD38cpx-1	1.56	0.05	0.75	0.77	0.03	0.01
OD38cpx-2	1.70	0.04	1.38	1.98	0.81	0.06
OD42cpx-4	2.02	0.05	67.38	7.29	0.12	0.03
OD48cpx-4	1.29	0.03	0.96	0.52	1.88	0.05
OD52cpx3	1.51	0.06	5.43	2.06	0.01	0.01
Serpentine minerals						
OD32ba-2	0.59	0.02	0.69	0.85	9.53	0.27
OD34ba3	9.38	0.16	0.46	0.58	58.10	0.81
OD42ba-3	0.90	0.02	15.72	2.95	1.46	0.11
OD48ba-1	2.08	0.26	0.65	0.58	63.04	3.80
OD49ba-1	0.19	0.01	0.26	0.34	50.21	0.39
OD52ba3	0.43	0.02	6.13	2.30	69.57	0.61
OD38ba-3	0.19	0.02	0.39	0.79	21.64	0.17
OD38ba-5	1.23	0.05	0.21	0.41	40.58	0.51
OD42se-1	0.05	0.00	1.93	0.82	4.28	0.20
OD42ser-4	0.20	0.02	3.44	0.0	0.09	0.02
OD38ser-3	0.10	0.01	0.60	0.61	11.65	0.13
OD38ser-4	0.12	0.01	b.d.l.	—	3.81	0.15
OD32sol-2	0.09	0.01	b.d.l.	—	0.44	0.12
OD48ser-l	0.08	0.01	0.12	0.25	9.96	0.15
OD48sv-2	0.64	0.02	2.21	1.82	14.02	0.24
OD52sev2	0.09	0.01	0.00	0.00	24.45	0.22
OD52sev4	0.13	0.02	0.90	0.94	40.39	0.47
OD32serol-1	0.12	0.01	0.35	0.46	2.85	0.56
Chrysotile vein						
OD32chry-2	0.37	0.03	0.96	0.86	15.54	0.24
OD34chry2	0.29	0.02	0.24	0.45	20.08	0.36
OD42chry-1	0.11	0.01	0.88	0.54	4.04	0.11
OD48chry-l	0.14	0.02	0.51	1.02	24.10	0.91
OD49chry-2	0.08	0.01	1.85	1.68	19.33	1.42
OD52chry2	0.07	0.01	0.64	0.62	26.04	0.14
OD52chry4	0.07	0.01	0.45	0.57	26.25	0.27

1σ showed as example of measurement errors (b.d.l., below dedection limit; OD2c29cp1, sample OD 2; circle 2 cpx grain 4). Detection limits are: 1.4 ng/g (Li), 1.0 ng/g (Be), 7.5 ng/g (B).

Complete SIMS-data set can be found at the end of this chapter

Spinel in the studied samples from ODP Leg 209 is among the most depleted of all abyssal peridotites, indicating partial melting exceeding 20% (Fig. 2.7.A; see also Godard et al., 2008). A similar conclusion can be drawn on the degree of partial melting when considering the relation between Mg# of olivine and Cr# of spinel (Fig. 2.7.B). Based on mineral compositions from Site 1274A, Seyler et al. (2007) explain this high degree of depletion with a two-stage partial melting/ melt–rock reaction history, with an early melting in the garnet stability field.

In the studied samples, there is little textural, but widespread chemical evidence that the peridotite at both studied sites was infiltrated by mafic melts prior to serpentinization. Interstitial clinopyroxene forms textures with primary minerals (now pseudomorphosed by serpentine; Fig. 2.3.A) that strongly resemble textures of melt pockets and primary minerals obtained with mantle rocks during deformation experiments (e.g. Bussod and Christie, 1991; Kohlstedt and Zimmerman, 1996; de Kloe et al., 2000). Seyler et al. (2001, 2007) interpreted similar clinopyroxene as left over from an interstitial melt. We thus interpret the interstitial clinopyroxene as crystallized from a melt, as described for ophiolites (e.g. Dijkstra et al., 2001; Müntener and Piccardo, 2003; Müntener et al., 2004).

Most of the clinopyroxene grains measured in this study show no TiO_2 enrichment and plot within the abyssal peridotites field (Fig. 2.6). In contrast, sample OD 42 shows a trend towards melt enrichment, while the samples OD 38 and OD 48 show pronounced signatures of TiO_2 enrichment. The major element compositions of clinopyroxene obtained in this study (Figs. 2.4–2.7) are consistent with the earlier microprobe data from ODP Leg 209 Site 1274A (Seyler et al., 2007; Moll et al., 2007).

The B and Li contents of interstitial clinopyroxene are in line with the hypothesis that these grains crystallized from an infiltrating melt. Compared to normal mantle clinopyroxene, interstitial clinopyroxene is variably enriched in B and Li, with a trend towards the MORB field (Fig. 2.9). According to Seitz and Woodland (2000), Li enrichment in clinopyroxene compared to olivine and orthopyroxene can be related to metasomatism by mafic silicate melts or hydrous fluids. The preferential incorporation of Li in clinopyroxene during impregnation of peridotite by mafic melt was also reported by Eggins et al. (1998), McDade et al. (2003), Ottolini et al. (2004), Woodland et al. (2004) and Pelletier (2008).

An alternative explanation for the preferential enrichment of Li would be fractionation upon cooling. Coogan et al. (2005) performed experiments on Li diffusion in clinopyroxene

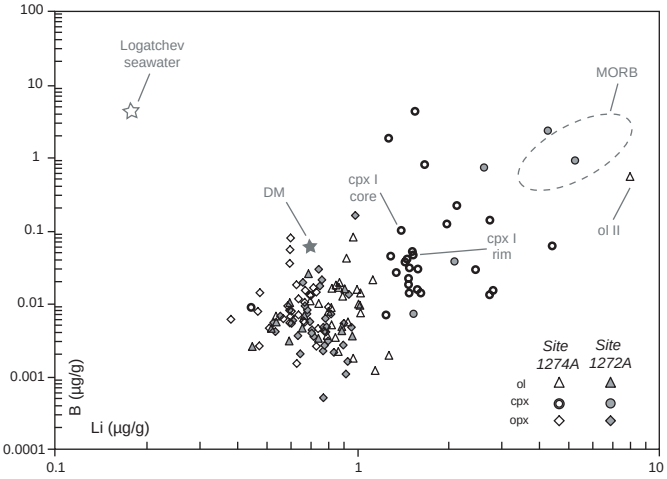

Fig. 2.9. Light element data obtained by SIMS analysis of primary minerals from ODP Leg 209 Sites 1272A and 1274A. Cpx I, primary cpx (OD 32); ol II, magmatic olivine. (OD42), Depleted mantle value after Salters and Stracke (2004), errors on these values are 8% for Li and 91% for B. Seawater value after Schmidt et al. (2007), MORB-field after Ryan and Langmuir (1987); Ryan and Langmuir (1993).

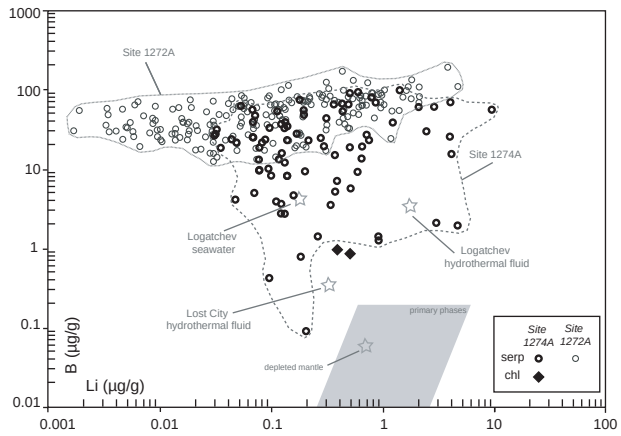

Fig. 2.10. Light element data of serpentine minerals obtained by SIMS-analysis of secondary minerals from ODP Leg 209 Site 1272A and 1274A. Depleted mantle value after Salters and Stracke (2004). Seawater and hydrothermal fluid value after Schmidt et al. (2007), Lost City data (Boschi, 2006).

at 800–1000°C and observed that Li diffused into clinopyroxene within hours. Jeffcoate et al. (2007) also suggested higher diffusivity of Li in clinopyroxene compared to olivine for phenocrysts from Hawaiian basalts. In the studied samples, however, we observe that olivine and orthopyroxene show Li abundances typical of minerals from the depleted mantle (Fig. 2.9), while clinopyroxene is enriched in Li. Inter-mineral diffusive re-equilibration would have depleted olivine and orthopyroxene in Li. Also, the only primary clinopyroxene grain that could be analyzed shows no zoning in Li, which could support the hypothesis of fractionation upon cooling. We therefore conclude that the principal process controlling Li enrichment in clinopyroxene is melt infiltration.

2.6.3. The impact of serpentinization

As shown above, serpentinization had almost no impact on the composition of primary phases, but it modified the whole rock composition, in particular B contents, by formation of serpentine. Fig. 2.10 and Table 4 reveal that B contents of serpentine are much higher than those of primary minerals and than values for the depleted mantle. Most serpentine grains show B abundances between 10 and 100 µg/g. The variability of B abundances in serpentine is higher at Site 1274A (on average less serpentinized) than at Site 1272A (almost completely serpentinized), the latter showing generally higher absolute values (Fig. 2.10). There is no simple positive correlation between the degree of serpentinization and B whole rock contents (Fig. 2.8). However, the variability of B abundances in whole rock samples is higher at Site 1274A than at Site 1272A, the latter showing generally higher values (Fig. 2.11). A similar conclusion can be drawn from sulfur and from oxygen isotopes (Alt et al., 2007). At site 1274A, more primary sulfide minerals are preserved (e.g. pentlandite, chalcopyrite, bornite) and oxygen isotopic composition is within the range for depleted mantle (Alt et al., 2007). At Site 1272A, primary sulfides are almost completely transformed to awaruite and heazlewoodite, testifying to desulfurization under reducing conditions due to serpentinization (Bach et al., 2004), and $\delta^{18}O$ values are enriched, pointing to more extensive interaction with seawater or a seawater-derived fluid than at site 1274A (Alt et al., 2007).

The positive correlation of B, Cl and H_2O implies that serpentinzation is the main process for B and Cl enrichment in ultramafic rocks. Cl contents correspond to average values for serpentinized mantle samples (Barnes and Sharp, 2006; Bonifacie et al., 2007), and show trends similar to H_2O.

Literature data confirm that serpentinization increases the B contents of oceanic mantle rocks (e.g. Bonatti et al., 1984; Thompson and Melson, 1970). Serpentinization at oceanic ridges is commonly triggered by heated seawater that cycles through the crust and parts of the lithospheric mantle and slowly alters the oceanic plate. As B is abundant in seawater (4.6 µg/g, Quinby-Hunt and Turekian, 1983; Jean-Baptise et al., 1991) compared to depleted mantle (0.04 µg/g, Table 6), seawater–peridotite interaction should enrich the mantle in B. Various studies on dredged abyssal peridotites have confirmed this enrichment in serpentinite (Thompson and Melson, 1970; Bonatti et al., 1984; Spivack and Edmond, 1987; Boschi et al., 2008), and studies on alpine serpentinite have demonstrated a large variability of B contents in serpentine (Scambelluri et al., 2004; Pelletier et al., 2008).

Experiments on chemical exchange between seawater and peridotite showed that at high temperature B is probably not incorporated into the rock but remains in solution (Seyfried and Dibble, 1980). However, during slow cooling below 300°C, a B loss from the fluid was observed (partially driven by a change in pH). This implies that the major uptake of B by peridotites takes place at temperatures below 300°C (Seyfried and Dibble, 1980).

The variation of B concentrations in the studied samples could also be due to changes in pH and temperature of the reacting fluid. For incorporating B in silicates, tetrahedrally coordinated boron, $B(OH)_4$, is required (Spivack and Edmond, 1987). Palmer and Swihart (1996) demonstrated the pH dependency of $B(OH)_4$ availability in fluids. Their results show that only at pH >8 significant concentrations of tetrahedrally coordinated boron complexes are present. At pH values lower than 6, $B(OH)_4$ is absent in the fluid and B is not enriched in the minerals (Palmer and Swihart, 1996). Bonatti et al. (1984) showed a negative correlation between

temperature and B concentration in abyssal peridotites from the Vema and Romanche Fracture zones, using O^{18}/O^{16} fractionation between coexisting magnetite and serpentine as a thermometer (Wenner and Taylor, 1971). This simple relationship has been questioned by Plas (1997). His results from abyssal peridotites of different MOR (ODP Leg 107, 147, 149) for B and $\delta^{18}O$ showed that there is no simple correlation between temperature, serpentine mineral type and B content (Plas, 1997). For Lost City, Boschi et al. (2008) report B incorporation into serpentine at moderate temperatures, with random B - $\delta^{18}O$ distribution, supporting the hypothesis of Plas (1997).

The Li contents of serpentine in the studied samples range from 0.001 to 9.38 µg/g. The high abundances may in part be due to analyses of mixtures of serpentine with primary (cpx, opx, and ol) or secondary phases (brucite and iowaite). If the latter show the same light element characteristics as clay minerals they should be rich in Li.

In any case, the Li contents of serpentine from Sites 1272A and 1274A are on the average lower than those of primary minerals (Fig. 2.10). Serpentinization, on average, should thus decrease Li contents of the whole rock samples. Serpentine from Site 1274A (less serpentinized) shows a smaller variation in Li contents and tends to higher values compared to serpentine from Site 1272A (almost completely serpentinized), which shows a larger variation and tends to lower values (Fig. 2.10).

The Li whole rock contents range from 0.72 to 1.04 µg/g (Vils et al., 2008) and are within the range measured by Paulick et al. (2006) and Godard et al. (2008; 0.04–1.37 µg/g). They are, on average, lower than values for the depleted mantle (Fig. 2.11). Samples from the less serpentinized Site 1274A tend to higher and more uniform values than samples from Site 1272A, which show a larger variation and a lower average of Li contents (Fig. 2.11). As for B, there is no simple linear correlation between the degree of serpentinization and Li whole rock contents. On the other hand, Fig. 2.11 shows a significant difference between Mariana forearc samples (ODP Leg 125) and ODP Leg 209. Pore water measurements at the Mariana forearc showed high B (0.96–42.9 µg/g) and low Li abundance in the fluids (0.0001–0.07

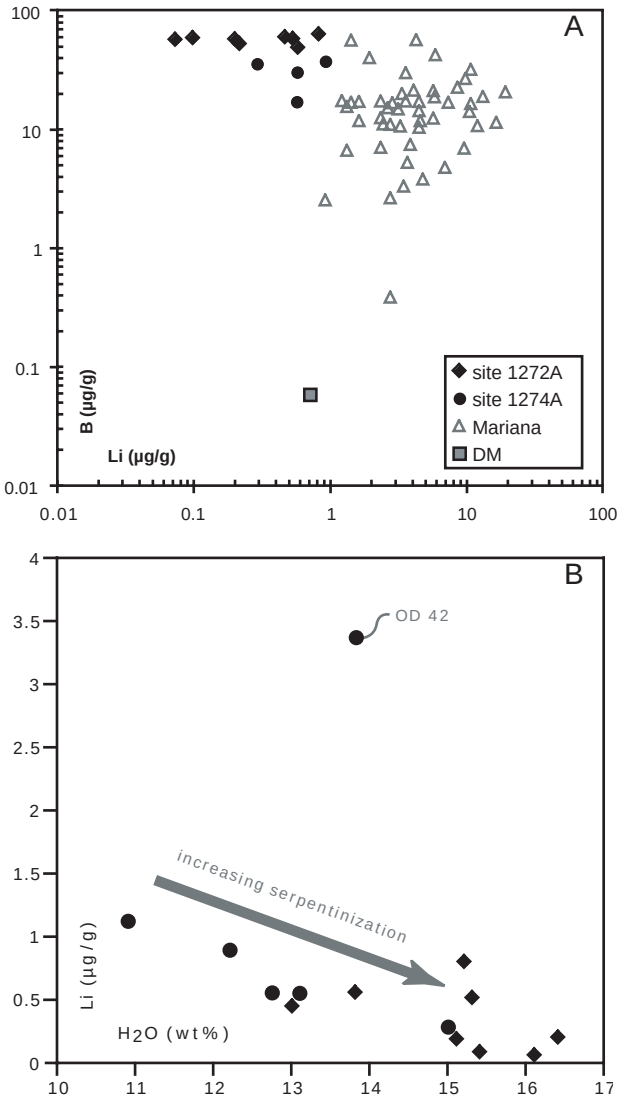

Fig. 2.11. A) Diagram showing measured Li and B contents of whole rock samples from the oceanic domain. Data for samples from Mariana forearc mud volcanoes (ODP Leg 215) are from Savov et al. (2005); the value for the depleted mantle (DM) is from Salters and Stracke (2004). B) Diagram showing measured Li and H_2O contents of whole rock samples, indicating Li loss with increasing serpentinization.

µg/g; Mottl et al., 2004), the latter being probably the source of the enriched B and Li concentrations of the Mariana samples with respect to the ODP Leg 209 samples.

Less is known about the incorporation of Li into serpentine and serpentinite than for B. Whole rock studies on dredged abyssal peridotites have shown a considerable enrichment of serpentinized peridotite in Li compared to depleted mantle values, but with large variations (0.6– 13.4 µg/g; Decitre et al., 2002; Niu, 2004). In-situ analysis of serpentine for Li revealed even larger variability (Decitre et al., 2002). In analogy to

Table 5
Whole rock PGAA analyses from ODP leg 209

	SiO_2		H_2O		H		B		S		Cl	
	wt%	±	wt%	±	wt%	±	$\mu g\ g^{-1}$	±	$\mu g\ g^{-1}$	±	$\mu g\ g^{-1}$	±
Site 1272A												
OD 2	33.85	*0.90*	16.13	*0.43*	1.80	*0.04*	58.7	*1.11*		*0*	10114	*446*
OD 6	35.73	*0.93*	15.42	*0.41*	1.73	*0.04*	60.3	*1.10*	1380	*84*	7759	*343*
OD 11	35.10	*0.92*	16.40	*0.43*	1.84	*0.04*	53.9	*1.01*	1353	*107*	6389	*291*
OD 15	35.77	*0.93*	15.11	*0.40*	1.69	*0.04*	59.3	*1.08*	1330	*96*	6682	*314*
OD 18	35.84	*0.94*	15.34	*0.41*	1.72	*0.04*	59.8	*1.12*	1909	*132*	6355	*251*
OD 22	36.21	*0.92*	15.17	*0.40*	1.70	*0.04*	65.0	*1.18*	1402	*118*	7291	*289*
OD 26	30.64	*1.03*	13.00	*0.43*	1.45	*0.03*	61.5	*1.12*	2229	*74*	6032	*244*
OD 29	36.48	*0.94*	13.79	*0.37*	1.54	*0.03*	50.3	*0.92*	1399	*109*	6855	*247*
Site 1274A												
OD 34	36.74	*0.94*	12.75	*0.34*	1.43	*0.03*	31.2	*0.59*	781	*80*	2242	*90*
OD 38	37.30	*0.94*	13.12	*0.35*	1.47	*0.03*	17.5	*0.33*	825	*66*	2746	*129*
OD 42	36.33	*0.92*	13.82	*0.37*	1.55	*0.03*	<0.2	–	561	*66*	1553	*33*
OD 45	38.50	*0.98*	10.90	*0.30*	1.22	*0.03*	10.4	*0.20*	<500	–	1061	*44*
OD 48	37.50	*0.95*	12.20	*0.33*	1.37	*0.03*	38.5	*0.72*	<500	–	1823	*77*
OD 49	34.57	*0.92*	14.99	*0.40*	1.68	*0.04*	36.6	*0.69*	1056	*79*	3566	*144*

the results of heating experiments conducted on altered basalt (Seyfried et al., 1998), it may be concluded that Li incorporation in serpentine is favored at temperatures below 350°C.

In summary, the systematics of B and Li observed in serpentine and serpentinite from Sites 1272A and 1274A suggest that the B and Li budget is strongly controlled by the degree of serpentinization, although there are large variations on the sample and the thin section scale. This suggests that the light element budget should depend strongly on water/rock ratios. In their study on serpentinized peridotites from Lost City, Boschi et al. (2008) observed that B content and $\delta^{11}B$ values show a strong positive correlation with water/rock ratios, the latter calculated by using the Sr isotopic composition of the rocks. For ODP Leg 209, we measured high $\delta^{11}B$ and high B content and calculated high water/rock ratios using the Sr isotopic composition of the serpentinites (Vils et al., 2008).

The potential role of temperature and pH is difficult to assess, because there are no direct indications from the two sites. Concerning temperature, we assume that within each of the two sites any temperature gradient must have been negligible given that the rocks cover a vertical distance of only 147 m (Table 1). There may have been a systematic temperature difference between the two sites given the large horizontal distance (Fig. 2.1), but Alt et al. (2007) derive serpentinization temperatures around 150°C at both sites on the basis of oxygen isotope data of serpentinites and gabbros. In addition there seems to be a chemical difference between the two Sites (Fig. 2.4–2.7). Spinel compositions show a lower degree of partial melting at Site 1272A compared to Site 1274A.

Indications of temperature and pH during water-rock interaction on the ocean floor come from two hydrothermal fields at the MAR, Logatchev and Lost City. The Logatchev hydrothermal field lies approximately 50 km south of Site 1272A. Fluids emerging from this site have temperatures of 353°C and a pH of 3.3 (Douville et al., 2002 and Schmidt et al., 2007). They contain 3.63 µg/g B and 1.75 µg/g Li and are interpreted as chemically buffered by ultramafic and mafic rocks (Schmidt et al., 2007). The Li content in fluids buffered by only mafic rocks should be generally higher than for ultramafic systems (e.g. Snakepit 5.85 µg/g Li, Douville et al., 2002), but may be difficult to predict for mixed systems. At the Logatchev hydrothermal field, serpentinization enriched the reacting seawater in Li and depleted it in B. The ODP Leg 209 mineral and whole rock B and Li data are in line with such a process, although the fluids from Logatchev contain too much B to be in equilibrium with peridotites only from Sites 1272A and 1274A. However, this difference may be explained by the fact that we studied an (almost) pure ultramafic system, while the Logatchev fluids represent a mafic-ultramafic system.

In 2000, an expedition discovered an off-axis hydrothermal field near the summit of the Atlantic massif: Lost City, a cold hydrothermal system driven by the exothermic serpentinization reaction (Kelley et al., 2001; Früh-Green et al., 2003; Kelley et al., 2005). From the white smokers a fluid with 40–75°C

and a pH of 9–9.8 emerges (Kelley et al., 2001). These hydrothermal fluids from Lost City are depleted in B and slightly enriched in Li compared to seawater (0.34 µg/g B and 0.33 µg/g Li; Boschi, 2006). Thus, also the data from this hydrothermal field show that the reacting fluid is enriched in Li and depleted in B after percolation through ultramafic rocks, although temperature and pH are very different from the Logatchev hydrothermal field. This suggests that these two parameters may be less important for the B and Li budget of the serpentinite samples from Sites 1272A and 1274A than the water/rock ratios.

2.6.4. Model of the B and Li budget of the oceanic lithosphere

The data presented in this study have shown that serpentinized oceanic mantle can be considerably enriched in B and slightly depleted in Li compared to depleted mantle values. B contents seem to increase with the degree of serpentinization, while Li seems to show the opposite trend. This implies that serpentinization of oceanic mantle fractionates B from Li. This is opposite to what is found in igneous oceanic crust, where both B and Li are added by alteration processes (see Section 1).

Based on field and experimental data, Scambelluri et al. (2004) and Tenthorey and Hermann (2004) proposed that serpentinites are a major source of B into subduction zones. On the other hand, previous studies (see Section 1) have shown that—although volumetrically less important—the oceanic crust may also be an important reservoir of light elements. In addition, the proportions of igneous crust and mantle, the degree of hydrothermal alteration of the mantle, and the thickness of the lithosphere can vary considerably from one oceanic plate to another. Based on our results and on literature data, we model the budget of B and Li contained in the oceanic lithosphere, and its partitioning between crust and mantle as a function of plate characteristics. This represents an estimate of total B and Li potentially available in a subducting oceanic plate. We will first discuss the rationale and the parameters of our model. Then, we will present the results and discuss them against

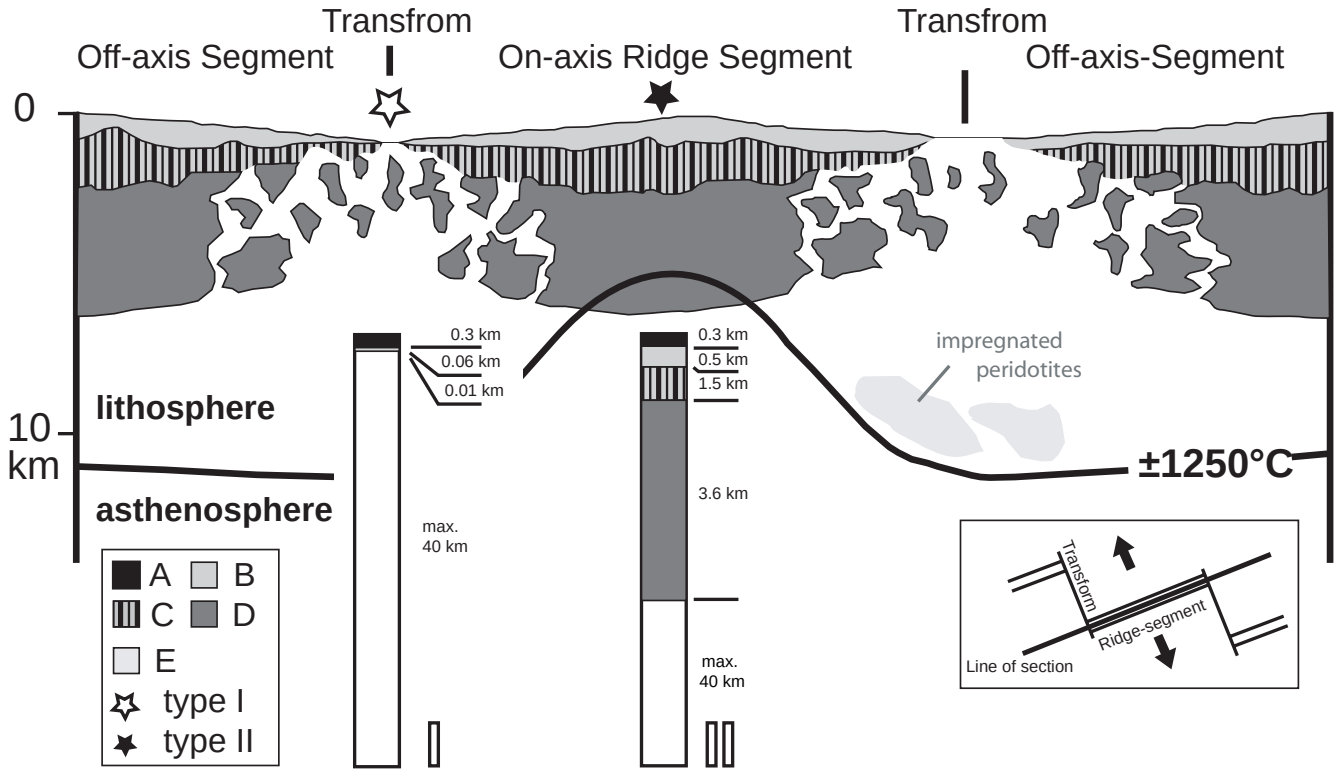

Fig. 2.12. Cross section through a mid-ocean ridge (modified after Ghose et al., 1996; Dijkstra et al., 2001). Type I: modified cross-section through ODP 209-type lithosphere after 75 Ma (modified after Bach et al., 2004). Type II: simplified cross-section through a Semail-type lithosphere after 75 Ma (modified after Boudier and Nicolas, 1985). (A) Sedimentary cover, (B) pillow basalts (completely altered), (C) sheeted dykes (fresh basalt), (D) gabbros, (E) plagioclase peridotites, white: mantle. Stars indicate possible location of type I and II on a mid-ocean ridge.

the background of published estimates of B and Li loss in subduction zones. Beryllium was not considered in our model because our data shows Be to be mostly around the critical value (<3 ng/g), independent of the degree of serpentinization. Also, the depleted mantle in general has very low Be contents (25 ng/g, Salters and Stracke, 2004). The Be content would be largely dominated by the sedimentary cover, because sediments can be enriched in Be up to the µg/g-level (e.g. Gao et al., 1998) and/or by the mafic crust (see compilation in Ryan, 2002).

2.6.5. Model parameters and rationale

Two parameters need to be considered when modeling the B and Li budget of the oceanic lithosphere. The first parameter is primary lithology. Geophysical data obtained in the oceanic domain (e.g. The MELT seismic team, 1998) and studies on ophiolites with largely coherent crust–mantle sections (Semail, Oman; Boudier and Nicolas, 1985) have shown that at fast-spreading ridges the igneous crust may be up to 7 km thick. On the other hand, at slow-spreading ridges such as the MAR, the igneous crust can be completely absent and the mantle exposed on the ocean floor (such as at Site 1274A, ODP Leg 209). Also, petrostructural studies on the Romanche and Vema fracture zones (mid-Atlantic ridge) have stressed the importance of oceanic fracture zones for locally exhuming serpentinized mantle to shallow depths, creating lithologically variable crust-mantle sections (Bonatti and Honnorez, 1976). As 'endmember' cases of oceanic lithosphere for our modeling we therefore use a lithospheric mantle with an igneous crust corresponding to that of the Semail ophiolite (Fig. 2.12, Table 6) and one with almost no igneous crust, such as that of to ODP Leg 209, Sites 1274A and 1272A (Fig. 2.12, Table 6). For both types of lithosphere, the published stratigraphic logs (Semail ophiolite: Boudier

Table 6
Lithium and boron budget into subduction zone

	Sediment (clay)	MORB (altered)	MORB (fresh)	Gabbro	Peridotite (80% serp)	DM (harz)	
Density (kg m^{-3})	2700	2690	2900	2900	2530	3300	
Li (µg/g)	44.65	14.89	5.65	1	0.62	0.8	
B (µg/g)	83.91	40	1.99	2.7	40.92	0.04	
Data source	1	4 and 5	2 and 3	6 and 7	This study	This study	
1 m^3 contains							
Total Li (g)	120.56	16.39	40.05	2.90	2.05*	2.64	
Total B (g)	226.56	5.77	107.60	7.83	135.04*	0.13	
Semail-type lithosphere							Total
1-Ma-old plate					Total serp*		(t/col)
Thickness (km)	0	0.2	1.8	3.6	0		
% Li	–	16.71	61.52	21.78	–		0.048
% B	–	35.81	17.29	46.91	–		0.060
75-Ma-old plate							
Thickness (km)	0.3	1.5	0.5	3.6	20	54.1	
% Li	11.80	19.60	2.67	3.41	15.95	46.58	0.307
% B	7.52	17.85	0.32	3.12	70.66	0.79	0.904
ODP Leg 209-typ lithosphere							
1-Ma-old plate							
Thickness (km)	0	0.06	0	0.01	0.13	5.4	
% Li	–	14.17	–	0.17	1.57	84.09	0.017
% B	–	26.03	–	0.32	70.78	2.87	0.025
75-Ma-old plate							
Thickness (km)	0.3	0.06	0	0.01	20	59.63	
% Li	14.77	0.98	–	0.01	19.96	64.28	0.245
% B	9.45	0.90	–	0.01	88.86	1.09	0.719
DM (harzburgite)							
	Ol	Cpx	Opx	Spl	Total		
% Modal	66	3	30	1	100		
Li (µg/g)	0.80	2.04	0.69	0.51	0.80		
B (µg/g)	0.011	1.035	0.012	0.008	0.042		

Unit thickness see Fig. 14; DM (depleted mantle) calculation based on mineral average content from ODP leg 209. *first 3 km 80% serpentinization, rest 20% serpentinization used in the model (Li = 2.39 g and B = 27.11 g); col, column with x km depth and 1 m^2 surface; Li and B content are average data after: (1) Ishikawa and Nakamura (1993); (2) Ryan and Langmuir (1987); (3) Ryan and Langmuir (1993); (4) Bouman et al. (2004); (5) Thompson and Melson (1970); (6) Chan et al. (2002); (7) Smith et al. (1995).

and Nicolas, 1985, ODP Leg 209: Bach et al., 2004) were simplified into six units: sediment, altered MORB, MORB, gabbro, serpentinized peridotite and depleted mantle (Fig. 2.12 and Table 6).

The second parameter, the age of the oceanic lithosphere, is important as it controls a considerable number of physical and chemical features. The total thickness of the oceanic lithosphere increases as the plate moves away from the ridge. In our model, we use plate ages of 1 and 75 Ma; the latter, because it corresponds to the average age of currently subducted oceanic plates (Li and Lee, 2006); the former because there are examples of very young oceanic lithosphere currently subducted, e.g. the Chile ridge (e.g. Tebbens et al., 1997), various oceanic basins in the western Pacific (e.g. Heaton and Hartzell, 1987), or about to be subducted (e.g. Macquarie Island, Sutherland, 1995; Lamarche et al., 1997).

Total lithospheric thickness as a function of age can be calculated with the GDH1 plate model of Stein and Stein (1992, 1996). According to this model, an oceanic plate has a total thickness of around 5 km after 1 Ma. In the case of a Semail-type lithosphere, this will correspond to the thickness of the igneous crust. In the case of an ODP Leg 209-type lithosphere, there will be 5 km of lithospheric mantle with minor volumes of igneous crust. After 75 Ma, both types of oceanic plates will have acquired a total thickness of approximately 80 km (Table 6).

The age of the lithosphere also controls the thickness of the sedimentary layer. To simplify modeling, we assume that any oceanic lithosphere will have no sedimentary cover at an age of 1 Ma and a 300-m sedimentary cover after 75 Ma (as is the case for the Semail ophiolite). We thus model in total four cases, an ODP Leg 209-type lithosphere, and a Semail-type lithosphere at 1 and 75 Ma, respectively (Table 6 and, Figs. 2.13 and 2.14).

The age of the lithosphere controls the vertical temperature gradient and hence the depth to which alteration by seawater-derived fluids plays a role/is possible. For the mantle part of the oceanic lithosphere it is important to note that the depth of serpentinization does not necessarily correspond to the depth of B enrichment/Li depletion. The major B incorporation in peridotites takes place at low temperatures (<300°C, Seyfried and Dibble, 1980; Spivack and Edmond, 1987). In contrast, experiments showed that serpentine can be stable up to 650°C at 3 GPa and up to 475°C at 1 atm (Ulmer and Trommsdorff, 1995; Ulmer and Trommsdorff, 1999). For our model, we arbitrarily fixed the temperature limit of B enrichment/Li depletion at 300°C and that of serpentinization at 550°C and calculated the depth of both isotherms in the four endmember cases (Table 6) using the model of Parker and Oldenburg (1973) and Stein and Stein (1996). For the sake of simplicity, we assume the 300°C also represents the limit of alteration in the igneous oceanic crust with respect to B and Li.

It is important to know to which degree the mantle at temperatures below the 300°C isotherm is serpentinized. Experiments on water flow through partially serpentinized peridotite showed that serpentinization rates vary between 10.8 cm^2/s at 34°C to 10.4 cm^2/s at 300°C (MacDonald and Fyfe, 1985), indicating that in 1 Ma, 1 km of serpentinite layer can form at 300°C, 260 m at 200°C, and 60 m at 100°C. These results indicate that serpentinization is a rather efficient process. It could be argued, however, that serpentine formation is also controlled by water availability and that this limit could be at shallower depth than the 300°C isotherm. Although the oceans represent a virtually infinite reservoir, water can only penetrate the oceanic lithosphere through fractures or by diffusion. To our knowledge, there are no quantitative data on the penetration depth of water and the degree of serpentinization in off-ridge settings. However, MacDonald and Fyfe (1985) have shown that serpentinization proceeds by an efficient interplay of water diffusion and crack propagation due to volume increase during serpentinization. We therefore assume in our model that the mantle at temperatures below the 300°C isotherm is serpentinized. The degree of serpentinization is difficult to assess. Escartin et al. (2001) showed that serpentinization degrees of 35% to 55% are necessary to obtain the reduced P-wave velocities of 6.5–7.5 km/s commonly observed in the oceanic lithosphere between normal crust and normal mantle. This layer has often been interpreted as serpentinized peridotite (e.g. Minshull et al., 1998). A wide-angle seismic experiment at the Atlantis II Fracture Zone, Southwest

Indian Ridge (Muller et al., 1997) shows that a 3- to 4-km-thick igneous crust is underlain by a 2- to 3-km-thick layer of serpentinized mantle peridotite. The P-wave velocity of 6.9 km/s for the serpentinized peridotite layer corresponds to a 35 ± 10 vol% serpentine content (Escartin et al., 2001). A compilation of velocity structures of the oceanic crust/ mantle in various tectonic settings (Minshull et al., 1998) shows that P-wave velocity of around 7 km/s, that can eventually be attributed to serpentinized mantle, are found between 1 and 6 km depth.

Taking all these lines of evidence into consideration, we fix the degree of serpentinization in our model to 80% (average

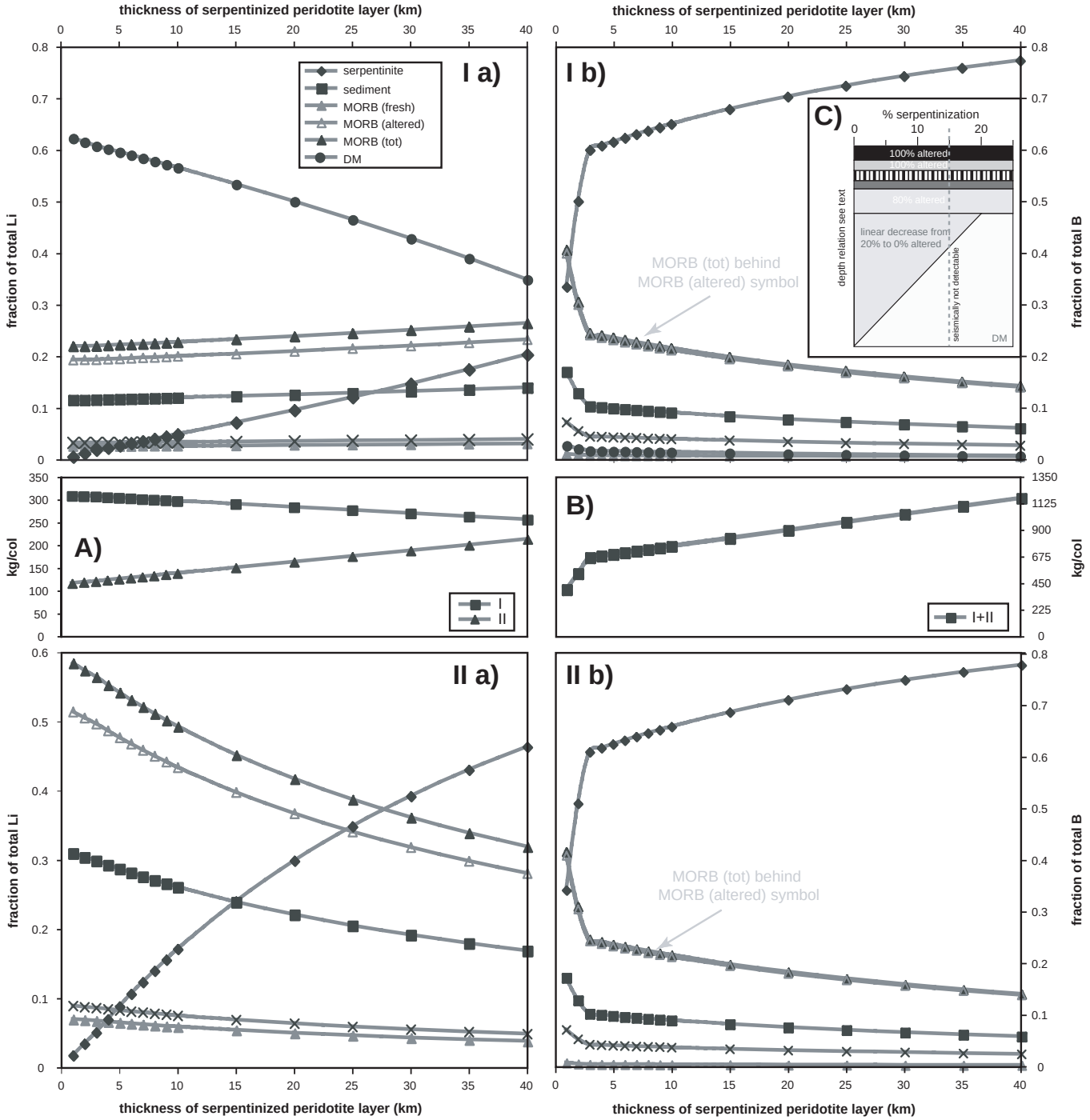

Fig. 2.13. Modeled evolution of the B and Li contents in a Semail-type lithosphere as a function of the thickness of the serpentinized layer, considering two cases: (I) the total thickness of the oceanic lithosphere is fixed to 80 km and (II) the total lithospheric thickness increases with age and serpentinization. (A and B) The total amount of Li and B content in a column of x km depth with 1 m² surface (x= thickness of the lithosphere). Input values are given in Table 6. (C) Simplified cross-section through an ocean plate, indicating degree of alteration/ serpentinization with depth, as described in the text. Same symbols used as in Fig. 12 (figure not to scale).

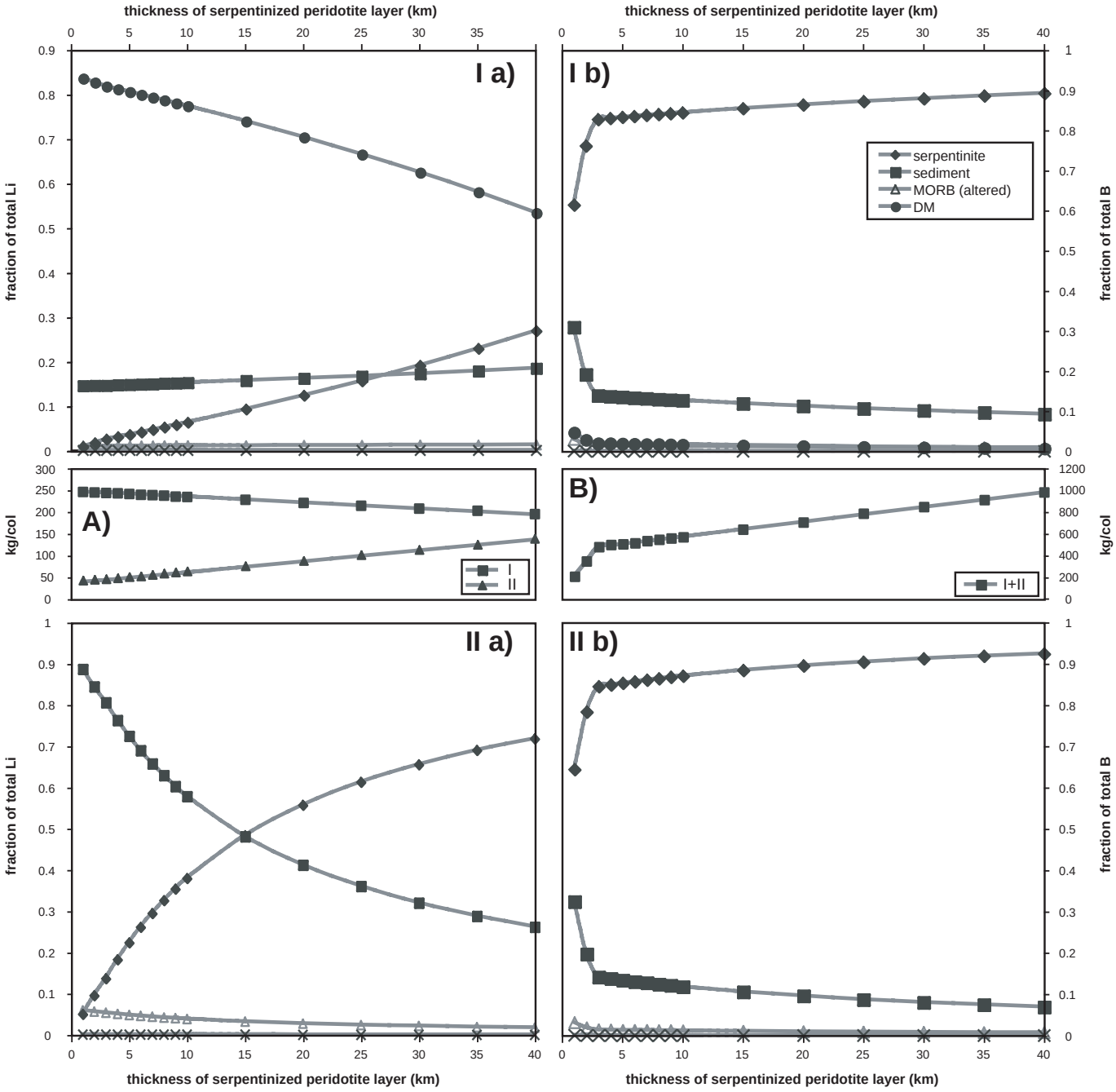

Fig. 2.14. Modeled evolution of the B and Li contents in a ODP Leg 209-type lithosphere as a function of the thickness of the serpentinized layer, considering two cases: (I) the total thickness of the oceanic lithosphere is fixed to 80 km and (II) the total lithospheric thickness increases with age and serpentinization. (A and B) The total amount of Li and B content in a column of x km depth with 1 m² surface (x= thickness of the lithosphere). Input values are given in Table 6.

degree observed in our samples: Tables 1 and 6) to a depth of 3 km. Below follows a much thicker layer where serpentinization decreases linearly from 20% to 0% (Fig. 2.13). Various test calculations, varying the thickness of the top layer between 1 and 3 km, have shown no significant difference.

B and Li input values for the mass balance are reported in Table 6. For the B and Li contents of the sedimentary layer, the data of Ishikawa and Nakamura (1993) were used, assuming the sediment to be composed only of clay minerals, known to incorporate high amounts of Li and B (Wunder et al., 2005; Wunder et al., 2006).

2.6.6. Results of mass balance calculations

The Li and B budgets are given in kilogram per column (kg/col). 1 column corresponds to 1 m x 1 m at the surface the thickness of the

lithosphere. As the thickness of the oceanic lithosphere varies with age, indicating kg/m^3 would not be useful. For case 1 (Semail-type lithosphere at an age of 1 Ma), the lithosphere is 5.6 km thick (total thickness of igneous crust in the Semail ophiolite), the 300 and 550°C isotherms are located at 0.2 and 0.4 km depth, respectively (Table 6). The section is made up entirely of igneous crust (0.2 km of altered MORB, 1.8 km of MORB, 3.6 km of gabbro). At these conditions, the oceanic lithosphere contains on the average 48 kg/col Li and 60 kg/col B. Li is essentially hosted by MORB (61.5%). The major carriers of B are altered MORB (35.8%) and gabbro (46.9%). After 75 Ma, the 300 and 550°C isotherms are located at 20 and 34 km depth, respectively. The section comprises from top to bottom: 0.3 km of sediment, 1.5 km of altered MORB, 0.5 km of MORB, 3.6 km of gabbro, 20 km of serpentinized peridotite enriched in B/depleted in Li, and 54.1 km of depleted mantle (Table 6). In this situation, the oceanic lithosphere contains on the average 307 kg/col Li and 904 kg/col B. Li resides mainly within the depleted mantle. It is hosted to a lesser degree by altered MORB (19.6%), serpentinized peridotites (16.0%) and sediment (11.8%). B is almost entirely hosted by serpentinized peridotite (70.8%).

For case 3 (ODP Leg 209-type lithosphere at an age of 1 Ma), the total lithospheric thickness is 5.6 km, the 300 and 550°C isotherms are located at 0.2 and 0.4 km depth, respectively. At these conditions, the section comprises from top to bottom: 0.06 km of altered MORB, 0.01 km of gabbro, 0.13 km of serpentinized peridotite enriched in B/depleted in Li, and 5.4 km of depleted mantle (Table 6). In this situation, the oceanic lithosphere contains on the average 17 kg/col Li and 25 kg/col B. Table 6 shows that the Li budget of a slow spreading ridge will be predominantly hosted by the depleted mantle (84.1%), whereas B resides in serpentinized peridotite (70.8%) and in altered MORB (26.0%). After 75 Ma (case 4), the 300 and 550°C isotherms will be located at 20 and 34 km depth, respectively. The oceanic lithosphere will have the same thickness of the igneous crust as at 1 Ma (0.06 km of altered MORB, 0.01 km of gabbro), but 0.30 km of sediment will have accumulated on top. Serpentinized peridotite will have increased to 20 km and depleted mantle to 59.63 km thickness. At these conditions, the oceanic lithosphere contains on average 245 kg/col Li and 719 kg/col B. The Li budget is dominated by the depleted mantle (64.3%), serpentinized peridotite (20.0%) and less by the sedimentary cover (14.8%). The B budget is largely controlled by serpentinized peridotite (88.9%). The (igneous) crust plays virtually no role for the Li and B budget in the ODP Leg 209-case.

2.6.7. Temporal evolution of the B and Li budget within the upper 40 km of the oceanic lithosphere—implications for subduction zones

From the mass balance calculations presented in the previous section, it is apparent that with increasing age of the lithosphere, the role of the depleted mantle as a reservoir for B and Li becomes increasingly important. In the context of B and Li recycling at subduction zones it can be argued that not the entire mantle volume dehydrates and liberates B and Li. For this setting, it may be more appropriate to consider only the B and Li budget of the upper part of the oceanic lithosphere (the 'dehydratable' part).

Moreover, there is evidence that additional serpentinization occurs due to fracturing during plate bending (e.g. Ranero et al., 2003; Ranero and Sallarès, 2004; Li and Lee, 2006), and may proceed to depth greater than 20 km (depth of the 300°C isotherm in a 75-Ma-old plate) because of lower geothermal gradients and better water availability. By modeling seismic velocities of bending-related extensional faulting, Ranero and Sallarès (2004) predict a 20-km-thick mantle layer serpentinized to 17% for the Nazca plate at the North Chile trench. Based on geochemical data and modeling, Li and Lee (2006) estimate the paleo-serpentinization depth of the Feather River Ophiolite (subduction context) to be around 40 km.

In order to better account for this geodynamic context, we modeled the evolution of the B and Li budget only in the upper 40 km of the oceanic lithosphere, using the same input parameters as for our previous model, and applying it to two 'endmembers': a Semail-type lithosphere (Fig. 2.13) and an ODP Leg 209-type lithosphere (Fig. 2.14). In model cases I (Figs. 2.13.Ia, b and 2.14.Ia, b) we assume that the oceanic lithosphere has a constant thickness of 80 km, with the mantle

part becoming increasingly serpentinized at conditions below 300°C. This implies that initially, there are almost 80 km of depleted mantle, which are successively replaced by peridotites serpentinized at temperatures below 300°C. In model cases II (Figs. 2.13. IIa, b, and 2.14.IIa, b) we assume that the lithospheric thickness increases by adding peridotite serpentinized at temperatures below 300°C. This implies that there is no depleted mantle.

For boron, running the two models for the two endmembers provides similar results in all cases (Figs. 2.13.Ib, IIb and 2.14.Ib, IIb). Independent of the lithology of the oceanic plate, the B budget will be almost entirely controlled by serpentinized peridotite. Even in Semail-type lithosphere with a 5.6-km-thick igneous crust, a 3-km-thick section of serpentinized peridotite will be sufficient to host approximately 40% of the lithospheric B budget. These results suggest that large quantities of B reside in the uppermost part of the plate and could hence be easily liberated during slab dehydration.

For lithium, running the two models shows that the lithology of the oceanic plate controls the partitioning and availability of this element (Figs. 2.13.Ia, IIa and 2.14. Ia, IIa). In oceanic lithosphere containing a considerable fraction of depleted mantle (40%–50%), the Li budget is dominated by the latter (Figs. 2.13.Ia and 2.14.Ia). In oceanic lithosphere where depleted mantle is absent, Li is essentially hosted in sediments and in MORB (Figs. 2.13.Ib and 2.14.Ib).

All of the figures related to Li show that serpentinized peridotites only becomes important for the Li budget once its thickness exceeds 20–25 km. These results suggest that the most prominent input of Li into subduction zones is to be expected from Semail-type lithosphere with a significant crustal section and a depleted mantle section, because in this situation most of the Li is stored at shallow levels in the plate. Subducting an ODP Leg 209-type lithosphere and assuming that most of the Li is liberated from the upper part of the plate would mean only very little Li output from the slab.

2.7. Summary and Conclusions

The results of our study of serpentinized peridotites from the mid-Atlantic ridge show that the B, Li and Be contents of the mantle minerals olivine, orthopyroxene and clinopyroxene remain unchanged during serpentinization and still reflect older processes such as melt infiltration. As serpentine has high B and fairly low Li contents, the process of serpentinization increases the B (and H_2O and Cl) and lowers the Li contents of the whole rock. These findings are in line with the composition of hydrothermal fluids sampled from the ocean floor, which are enriched in Li and depleted in B after percolation through ultramafic rocks.

The results of our mass balance calculations show that the Li contents of the oceanic lithosphere are highly variable and controlled by primary lithology whereas the B contents depend entirely on serpentinization. In all cases, large quantities of B reside in the uppermost part of the plate and could hence be easily liberated during slab dehydration. Late-stage serpentinization during slab bending will probably further increase the B content in the downgoing slab. The most prominent input of Li into subduction zones is to be expected from Semail-type lithosphere whereas subducting an ODP Leg 209-type lithosphere would be a far less efficient mechanism. Serpentinized mantle thus plays an important role in B recycling in subduction zones, but it is of lesser importance for Li.

ACKNOWLEDGMENTS

This research used samples provided by the Ocean Drilling Program (ODP). ODP is sponsored by the U.S. National Science Foundation (NSF) and participating countries under management of Joint Oceanographic Institutions (JOI), Inc.. Funding for this research was provided by the Swiss National Science Foundation (Grants 200021-10361 and 200021-103479/1). We thank E. Reusser (ETH Zürich, Switzerland), E. Gnos and A. Berger (Bern, Switzerland), H.-P. Meyer (Heidelberg, Germany) and H. Siegfried-Müller (Freiburg, Germany) for technical support at their microprobe and the PGAA team in Budapest for supplying B, H_2O and Cl whole rock data. Reviews by I. Savov, M. Godard and W. Bach helped to improve the manuscript.

REFERENCES

Alt, J. C., Shanks III, W. C., Bach, W., Paulick, H., Garrido, C. J., and Beaudoin, G., 2007. Hydrothermal alteration and microbial sulfate reduction in peridotite and gabbro exposed by detachement faulting at the mid-Atlantic ridge, 15°20'N (ODP Leg 209): A sulfur and oxygene isotope study. Geochemistry Geophysics Geosystems 8, 1-22.

Anders, E. and Grevesse, N., 1989. Abundance of the elements: Meteoritic and solar. Geochimica et Cosmochimica Acta 53, 197-214.

Anderson, D. L. and Kasztovszky, Z., 2004. Application of PGAA with neutron beam. In: Molnar, G. L. (Ed.), Handbook of prompt gamma activation analysis with neutron beams. Kluwer.

Arai, S., 1994. Compositional variation of olivine-chromian spinel in Mg-rich magmas as a guide to their residual spinel peridotites. Journal of Volcanology and Geothermal Research 59, 279-293.

Bach, W., Garrido, C. J., Paulick, H., Harvey, J., and Rosner, M., 2004. Seawater-peridotite interactions: First insights from ODP Leg 209, MAR 15°N. Geochemistry Geophysics Geosystems 5, 1-22.

Barnes, J. D. and Sharp, Z. D., 2006. A chlorine isotope study of DSDP/ODP serpentinized ultramafic rocks: Insights into the serpentinization process. Chemical Geology 228, 246-265.

Benninghoven, A., Rüdenauer, F. G., and Werner, H. W., 1987. Secondary ion mass spectrometry: Basic concepts, instrumental aspects, applications and trends. John Wiley & Sons, New York Chichester Brisbane Toronto Singapore.

Benton, L. D., Ryan, J. G., and Savov, I. P., 2004. Lithium abundance and isotopic systematics of forearc serpentinites, Conical Seamount, Mariana forearc: Insights into the mechanics of slab-mantle exchange during subduction. Geochemistry Geophysics Geosystems 5, 1-14.

Benton, L. D., Ryan, J. G., and Tera, F., 2001. Boron isotope systematics of slab fluids as inferred from a serpentine seamount, Mariana forearc. Earth and Planetary Science Letters 187, 273-282.

Bonatti, E. and Honnorez, J., 1976. Section of the Earth's crust in the Equatorial Atlantic. Journal of Geophysical Research 81, 4104-4116.

Bonatti, E., Lawrence, J., and Morandi, N., 1984. Serpentinization of oceanic peridotites: Temperature dependence of mineralogy and boron content. Earth and Planetary Science Letters 70, 88-94.

Bonifacie, M., Busigny, V., Mével, C., Philippot, P., Agrinier, P., Jendrzejewski, N., Scambelluri, M., and Javoy, M., 2007. Chlorine isotope composition in seafloor serpentinites and high-pressure metaperidotites. Insights into oceanic serpentinization and subduction processes. Geochimica et Cosmochimica Acta 72, 126-139.

Boschi, C., 2006. Building Lost City: serpentinization, mass transfer and fluid flow in an oceanic core complex, Ph.D. thesis, Swiss Federal Institute of Technology Zurich (ETH Zürich).

Boschi, C., Früh-Green, G., Delacour, A., Karson, J. A., and Kelley, D. S., 2006. Mass transfer and fluid flow during detachment faulting and development of an oceanic core complex, Atlantis Massif (MAR 30°N). Geochemistry Geophysics Geosystems 7, 1-39.

Boschi, C., Dini, A., Fruh-Green G.L., 2008. Isotopic and element exchange during serpentinization and metasomatism at the Atlantis Massif (MAR 30 degrees N): Insights from B and Sr isotope data. Geochimica et Cosmochimica Acta 72, 1801-1823.

Boudier, F. and Nicolas, A., 1985. Harzburgite and lherzolite subtypes in ophiolitic and oceanic environment. Earth and Planetary Science Letters 76, 81-92.

Bouman, C., Elliott, T., and Vroon, P. Z., 2004. Lithium inputs to subduction zones. Chemical Geology 212, 59-79.

Brenan, J. M., Neroda, E., Lundstrom, C. C., Shaw, H. F., Ryerson, G. F. J., and Phinney, D. L., 1998. Behaviour of boron, beryllium and lithium during melting and crystallization: Constraints from mineral-melt partitioning experiments. Geochimica et Cosmochimica Acta 62, 2129-2141.

Bussod, G. Y. and Christie, J. M., 1991. Textural development and melt topology in spinel lherzolite experimentally deformed at hypersolidus conditions. Journal of Petrology, 17-39.

Cannat, M., 1993. Emplacement of mantle rocks in the seafloor at mid-ocean ridges. Journal of Geophysical Research 98, 4163-4172.

Chan, L. H., Alt, J. C., and Teagle, D. A. H., 2002. Lithium and lithium isotope profiles through the upper oceanic crust: A study of seawater-basalt exchange at ODP Sites 504B and 896A. Earth and Planetary Science Letters 201, 187-201.

Coogan, L. A., Kasemann, S. A., and Chakraborty, S., 2005. Rates of hydrothermal cooling of new oceanic upper crust derived from lithium-geospeedometry. Earth and Planetary Science Letters 240, 415-424.

Currie, L. A., 1968. Limits for qualitative detection and quantitative determination. Analytical Chemistry 40, 586-593.

de Kloe, R., Drury, M. R., and van Roermund, H. L. M., 2000. Evidence for stable grain boundary melt films in experimentally deformed olivine-

orthopyroxene rocks. Physics and Chemistry of Minerals 27, 480-494.

Decitre, S., Deloule, E., Reisberg, L., James, R., Agrinier, P., and Mével, C., 2002. Behavior of Li and its isotopes during serpentinization of oceanic peridotites. Geochemistry Geophysics Geosystems 3.

Dick, H. J. B. and Bullen, T., 1984. Chromian spinel as a petrogenetic indicator in abyssal and alpine-type peridotites and spatially associated lavas. Contributions to Mineralogy and Petrology 86, 54-76.

Dick, H. J. B., Lin, J., and Schouten, H., 2003. An ultraslow-spreading class of ocean ridges. Nature 426, 405-412.

Dijkstra, A. H., Drury, M. R., and Vissers, R. L. M., 2001. Structural petrology of plagioclase peridotites in the West Othris Mountains (Greece): Melt impregnation in mantle lithosphere. Journal of Petrology 42, 5-24.

Douville, E., Charlou, J. L., Oelkers, E. H., Bienvenu, P., Jove Colon, C. F., Donval, J. P., Fouquet, Y., Prieur, D., and Appriou, P., 2002. The rainbow vent fluids (36°14'N, MAR): The influence of ultramafic rocks and phase separation on trace metal content in mid-Atlantic ridge hydrothermal fluids. Chemical Geology 184, 37-48.

Eggins, S. M., Rudnick, R. L., and McDonough, W. F., 1998. The composition of peridotites and their minerals: A laser-ablation ICP-MS study. Earth and Planetary Science Letters 154, 53-71.

Elliott, T., Thomas, A., Jeffcoate, A., and Niu, Y., 2006. Lithium isotope evidence for subduction-enriched mantle in the source of mid-ocean-ridge basalts. Nature 443, 565-568.

Escartin, J. and Cannat, M., 1999. Ultramafic exposures and the gravity signature of the lithosphere near the Fifteen-Twenty Fracture Zone (mid-Atlantic ridge, 14°-16.5°N). Earth and Planetary Science Letters 171, 411-424.

Escartin, J., Hirth, G., and Evans, B., 2001. Strength of slightly serpentinized peridotites: Implications for the tectonics of the oceanic lithosphere. Geology 29, 1023-1026

Escartin, J., Mével, C., MacLeod, C. J., and McCaig, A. M., 2003. Constraints on deformation conditions and the origin of oceanic detachments: The mid-Atlantic ridge core complex at 15°45'N. Geochemistry Geophysics Geosystems 4, 1-37.

Früh-Green, G., Kelley, D. S., Bernasconi, S. M., Karson, J. A., Ludwig, K. A., Butterfield, D. A., Boschi, C., and Proskurowski, G., 2003. 30'000 years of hydrothermal activity at the Lost City vent field. Science 301, 495-498.

Fujiwara, T., Lin, J., Matsumoto, T., Kelemen, P. B., Tucholke, B. E., and Casey, J. F., 2003. Crustal evolution of the mid-Atlantic ridge near the Fifteen-Twenty Fracture zone in the last 5 Ma. Geochemistry Geophysics Geosystems 4, 1-25.

Gao, S., Luo, T.-C., Zhang, B.-R., Zhang, H.-F., Han, Y.-W., Zhao, Z.-D., and Hu, Y.-K., 1998. Chemical composition of the continental crust as revealed by studies in East China. Geochimica et Cosmochimica Acta 62, 1959-1975.

Ghose, I., Cannat, M., and Seyler, M., 1996. Transform fault effect on mantle melting in the MARK area (mid-Atlantic ridge south of the Kane transform). Geology 24, 1139-1142.

Gméling, K., Harangi, S., and Kasztovszky, Z., 2005. Boron and chlorine concentrations of volcanic rocks: An application of prompt gamma activation analysis. Journal of Radioanalytical and Nuclear Chemistry 265, 204-214.

Godard, M., Lagabrielle, Y., Alard, O., and Harvey, J., 2008. Geochemistry of the highly depleted peridotites drilled at ODP Sites 1272 and 1274 (Fiffteen-Twenty Fracture Zone, mid-Atlantic ridge): Implications for mantle dynamics beneath a slow spreading ridge. Earth and Planetary Science Letters 267, 410-425.

Hamlyn, P. R. and Bonatti, E., 1980. Petrology of mantle-derived ultramafics from the Owen fracture zone, northwest Indian ocean: Implications for the nature of the oceanic upper mantle. Earth and Planetary Science Letters 48, 65-79.

Heaton, T. H. and Hartzell, S. H., 1987. Earthquake hazards on the Cascadia subduction zone. Science 236, 162-168.

Hellebrand, E., Snow, J. E., and Mühe, R., 2002. Mantle melting beneath Gakkel Ridge (Arctic Ocean): Abyssal peridotite spinel compositions. Chemical Geology 182, 227-235.

Hellebrand, E., Snow, J. E., Dick, H. J. B., and Hofmann, A. W., 2001. Coupled major and trace elements as indicators of the extent of melting in mid-ocean-ridge peridotites. Nature 410, 677-681.

Ildefonse, B., Blackman, D. K., John, B., Ohara, Y., Miller, D. J., and MacLeod, C. J., 2007. Oceanic core complexes and crustal accretion at slow-spreading ridges. Geology 35, 623-626.

Ishikawa, T. and Nakamura, E., 1993. Boron isotope systematics of marine sediments. Earth and Planetary Science Letters 117, 567-580.

James, R. H. and Palmer, M. R., 2000. Marine geochemical cycle of the alkali elements and boron: The role of sediments. Geochimica et Cosmochimica Acta 64, 3111-3122.

Jean-Baptise, P., Charlou, J. L., Stievenard, M., Donval, J. P., Bougault, H., and Mével, C., 1991. Helium and methan measurements in hydrothermal fluids from the mid-Atlantic ridge: The Sanke Pit Site at 23°N. Earth and Planetary Science Letters 106, 17-28.

Jeffcoate, A., Elliott, T., Kasemann, S. A., Ionov, D., Cooper, K., and Brooker, R. A., 2007. Li isotope fractionation in peridotites and mafic

melts. Geochimica et Cosmochimica Acta 71, 22-218.

Kelemen, P.B., Kikawa, E., and Miller, D.J. (Eds.), 2007. Proc. ODP, Sci. Results, 209: College Station, TX (Ocean Drilling Program).

Kelemen, P. B., Kikawa, E., and Miller, D. J., 2004a. Proceedings of the Ocean Drilling Programm. Preliminary Report Leg 209.

Kelemen, P. B., Kikawa, E., and Miller, D. J., 2004b. Proceedings of the Ocean Drilling Programm. Initial Reports 209.

Kelley, D. S., Karson, J. A., Blackman, D. K., Früh-Green, G., Butterfield, D. A., Lilley, M. D., Olson, E. J., Schrenk, M. O., Roe, K., Lebon, G. T., and Rivizzigno, P., 2001. An off-axis hydrothermal field near the mid-Atlantic ridge at 30°N. Nature 412, 145-149.

Kelley, D. S., Karson, J. A., Früh-Green, G., Yoerger, D. R., Shank, T. M., Butterfield, D. A., Hayes, J. M., Schrenk, M. O., Olson, E. J., Proskurowski, G., Jakuba, M., Bradley, A., Larson, B., Ludwig, K., Glickson, D., Buckman, K., Bradley, A. S., Brazelton, W. J., Roe, K., Elend, M. J., Delacour, A., Bernasconi, S. M., Lilley, M. D., Baross, J. A., Summons, R. E., and Sylva, S. P., 2005. A serpentinite-hosted ecoystem: The Lost City hydrothermal field. Science 307, 1428-1434.

Kisakürek, B., Widdowson, M., and James, R. H., 2004. Behavior of Li isotopes during continental weathering: The Bidar laterite profile, India. Chemical Geology 212, 27-44.

Kohlstedt, D. L. and Zimmerman, M. E., 1996. Rheology of partially molten mantle rocks. Annual review of Earth and Planetary Sciences 24, 41-62.

Kuhn et al., 2004. The hydrothermal field - revisited: preliminary results of the R/V Meteor cruise hydromar I (M60/3). Interridge News 13, 1-4.

Lagabrielle, Y., Bideau, D., Cannat, M., Karson, J. A., and Mével, C., 1998. Ultramafic-mafic plutonic rock suites exposed along the mid-Atlantic ridge (10°N-30°N). Symmetrical-asymmetrical distribution and implications for seafloor spreading processes. Faulting and magmatism at mid-ocean ridges Geophysical Monograph 106, 153-176.

Lamarche, G., Collot, J.-Y., Wood, R. A., Sosson, M., Sutherland, R., and Delteil, J., 1997. The oligocene-miocene pacific australia plate boundary, south of New Zealand: Evolution from ocean spreading to strike-slip faulting. Earth and Planetary Science Letters 148, 129-139.

Leeman, W. P., Tonarini, S., Chan, L. H., and Borg, L. E., 2004. Boron and lithium isotopic variations in a hot subduction zone - the southern Washington Cascades. Chemical Geology 212, 101-124.

Li, Z.-X. A. and Lee, C.-T. A., 2006. Geochemical investigation of serpentinized oceanic lithospheric mantle in the Feather River Ophiolite, California: Implications for the recycling rate of water by subduction. Chemical Geology 235, 161-185.

Lyubetskaya, T. and Korenaga, J., 2007. Chemical composition of Earth's primitive mantle and its variance: 1. Method and results. Journal of Geophysical Research 112.

MacDonald, A. H. and Fyfe, W. S., 1985. Rate of serpentinization in seafloor environments. Tectonophysics 116, 123-135.

Marschall, H., Altherr, R., Ludwig, T., Kalt, A., Gméling, K., and Kasztovszky, Z., 2006. Partitioning and budget of Li, Be and B in high-pressure metamorphic rocks. Geochimica et Cosmochimica Acta 70, 4750-4769.

Marschall, H., Kasztovszky, Z., Gméling, K., and Altherr, R., 2005. Chemical analysis of high-pressure metamorphic rocks by PGNAA: Comparison with results from XRF and solution ICP-MS. Journal of Radioanalytical and Nuclear Chemistry 265, 339-348.

Marschall, H. R. and Ludwig, T., 2004. The low-boron contest. Minimising surface contaminiation and analysing boron concentration at the ng/g-level by secondary ion mass spectrometry. Mineralogy and Petrology 81, 265-278.

McDade, P., Blundy, J. D., and Wood, B. J., 2003. Trace element partitioning on the Tinaquillo lherzolite solidus at 1.5 GPa. Physics of the Earth and Planetary Interiors 139, 129-147.

McDonough, W. F. and Sun, S.-S., 1995. The composition of the Earth. Chemical Geology 120, 223-253.

Michael, P. J., Langmuir, C. H., Dick, H. J. B., Snow, J. E., Goldstein, S. L., Graham, D. W., Lehnert, K., Kurras, G., Jokat, W., Mühe, R., and Edmonds, H. N., 2003. Magmatic and amagmatic seafloor generation at the ultraslow-spreading Gakkel ridge, Arctic Ocean. Nature 423, 956-961.

Moll, M., Paulick, H., Suhr, G. and Bach, W., 2007. Data report: Microprobe analyses of primary phases (olivine, pyroxene, and spinel) and alteration products (serpentine, iowaite, talc, magnetite, and sulfides) in Holes 1268A, 1272A, and 1274A. In: P.B. Kelemen, E. Kikawa and D.J. Miller (Editors), Proc. ODP, Sci. Results 209. pp. 1–13.

Molnar, G. L., 2004. Handbook of prompt gamma activation analysis with neutron beams. Kluwer Academic Pubisher.

Mottl, M. J., Wheat, G. C., Fryer, P., Gharib, J., and Martin, J. B., 2004. Chemistry of springs across the Mariana forearc shows progressive devolatilization of the subducting plate. Geochimica et Cosmochimica Acta 68, 4915-4933.

Minshull, T. A., Muller, M. R., Robinson, C. J., White, R. S., and Bickle, M. J., 1998. Is the oceanic Moho a serpentinization front? In: Mills, R. A. and Harrison, K. Eds.), Modern ocean floor

processes and geological record. Geological Society, London. 148, 71-80.

Muller, M.R., Robinson, C.J., Minshull, T.A., White, R.S. and Bickle, M.J., 1997. Thin crust beneath ocean drilling program borehole 735B at the Southwest Indian Ridge? Earth and Planetary Science Letters 148, 93-107.

Müntener, O. and Piccardo, G. B., 2003. Melt migration in ophiolitic peridotites: The message from Alpine-Apennine peridotites and implications from embryonic ocean basins. In: Ophiolites in Earth History (eds Dilek, Y. and Robinson, P. T.). Geological Society of London, Special Publications 218, 69-89.

Müntener, O., Pettke, T., Desmurs, L., Meier, M., and Schaltegger, U., 2004. Refertilization of mantle peridotite in embryonic ocean basins: Trace element and Nd-isotopic evidence and implications for crust-mantle relationships. Earth and Planetary Science Letters 221, 293-308.

Niida, K., 1997. Mineralogy of MARK peridotites: replacement through magma channeling examined from hole 920D, MARK area. Proceedings of Ocean Drilling Program, Scientific Results 153, 265-275.

Niu, Y., 2004. Bulk-rock major and trace element compositions of abyssal peridotites: Implications for mantle melting, melt extraction and post-melting processes beneath mid-ocean ridges. Journal of Petrology 45, 2423-2458.

O'Hanley, D. S., 1996. Serpentinites, records of teconic and petrological history. Oxford Monographs on Geology and Geophysics 34.

Ottolini L., Bottazzi P., Vannucci R., 1993. Quantification of lithium, beryllium and boron in silicates by Secondary Ion Mass Spectrometry using conventional energy filtering. Analytical Chemistry 65, 1960-1968.

Ottolini, L., Le Fèvre, B., and Vannucci, R., 2004. Direct assessment of mantle boron and lithium contents and distribution by SIMS analyses of peridotite minerals. Earth and Planetary Science Letters 228, 19-36.

Palmer, M. R. and Swihart, G. H., 1996. Boron isotope geochemistry: an overview. Mineralogical Society of America, Washington, D.C.

Parker, R. L. and Oldenburg, D. W., 1973. Thermal model of ocean ridges. Nature Physical Science 242, 137-139.

Parkinson, I. J. and Pearce, J. A., 1998. Peridotites from the Izu-Bonin-Mariana Forearc (ODP Leg 125): Evidence for Mantle Melting and Melt-Mantle Interaction in a Supra-Subduction Zone Setting. Journal of Petrology 339, 1577-1618.

Paulick, H., Bach, W., Godard, M., De Hoog, J. C. M., Suhr, G., and Harvey, J., 2006. Geochemistry of abyssal peridotites (mid-Atlantic ridge, 15°20'N, ODP Leg 209): Implications for fluid/rock interaction in slow spreading environments. Chemical Geology 234, 179-210.

Pearce, N., Perkins, W. T., Westgate, J. A., Gorton, M. P., Jackson, S. E., Neal, C. R., and Chenery, S. P., 1997. A compilation of new and published major and trace element data for NIST SRM 610 and NIST SRM 612 glass reference materials. Geostandards Newsletter 21, 115-144.

Pelletier, L., 2008. The oceanic mantle as an important repository for the light elements Li, Be and B. Ph.D. thesis, University of Neuchâtel

Pelletier, L., Müntener, O., Kalt, A., Vennemann, T.W., Belgya, T., 2008. Emplacement of ultramafic rocks into the continental crust monitored by light and other trace elements: an example from the Geisspfad body (Swiss-Italian Alps). Chemical Geology, 255, 143-159.

Pistiner, J. S. and Henderson, G. M., 2003. Lithium-isotope fractionation during continental weathering processes. Earth and Planetary Science Letters 214, 327-339.

Plas, A., 1997. Petrologic and stable isotope constraints on fluid-rock interaction, serpentinization and alteration of oceanic ultramafic rocks. Ph. D. thesis, Swiss Federal Institute of Technology Zurich (ETH Zürich).

Prichard, H. M., 1979. A petrographic study of the process of serpentinisation in ophiolites and the ocean crust. Contributions to Mineralogy and Petrology 68, 231-241.

Quinby-Hunt, M. S. and Turekian, K. K., 1983. Distribution of elements in sea water. EOS 64, 130-132.

Ranero, C. R. and Sallarès, V., 2004. Geophysical evidence for hydration of the crust and mantle of the Nazca plate during bending at the north Chile trench. Geology 32, 549-552.

Ranero, C. R., Morgan, P. J., McIntosh, K., and Reichert, C., 2003. Bending-related faulting and mantle serpentinization at the Middle America trench. Nature 45, 367-373.

Révay, Z., Molnar, G. L., Belgya, T., Kasztovszky, Z., and Firestone, R. B., 2001. A new gamma-ray spectrum catalog and library for PGAA. Journal of Radioanalytical and Nuclear Chemistry 248, 395-399.

Ross, K. and Elthon, D., 1997. Extreme incompatible trace-element depletion of diopside in residual mantle from south of the Kane fracture zone. In: Karson, J. A., Cannat, M., Miller, D. J., and Elthon, D. Eds.), Proceedings of the ocean drilling program. 153, 277-284.

Rudnick, R. L., Tomascak, P. B., Njo, H. B., and Gardner, R. l., 2004. Extreme lithium isotopic fractionation during continental weathering revealed in saprolites from South Carolina. Chemical Geology 212, 45-57.

Ryan, J. G., 2002. Trace-element systematics of beryllium in terrestrial materials. In: Grew, E. S., Ribbe, P. H., and Rosso, J. J. Eds.), Beryllium: Mineralogy, Petrology and Geochemistry.

Mineralogical Society of America, Washington DC.

Ryan, J. G. and Langmuir, C. H., 1987. The systematics of lithium abundances in young volcanic rock. Geochimica et Cosmochimica Acta 51, 1727-1741.

Ryan, J. G. and Langmuir, C. H., 1993. The systematics of boron abundances in young volcanic rocks. Geochimica et Cosmochimica Acta 57, 1489-1498.

Salters, V. J. M. and Stracke, A., 2004. Composition of the depleted mantle. Geochemistry Geophysics Geosystems 5, 1-27.

Savov, I. P., Ryan, J. G., D'Antonio, M., and Fryer, P., 2007. Shallow slab fluid release across and along the Mariana arc-basin system: Insights from geochemistry of serpentinized peridotites from the Mariana Forearc. Journal of Geophysical Research 112, B09205, doi:10.1029/2006JB004749

Savov, I. P., Ryan, J. G., D'Antonio, M., Kelley, K., and Mattie, P., 2005. Geochemistry of serpentinized peridotites from the Mariana Forearc Conical Seamount, ODP Leg 125: Implications for the elemental recycling at subduction zones. Geochemistry Geophysics Geosystems 6, 1-24.

Scambelluri, M., Müntener, O., Ottolini, L., Pettke, T., and Vannucci, R., 2004. The fate of B, Cl and Li in the subducted oceanic mantle and in the antigorite breakdown fluids. Earth and Planetary Science Letters 222, 217-234.

Schmidt, K., Koschinsky, A., Garbe-Schönberg, D., de Carvalho, L. M., and Seifert, R., 2007. Geochemistry of hydrothermal fluids from the ultramafic-hosted hydrothermal field, 15°N on the mid-Atlantic ridge: Temporal and spatial investigation. Chemical Geology 242, 1-21.

Scotese, C. R., Gahagan, L. M., and Larson, R. L., 1988. Plate tectonic reconstructions of the Cretaceous and Cenozoic ocean basins. Tectonophysics 155, 27-48.

Seitz, H.-M. and Woodland, A. B., 2000. The distribution of lithium in peridotitic and pyroxenitic mantle lithologies - an indicator of magmatic and metasomatic processes. Chemical Geology 166, 47-64.

Seyfried Jr., W. E., Chen, X., and Chan, L. H., 1998. Trace element mobility and lithium isotope exchange during hydrothermal alteration of seafloor weathered basalt: an experimental study at 350°C, 500 bars. Geochimica et Cosmochimica Acta 62, 949-960.

Seyfried Jr., W. E. and Dibble Jr., W. E., 1980. Seawater-peridotite interaction at 300°C and 500 bars: Implications of the origin of oceanic serpentinites. Geochimica et Cosmochimica Acta 44, 309-321.

Seyler, M., Lorand, J.-P., Dick, H. J. B., and Drouin, M., 2007. Pervasive melt percolation reactions in ultra-depleted refractory harzburgites at the mid-Atlantic ridge, 15°20'N: ODP Hole 1274A. Contributions to Mineralogy and Petrology 153, 303-319.

Seyler, M., Toplis, M. J., Lorand, J.-P., Luguet, A., and Cannat, M., 2001. Clinopyroxene microtextures reveal incompletely extracted melts in abyssal peridotites. Geology 29, 155-158.

Sharapov, V. N. and Simonov, V. A., 1991. Geologic investigations in the Central Atlantic, Novosibirsk institute of geology and geophysics, siberian branch of the USSR academy of science (in Russian, 192pp.).

Shaw, D. M., Higgins, M. D., Truscott, M. G., and Middleton, T. A., 1988. Boron contaminiation in polished thin sections of meteorites: Implications for the trace-elements studies by alpha-track image or ion microprobe. American Mineralogist 73, 894-900.

Shibata, T. and Thompson, G., 1986. Peridotites from the mid-Atlantic ridge at 43°N and their petrogenetic relation to abyssal tholeiites. Contributions to Mineralogy and Petrology 93, 144-159.

Spivack, A. J. and Edmond, J., 1987. Boron isotope exchange between seawater and oceanic crust. Geochimica et Cosmochimica Acta 51, 1033-1043.

Stein, C. A. and Stein, S., 1992. A model for the global variations in oceanic depth and heat flow with lithospheric age. Nature 359, 123-129.

Stein, S. and Stein, C. A., 1996. Thermo-mechanical evolution of oceanic lithosphere: Implications for the subduction process and deep earthquakes (overview). In: Bebout, G. E., Scholl, D. W., Kirby, S. H., and Platt, J. P. Eds.), Subduction: top to bottom.

Sudarikov, S. M. and Roumiantsev, A. B., 2000. Structure of hydrothermal plumes at the vent field, 14°45'N, mid-Atlantic ridge: Evidence from geochemical and geophysical data. Journal of Volcanology and Geothermal Research 101, 245-252.

Sutherland, R., 1995. The Australia-Pacific boundary and Cenozoic plate motions in the SW Pacific: Some constraints from Geosat data. Tectonics 4, 819-831.

Takahashi, E., Uto, K., and Schilling, J. G., 1987. Primary magma compositions and Mg/Fe ratios of their mantle residues along Mid Atlantic Ridge 29°N to 73°N. Technical Report ISEI, Okayama University Ser. A, 1-14.

Taura, H., Yurimoto, H., Kurita, K., and Sueno, S., 1998. Pressure dependence on partition coefficients for trace elements between olivine and the coexisting melts. Physics and Chemistry of Minerals 25, 469-484.

Tebbens, S. F., Cande, S. C., Kovacs, L., Parra, J. C., LaBrecque, J. L., and Vergara, H., 1997. The Chile ridge: a tectonic framework. Journal of Geophysical Research 102, 12035-12060.

Tenthorey, E. and Hermann, J., 2004. Composition of fluids during serpentinite breakdown in subduction zones: Evidence for limited boron mobility. Geology 32, 865-868.

The MELT seismic team, 1998. Imaging the deep seismic structure beneath a mid-ocean ridge: The MELT experiment. Science 280, 1215-1218.

Thompson, G. and Melson, W. G., 1970. Boron contents of serpentinites and metabasalts in the oceanic crust: Implications for the boron cycle in the oceans. Earth and Planetary Science Letters 8, 61-65.

Tucholke, B. E., Lin, J., and Kleinrock, M. C., 1998. Megamullions and mullion structure defining oceanic metamorphic core complexes on the mid-Atlanic ridge. Journal of Geophysical Research 103, 9857-9866.

Ulmer, P. and Trommsdorff, V., 1995. Serpentine stability to mantle depths and subduction-related magmatism. Science 268, 858-861.

Ulmer, P. and Trommsdorff, V., 1999. Phase relations of hydrous mantle subducting to 300 km. In: Fei, Y., Bertka, C. M. & Mysen, B. O. (eds.) Mantle petrology: Field observations and high pressure experimentation: A tribute to Francis R. (Joe) Boyd: The Geochemical Society, Special Publication No. 6, 259-281.

Vils, F., Tonarini, S., Seitz, H.-M., Kalt, A., and Pelletier, L., 2008. Are Li, B and Sr-isotopes tracers for serpentinization? Geochimica et Cosmochimica Acta 72, A985.

Viti, C., Mellini, M., and Rumori, C., 2005. Exsolution and hydration of pyroxenes from partially serpentinized harzburgites. Mineralogical Magazine 69, 491-507.

Wei, W., Kastner, M., Dehyle, A., and Spivack, A. J., 2005. Geochemical cycling of fluorine, chlorine, bromine, boron and implications for fluid-rock reactions in Mariana forarc, South Chamorro Seamount, ODP Leg 195. Proceedings of Ocean Drilling Program, Scientific Results 195, 1-23.

Wenner, D. B. and Taylor, H. P. J., 1971. Temperatures of serpentinization of ultramafic rocks based on O^{18}/O^{16} fractionation between coexisting serpentine and magnetite. Contributions to Mineralogy and Petrology 32, 165-185.

Wicks, F. J. and Whittaker, E. J. W., 1977. Serpentine textures and serpentinization. Canadian Mineralogist 15, 459-488.

Woodland, A. B., Seitz, H.-M., and Yaxley, G. M., 2004. Varying behavior of Li in metasomatised spinel peridotite xenoliths from western Victoria, Australia. Lithos 75, 55-66.

Wunder, B., Meixner, A., Romer, R. L., and Heinrich, W., 2006. Temperature-dependent isotopic fractionation of lithium between clinopyroxene and high-pressure hydrous fluids. Contributions to Mineralogy and Petrology 151, 112-120.

Wunder, B., Meixner, A., Romer, R. L., Wirth, R., and Heinrich, W., 2005. The geochemical cycle of boron: Constraints from boron isotope partitioning experiments between mica and fluid. Lithos 84, 206-216.

Zack, T., Foley, S. F., and Rivers, T., 2002. Equilibrium and disequilibrium trace element partitioning in hydrous eclogites (Trescolmen, Central Alps). Journal of Petrology 43, 1947-1974.

Zanetti, A., D'Antonio, M., Spadea, P., Raffone, N., and Vannucci, R., 2006. Petrogenesis of mantle peridotites from the Izu-Bonin-Mariana (IBM) Forearc. Ofioliti 31, 189-206.

3c (*continued*)

Mineral	Orthopyroxene (normalized to 6 oxygens)																
Sample	OD 22 o22z3op2	OD 26 o26c2op1	OD 28 o28c1op7	OD 28 o28c2op1	OD 29 o29c2op1	OD 32 dp32op1	OD 32 dp32op1	OD 34 dp34op1	OD 34 dp34op3b	OD 38 dp38opc1	OD 38 dp38opc3	OD 42 42op2	OD 42 42op7	OD 48 48op1	OD 48 48op2	OD 48 48op5b	OD 52 odp52op4
SiO_2	56.08	55.47	55.39	55.75	56.09	56.41	56.74	54.88	56.16	55.79	56.58	56.03	55.62	56.09	55.59	56.73	56.12
TiO_2	<0.01	0.02	<0.01	0.01	0.01	0.01	0.03	0.02	0.02	0.03	0.01	<0.01	0.04	0.07	0.06	0.05	0.05
Cr_2O_3	0.80	0.68	0.73	0.86	0.66	0.86	2.17	0.66	0.86	0.82	1.05	2.44	2.54	2.66	2.82	2.08	0.87
Al_2O_3	2.13	2.10	2.24	2.22	2.29	0.77	0.44	3.05	2.80	3.40	2.96	0.78	0.76	0.86	0.84	0.51	2.57
FeO	6.38	5.47	5.52	5.52	5.25	6.13	6.21	5.12	5.14	5.64	0.00	5.63	6.03	5.31	5.63	5.77	5.16
MnO	0.13	0.12	0.14	0.09	0.17	0.15	0.13	0.13	0.18	0.13	6.01	0.18	0.19	0.11	0.10	0.18	0.06
NiO	0.10	0.14	0.12	0.08	0.13	0.06	0.08	0.09	0.08	0.13	0.03	0.10	0.10	0.13	0.15	0.06	0.15
MgO	33.49	34.68	34.20	34.14	32.62	33.73	34.65	32.95	33.68	32.07	0.18	33.58	33.62	33.47	33.82	34.55	33.53
CaO	1.76	1.50	2.01	1.63	2.75	1.67	0.99	1.80	1.14	2.01	32.69	1.71	1.42	1.86	1.29	0.88	1.34
Na_2O	<0.01	<0.01	0.01	<0.01	<0.01	<0.01	0.01	<0.01	<0.01	0.01	1.48	0.01	0.01	0.04	0.01	<0.01	0.03
K_2O	<0.01	0.01	<0.01	0.01	<0.01	0.01	0.02	<0.01	<0.01	<0.01	0.02	0.01	<0.01	<0.01	0.01	0.03	0.01
Total	100.86	100.19	100.38	100.30	100.26	101.66	101.47	98.70	100.06	100.03	101.02	100.47	100.33	100.60	100.32	100.84	99.88
Si	1.932	1.917	1.914	1.924	1.939	1.936	1.946	1.920	1.934	1.929	1.938	1.941	1.934	1.940	1.930	1.952	1.937
Ti	0.000	0.000	0.000	0.000	0.000	0.000	0.001	0.001	0.001	0.001	0.000	0.000	0.001	0.002	0.002	0.001	0.001
Cr	0.022	0.019	0.020	0.023	0.026	0.074	0.059	0.018	0.023	0.022	0.028	0.067	0.070	0.073	0.077	0.057	0.024
Al	0.087	0.086	0.091	0.090	0.093	0.031	0.018	0.126	0.114	0.139	0.0120	0.032	0.031	0.035	0.034	0.021	0.104
Fe	0.184	0.158	0.160	0.159	0.152	0.176	0.178	0.150	0.148	0.163	0.172	0.163	0.175	0.154	0.163	0.166	0.149
Mn	0.004	0.004	0.004	0.003	0.005	0.004	0.004	0.004	0.005	0.004	0.001	0.005	0.006	0.003	0.003	0.005	0.002
Ni	0.003	0.004	0.003	0.002	0.003	0.002	0.002	0.003	0.002	0.004	0.005	0.003	0.003	0.004	0.004	0.002	0.004
Mg	1.719	1.787	1.761	1.756	1.681	1.726	1.771	1.718	1.728	1.653	1.669	1.734	1.742	1.725	1.750	1.772	1.725
Ca	0.065	0.056	0.074	0.060	0.102	0.061	0.036	0.067	0.042	0.074	0.054	0.063	0.053	0.069	0.048	0.032	0.049
Na	0.000	0.000	0.001	0.000	0.000	0.000	0.001	0.000	0.000	0.001	0.002	0.001	0.001	0.003	0.001	0.000	0.002
K	0.000	0.000	0.000	0.000	0.000	0.000	0.001	0.000	0.000	0.000	0.000	0.000	0.000	0.000	0.000	0.001	0.000
Cat	4.014	4.030	4.030	4.019	4.001	4.011	4.016	4.007	3.997	3.990	3.989	4.010	4.015	4.006	4.013	4.009	3.998
Mg#	0.90	0.92	0.92	0.92	0.92	0.91	0.91	0.92	0.92	0.91	0.91	0.91	0.91	0.92	0.91	0.91	0.92

3b (*continued*)

Mineral	Clinopyroxene (normalized to 6 oxygens)																
Sample	OD 26 o26c5cp2c	OD 28 o28c2cp2c	OD 29 o29c1cp2c	OD 38 dp38cpc9	OD 32 dp32cpc1	OD 32 dp32cpc1	OD 32 dp32cpc1	OD 32 dp32cpc1	OD 32 dp32cpx2	OD 32 dp32cpx5	OD 34 odp34cpi3	OD 42 42cpr1	OD 42 42cpr3	OD 42 42cp3b	OD 48 48cp5	OD 48 48cp6	OD 52 odp52cp1
SiO_2	52.00	52.43	53.30	52.86	51.94	52.22	51.35	53.69	52.92	52.72	52.36	52.77	52.85	52.93	52.34	52.50	52.60
TiO_2	0.05	0.01	0.03	0.04	0.01	0.06	0.02	0.06	0.04	0.05	0.03	0.05	0.05	0.04	0.14	0.13	0.13
Cr_2O_3	1.32	1.21	1.04	1.16	1.58	1.55	1.61	0.57	1.18	1.24	1.45	2.92	3.28	3.21	1.40	1.13	1.57
Al_2O_3	3.11	2.77	2.65	3.83	4.11	4.00	4.31	1.86	3.45	3.53	3.40	1.3	1.20	1.35	3.44	2.99	3.47
FeO	2.20	2.67	2.72	2.66	2.74	2.75	2.86	2.55	2.62	2.60	2.22	1.93	2.28	2.44	2.25	2.17	2.26
MnO	0.10	0.07	0.06	0.00	0.13	0.09	0.14	0.03	0.09	0.09	0.00	0.03	0.03	0.07	0.08	0.10	0.00
NiO	0.07	0.06	0.05	0.09	n.a.	n.a.	n.a.	n.a.	n.a.	n.a.	0.11	0.08	0.06	0.07	0.00	0.00	0.02
MgO	17.66	18.84	18.58	16.98	17.44	17.04	16.91	18.29	18.28	17.77	17.53	17.30	17.36	17.63	16.84	17.26	16.68
CaO	24.24	22.15	22.28	23.12	22.69	22.78	22.83	23.22	21.51	22.69	22.58	23.82	23.47	23.13	23.49	23.59	22.57
Na_2O	0.04	0.07	0.04	0.10	0.06	0.06	0.06	0.05	0.05	0.05	0.06	0.11	0.12	0.07	0.20	0.15	0.48
K_2O	<0.01	0.01	<0.01	<0.01	0.02	<0.01	0.01	<0.01	<0.01	<0.01	0.01	<0.01	0.02	<0.01	<0.01	<0.01	0.01
Total	100.78	100.28	100.75	100.84	100.72	100.55	100.10	100.32	100.14	100.74	99.75	100.14	100.72	100.94	100.18	100.02	99.80
Si	1.886	1.902	1.920	1.906	1.879	1.891	1.873	1.943	1.913	1.902	1.906	1.928	1.923	1.920	1.903	1.911	1.915
Ti	0.001	0.000	0.001	0.001	0.000	0.002	0.001	0.002	0.001	0.001	0.001	0.001	0.001	0.001	0.004	0.004	0.004
Cr	0.038	0.035	0.030	0.033	0.045	0.044	0.046	0.016	0.034	0.035	0.042	0.084	0.094	0.092	0.040	0.033	0.045
Al	0.133	0.118	0.113	0.163	0.175	0.171	0.185	0.079	0.147	0.150	0.146	0.049	0.051	0.058	0.147	0.128	0.149
Fe	0.067	0.081	0.082	0.080	0.083	0.083	0.087	0.077	0.079	0.079	0.068	0.059	0.069	0.074	0.068	0.066	0.069
Mn	0.003	0.002	0.002	0.000	0.004	0.003	0.004	0.001	0.003	0.003	0.000	0.001	0.001	0.002	0.002	0.003	0.000
Ni	0.002	0.002	0.001	0.003	n.a.	n.a.	n.a.	n.a.	n.a.	n.a.	0.003	0.002	0.002	0.002	0.000	0.000	0.001
Mg	0.955	1.018	0.998	0.913	0.94	0.92	0.92	0.9	0.98	0.96	0.951	0.942	0.941	0.953	0.91	0.94	0.905
Ca	0.942	0.861	0.860	0.893	0.880	0.884	0.892	0.900	0.833	0.877	0.881	0.933	0.915	0.899	0.915	0.920	0.880
Na	0.003	0.005	0.003	0.007	0.014	0.014	0.014	0.014	0.014	0.003	0.014	0.008	0.008	0.005	0.014	0.011	0.034
K	0.000	0.000	0.000	0.000	0.001	0.000	0.000	0.000	0.000	0.000	0.000	0.000	0.001	0.000	0.000	0.000	0.001
Cat	4.029	4.024	4.009	3.999	4.013	4.002	4.013	4.009	3.998	4.006	4.001	4.008	4.008	4.006	4.007	4.011	4.002
Mg#	0.93	0.93	0.92	0.92	0.92	0.92	0.91	0.93	0.93	0.92	0.93	0.94	0.93	0.93	0.93	0.93	0.93

(*continued on next page*)

3d (*continued*)

Mineral	Spinel (normalized to 3 cations)																
Sample	OD 2 o2c5sp3	OD 06 o6c3sp4	OD 7 o7c1sp3	OD 15 o15c4sp2	OD 18 o18c5sp2	OD 26 o26c2sp1	OD 28 32spc1	OD 29 o29c4sp1	OD 32 dp32spc2	OD 32 dp32spc	OD 42 42sp3	OD 48 48sp1	OD 48 48sp5	OD 48 48sp1b	OD 48 48sp1	OD 48 48sp7	OD 49 dp49chr1
SiO_2	0.01	<0.01	<0.01	0.03	0.04	0.12	0.15	0.04	0.04	0.04	0.04	0.01	0.03	0.04	0.01	0.02	0.00
TiO_2	0.07	0.03	0.02	0.01	0.04	<0.01	0.02	0.05	0.05	0.05	0.08	0.13	0.12	0.09	0.13	0.17	0.05
Cr_2O_3	43.65	41.63	43.93	43.00	40.51	40.62	43.73	42.83	29.07	29.52	12.23	34.55	31.5	37.25	34.55	28.77	31.38
Al_2O_3	26.36	27.04	25.48	27.03	28.91	27.77	24.84	25.90	40.23	41.35	52.58	35.07	38.85	32.40	35.07	41.00	37.18
Fe_2O_3	2.84	2.53	2.15	2.18	2.31	3.44	3.29	2.70	2.48	1.04	4.41	1.48	1.14	1.16	1.48	0.89	3.00
FeO	13.47	13.70	13.85	13.81	13.75	13.59	13.94	13.70	12.90	14.16	24.84	13.11	14.33	12.80	13.11	14.85	15.33
MnO	<0.01	0.02	0.03	<0.01	<0.01	0.26	0.31	0.39	0.09	0.06	0.11	0.03	0.11	0.07	0.03	0.07	0.10
NiO	0.13	0.14	0.12	0.11	0.10	0.12	0.13	0.10	0.14	0.11	0.09	0.16	0.10	0.15	0.16	0.12	0.09
MgO	15.16	14.63	14.44	14.79	14.99	14.91	14.38	14.38	15.44	14.89	5.86	15.87	14.66	16.30	15.87	14.08	14.36
ZnO	n.a.	n.a.	n.a.	n.a.	n.a.	n.a.	n.a.	n.a.	0.10	0.12	0.14	0.17	0.20	0.16	0.17	0.17	n.a.
Total	101.69	99.71	100.02	101.00	100.70	100.86	100.79	100.11	100.59	101.37	100.39	100.62	100.62	100.48	100.62	100.17	101.52
Si	0.000	0.000	0.000	0.001	0.001	0.004	0.004	0.001	0.001	0.001	0.001	0.000	0.001	0.001	0.000	0.001	0.000
Ti	0.001	0.001	0.000	0.000	0.001	0.000	0.000	0.001	0.001	0.001	0.002	0.003	0.003	0.002	0.003	0.004	0.001
Cr	1.017	0.986	1.046	1.007	0.943	0.949	1.038	1.018	1.007	1.017	0.485	1.168	1.071	1.244	1.168	1.009	1.076
Al	0.916	0.955	0.904	0.944	1.003	0.968	0.879	0.917	0.934	0.956	1.398	0.795	0.899	0.726	0.795	0.964	0.856
Fe_3	0.063	0.057	0.049	0.049	0.051	0.076	0.074	0.061	0.055	0.023	0.112	0.032	0.025	0.025	0.032	0.020	0.066
Fe_2	0.332	0.343	0.349	0.342	0.339	0.336	0.350	0.344	0.317	0.346	0.699	0.315	0.351	0.303	0.315	0.369	0.373
Mn	0.000	0.001	0.001	0.000	0.000	0.007	0.008	0.010	0.003	0.003	0.003	0.004	0.002	0.004	0.004	0.003	0.003
Ni	0.003	0.003	0.003	0.003	0.002	0.003	0.003	0.002	0.002	0.003	0.002	0.004	0.004	0.003	0.004	0.004	0.002
Mg	0.666	0.654	0.648	0.653	0.658	0.657	0.643	0.644	0.676	0.649	0.294	0.678	0.640	0.688	0.678	0.624	0.623
ZnO	n.a.	n.a.	n.a.	n.a.	n.a.	n.a.	n.a.	n.a.	0.002	0.002	0.003	0.004	0.005	0.004	0.004	0.004	n.a.
Cat	3.000	3.000	3.000	3.000	3.000	3.000	3.000	3.000	3.000	3.000	3.000	3.000	3.000	3.000	3.000	3.000	3.000
Mg#	0.63	0.62	0.62	0.63	0.63	0.61	0.60	0.61	0.65	0.64	0.29	0.66	0.63	0.68	0.66	0.62	0.59
Cr#	0.53	0.51	0.54	0.52	0.48	0.50	0.54	0.53	0.33	0.32	0.70	0.40	0.35	0.44	0.40	0.32	0.36

(*continued on next page*)

3e (*continued*)

Mineral	**Magnetite (normalized to 3 cations)**						
Sample	OD2	OD 6	OD 7	OD 15	OD 18	OD 42	OD 48
	o2c2mt1	o6c2sp2	o7c1mt1	o15c3mt2	odp18c4m	42sp6	48mag1
SiO_2	0.75	0.73	1.02	0.57	0.77	0.07	1.06
TiO_2	<0.01	0.02	<0.01	<0.01	<0.01	0.27	0.01
Cr_2O_3	0.01	0.02	0.51	0.02	2.30	0.08	0.02
Al_2O_3	0.01	0.01	0.02	0.00	0.00	6.55	0.00
Fe_2O_3	67.04	67.89	66.36	66.04	64.44	61.22	67.23
FeO	30.62	31.76	32.19	30.77	31.55	32.32	29.96
MnO	0.42	0.14	0.13	0.16	<0.01	<0.01	0.25
NiO	0.12	0.01	0.03	0.03	<0.01	0.09	0.04
MgO	0.45	0.09	0.09	0.06	0.20	0.25	1.24
Total	**99.43**	**100.74**	**100.39**	**97.68**	**99.27**	**100.86**	**99.89**
Si	0.029	0.028	0.039	0.023	0.030	0.003	0.040
Ti	0.000	0.001	0.000	0.000	0.000	0.007	0.000
Cr	0.000	0.001	0.015	0.001	0.070	0.002	0.001
Al	0.001	0.000	0.001	0.000	0.000	0.284	0.000
Fe^{3+}	1.941	1.945	1.906	1.954	1.870	1.694	1.922
Fe^{2+}	0.985	1.011	1.027	1.012	1.018	0.994	0.952
Mn	0.014	0.005	0.004	0.005	0.000	0.000	0.008
Ni	0.004	0.000	0.001	0.001	0.000	0.003	0.001
Mg	0.026	0.005	0.005	0.003	0.011	0.014	0.070
Cat	**3.000**	**3.000**	**3.000**	**3.000**	**3.000**	**3.000**	**3.000**

chlorite (normalized to 18 oxygens)		
Sample	OD 42	OD 42
	42ch1	42ch2
SiO_2	34.07	33.37
TiO_2	0.03	0.01
Cr_2O_3	12.78	14.10
Al_2O_3	1.21	0.48
FeO	5.05	5.26
MnO	0.02	0.00
MgO	33.38	33.11
CaO	0.02	0.01
Na_2O	0.02	0.01
K_2O	0.04	0.03
Cl	0.03	0.01
H_2O	12.52	12.51
Total	**99.17**	**98.89**
Si	3.26	3.20
Ti	0.00	0.00
Al	1.44	1.59
Cr	0.09	0.04
Fe	0.40	0.42
Mn	0.00	0.00
Mg	4.76	4.73
Ca	0.00	0.00
Na	0.00	0.00
K	0.00	0.00
Cl	0.00	0.00
H	8.00	8.00
Cat	**17.97**	**17.99**

phlogopite (normalized to 11) oxygens		
Sample	OD 42	OD 42
	42bt1	42bt2
SiO_2	41.89	43.55
TiO_2	0.19	0.23
Cr_2O_3	1.26	1.35
Al_2O_3	12.17	12.23
FeO	4.64	3.97
MnO	0.05	0.02
MgO	25.71	25.58
CaO	0.03	0.03
Na_2O	0.21	0.21
K_2O	8.37	8.35
Cl	0.03	0.07
H_2O	4.60	4.62
Total	**99.30**	**100.55**
F,Cl=O	**0.04**	**0.09**
Total	**99.26**	**100.46**
Si	2.70	2.76
Ti	0.01	0.01
Cr	0.06	0.07
Al	0.93	0.91
Fe	0.25	0.21
Mn	0.00	0.00
Mg	2.47	2.42
Ca	0.00	0.00
Na	0.03	0.03
K	0.69	0.68
Cl	0.02	0.04
H	1.98	1.96
Cat	**7.15**	**7.09**

3f (*continued*)

Mineral	Serpentine (normalized to 9 oxygens)									Serpentine matrix (normalized to 9 oxygens)						
Sample	OD 6 o6c2s13	OD 7 o7c1sr1	OD 7 o7c5sr9	OD 11 O11c2sr2	OD 18 o18c4sr25	OD 22 o22z5sr7a	OD 26 o26c3sr1	OD 28 o28c2sr4	OD 29 o29c5sr5	OD 2 o2c5sr8	OD 11 o11c5s10	OD 15 o15c1sr3	OD 15 o15c1sr10	OD 18 o18c5sr12	OD 22 o22z3sr3	OD 26 o26c3sr7
SiO_2	40.38	39.26	42.02	40.94	40.89	40.41	40.57	40.00	39.06	37.47	35.33	35.89	38.75	36.52	38.77	36.56
TiO_2	<0.01	0.01	0.01	<0.01	0.01	<0.01	<0.01	0.03	<0.01	0.03	<0.01	0.01	0.01	0.02	0.01	0.01
Cr_2O_3	0.02	0.71	0.02	<0.01	0.03	<0.01	0.01	<0.01	0.81	0.99	<0.01	0.01	0.71	<0.01	0.74	<0.01
Al_2O_3	0.03	1.20	0.24	0.07	0.11	0.95	0.64	0.89	1.48	0.60	0.23	0.28	1.77	0.36	1.77	0.26
FeO	4.85	4.82	2.83	3.30	3.87	5.31	2.58	5.49	5.70	5.89	2.93	1.86	4.69	3.03	6.31	3.81
MnO	0.11	0.14	0.01	0.05	0.01	0.05	0.09	0.12	0.15	0.09	0.07	0.05	0.13	<0.01	0.18	0.06
NiO	0.43	0.16	0.05	0.44	0.35	<0.01	<0.01	0.02	0.07	0.07	0.12	0.04	0.01	<0.01	<0.01	0.05
MgO	40.08	36.79	40.73	40.43	38.84	38.49	40.13	37.67	37.05	35.74	33.80	34.96	36.59	35.19	35.93	34.82
CaO	0.02	0.03	0.04	0.02	0.01	0.02	0.03	0.03	0.07	0.03	0.01	0.01	0.03	0.02	0.05	0.03
Na_2O	0.06	0.09	0.04	0.04	0.04	0.02	<0.01	0.02	<0.01	0.07	0.12	0.07	0.05	0.03	<0.01	0.01
K_2O	<0.01	0.01	<0.01	0.01	0.01	0.01	0.01	<0.01	<0.01	<0.01	0.01	<0.01	<0.01	0.01	0.01	<0.01
Cl	1.34	1.13	1.23	0.47	0.45	0.38	1.08	0.94	1.36	1.41	2.56	3.62	1.12	2.57	0.67	0.70
H_2O	12.09	11.77	12.34	12.35	12.18	12.28	12.09	11.97	11.82	11.26	9.99	9.88	11.72	10.38	11.87	10.86
Total	99.42	96.12	99.56	98.11	96.80	97.92	97.24	97.18	97.56	93.66	85.17	86.67	95.56	88.11	96.31	87.16
Cl=O	0.30	0.25	0.28	0.11	0.10	0.08	0.24	0.21	0.31	0.32	0.58	0.82	0.25	0.58	0.15	0.16
Total	99.11	95.86	99.28	98.01	96.70	97.83	96.99	96.97	97.27	93.34	84.59	85.85	95.31	87.54	96.15	87.01
Si	1.947	1.953	1.991	1.970	1.995	1.959	1.967	1.965	1.926	1.934	1.991	1.992	1.936	1.986	1.930	1.987
Ti	0.000	0.000	0.000	0.000	0.000	0.000	0.000	0.001	0.000	0.001	0.000	0.000	0.000	0.001	0.000	0.000
Cr	0.001	0.028	0.001	0.000	0.001	0.000	0.000	0.000	0.032	0.040	0.000	0.000	0.028	0.000	0.029	0.000
Al	0.002	0.070	0.013	0.004	0.006	0.054	0.037	0.051	0.086	0.036	0.015	0.018	0.104	0.023	0.104	0.017
Fe	0.196	0.200	0.112	0.133	0.158	0.215	0.105	0.225	0.235	0.254	0.138	0.086	0.196	0.138	0.263	0.173
Mn	0.004	0.006	0.000	0.002	0.000	0.002	0.004	0.005	0.006	0.004	0.003	0.002	0.006	0.000	0.008	0.003
Ni	0.017	0.006	0.002	0.017	0.014	0.000	0.000	0.001	0.003	0.003	0.005	0.002	0.000	0.000	0.000	0.002
Mg	2.881	2.727	2.877	2.899	2.824	2.781	2.900	2.757	2.723	2.749	2.840	2.892	2.725	2.852	2.666	2.820
Ca	0.001	0.002	0.002	0.001	0.001	0.001	0.002	0.002	0.004	0.002	0.001	0.0010	0.001	0.001	0.002	0.001
Na	0.006	0.009	0.004	0.004	0.004	0.002	0.000	0.002	0.000	0.007	0.013	0.008	0.004	0.003	0.000	0.001
K	0.000	0.001	0.000	0.001	0.001	0.000	0.000	0.000	0.000	0.000	0.001	0.000	0.000	0.000	0.001	0.000
Cl	0.110	0.095	0.099	0.038	0.037	0.031	0.089	0.078	0.113	0.124	0.224	0.340	0.095	0.237	0.057	0.064
Cat	5.054	5.002	5.003	5.030	5.004	5.015	5.015	5.009	5.015	5.030	5.008	5.002	5.000	5.004	5.003	5.005

H_2O calculated assuming stoichiometry.

sample Site 1272A	Min	Li ug/g	sigma Li	Be µg/g	sigma Be	B ug/g	sigma B
Olivine							
ODP29C1ol1	ol	0.980	5.1%	b.d.l.	-	0.003	86%
ODP29C1ol1	ol	0.904	5.4%	b.d.l.	-	0.005	98%
ODP29C1ol2	ol	0.903	6.1%	b.d.l.	-	0.004	136%
ODP29C5olp3a	ol	0.754	5.3%	b.d.l.	-	0.003	116%
ODP29C5olp3	ol	0.602	6.6%	b.d.l.	-	0.003	105%
ODP26C3ol2	ol	0.667	7.7%	b.d.l.	-	0.004	116%
ODP26C3ol3	ol	0.677	11.3%	b.d.l.	-	0.007	122%
ODP26C3ol1	ol	0.699	8.9%	b.d.l.	-	0.025	58%
ODP28C1ol1	ol	0.525	10.5%	b.d.l.	-	0.004	116%
ODP28C3ol3	ol	0.606	6.7%	0.003	210.8%	0.010	112%
ODP28C3ol1	ol	0.545	7.4%	b.d.l.	-	0.006	82%
ODP28C5ol2	ol	0.454	8.1%	b.d.l.	-	b.d.l.	-
ODP28C5ol1	ol	0.546	6.6%	b.d.l.	-	0.005	97%
Odp6C2ol1	ol	1.039	3.5%	b.d.l.	-	0.009	108%
Odp6C2osp1	ol	0.924	5.2%	b.d.l.	-	0.015	70%
ODP2c6ol1	ol	0.498	11.1%	b.d.l.	-	0.022	74%
ODP2sol1 C1	ol	0.892	6.0%	b.d.l.	-	0.026	69%
ODP2sol3 C1	ol	0.824	6.4%	b.d.l.	-	0.027	67%
Orthopyroxene							
ODP22C4op2	opx	0.669	5.2%	b.d.l.	-	0.019	43%
ODP22C3opp1-1	opx	0.718	9.7%	b.d.l.	-	0.004	164%
ODP22C3opp1-2	opx	0.691	19.5%	0.001	129.1%	0.007	159%
ODP22C3opp1-3	opx	0.564	10.2%	b.d.l.	-	0.006	162%
ODP22C3opp1-4	opx	0.796	46.7%	0.002	206.5%	0.006	136%
ODP22C3opp1-5	opx	0.542	8.7%	b.d.l.	-	0.004	79%
ODP22C3opp1-6	opx	0.785	20.7%	b.d.l.	-	0.005	95%
ODP22C3oppr1a	opx	0.693	3.4%	b.d.l.	-	0.008	107%
ODP22C3oppr1b	opx	0.756	5.2%	b.d.l.	-	0.029	17%
ODP22C3oppr1c	opx	0.728	4.3%	b.d.l.	-	0.003	96%
ODP22C3oppr1d	opx	0.813	2.6%	b.d.l.	-	0.003	116%
ODP22C3oppr1e	opx	0.775	4.0%	b.d.l.	-	0.020	59%
ODP22C3oppr1f	opx	0.784	5.0%	b.d.l.	-	0.000	316%
ODP22C3op21	opx	0.645	4.8%	b.d.l.	-	0.003	118%
ODP22C3op14	opx	0.782	5.3%	0.004	161.0%	b.d.l.	-
ODP29C2op2	opx	0.656	7.9%	b.d.l.	-	b.d.l.	-
ODP29C2opp1-1	opx	0.707	6.3%	b.d.l.	-	0.005	90%
ODP29C2opp1-2	opx	0.792	4.5%	b.d.l.	-	0.003	105%
ODP29C2opp1-3	opx	0.850	5.3%	b.d.l.	-	b.d.l.	-
ODP29C1op3	opx	0.946	4.8%	b.d.l.	-	b.d.l.	-
ODP29C5op1	opx	0.763	4.7%	0.001	97.8%	0.017	72%
ODP29C1opp3-1	opx	0.974	3.8%	b.d.l.	-	0.005	82%
ODP29C1opp3-2	opx	0.919	4.7%	b.d.l.	-	0.005	116%
ODP29C1opp3-3	opx	0.933	6.8%	b.d.l.	-	b.d.l.	-
ODP29C1opp3-4	opx	0.914	4.7%	b.d.l.	-	0.003	142%
ODP26C4op3	opx	0.620	7.8%	b.d.l.	-	0.006	62%
ODP26C4op2	opx	0.955	3.0%	b.d.l.	-	0.013	87%
ODP26C4op1	opx	0.800	9.0%	b.d.l.	-	0.004	159%
ODP26C3op3	opx	0.716	4.9%	b.d.l.	-	0.004	117%
ODP26C3op2	opx	0.803	8.6%	b.d.l.	-	0.005	118%
ODP26C3op1	opx	0.831	6.4%	b.d.l.	-	0.007	79%
ODP28C2oppr3	opx	0.605	8.1%	b.d.l.	-	0.008	103%
ODP28C2op3	opx	0.534	7.6%	b.d.l.	-	0.005	98%
ODP28C2op2	opx	0.681	6.3%	b.d.l.	-	0.009	97%
ODP28C2op6	opx	0.613	4.2%	b.d.l.	-	0.005	152%
ODP28C1op1	opx	0.000	6.6%	b.d.l.	-	b.d.l.	-
ODP28C1op3	opx	1.001	4.1%	b.d.l.	-	0.158	13%
Clinopyroxene							
ODP29C5CP1	cpx	2.051	6.6%	b.d.l.	-	20.80	8%
ODP29C2cp4	cpx	5.413	4.3%	b.d.l.	-	0.928	14%
ODP29C2cp5	cpx	4.392	4.5%	b.d.l.	-	2.394	8%
ODP29C2cp1	cpx	2.685	1.6%	b.d.l.	-	0.740	9%
ODP28C2cp2	cpx	1.561	4.3%	b.d.l.	-	0.007	129%
ODP28C1cp5	cpx	2.141	4.6%	b.d.l.	-	0.038	39%

sample Site 1274A	Min	Li ug/g	sigma Li	Be µg/g	sigma Be	B ug/g	sigma B
Olivine							
odp32oli-1	ol	0.860	3.4%	b.d.l.	-	0.003	81.7%
odp32oli-2	ol	0.836	5.1%	b.d.l.	-	0.005	73.8%
ODP34oli1	ol	0.708	4.5%	b.d.l.	-	0.011	60.2%
ODP34oli2	ol	0.814	4.7%	b.d.l.	-	0.008	59.2%
ODP34oli3	ol	1.147	3.7%	b.d.l.	-	0.020	55.0%
ODP34oli4	ol	0.986	3.0%	b.d.l.	-	0.079	22.5%
odp38ol-1	ol	0.852	5.0%	b.d.l.	-	0.009	51.4%
odp38ol-2	ol	0.921	3.7%	0.001	101.8%	0.012	60.7%
odp38ol-3	ol	0.852	3.7%	b.d.l.	-	0.016	36.6%
odp38ol-4	ol	1.018	3.5%	b.d.l.	-	0.015	49.0%
odp38ol-5	ol	1.040	4.5%	0.001	101.9%	0.010	63.6%
odp42oli-1	ol	1.299	3.1%	b.d.l.	-	b.d.l.	-
odp42oli-2	ol	1.168	3.4%	b.d.l.	-	b.d.l.	-
odp42oli-3	ol	0.948	3.9%	b.d.l.	-	0.005	70.0%
odp42oli-4	ol	1.044	2.1%	0.001	110.7%	0.007	60.0%
odp42oli-5	ol	8.291	1.1%	0.010	29.6%	0.545	6.7%
odp48oli-1	ol	0.808	3.9%	b.d.l.	-	0.003	88.8%
odp48oli-2	ol	0.937	2.5%	0.001	152.3%	0.041	37.6%
odp48oli-3	ol	0.987	2.5%	0.001	153.1%	b.d.l.	-
odp48oli-4	ol	0.864	2.9%	b.d.l.	-	0.017	40.4%
ODP52ol1	ol	0.879	3.8%	0.001	126.5%	0.002	126.5%
ODP52ol2	ol	0.887	6.0%	0.001	77.5%	0.019	44.1%
ODP52ol3	ol	1.043	4.8%	0.001	189.7%	0.013	31.7%
ODP52olb1	ol	0.756	4.5%	b.d.l.	-	0.010	48.4%
ODP52olb2	ol	0.884	3.5%	0.001	104.4%	0.016	57.7%
Orthopyroxene							
ODP52opxb1	opx	0.638	4.6%	0.004	50.0%	0.017	45.2%
ODP52opxb2	opx	0.609	3.5%	0.004	43.2%	0.077	25.4%
ODP52opxb3	opx	0.647	4.4%	0.003	51.9%	0.011	43.4%
ODP52opxb4	opx	0.605	5.9%	0.004	46.8%	0.034	20.9%
ODP52opxc1	opx	0.682	5.2%	0.003	38.2%	0.015	56.7%
ODP52opxc2	opx	0.744	3.1%	0.003	45.6%	0.014	39.4%
ODP52opxc3	opx	0.727	5.6%	0.003	47.4%	0.016	41.4%
ODP52opxc4	opx	0.711	3.8%	0.002	77.9%	0.012	42.1%
ODP34opxb1	opx	0.596	2.3%	b.d.l.	-	0.009	40.0%
ODP34opxb2	opx	0.482	6.5%	0.001	105.5%	0.014	53.3%
ODP34opxb3	opx	0.607	6.0%	0.001	96.6%	0.053	23.3%
ODP34opxb4	opx	0.576	5.1%	b.d.l.	-	0.006	57.9%
ODP34opxc1	opx	0.672	5.8%	b.d.l.	-	0.005	90.2%
ODP34opxc2	opx	0.680	3.7%	b.d.l.	-	0.010	56.3%
ODP34opxc3	opx	0.648	4.4%	b.d.l.	-	0.007	47.2%
ODP34opxc4	opx	0.614	4.5%	b.d.l.	-	0.008	58.7%
odp38opx-1	opx	0.828	3.0%	0.001	89.9%	0.009	64.4%
odp38opx-2	opx	0.712	2.8%	0.001	142.1%	0.013	46.4%
odp38opx-3	opx	0.682	5.5%	b.d.l.	-	0.005	74.3%
odp38opx-4	opx	0.618	5.9%	b.d.l.	-	0.005	85.0%
odp42opx-1	opx	0.791	3.0%	b.d.l.	-	0.004	72.7%
odp42opx-2	opx	0.744	3.8%	b.d.l.	-	b.d.l.	-
odp48opx-1	opx	0.479	3.5%	b.d.l.	-	b.d.l.	-
odp48opx-2	opx	0.517	4.9%	b.d.l.	-	0.004	77.1%
odp48opx-3	opx	0.385	4.2%	b.d.l.	-	0.006	41.5%
odp48opx-4	opx	0.473	3.8%	b.d.l.	-	0.007	66.5%
odp32opxI-1	opx	0.610	3.4%	0.001	101.8%	0.006	61.2%
odp32opxI-2	opx	0.754	3.9%	b.d.l.	-	0.004	74.0%
odp32opxI-3	opx	0.639	4.2%	b.d.l.	-	b.d.l.	-
Clinopyroxene							
odp32cpxI-1	cpx	1.559	3.3%	b.d.l.	-	0.046	19.2%
odp32cpxI-2	cpx	1.420	4.7%	b.d.l.	-	0.100	15.5%
odp32cpxII-1	cpx	2.877	1.9%	0.001	122.3%	0.015	46.8%
odp32cpxII-2	cpx	2.517	1.8%	0.001	142.3%	0.029	22.4%
ODP34cpxc1	cpx	2.801	2.9%	0.001	115.8%	0.013	43.9%
ODP34cpxc2	cpx	1.504	3.2%	0.001	135.8%	0.022	45.5%
ODP34cpxc3	cpx	0.447	5.4%	0.001	77.5%	0.009	59.9%
ODP34cpxc4	cpx	1.309	5.0%	0.001	96.6%	0.044	29.3%
odp38cpx-3	cpx	1.504	3.4%	b.d.l.	-	0.018	50.3%
odp38cpx-4	cpx	4.601	12.1%	0.001	133.3%	0.062	29.7%
odp38cpx-5	cpx	1.663	3.2%	0.001	66.7%	0.014	43.2%

sample Site 1272A	Min	Li ug/g	sigma Li	Be µg/g	sigma Be	B ug/g	sigma B
Serpentine minerals							
ODP22C3sr15	serp	0.006	57.0%	b.d.l.	-	66.7	0.72%
ODP22C3sr3	serp	0.141	19.8%	b.d.l.	-	117.5	0.67%
ODP22C3sr1	serp	0.324	4.0%	b.d.l.	-	107.5	2.19%
ODP22C4sr4	serp	0.121	12.7%	b.d.l.	-	104.0	2.66%
ODP22C4sr6	serp	0.724	6.3%	b.d.l.	-	126.9	3.02%
ODP22C3sr1	serp	0.014	6.3%	b.d.l.	-	29.1	3.56%
ODP22C3sr4	serp	0.018	47.9%	b.d.l.	-	31.6	2.42%
ODP22C3sr5	serp	0.056	14.7%	b.d.l.	-	60.1	3.24%
ODP29C5sr3	serp	0.051	20.3%	b.d.l.	-	65.2	4.24%
ODP29C5sr5	serp	0.191	8.9%	b.d.l.	-	72.1	1.88%
ODP29C5sr7	serp	0.018	44.3%	b.d.l.	-	77.6	3.68%
ODP29C1sr1	serp	0.437	7.4%	b.d.l.	-	102.7	0.78%
ODP29C1sr2	serp	0.119	15.9%	b.d.l.	-	68.0	1.65%
ODP29C1sr3	serp	0.307	8.3%	b.d.l.	-	129.2	0.50%
ODP29C4sr2	serp	0.536	5.8%	b.d.l.	-	136.3	2.41%
ODP29C2sr5	serp	4.650	3.7%	b.d.l.	-	114.1	1.04%
ODP29C4sr4	serp	0.284	8.8%	b.d.l.	-	88.1	1.13%
ODP26C4sr3	serp	2.091	36.6%	b.d.l.	-	112.4	3.02%
ODP26C4sr2	serp	0.142	8.6%	b.d.l.	-	77.1	3.67%
ODP26C1sr3	serp	0.015	45.2%	b.d.l.	-	61.8	4.61%
ODP26C1sr7	serp	0.102	19.8%	0.005	68.7%	21.9	2.26%
ODP26C1sr11	serp	0.007	89.5%	b.d.l.	-	19.9	4.87%
ODP26C1sr10	serp	0.026	30.9%	b.d.l.	-	54.7	1.65%
ODP26C3sr2	serp	0.443	4.5%	0.001	118%	58.1	4.99%
ODP26C3sr1	serp	0.696	8.6%	0.001	116%	86.4	1.54%
ODP26C3sr9	serp	0.018	47.3%	b.d.l.	-	28.6	2.98%
ODP26C3sr3	serp	0.013	49.0%	0.001	129%	58.9	1.91%
ODP26C1sr5	serp	6.593	99.7%	0.273	316%	166.0	39%
ODP26C1sr6	serp	3.787	97.7%	0.749	217%	200.0	35%
ODP28C2sr1	serp	0.304	12.0%	b.d.l.	-	17.8	3.37%
ODP28C2sr17	serp	0.802	5.6%	b.d.l.	-	84.8	2.25%
ODP28C2sr16	serp	1.013	6.2%	0.001	117%	67.5	1.10%
ODP28C2sr15	serp	2.089	1.4%	b.d.l.	-	71.4	3.27%
ODP28C2sr20	serp	1.026	3.2%	b.d.l.	-	103.5	1.55%
ODP28C2sr5	serp	0.899	3.8%	b.d.l.	-	90.6	3.13%
ODP28C2sr4	serp	0.642	7.0%	b.d.l.	-	65.4	1.04%
ODP28C1sr1	serp	0.013	49.0%	b.d.l.	-	28.6	4.76%
ODP28C1sr8	serp	1.796	3.2%	b.d.l.	-	138.2	2.29%
ODP28C1sr3	serp	0.429	8.8%	b.d.l.	-	177.7	2.30%
ODP28C1sr11	serp	1.676	3.9%	b.d.l.	-	113.4	3.57%
ODP28C3sr2	serp	0.401	6.4%	b.d.l.	-	40.3	4.22%
ODP28C3sr3	serp	0.537	6.5%	b.d.l.	-	53.0	6.49%
ODP28C3sr6	serp	0.948	6.2%	b.d.l.	-	94.1	1.07%
ODP28C5sr1	serp	0.014	66.7%	0.001	134%	24.0	1.82%
Odp6C1sr4	serp	0.009	44.8%	b.d.l.	-	38.9	2.91%
Odp6C2sr1	serp	2.113	2.2%	b.d.l.	-	85.1	1.54%
Odp6C5sr2	serp	0.705	14.8%	b.d.l.	-	66.1	3.83%
Odp6C5sr3	serp	0.602	9.8%	b.d.l.	-	63.0	5.82%
Odp6C2sr13	serp	0.009	54.8%	b.d.l.	-	42.6	4.58%
Odp6C2sr5	serp	0.005	76.3%	b.d.l.	-	34.4	3.81%
Odp6C5sr4	serp	0.043	15.9%	b.d.l.	-	25.0	2.64%
Odp6C5sr8	serp	0.190	10.5%	b.d.l.	-	21.0	1.61%
Odp6C5sr9	serp	0.202	9.7%	b.d.l.	-	19.6	1.49%
Odp6C1sr1	serp	0.028	26.5%	b.d.l.	-	37.6	3.41%
Odp6C1sr5	serp	0.211	16.2%	b.d.l.	-	74.1	4.46%
Odp6C1sr6	serp	0.068	16.1%	b.d.l.	-	33.5	1.61%
Odp6C2sr15	serp	0.010	69.8%	b.d.l.	-	32.8	4.36%
Odp6C2sr3	serp	0.008	48.8%	b.d.l.	-	45.2	1.23%
Odp6C3sr4	serp	0.002	98.7%	b.d.l.	-	31.6	1.76%
Odp6C3sr4b	serp	0.097	35.6%	0.001	152%	66.6	0.89%
Odp6C1sr12	serp	0.005	83.3%	b.d.l.	-	59.1	1.55%
Odp6C1sr10	serp	0.007	60.7%	b.d.l.	-	48.6	1.73%
Odp6C1sr9	serp	0.006	56.0%	b.d.l.	-	73.1	1.69%
Odp6C2sr10	serp	0.056	19.8%	b.d.l.	-	82.1	1.00%
Odp6C2sr8	serp	0.089	31.2%	b.d.l.	-	50.1	6.36%
Odp6C2sr7	serp	0.005	84.8%	b.d.l.	-	40.1	2.23%
Odp7C9sr4	serp	0.117	13.7%	b.d.l.	-	48.7	1.14%
Odp7C9s2	serp	0.124	8.6%	b.d.l.	-	43.5	1.65%
Odp7C9sr5	serp	0.133	12.8%	b.d.l.	-	43.5	2.09%

sample Site 1274A	Min	Li ug/g	sigma Li	Be µg/g	sigma Be	B ug/g	sigma B
Clinopyroxene							
odp38cpx-1	cpx	1.558	3.4%	0.001	101.8%	0.032	39.3%
odp38cpx-2	cpx	1.695	2.5%	0.001	142.8%	0.810	7.5%
odp38cpx-6	cpx	1.573	3.6%	b.d.l.	-	0.052	18.7%
odp42cpx-1	cpx	1.616	2.6%	0.030	14.2%	0.029	40.8%
odp42cpx-2	cpx	1.464	3.2%	0.002	36.0%	0.037	20.9%
odp42cpx-3	cpx	2.179	2.6%	0.113	8.1%	0.221	15.1%
odp42cpx-4	cpx	2.021	2.6%	0.067	10.8%	0.124	26.5%
odp42cpx-5	cpx	2.812	2.1%	0.017	24.2%	0.139	18.9%
odp48cpx-1	cpx	1.609	11.8%	b.d.l.	-	0.015	37.6%
odp48cpx-2	cpx	1.485	3.1%	b.d.l.	-	0.041	20.9%
odp48cpx-3	cpx	1.263	2.9%	b.d.l.	-	0.007	66.6%
odp48cpx-4	cpx	1.290	2.0%	0.001	54.4%	1.878	2.7%
ODP52cpx1	cpx	1.367	3.5%	0.007	39.6%	0.026	25.0%
ODP52cpx2	cpx	1.579	4.7%	0.008	26.3%	4.417	3.5%
ODP52cpx3	cpx	1.511	4.1%	0.005	37.9%	0.014	56.8%
Serpentine minerals							
odp32ba-1	serp	0.137	6.3%	0.001	269.2%	8.51	7.1%
odp32ba-1	serp	0.137	4.0%	0.001	170.3%	8.51	4.5%
odp32ba-2	serp	0.587	2.8%	0.001	123.1%	9.53	2.8%
odp32chry-1	serp	0.181	7.7%	b.d.l.	-	0.81	2.0%
odp32chry-2	serp	0.368	7.9%	0.001	89.4%	15.54	1.5%
odp32sercp-2	serp	8.232	5.6%	0.001	133.3%	10.54	6.6%
odp32serol-1	serp	0.121	7.1%	b.d.l.	-	2.85	19.6%
odp32serol-2	serp	0.095	8.9%	b.d.l.	-	0.44	26.9%
ODP34ba1	serp	3.953	2.6%	b.d.l.	-	26.61	1.0%
ODP34ba2	serp	2.859	2.4%	0.001	96.6%	63.05	0.6%
ODP34ba3	serp	9.377	1.7%	b.d.l.	-	58.10	1.4%
ODP34chry1	serp	0.275	5.9%	0.001	189.7%	25.64	1.3%
ODP34chry2	serp	0.293	6.1%	b.d.l.	-	20.08	1.8%
ODP34chry3	serp	0.307	5.8%	0.002	84.3%	45.24	1.3%
ODP34sem1	serp	0.076	12.4%	0.001	144.5%	13.60	2.4%
ODP34sem2	serp	0.048	23.2%	b.d.l.	-	22.38	1.7%
ODP34seo1	serp	0.852	2.7%	b.d.l.	-	71.89	0.8%
ODP34seo2	serp	0.781	3.3%	0.001	96.6%	83.02	1.5%
ODP34seo3	serp	0.035	27.3%	b.d.l.	-	19.21	2.4%
odp38ba-1	serp	0.666	4.1%	0.001	152.8%	26.39	1.7%
odp38ba-2	serp	0.717	5.4%	b.d.l.	-	23.22	1.0%
odp38ba-3	serp	0.194	11.9%	b.d.l.	-	21.64	0.8%
odp38ba-4	serp	2.427	3.4%	b.d.l.	-	30.96	1.3%
odp38ba-5	serp	1.231	4.0%	b.d.l.	-	40.58	1.3%
odp38chry-1	serp	0.473	3.8%	0.002	81.7%	5.52	2.6%
odp38chry-2	serp	0.359	6.8%	0.001	106.8%	5.27	2.4%
odp38chry-3	serp	0.403	7.9%	0.004	46.8%	7.69	2.7%
odp38chry-4	serp	0.193	8.9%	0.001	89.0%	9.43	1.3%
odp38chry-5	serp	0.322	5.7%	0.002	72.8%	3.50	4.0%
odp38ser-1	serp	0.083	7.9%	b.d.l.	-	10.91	1.5%
odp38ser-2	serp	0.150	6.2%	0.001	73.5%	14.53	1.7%
odp38ser-3	serp	0.103	11.7%	0.001	101.8%	11.65	1.1%
odp38ser-4	serp	0.122	6.7%	b.d.l.	-	3.81	3.9%
odp38ser-5	serp	0.104	8.2%	b.d.l.	-	9.09	2.7%
odp42ba-1	serp	2.979	3.0%	0.010	27.6%	2.17	8.4%
odp42ba-2	serp	4.090	13.7%	0.017	35.9%	16.01	6.0%
odp42ba-3	serp	0.902	2.7%	0.016	18.8%	1.46	7.3%
odp42ba-4	serp	4.635	3.1%	0.016	21.6%	2.01	8.3%
odp42chry-1	serp	0.109	8.5%	0.001	61.2%	4.04	2.7%
odp42chry-2	serp	0.130	13.4%	0.001	136.9%	2.82	2.3%
odp42se-1	serp	0.047	8.9%	0.002	42.5%	4.28	4.7%
odp42se-2	serp	0.156	13.3%	0.006	39.3%	4.82	6.1%
odp42ser-3	serp	0.258	3.6%	0.004	27.3%	1.46	16.3%
odp42ser-4	serp	0.202	7.7%	0.003	37.8%	0.09	19.7%
odp42ser-5	serp	0.907	2.8%	0.018	19.2%	1.30	20.3%
odp48ba-1	serp	2.076	12.4%	0.001	89.2%	63.04	6.0%
odp48ba-2	serp	3.986	3.2%	b.d.l.	-	72.38	0.9%
odp48chry-1	serp	0.137	11.0%	0.001	200.0%	24.10	3.8%
odp48chry-2	serp	0.167	18.1%	0.001	97.6%	28.88	2.5%
odp48ser-1	serp	0.077	13.6%	b.d.l.	-	9.96	1.5%
odp48ser-2	serp	0.069	11.5%	b.d.l.	-	5.19	3.1%
odp48sercp-1	serp	0.486	3.9%	0.002	88.7%	67.94	0.5%

sample Site 1272A	Min	Li ug/g	sigma Li	Be µg/g	sigma Be	B ug/g	sigma B
Serpentine minerals							
Odp7C9sr6	serp	0.599	5.2%	b.d.l.	-	50.5	3.46%
Odp7C9sr7	serp	0.023	34.5%	b.d.l.	-	18.5	3.13%
Odp7C9sr1	serp	0.003	52.8%	b.d.l.	-	50.1	1.81%
Odp7C9sr8	serp	0.450	5.8%	b.d.l.	-	38.4	1.43%
Odp7C9sr12	serp	0.436	6.0%	b.d.l.	-	45.2	1.58%
Odp7C1sr11	serp	0.090	18.8%	b.d.l.	-	37.7	2.23%
Odp7C1sr14	serp	0.017	29.6%	b.d.l.	-	24.1	2.17%
Odp7C1sr3	serp	0.053	14.4%	b.d.l.	-	87.7	2.07%
Odp7C1sr1	serp	0.532	5.4%	b.d.l.	-	80.2	1.65%
Odp7C1sr8	serp	0.044	27.4%	b.d.l.	-	80.1	4.78%
Odp7C1sr7	serp	1.772	10.6%	b.d.l.	-	79.7	1.79%
Odp7C5sr3	serp	0.160	11.9%	b.d.l.	-	19.1	1.06%
Odp7C5sr4	serp	0.142	23.1%	b.d.l.	-	23.7	2.20%
Odp7C5sr6	serp	0.065	17.7%	b.d.l.	-	71.5	2.41%
Odp7C5sr2	serp	0.365	10.7%	b.d.l.	-	76.1	2.79%
Odp7C5sr11	serp	0.108	12.5%	b.d.l.	-	14.8	1.96%
Odp7C5sr8	serp	0.010	75.4%	b.d.l.	-	24.3	6.21%
Odp7C3sr8	serp	0.218	10.3%	b.d.l.	-	84.6	2.56%
Odp7C3sr6	serp	0.029	23.8%	b.d.l.	-	31.3	1.49%
Odp7C3sr1	serp	0.219	12.4%	b.d.l.	-	80.5	2.87%
Odp7C3sr4	serp	0.107	8.3%	b.d.l.	-	37.0	1.70%
Odp7C3sr11	serp	0.029	18.7%	b.d.l.	-	28.0	3.73%
Odp7C9sr9	serp	0.073	18.1%	b.d.l.	-	36.7	1.67%
Odp7C9sr10	serp	0.053	20.6%	b.d.l.	-	39.3	1.40%
Odp11C5sr6	serp	0.497	8.0%	b.d.l.	-	33.8	5.37%
Odp11C5sr8	serp	0.032	27.1%	b.d.l.	-	14.7	5.78%
Odp11C5sr9	serp	0.030	23.1%	b.d.l.	-	12.9	2.62%
Odp11C5sr11	serp	0.068	16.5%	b.d.l.	-	37.9	3.48%
Odp11C4sr10	serp	0.189	8.5%	b.d.l.	-	47.2	2.56%
Odp11C4sr4	serp	0.178	11.9%	b.d.l.	-	29.6	1.80%
Odp11C4sr3	serp	0.176	13.3%	b.d.l.	-	28.6	5.06%
Odp11C4sr8	serp	0.039	20.6%	b.d.l.	-	48.9	3.97%
Odp11C3sr1	serp	0.021	20.0%	b.d.l.	-	36.6	3.22%
Odp11C3sr4	serp	0.070	10.5%	b.d.l.	-	43.2	6.61%
Odp11C3sr6	serp	0.645	6.6%	b.d.l.	-	75.7	3.62%
Odp11C3sr5	serp	0.949	9.0%	b.d.l.	-	72.1	3.56%
Odp11C3sr7	serp	0.015	48.5%	b.d.l.	-	26.0	1.99%
Odp11C3sr7	serp	0.030	16.4%	b.d.l.	-	74.4	3.52%
Odp11C2sr4	serp	0.646	4.7%	b.d.l.	-	66.5	4.53%
Odp11C2sr5	serp	0.193	12.6%	b.d.l.	-	52.8	3.69%
Odp11C4sr2	serp	0.477	14.6%	0.002	316%	47.5	6.79%
Odp11C4sr15	serp	0.480	18.2%	0.005	161%	34.4	5.07%
Odp11C4sr11	serp	0.117	46.1%	0.005	129%	48.5	4.44%
ODp2C5sr10	serp	0.108	16.7%	b.d.l.	-	68.8	3.26%
ODP2c1sr14	serp	1.193	4.6%	b.d.l.	-	55.9	2.56%
ODP2c1sr15	serp	0.003	93.7%	b.d.l.	-	37.2	2.18%
ODP2c1sr16	serp	0.006	78.8%	b.d.l.	-	30.7	1.77%
ODP2C1sr4	serp	0.073	22.2%	b.d.l.	-	61.5	2.31%
ODp2C2sr1	serp	0.052	27.4%	b.d.l.	-	36.0	2.40%
ODp2C2sr10	serp	0.030	27.4%	b.d.l.	-	37.1	2.06%
ODp2C2sr12	serp	0.100	14.6%	b.d.l.	-	47.7	2.34%
ODp2C2sr20	serp	0.016	47.1%	b.d.l.	-	40.3	2.06%
ODp2C2sr20	serp	0.016	47.1%	b.d.l.	-	40.3	2.06%
ODp2C2sr22	serp	0.150	12.3%	b.d.l.	-	70.9	4.46%
ODp2C2sr29	serp	0.295	8.9%	b.d.l.	-	67.9	1.14%
ODp2C2sr31	serp	0.393	10.7%	b.d.l.	-	72.4	4.71%
ODp2C2sr34	serp	0.829	6.5%	b.d.l.	-	45.9	5.44%
ODp2C2sr4	serp	0.969	17.6%	0.002	109%	88.6	1.80%
ODp2C3sr1	serp	0.009	45.3%	b.d.l.	-	64.1	1.74%
ODp2C3sr19	serp	0.132	13.6%	b.d.l.	-	58.8	1.77%
ODp2C3sr2	serp	0.014	44.2%	b.d.l.	-	33.2	2.31%
ODp2C3sr21	serp	0.332	15.6%	b.d.l.	-	86.3	1.64%
ODp2C3sr7	serp	0.073	21.4%	b.d.l.	-	13.8	3.83%
ODp2C3sr8	serp	0.086	23.9%	b.d.l.	-	17.9	1.14%
ODp2C5sr1	serp	0.281	10.3%	b.d.l.	-	82.7	2.94%
ODp2C5sr11	serp	0.056	24.7%	b.d.l.	-	65.1	1.45%
ODp2C5sr15	serp	0.057	14.0%	b.d.l.	-	70.8	0.63%
ODp2C5sr2	serp	0.786	8.8%	b.d.l.	-	94.7	1.96%

sample Site 1274A	Min	Li ug/g	sigma Li	Be µg/g	sigma Be	B ug/g	sigma B
Serpentine minerals							
odp48sercp-2	serp	0.431	6.1%	0.001	66.7%	55.57	1.0%
odp48serv-1	serp	0.644	3.4%	0.001	96.6%	19.92	1.3%
odp48serv-2	serp	0.638	3.6%	0.002	82.3%	14.02	1.7%
odp49ba-1	serp	0.194	6.5%	b.d.l.	-	50.21	0.8%
odp49ba-2	serp	0.192	8.1%	b.d.l.	-	57.16	1.3%
odp49chry-1	serp	0.082	8.4%	b.d.l.	-	22.41	3.5%
odp49chry-2	serp	0.077	9.9%	0.002	90.9%	19.33	7.4%
odp49se-1	serp	0.112	13.4%	0.001	133.5%	55.53	1.4%
odp49se-2	serp	0.071	12.4%	0.001	104.5%	49.18	3.4%
odp49serc-1	serp	0.122	8.5%	0.001	81.7%	16.45	2.2%
odp49serc-2	serp	0.115	10.6%	0.002	119.8%	13.71	2.1%
odp49sercp-1	serp	0.500	12.8%	0.001	73.6%	19.50	1.5%
odp49sercp-2	serp	0.359	4.8%	0.001	110.7%	67.69	3.2%
odp49sero-1	serp	0.067	9.8%	0.003	69.0%	58.15	1.1%
odp49sero-2	serp	0.053	10.4%	b.d.l.	-	64.59	0.5%
odp49sero-3	serp	0.032	14.3%	0.001	74.4%	32.82	2.0%
odp49sero-4	serp	0.031	15.5%	0.001	129.1%	28.78	3.2%
ODP52ba1	serp	1.405	15.2%	0.004	37.3%	102.42	2.1%
ODP52ba2	serp	0.178	13.9%	0.002	58.4%	77.55	4.7%
ODP52ba3	serp	0.425	4.2%	0.006	37.6%	69.57	0.9%
ODP52chry1	serp	0.095	10.8%	b.d.l.	-	34.36	0.8%
ODP52chry2	serp	0.068	10.5%	0.001	96.6%	26.04	0.5%
ODP52chry3	serp	0.121	10.4%	b.d.l.	-	38.16	0.8%
ODP52chry4	serp	0.067	18.7%	b.d.l.	-	26.25	1.0%
ODP52seol1	serp	0.499	7.7%	b.d.l.	-	94.19	0.6%
ODP52seol2	serp	0.593	2.7%	0.001	105.1%	97.19	1.0%
ODP52seol3	serp	0.043	18.9%	0.001	126.5%	24.54	1.7%
ODP52seol4	serp	0.030	12.5%	0.001	77.5%	27.31	1.2%
ODP52seol5	serp	0.067	14.5%	b.d.l.	-	40.59	1.0%
ODP52sev1	serp	0.138	10.3%	b.d.l.	-	35.93	0.6%
ODP52sev2	serp	0.087	9.9%	b.d.l.	-	24.45	0.9%
ODP52sev3	serp	0.130	9.9%	b.d.l.	-	33.92	1.0%
ODP52sev4	serp	0.132	12.4%	0.001	105.1%	40.39	1.2%

sample Site 1272A	Min	Li ug/g	sigma Li	Be µg/g	sigma Be	B ug/g	sigma B
Serpentine minerals							
ODp2C5sr5	serp	0.049	23.8%	b.d.l.	-	21.8	1.77%
ODp2C5sr6	serp	0.072	17.0%	b.d.l.	-	18.9	6.45%
ODP2c6sr1	serp	0.030	36.4%	b.d.l.	-	41.5	2.12%
ODP15c2sr1	serp	0.021	45.9%	b.d.l.	-	31.7	7.78%
ODP15c2sr8	serp	0.115	19.7%	b.d.l.	-	58.5	1.99%
ODP15c2sr6	serp	0.060	24.7%	b.d.l.	-	54.7	2.37%
ODP15c2sr7	serp	0.188	6.7%	b.d.l.	-	76.1	1.11%
ODP15c2sr17	serp	0.311	10.0%	b.d.l.	-	37.3	1.14%
ODP15c2sr19	serp	0.306	8.6%	b.d.l.	-	32.3	3.38%
ODP15c2sr20	serp	0.045	30.3%	b.d.l.	-	27.0	1.64%
ODP15c2sr21	serp	0.061	24.7%	b.d.l.	-	28.0	1.71%
ODP15c2sr23	serp	0.614	7.0%	b.d.l.	-	81.5	2.50%
ODP15c2sr22	serp	0.483	2.7%	b.d.l.	-	84.6	4.49%
ODP15c2sr16	serp	0.009	58.4%	b.d.l.	-	32.4	1.58%
ODP15c1sr6	serp	0.005	84.8%	b.d.l.	-	35.0	1.93%
ODP15c1sr7	serp	0.004	59.5%	b.d.l.	-	31.3	1.39%
ODP15c1sr4	serp	0.003	75.9%	b.d.l.	-	30.5	2.72%
ODP15c1sr16	serp	0.801	12.1%	b.d.l.	-	93.9	2.09%
ODP15c1sr14	serp	0.626	3.4%	b.d.l.	-	86.9	1.26%
ODP15c1sr18	serp	0.002	110%	b.d.l.	-	56.9	0.79%
ODP15c1sr21	serp	0.169	11.3%	b.d.l.	-	84.8	0.73%
ODP15c1sr9	serp	0.948	6.2%	b.d.l.	-	61.6	1.74%
ODP15c1sr10	serp	0.267	14.8%	b.d.l.	-	92.5	1.26%
ODP15c4sr2	serp	0.045	22.3%	b.d.l.	-	58.0	1.30%
ODP15c4sr5	serp	0.030	31.2%	b.d.l.	-	22.6	2.94%
ODP15c4sr6	serp	0.016	39.2%	b.d.l.	-	45.0	1.80%
ODP15c4sr3	serp	0.034	36.1%	b.d.l.	-	50.6	1.61%
ODP15c4sr7	serp	0.105	20.1%	b.d.l.	-	67.2	1.80%
ODP15c4sr8	serp	1.170	27.2%	b.d.l.	-	25.1	2.91%
ODP15c4sr12	serp	0.105	25.8%	b.d.l.	-	56.3	4.11%
ODP15c3sr2	serp	0.166	13.4%	b.d.l.	-	20.3	4.43%
ODP15c3sr4	serp	0.182	18.1%	b.d.l.	-	27.7	1.11%
ODP15c3sr11	serp	1.610	5.9%	b.d.l.	-	101.5	2.06%
ODP15c3sr8	serp	0.003	101%	b.d.l.	-	60.2	1.30%
ODP15c3sr12	serp	0.225	11.0%	b.d.l.	-	67.5	1.17%
ODP18c5sr1	serp	0.199	17.3%	b.d.l.	-	75.1	1.04%
ODP18c5sr6	serp	0.091	20.4%	b.d.l.	-	82.0	5.57%
ODP18c5sr8	serp	0.050	23.1%	b.d.l.	-	64.4	1.39%
ODP18c5sr2	serp	0.009	70.5%	0.003	91%	26.6	3.57%
ODP18c5sr13	serp	0.021	21.3%	b.d.l.	-	18.0	2.18%
ODP18c5sr18	serp	0.048	27.6%	b.d.l.	-	17.7	2.62%
ODP18c5sr17	serp	0.008	73.7%	b.d.l.	-	29.5	1.83%
ODP18c5sr22	serp	0.006	59.2%	b.d.l.	-	26.6	1.36%
ODP18c3sr1	serp	0.010	55.4%	0.001	110%	22.9	6.23%
ODP18c3sr10	serp	1.388	11.2%	b.d.l.	-	56.9	3.42%
ODP18c3sr2	serp	0.030	41.5%	b.d.l.	-	16.3	2.21%
ODP18c3sr3	serp	0.028	35.8%	b.d.l.	-	16.4	2.72%
ODP18c3sr17	serp	0.038	34.2%	b.d.l.	-	24.1	1.74%
ODP18c3sr25	serp	0.053	19.8%	b.d.l.	-	47.1	8.41%
ODP18c4sr27	serp	0.041	22.1%	b.d.l.	-	69.5	1.36%
ODP18c4sr4	serp	0.017	34.1%	b.d.l.	-	38.6	1.36%
ODP18c4sr2	serp	0.019	43.6%	b.d.l.	-	62.0	1.80%
ODP18c2sr5	serp	0.621	6.5%	b.d.l.	-	88.9	3.19%
ODP18c2sr13	serp	0.025	37.0%	b.d.l.	-	26.4	1.74%
ODP18C2sr1	serp	0.128	23.4%	b.d.l.	-	61.7	2.28%
ODP18C2sr8	serp	1.497	10.7%	b.d.l.	-	83.7	1.90%
ODP18C2sr3	serp	0.095	27.6%	0.001	186%	87.1	1.99%
ODP18C5sr27	serp	0.005	104%	b.d.l.	-	24.7	1.61%
ODP18C4sr19	serp	0.018	40.2%	b.d.l.	-	40.5	1.26%
ODP18C4sr14	serp	0.308	16.3%	b.d.l.	-	78.1	1.64%

Chapter III

Boron, lithium and strontium isotopes as tracers of seawater-serpentinite interaction at mid-Atlantic ridge, ODP Leg 209

Submitted to Earth and Planetary Science Letters

ABSTRACT

Spinel harzburgites from ODP Leg 209 (Sites 1272A, 1274A) drilled at the mid-Atlantic ridge between 14°N and 16°N are highly serpentinized (50-100%), but still preserve relics of primary phases (olivine ≥ orthopyroxene >> clinopyroxene). We determined whole-rock B and Li isotope compositions in order to constrain the effect of serpentinization on $\delta^{11}B$ and $\delta^{7}Li$. Our data indicate that during serpentinization Li is leached from the rock, while B is added. The samples from ODP Leg 209 show the heaviest $\delta^{11}B$ (+29.6 to +40.52‰) and lightest $\delta^{7}Li$ (-28.46 to +7.17‰) found so far in oceanic mantle. High $^{87}Sr/^{86}Sr$ ratios (0.708536 to 0.709130) indicate moderate water/rock ratios (3 to 273, on the average 39), in line with the high degree of serpentinization observed.

Applying the known fractionation factors for $^{11}B/^{10}B$ and $^{7}Li/^{6}Li$ between seawater and silicates, serpentinized peridotite in equilibrium with seawater at conditions corresponding to those of the studied drill holes (pH: 8.2; temperature: 200°C) should have $\delta^{11}B$ of +21.52‰ and $\delta^{7}Li$ of +9.7‰. As the data from ODP Leg 209 are clearly not in line with this, we modelled a process of seawater-rock interaction where $\delta^{11}B$ and $\delta^{7}Li$ of seawater evolve during penetration into the oceanic plate. Assuming chemical equilibrium between fluid and a rock with $\delta^{11}B$ and $\delta^{7}Li$ of ODP Leg 209 samples, we obtain $\delta^{11}B$ and $\delta^{7}Li$ values of +50 to +60‰, -2 to +12‰, respectively, for the co-existing fluid. In the oceanic domain, no hydrothermal fluids with such high $\delta^{11}B$ have yet been found, but are predicted by theoretical calculations. Combining the calculated water/rock ratios with the $\delta^{7}Li$ and $\delta^{11}B$ evolution in the fluid, shows that modification of $\delta^{7}Li$ during serpentinization requires higher water/rock ratios than modification of $\delta^{11}B$.

Extremely heavy $\delta^{11}B$ in serpentinized oceanic mantle can potentially be transported into subduction zones, as the B budget of the oceanic plate is dominated by serpentinites. Extremely light $\delta^{7}Li$ is unlikely to survive as the Li budget is dominated by the oceanic crust, even at small fractions.

3.1. Introduction

At mid-ocean ridges, new oceanic crust is formed, and mantle may be exhumed at the ocean floor (e.g. Cannat, 1993; Escartin et al., 2003; Michael et al., 2003). The oceanic plate cools continuously as it moves away from the ridge. Hydrothermal activity is thought to play a major role in this cooling process and may be responsible for the discrepancies between observed and modelled heat flow values (Stein and Stein, 1992; Stein and Stein, 1996). Interaction between seawater and the oceanic plate alters the latter as secondary hydrous minerals precipitate (e.g. serpentine, chlorite, zeolites, clay or carbonate minerals). At relatively low temperatures, the light elements B and Li are preferentially incorporated in these secondary minerals (Vils et al., 2008), and fractionation of ^{11}B from ^{10}B and of ^{7}Li from ^{6}Li takes place. During its residence in the ocean, the oceanic plate can become highly enriched in these secondary minerals, containing more Li and B than unaltered mantle or crust and is isotopically distinguishable (e.g. Chan et al., 1992; Bouman et al., 2004; Elliott et al., 2004; Tomascak, 2004; Vils et al., 2008). Alteration is therefore an important parameter controlling the input of light elements and their isotopes into subduction zones (e.g. Elliott et al., 2004; Savov et al., 2005; Savov et al., 2007; Vils et al., 2008).

At temperatures < 100°C, basalts exposed on the seafloor usually take up seawater B and Li through formation of alteration phases such as clay minerals (e.g. Seyfried et al., 1984; Chan et al., 1992; Ishikawa and Nakamura, 1992; Palmer and Swihart, 1996). The isotope fractionation is in general such that the heavy isotopes (^{7}Li, ^{11}B) are partitioned into the fluid whereas the light isotopes (^{6}Li, ^{10}B) are preferentially retained in the rock (e.g. Palmer and Swihart, 1996; Tomascak et al., 2008). However, as the clay minerals equilibrate with a reservoir of heavy Li and B, they will acquire relatively high $\delta^{11}B$ and $\delta^{7}Li$ values compared to the unaltered rock. This has been shown in studies on altered basalts from the ocean floor (Chan et al., 1992; Ishikawa and Nakamura, 1992; Ishikawa and Nakamura, 1993) and by experimental equilibration of clay minerals and clay-rich sediments with seawater (e.g. Palmer et al., 1987; You et al., 1995; Vigier et al., 2008).

At temperatures above the upper stability limit of clay minerals (ca. 200°C), chlorite becomes the most important secondary hydrous mineral in basalts and serpentine in peridotite. Although these phyllosilicates can potentially accommodate Li and B in their structures, it has been documented in several instances that at elevated temperatures, Li and B are leached from basalt (e.g. Ishikawa and Nakamura, 1992; Chan et al., 1993; Seyfried et al., 1998). As the fractionation in both isotope systems decreases with increasing temperature (e.g Palmer and Swihart, 1996; Tomascak, 2004), it might be expected that hydrothermally altered basalts and peridotites have $\delta^{11}B$ and $\delta^{7}Li$ values between those of their low-temperature equivalents and seawater. However, neither the elemental partition coefficients nor the isotope fractionation is known for chlorite-seawater and serpentine-seawater.

In addition to temperature, B isotope fractionation during fluid-rock interaction is controlled by pH (Spivack and Edmond, 1987; Liu and Tossell, 2005; Boschi et al., 2008). Low pH favours trigonally over tetragonally coordinated B and hence ^{11}B increases in fluid and decreases in solid (Spivack and Edmond, 1987). This is confirmed by down-hole trends in drilled serpentine mud and clasts at the Mariana forearc, showing a decrease of $\delta^{11}B$ with depth from +25 to +10‰, with pH of the coexisting fluid increasing from 8 to 12 (Benton et al., 2001).

Against this complex background, an increasing dataset on oceanic peridotite that interacted with seawater at ridges or fracture zones shows that serpentine minerals and serpentinite are generally enriched in B during alteration (10-100 µg/g), whereas they can be enriched (up to 13.7 µg/g) or depleted (down to 0.1 µg/g) in Li (Thompson and Melson, 1970; Bonatti et al., 1984; Spivack and Edmond, 1987; Niu, 2004; Boschi et al., 2008; Vils et al., 2008) compared to the values for depleted mantle (B: 0.06 µg/g, Li: 0.7 µg/g; Salters & Stracke, 2004). Samples of serpentinized peridotites from the Atlantis Massif (Boschi et al., 2008) and from the Atlantic ocean (Spivack and Edmond, 1987; Simon et al., 2006) show heavy $\delta^{11}B$ compared to mantle peridotites (+7.0 to +25.3‰ versus -3‰; Hart et al., 1999), but the spread is large. In-situ Li and $\delta^{7}Li$ measurements on serpentine from the Southwest Indian Ridge

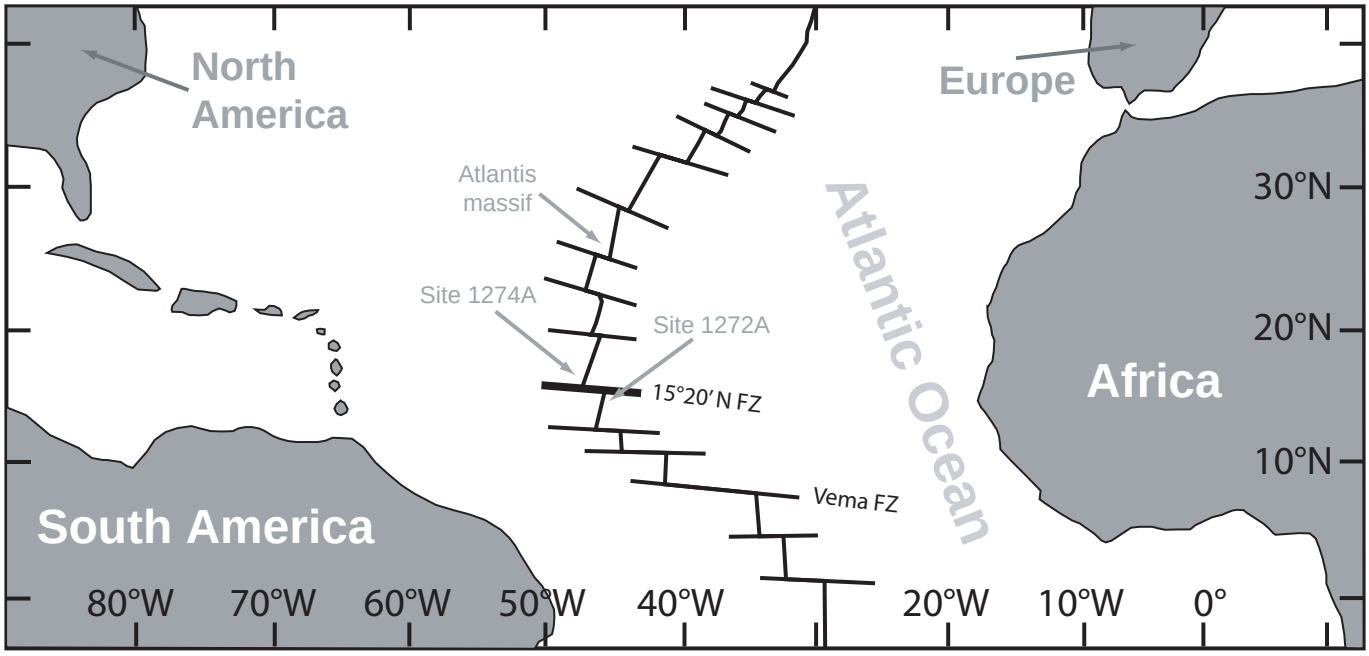

Fig. 3.1. Simplified map of the axial zone of the mid-Atlantic ridge, with situation of the ODP 209 drilling site north and south of the Fifteen-Twenty fracture zone (modified after Paulick et al., 2006). FZ fracture zone.

showed a range in $\delta^{7}Li$ from +25.5 to -19.1‰ (Decitre et al., 2002).

In order to explain the range in concentration (and isotopic composition) often found in serpentinized peridotites at one single site and displayed by fluids emerging from hydrothermal vents, several authors have invoked the importance of fluid-rock ratio and fluid evolution (Decitre et al., 2002; McCaig et al., 2007; Boschi et al., 2008). In our previous work (Vils et al., 2008) on serpentinized peridotites from ODP Leg 209 (Sites 1272A and 1274A) we showed by in-situ measurement of B and Li concentrations in minerals and whole-rock samples that during serpentinization B is taken up from seawater while Li is lost. Based on the correlation between degree of serpentinization and B and Li contents and on the absence of temperature gradients, we concluded that the B and Li budget was largely controlled by serpentinization and thus by water/rock ratios. Here, we present $\delta^{11}B$, $\delta^{7}Li$ and $^{87}Sr/^{86}Sr$ values and Li concentrations of 17 whole-rock samples from the same ODP drilling sites. We discuss the results against the background of theoretical and observed B and Li isotope fractionation during seawater-peridotite interaction and model the latter for our case.

3.2. ODP Leg 209

ODP Leg 209 was drilled at the mid-Atlantic ridge (Fig. 3.1) north and south of the Fifteen-Twenty-fracture zone (Bach et al., 2004; Kelemen et al., 2004; Kelemen et al., 2007). Samples presented in this study are serpentinized harburgites from Site 1272A and Site 1274A. The primary geochemical features of the mantle rocks at the two sites are slightly different, which is reflected in the REE patterns of whole rock samples (Godard et al., 2008), but at both sites the peridotites show high degrees of partial melting and melt extraction (Seyler et al., 2007; Godard et al., 2008; Suhr et al., 2008). The degree of serpentinization varies between 51 and 99%. The rocks of Site 1272A are generally serpentinized to a higher degree as those of Site 1274A, with a down-hole decrease of serpentinization in the former. For detailed sample descriptions, major and light element contents of minerals and B contents of whole-rock samples, we refer to our previous study (Vils et al., 2008). The samples are composed of primary phases (olivine, orthopyroxene and two generations of clinopyroxene), and serpentine (mostly lizardite; Pelletier, 2008). Sample OD 42 contains one cluster of magmatic olivine left over from a passing melt (Vils et al., 2008). Primary phases (ol, opx and cpx), except second-generation clinopyroxene, show

Table 1 Li, B and Sr isotopic and Li, B and H_20 composition of samples from ODP Leg 209

Sample	Depth [m.b.s.f.]	$\delta^{11}B$ [‰]	±2SD	$^{87}Sr/^{86}Sr$ [‰]	±2SD	n_{Sr}	B* [µg/g]	H_20* [wt%]	Li [µg/g]	±2SD	$\delta^{7}Li$ [‰]	±2SD	n_{Li}
Leg 1272A													
OD 2	61.75	+32.36	0.41	0.708954	0.000010	2	58.70	16.10	0.07	*0.00*	-28.46	*0.13*	3
OD 6	76.53	+37.64	0.71	0.708873	0.000035	1	60.30	15.40	0.10	*0.01*	-14.25	*1.37*	4
OD 6/2		+37.82	0.40	n.a.			n.a.	n.a.	n.a.		n.a.		
OD 7	80.18	+37.99	0.36	n.a.			n.a.	n.a.	0.48	*0.00*	+7.17	*0.78*	4
OD 11	89.92	+35.79	0.41	0.708792	0.000010	2	53.90	16.40	0.21	*0.00*	-4.34	*0.76*	3
OD 15	99.85	+34.09	0.43	0.709130	0.000036	1	59.30	15.10	0.20	*0.01*	+1.24	*0.89*	3
OD 15/2		n.a.		n.a.			n.a.	n.a.	0.22	*0.01*	-0.03	*1.37*	4
OD 18	110.19	+38.47	0.71	0.708599	0.000027	1	59.80	15.30	0.52	*0.11*	+2.31	*1.53*	4
OD 18/2	110.19	+39.00	0.24	n.a.			n.a.	n.a.	0.52	*0.08*	-3.37	*1.05*	5
OD 22	120.05	+35.35	0.26	0.708820	0.000123	1	65.00	15.20	0.81	*0.13*	-0.38	*0.46*	3
OD 26	125.08	+39.13	0.21	0.709064	0.000022	1	61.50	13.00	0.46	*0.04*	-3.37	*0.19*	3
OD 29	129.42	+35.00	0.33	0.708983	0.000041	2	50.30	13.80	0.57	*0.04*	-6.83	*1.47*	4
OD 29/2									0.52	*0.05*	-4.88	*1.35*	4
Leg 1274A													
OD 32	0.89	n.a.		0.708792	0.000031	2	n.a.	n.a.	1.04	*0.20*	-6.80	*1.02*	4
OD 34	17.27	+34.68	0.26	0.708548	0.000010	2	31.20	12.70	0.56	*0.08*	-16.55	*0.72*	4
OD 38	27.54	+40.66	0.19	0.708536	0.000013	2	17.50	13.10	0.56	*0.04*	-15.57	*1.06*	3
OD 42	32.14	n.a.		0.707173	0.000010	3	n.a.	13.89	3.37	*0.77*	+2.84	*1.76*	3
OD 45	36.45	+33.69	0.48	0.708070	0.000010	2	10.40	10.90	1.13	*0.19*	-1.18	*0.20*	3
OD 48	69.79	+32.24	1.12	0.708654	0.000010	3	38.50	12.20	0.90	*0.05*	-12.13	*1.51*	3
OD 48/2		+32.61	0.33	n.a.			n.a.	n.a.	n.a.		n.a.		
OD 49	94.11	+34.11	1.07	0.708748	0.000010	3	36.60	15.00	0.28	*0.06*	-4.88	*0.75*	3
OD 49/2		+34.31	0.50	n.a.			n.a.	n.a.	n.a.		n.a.		
OD 52	146.69	+29.72	0.30	0.708539	0.000017	3	n.a.	n.a.	0.87	*0.12*	-0.86	*1.25*	4

*Data published in Vils et al. (2008), except OD 45 (same analytics as Vils et al., 2008); SD=standard deviation; n number of

low Li, Be and B concentrations (< 1µg/g). Serpentine minerals are the major carrier of B (up to 177 µg/g), and second-generation clinopyroxene is the major phase for Li (up to 5.4 µg/g). No clay minerals or low-temperature phases other than serpentine are reported in the studied samples, with the exception of chlorite in OD 42 and possibly iowaiite in OD 34 (Vils et al., 2008).

3.3. Analytical methods

Prior to any chemical treatment samples were cut in small pieces and external rims were systematically removed. Dust was washed off in an ultrasonic bath in MilliQ water for 10 minutes. 2-3 cm thick slabs from the drilled samples were crushed to µm size in an agate micromill at the ETH Zurich (CH).

B isotope composition was determined using a VG Isomass 54E positive ion thermal ionization mass spectrometer at IGG-CNR in Pisa, following B extraction and purification procedures described by Tonarini et al. (2003). B isotopic compositions of the samples are reported in the conventional delta notation ($\delta^{11}B$) as per mill deviation from accepted composition of NIST-SRM 951 (certified $^{11}B/^{10}B$= 4.04362; Catanzaro et al., 1970). One analysis corresponds to 25-40 blocks of 10 individual B ratio measurements; in-run statistic is based on the block average. Accuracy of the procedure was evaluated by repeated analyses of NIST-SRM 951 standard taken through the full chemistry procedure (Table 1). Isotopic fractionation associated with the mass spectrometer analysis was corrected using a fractionation factor calculated as $[(R_{cert}+0.00079)/R_{meas}]$; $^{11}B/^{10}B_{meas}$ (NIST-SRM 951)= 4.0520±0.0016(2SD). Replicate analyses of NIST-SRM 951 that did not undergo the chemical procedure gave $^{11}B/^{10}B_{meas}$ (SRM 951)= 4.0516 ± 0.0016 (2SD, supplementary Table 1). The reproducibility of analytical results for isotopically homogeneous samples treated with alkaline fusion chemistry is approximately ± 0.5‰. Blanc measurement was 20 - 30 ng, following the same procedure.

Strontium isotope analyses were performed on a Finnigan MAT 262V multicollector mass spectrometer at IGG-CNR in Pisa, after conventional HF-HNO_3 dissolution and ion exchange procedures using Sr-SpecELChroM resins for strontium separation from the matrix. Measured $^{87}Sr/^{86}Sr$ ratios were normalized to $^{86}Sr/^{88}Sr$= 0.1194. The quoted error on single measurement is the standard deviation of the mean (2 θ mean). During the collection of isotopic data, 6 replicate analyses of NIST SRM 987 ($SrCO_3$) gave an average value of 0.710244 ± 12 (2 SD, supplementary Table 1). All $^{87}Sr/^{86}Sr$ data were normalized to a value of 0.71025 for the NIST SRM 987 standard. Two total blanks prepared during sample analysis gave values of 0.15 ng.

Rock digestion and column chemistry for Li isotopes followed the procedure of Seitz et al. (2004). 10 - 20 mg sample powder was digested in 2 ml of 1:1 HF -HNO_3 on a hot plate (140°C) for several days. Subsequently, samples were dissolved in 6M HCl and finally reconstituted in 6M HNO_3 followed by chromatographic Li purification (see Seitz et al., 2004 for details). Li isotope analyses were carried out on a Neptun (ThermoFinnigan) multiple collector inductively coupled plasma mass spectrometer (MC-ICP-MS) at the J.W. Goethe University (Frankfurt). The MC-ICP-MS allows simultaneous measurement of both ^{6}Li and ^{7}Li, performed at dry plasma conditions using a Cetac Aridus® nebuliser fitted with a PFA spray chamber and an ESI microconcentric-nebuliser with an uptake rate of 20ml/s. The sample gas was dried at 160°C before being introduced to the plasma. With the ThermoElectron standard cones (H-Cones) an intensity of 40-50 pA, 10^{11} Ω resistor (4-5 V) for ^{7}Li at a 10 ng/g concentration level is achieved. The analytical blank (chemistry blank minus background signal) on double distilled 2% HNO_3 was usually 30-20 pg (~12-20 mV on ^{7}Li). Sample analysis was carried out sequentially by 'bracketing' the sample with the L-SVEC standard (Flesch et al., 1973), followed by a blank measurement. The total integration time for each Li isotope measurement was approximately 4 min, following a baseline measurement (at masses 5.9 to 6.1 and 6.9 to 7.1, respectively) of approximately 1 min. Isotope compositions are expressed as per mil deviations from the NIST L-SVEC standard: $\delta^{7}Li=[[^{7}Li/^{6}Li]_{sample}/[^{7}Li/^{6}Li]_{L\text{-}SVEC\ standard}-1]*1000$. Internal precision is typically between 0.2 and 0.6‰ (2 sigma mean) and the long-term reproducibility, determined on replicate measurements of the geological standard JB-2, is about 1.2‰ (2SD; supplementary Table 1).

Li concentrations of samples were determined

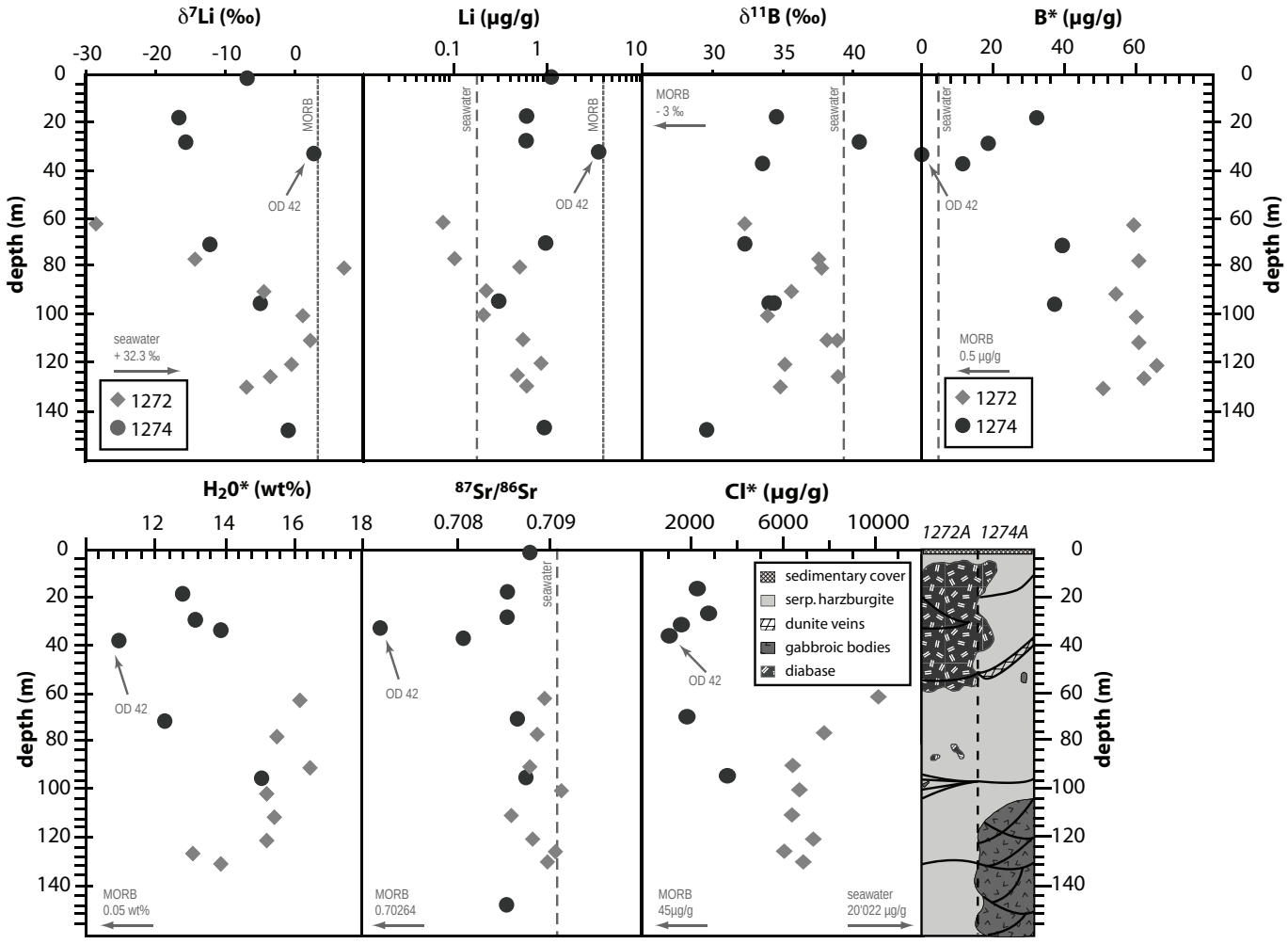

Fig. 3.2. Diagram showing δ7Li, δ11B, 87Sr/86Sr, Li, B, Cl* and H_2O* concentration versus depth for ODP Leg 209 Sites 1272A and 1274A. The data are reported in Table 2. * Data from Vils et al. (2008). Simplified lithologic log modified after Bach et al. (2004), and Vils et al. (2008). Seawater values from Palmer and Edmond (1989); Schmidt et al. (2007); mid-ocean ridge basalts (MORB) values from Edmond et al. (1979), Ryan and Langmuir (1987), Hart et al. (1999), Tomascak et al. (2008).*

along with the isotope measurements, by comparing the ion beam intensities with those of the 10 µg/g NIST L-SVEC standard solution. The uncertainty of this method was estimated by measuring international rock standards several times during a daily campaign. Daily precision of these concentration measurements was typically 10% (2 SD). Long-term reproducibility of the JB-2 basalt standard was 15% (2 SD, Seitz et al., 2004).

3.4. Analytical results

B and Li isotope data and Li concentrations of whole rock samples are reported in Table 2, completed by B, H_2O and Cl concentrations from Vils et al. (2008), and shown in Fig. 3.2 versus depth.

3.4.1. Site 1272A

87Sr/86Sr ranges from 0.708599 to 0.709130. δ11B is between +32.4 and +39.1‰ (average +36.6‰), while δ7Li varies from -28.5 to +7.2‰ (average -5.2‰).

87Sr/86Sr values are close to that of seawater (0.70916, Palmer and Edmond, 1989) and show no down-hole trend (Fig. 3.2). δ11B values show a large variation just below seawater values (+39.52‰; Smith et al., 1995). δ7Li values are far from those of seawater (+32‰; Chan et al., 1992), but more close to those of MORB (+4‰; Tomascak et al., 2008). A down-hole trend can be observed that starts with strongly negative values (-28‰), increasing to near-mantle values (+3‰) and goes back to negative values (-7‰). No systematic relationship between the three isotopic systems can be observed.

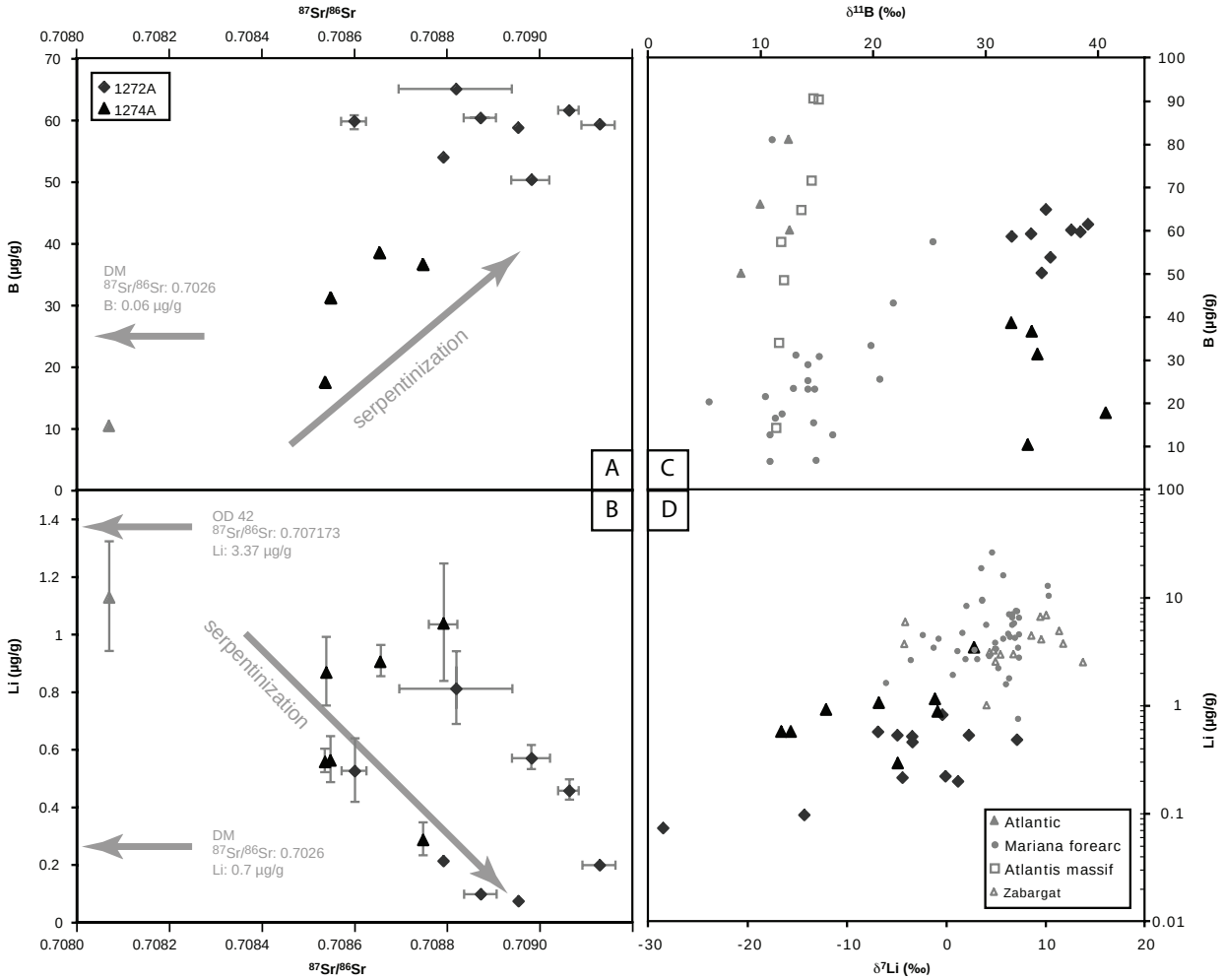

Fig. 3.3. B versus $^{87}Sr/^{86}Sr$ (A), Li versus $^{87}Sr/^{86}Sr$ (B) diagrams illustrating serpentinization, (C) $\delta^{11}B$ versus B and (D) $\delta^{7}Li$ versus Li. If no error bar visible, errors are smaller than data point. DM= depleted mantle value (after Salters and Stracke, 2004), Literature data after Spivack and Edmond (1987), Benton et al. (2001 & 2004), Brooker et al. (2004) and Boschi et al. (2008).

3.4.2. Site 1274A

$^{87}Sr/^{86}Sr$ ratio varies from 0.707173 to 0.708792 (Table 2). $\delta^{11}B$ is between +29.72 and +40.66‰ (average +34.0 ‰), while $\delta^{7}Li$ varies from -16.5 to +2.8‰ (average -7.7‰). Sample OD 42 contains a gabbroic pocket (Vils et al., 2008). This magmatic influence is reflected in lower $^{87}Sr/^{86}Sr$ ratios (0.707173), higher Li contents (3.37 µg/g) and heavier $\delta^{7}Li$ +2.84‰, while B contents (<0.2 µg/g) are lower than in average serpentinites.

$^{87}Sr/^{86}Sr$ ratios are generally close to those of seawater. $\delta^{7}Li$ starts at strongly negative values and approaches MORB values with increasing depth. $\delta^{11}B$ is close to seawater values at shallow levels and tends to decrease with depth.

3.5. Discussion of analytical results

3.5.1. Relation of the observed Li and B isotope fractionation with other chemical and isotope characteristics

In general, the analyzed samples show a narrow range of $^{87}Sr/^{86}Sr$ ratios close to the seawater value, overlapping with those of other oceanic serpentinites (Mével, 2003). The high H_2O contents and $^{87}Sr/^{86}Sr$ ratios measured indicate that the sampled peridotites have extensively interacted with seawater-derived fluid (Fig. 3.2). This process is also reflected by increasing B content and decreasing Li content with increasing $^{87}Sr/^{86}Sr$ ratios (Fig. 3.3). These observations are in line with the generally high degree of serpentinization occurring in the samples from both sites (up to 99%; Vils et al., 2008), although the rocks at Site 1272A are generally serpentinized to a higher degree.

This difference is reflected in the light element and Cl concentrations. As serpentine is the major carrier of B, H_2O and Cl, in serpentinites, the concentrations of these elements tend to higher values and scatter less at Site 1272A than at Site 1274A (Vils et al. 2008). As Li is mainly hosted by clinopyroxene, a primary mineral, Li concentrations are generally higher and scatter less at Site 1274A than at Site 1272A. Also, at Site 1272A, an overall decrease of H_2O, Cl, and B and an increase of Li with depth can be observed (Fig. 3.2), in line with the observed down-hole decrease in serpentinization (Vils et al. 2008). These observations led us to conclude that serpentinization added B to and removed Li from peridotite (Vils et al., 2008).

The B and Li isotope data presented here and their trends with B and Li concentrations (Fig. 3.3) indicate that isotope fractionation occurs during serpentinization. For Site 1274A, there is a positive correlation between Li concentrations and $\delta^{7}Li$ (Fig. 3.3). The strongly negative $\delta^{7}Li$ values and their trend towards less negative values in the uppermost part of Site 1272A are very likely due to the high degree of serpentinization (high H_2O, high $^{87}Sr/^{86}Sr$ ratios and low Li content in the sample), related to fluids entering through a fault gouge at 60 m.b.s.f. (meter below seafloor). The less negative $\delta^{7}Li$ values in the lower part of the borehole (and the higher Li concentrations) can be explained by the presence of larger fractions of clinopyroxene as the degree of serpentinization decreases from 99 to 70% and clinopyroxene occurrence increases (Vils et al., 2008). These observations indicate that during serpentinization, ^{7}Li is preferentially leached from the rocks.

There is no simple correlation between $\delta^{11}B$ and B concentration. On the average, the spread in $\delta^{11}B$ is larger and values tend to be lighter at Site 1274A (lower average degree of serpentinization) compared to Site 1272A (higher average degree of serpentinization; Figs. 3.2, 3.3). Also, when omitting the data points for sample OD42 (crosscut by a magmatic vein), $\delta^{7}Li$ and $\delta^{11}B$ show a negative correlation for Site 1274A at which relations are not complicated by a fault gouge (Fig. 3.2). These observations suggest that during serpentinization, ^{11}B is preferentially added to peridotites.

The $\delta^{11}B$ values obtained in this work (+29.7 to +40.7‰) are considerably higher than those found so far for any serpentinized oceanic peridotite (Fig. 3.3). Among the $\delta^{7}Li$ values obtained in this work (-28.5 to +7.2‰) are the most negative ones found so far for serpentinized oceanic peridotite, and our entire dataset tends to more negative values than previously found (Fig. 3.3).

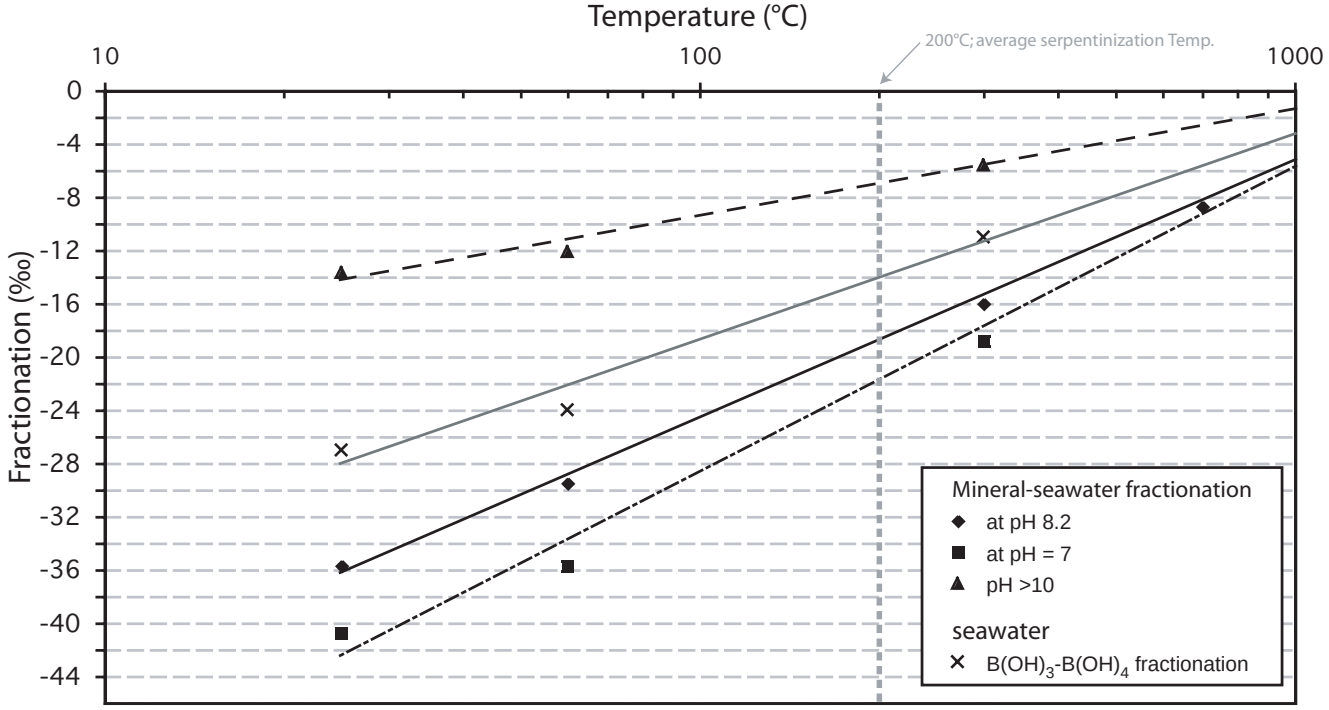

Fig. 3.4. Boron isotope fractionation versus temperature diagram (data from Liu and Tossell, 2005) showing the influence of pH on boron isotopes. Average serpentinization temperature chosen after Bonatti et al. (1984) and Bach et al. (2004).

3.5.2. Constraints on seawater-peridotite interaction for ODP Leg 209

During peridotite-seawater interaction, the observed B and Li isotope fractionation is controlled by temperature, by pH (B) and by water/rock ratio. Kakihana and Kotaka (1977) calculated the fractionation factor between BOH_3-BOH_4 in a fluid ($\alpha_{3/4}$=1.0193 at 300 K). New ab initio molecular orbital calculations for boron isotope fractionation on boric acids and borates of Liu and Tossell (2005) showed that the $B(OH)_3$-$B(OH)_4$ isotope fractionation is higher ($\alpha_{3/4}$=1.0245 at 300 K), moreover there is also a fractionation factor to consider between BOH_4 in aqueous solution and BO_4 in silicates. Combining the two fractionation factors, we obtain a data set illustrating the B isotope fractionation between seawater and silicates (≈ rock) as a function of temperature and pH (Appendix Table 1). Best-fit lines trough the calculated values are shown in Fig. 3.4. For example, assuming an average serpentinization temperature for oceanic mantle rocks of 200°C and seawater pH (8.2), we obtain $\Delta^{11}B_{silicate\text{-}seawater}$= -19‰ (Fig. 3.4).

For ODP Leg 209 Sites 1272A and 1274A, $\delta^{18}O$ isotopic composition and mineralogy indicate serpentinization temperatures between 150°C and 250°C (Bach et al., 2004; Alt et al., 2007). We consider 200°C as average serpentinization temperature at both sites. If we assume a single-stage seawater-peridotite equilibration, pH should be that of seawater (8.2). $\delta^{11}B$ values obtained in this work (+29.7 to +40.7‰) result in $\Delta^{11}B_{rock\text{-}seawater}$ values of +2 to -10‰. Using the fractionation factor of Liu and Tossell (2005) and considering a single-stage equilibrium process at 200°C, pH must have been considerably higher than 10, or, at pH of 8.2, temperature must have been between 400 and 1000°C. Moreover, Boschi et al. (2008) showed that during low-temperature seawater-rock interaction (0-25°C, pH 7.5-8.5), $\delta^{11}B$ in an equilibrated rock reaches a maximum value of +7‰. Hence, a single-stage equilibrium process, as is probably the case for weathering of peridotite on the ocean floor, is not a realistic model for seawater-peridotite interaction at Sites 1272A and 1274A.

It seems more reasonable to assume that batches of seawater penetrate into the oceanic plate and continuously evolve during interaction with the surrounding rocks (in our case peridotite). Such a process is in line with the composition of fluids emerging at oceanic hydrothermal vent sites hosted by ultramafic rocks (e.g. Li: 0.33 to 2.38 µg/g for Rainbow, Logatchev and Lost City hydrothermal fields; B: 0.34 to 3.69 µg/g for Logatchev and Lost City; Douville et al., 2002; Schmidt et al., 2007) which may be enriched or depleted in B or Li compared to seawater (0.18 µg/g Li, 4.5 µg/g B; Quinby-Hunt and Turekian, 1983; Schmidt et al., 2007). The chemical variability of such hydrothermal fluids was explained by a vent site evolution model (McCaig et al., 2007) in which single hydrothermal fields correspond to different evolution stages of low-angle detachment faults where emerging fluids interact with different rock types to different degrees (mafic and ultramafic lithologies). Hydrothermal fields have various pH (2.8 to 9.8; e.g. Kelley et al., 2001; Douville et al., 2002), depending on their solid buffer (pure ultramafic lithologies, pure basalt lithologies or mixtures of the two). Theoretical modelling of the behaviour of B during serpentinization revealed that changing pH during serpentinite formation at the Atlantic massif could be responsible for the observed $\delta^{11}B$ (Boschi et al., 2008).

Fractionation of Li isotopes does not seem to be dependent on pH, but is sensitive to temperature and pressure (Wunder et al., 2006). Pressure, however, plays no role for samples dredged or drilled from the ocean floor. Estimation of Li fractionation due to clay formation in weathered basalts ranges from -17 (4°C) to -3‰ (350°C; Chan et al., 1992; Chan et al., 1993). Recent experiments on incorporation of Li on the octahedral side of Mg-rich clay minerals showed strong temperature dependencies of Li fractionation (e.g. 200°C, $\Delta^{7}Li$= -3.6‰; Vigier et al., 2008). On serpentinites from the Southwest Indian Ridge, Decitre et al. (2002) obtained Li isotopic compositions lighter and heavier than the unaltered rocks. The authors interpreted this variation as internal recycling of Li from the hot MORB into the progressively forming serpentinites, rather than a direct exchange with seawater.

Calculation of the ocean $\delta^{7}Li$ budget by Huh et al. (1998) led to the conclusion that there needs to be a mineral phase in the oceans acting as a sink for Li, with $\Delta^{7}Li_{phase\text{-}seawater}$= -23‰. Adsorption and desorption experiments on phyllosilicates implied that

$\Delta^{7}Li_{phase\text{-}seawater}$ is > -20‰ (Zhang et al., 1998). These statements are in line with recalculation of the $\delta^{7}Li$ content of the ocean, assuming clay phases as the major Li sink, leading to $\Delta^{7}Li_{clay\text{-}seawater}$ between -12 to -21‰ (Vigier et al., 2008). As serpentine is also a phyllosilicate, fractionation factors for Li similar to those of clay minerals seem reasonable.

3.6. Modelling seawater and rock evolution during fluid-rock interaction

In the following, we model the evolution of seawater and the composition of coexisting rock in terms of $\delta^{11}B$ and $\delta^{7}Li$ values during continuous fluid-rock interaction in a closed system. Based on our previous results (Vils et al., 2008), we assume that during this process B is added to peridotite through serpentinization while Li is leached from the rock. The other parameters, e.g. $\delta^{11}B$ and $\delta^{7}Li$ values of seawater and peridotite, and fractionation factors, are given in the appendix and Table 3.2.

3.6.1. Results

In Fig. 3.5, the modeled process of fluid-rock interaction is illustrated by the stepwise evolution of a fluid batch reacting with ultramafic rocks. With each step, 10% of the fluid is adsorbed onto and integrated into the surrounding rocks. The fluid acquires increasingly heavy $\delta^{11}B$ (Figs. 3.5.A, B). The rock in equilibrium with such a fluid follows the same trend, if the fractionation factor ($\Delta^{11}B_{rock\text{-}seawater}$= -19‰) is kept constant. The influence of temperature at constant pH is shown in Fig. 3.5.A. At low reaction temperatures, fluids become more quickly enriched in ^{11}B and end up with higher $\delta^{11}B$ than at high temperatures. The influence of pH at constant temperature is shown in Fig. 3.5.B. As low pH favours the presence of trigonally coordinated B and thus ^{11}B, low-pH fluids become more quickly enriched in ^{11}B and end up with higher $\delta^{11}B$ than high-pH fluids. Figs. 3.5.A and 3.5.B show that fluids in equilibrium with rocks from ODP Leg 209 should have been isotopically heavier than seawater. Applying a fractionation of -19‰ at serpentinization temperature of 200°C on a batch of seawater (pH= 8.2), fluids in equilibrium with rocks of ODP Leg 209 should have had $\delta^{11}B$ of + 50 to +60 ‰ (Fig. 3.5.B).

Fig.3.5.C shows the evolution of $\delta^{7}Li$ in a fluid and co-existing rock during rock-water interaction. The line in Figure 3.5.C, which corresponds to seafloor weathering, does not intersect with the field outlined by samples from ODP Leg 209. Therefore, as already deduced from the B isotope systematic, seafloor weathering seems an unlikely process for the studied samples. In contrast, the line calculated using the fractionation of $\Delta^{7}Li$= -21‰ proposed by Vigier et al. (2008) intersects the data field for the ODP Leg 209 samples which have extremely light $\delta^{7}Li$. Applying a fractionation of -21‰, fluids in equilibrium with rocks of ODP Leg 209 should have had $\delta^{7}Li$ of - 2 to +12‰ (Fig. 3.5.B).

The modelling results from both isotope systems are consistent. First, they exclude that the peridotites of ODP Leg 209 were exposed to weathering at seafloor conditions during or after serpentinization. This result is in line with the conclusions from B and Li concentrations (Vils et al., 2008). Second, the model further show that the peridotites of ODP Leg 209 most likely acquired their extremely heavy $\delta^{11}B$ and their extremely light $\delta^{7}Li$ by reaction with an evolved fluid that had already exchanged 50-70% of its B and 60-80% of its Li with ultramafic rocks (Fig. 3.5).

3.6.2. Discussion

The measured isotope data are consistent with our model calculations, however, there may be alternative processes that could generate extremely heavy $\delta^{11}B$ and extremely light $\delta^{7}Li$ in serpentinized peridotites. The above-mentioned model is only valid under equilibrium conditions and closed-system behaviour. The penetrating fluid may not have been saturated in Li or B. In this case, even larger fractionation factors would have to be applied.

The modelled $\delta^{11}B$ of the fluid in equilibrium with ODP Leg 209 serpentinites tends towards higher values (+ 50 to +60 ‰) compared to those published for hydrothermal vent sites. Fluids emerging at hydrothermal fields have $\delta^{11}B$ between +10 and +37‰ (Palmer, 1991). Heavier values are reported for sediment-starved systems (+26.7 to +36.8‰) compared to sediment-hosted systems (+10.1 to +11.5‰; Palmer, 1991).

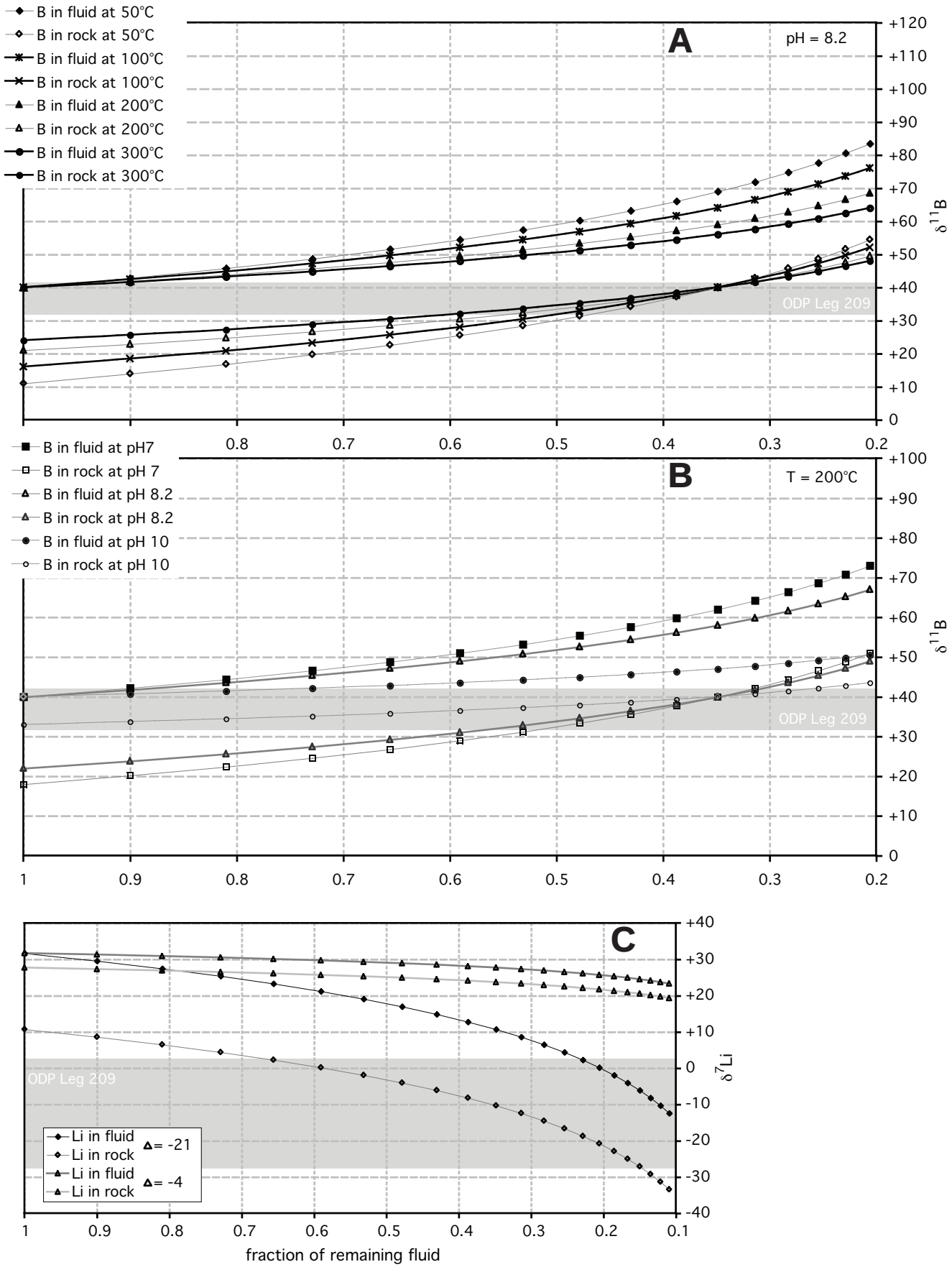

Fig. 3.5. Model of isotopic evolution of fluid and corresponding rock (in equilibrium) during closed-system stepwise fluid-rock interaction ($\delta_n=\delta(n-1)*0.1*\Delta$; n: step number). See appendix for further explanations. A: Results for $\delta^{11}B$ at different temperatures at constant pH (8.2). B: Results for $\delta^{11}B$ at different pH values at constant T (200°C). C: Results for $\delta^{7}Li$ using different fractionations (Chan et al., 1992; Vigier et al., 2008).

Table 2 Calculation of water-rock ratios

EQ 1

Leg 1272A	W/R	Ex.	*Leg 1274*	W/R	Ex.
OD 2	39	*97*	OD 32	21	*94*
OD 6	27	*96*	OD 34	12	*91*
OD 11	21	*94*	OD 38	12	*90*
OD 15	273	*100*	OD 42	3	*70*
OD 18	13	*91*	OD 45	6	*83*
OD 22	23	*95*	OD 48	15	*92*
OD 26	85	*99*	OD 49	19	*94*
OD 29	45	*97*	OD 52	12	*91*

EQ2

N (=W/R)	$(\delta^{11}B)_{w,f}$	$(\delta^{7}Li)_{w,f}$	$(^{87}Sr/^{86}Sr)_{w,f}$
0.001	16.4	25.0	0.70869
0.01	33.4	25.0	0.70892
0.1	54.6	25.0	0.70901
0.5	58.8	25.1	0.70902
1	59.4	25.2	0.70902
10	59.9	25.7	0.70903
20	60.0	25.8	0.70903
50	60.0	25.9	0.70903
100	60.0	26.0	0.70903
1000	60.0	26.0	0.70903

Input parameters		Boron	Lithium	Strontium
EQ1	c i,r (µg/g)	0.06§	0.7§	9.8§
EQ1	c i,w (µg/g)	4.5$	0.18£	7.8†
EQ1 & 2	ci,r / ci,w	0.013	3.89	1.26
EQ1 & 2	δ w,i (max)	+60*	+26*	0.70916¢
EQ1 & 2	δ w,i (min)	+51*	-8*	0.70916¢
EQ1 & 2	δ r,i	-3#	+4‘	0.703§
EQ2	Δw-r	-19*	-21*	0

EQ1 and EQ2 see text for details. N = water-rock ratio; Ex.= % of Sr-isotopic exchange; c= concentration (µg/g); i= initial; r= rock; w= fluid; δ= isotopic value or ratio; Δ= fractionation water-rock; § Salters and Stracke, 2004; $ Smith, 1995; £ Li et al., 1982; † Quint-Hunt et al., 1993;# Hart et al., 1999; ¢ Palmer and Edmond, 1989; ‘Tomascak et al., 2008; * values from Fig. 4 and 5

At the Lost City hydrothermal field (Atlantic massif), hosted by ultramafic rocks, $\delta^{11}B$ values of +25‰ are reported for end member fluids (Boschi, 2006). The results of Raleigh distillation models applied to the Lost City hydrothermal vent system predict, however, that at 100°C, initial seawater should acquire $\delta^{11}B$ of + 120‰ due to pH increase during serpentinization (Foustoukos et al., 2008). Also, at Lost City, hydrothermally precipitated aragonite (which incorporates preferably tetrahedrally coordinated B at low fractions; Sen et al., 1994; Hemming et al., 1995) has $\delta^{11}B$ up to +53‰ (Boschi, 2006), suggesting equilibration to fluids with $\delta^{11}B$ of around +71‰.

For Lost City, the discrepancy between the modelled high-^{11}B fluid composition (supported by the $\delta^{11}B$ of aragonite) and the measured fluid composition may be explained by the presence of brucite. Considerable quantities of brucite have been found at Lost City and are invoked by Boschi (2006) to be the cause of relatively low-^{11}B fluids. Based on the work of Pokrovsky et al. (2005), Foustoukos et al. (2008) suggested that brucite may preferentially incorporate trigonal B and hence lower the $\delta^{11}B$ of the coexisting fluid.

From ODP Leg 209 Sites 1272A and 1274A, brucite has been described as an accessory phase (Bach et al., 2004). Very likely, this is not sufficient to lower the $\delta^{11}B$ value of the reacting fluid. It may be more reasonable to consider our assumption of constant pH for the model as too simple. Using phase equilibria constraints, several authors (e.g. Frost and Beard, 2007) have predicted that pH should become increasingly alkaline during serpentinization reactions at very low temperatures. According to the model of Foustoukos et al. (2008), the pH effect is less pronounced at temperatures of 200°C, relevant for ODP Leg 209 samples. At these conditions, the $\delta^{11}B$ of a serpentinizing fluid would be + 50‰ (their Fig. 7), corresponding to our modelled values.

$\delta^{7}Li$ of hydrothermal fluids (Juan de Fuca ridge) ranges from +7.2 to +8.9‰, with Li content of 0.1 to 2.9 µg/g (Foustoukos et al., 2004). These data agree with our modelled fluid composition ($\delta^{7}Li$ of -2 to +12‰; Fig. 3.5.C). A similar evolution of Li in seawater through serpentinization is also invoked by Decitre et al. (2002) for serpentinites from the Southwest Indian ridge. However, their in-situ analyses of serpentine ($\delta^{7}Li$ up to +25.5‰) suggest that prior to serpentinization, fluids are heated up in the oceanic plate and doped with Li and $\delta^{7}Li$ through reaction with basalt.

3.7. Influence of water/rock ratios on B and Li isotopic composition

Similar abundances of strontium in the mantle (9.8 µg/g; Salters and Stracke, 2004) and in seawater (7.8 µg/g; Quinby-Hunt and Turekian, 1983) and the absence of fractionation of strontium isotopes during fluid-rock interaction leads to a linear mixing line between $^{87}Sr/^{86}Sr$ ratios of mantle (0.7025, Rehkamper and Hofmann, 1997) and seawater (0.7916, Palmer and Edmond, 1989). $^{87}Sr/^{86}Sr$ ratios are therefore a useful tool to quantify the fluid flow through a sample (expressed as water/rock ratio). We calculated water/rock ratios (N) for ODP Leg 209 samples assuming a closed system and a ‘single-pass-model’. We used EQ1 (Taylor, 1977; McCulloch et al., 1980), assuming $\delta_r^f = \delta_w^f - \Delta$ and for $^{87}Sr/^{86}Sr$ Δ=0. Results and input values are reported in Table 2.

$$N = \left(\frac{\delta_r^f - \delta_r^i}{\delta_w^i - \delta_w^f}\right) \times \frac{c_r^i}{c_w^i} \quad \text{(EQ1)}$$

r corresponds to rock, w to water or fluid, Δ to fractionation, f to final and i to initial. Calculation of N for ODP Leg 209 showed moderately high average N of 39. Values for Site 1272A (13 – 273) are higher than for Site 1274A (3 - 21), which is in line with the lower primary mineral content, the higher H_2O contents and the higher serpentinization degree at Site 1272A compared to Site 1274A (Vils et al., 2008). Compared to unaltered MORB (0.726; Hart et al., 1999), the serpentinites of ODP Leg 209 have exchanged a large fraction of their Sr with fluid (70-100%; $100x[^{87}Sr/^{86}Sr_{sample}-^{87}Sr/^{86}Sr_{MORB}]/[^{87}Sr/^{86}Sr_{seawater}-^{87}Sr/^{86}Sr_{MORB}]$ after Davies et al., 2003; Table 2), indicating extensive fluid-rock interaction. Similar water/rock ratios (18-234) and fractions of exchanged Sr (96-100%) were reported for Atlantis Massif serpentinites (Delacour et al., 2008). Spooner et al. (1977) and Delacour et al. (2008) concluded that during serpentinization, Sr was only locally mobilized (leached from primary minerals and precipitated in secondary minerals), and no Sr was added or removed. Similar exchange mechanisms seem to control the $^{87}Sr/^{86}Sr$ ratios of altered oceanic crust (e.g. Spooner et al., 1977).

Li, B and Sr isotope systematics from ODP Leg 209 indicate extensive seawater interaction, and the closed-system calculation showed high water-rock ratios (Table 2), which is in line with the high H_2O content of the samples (Vils et al., 2008). In hydrothermal systems at mid-ocean ridges, fluid-rock interaction is continuous. Nevertheless, emerging fluids at hydrothermal vent sites show highly variable Sr contents and $^{87}Sr/^{86}Sr$ ratios (3.5-24 µg/g; 0.70279 - 0.70997, respectively; Albarède et al., 1981; Palmer and Edmond, 1989). During its passage through the rock column, seawater continuously exchanges elements with the surrounding rock and hence changes its isotopic composition. As shown above, the $\delta^{11}B$ and $\delta^{7}Li$ data of ODP Leg 209 are coherent with such a fluid evolution. In order to model coupling between water/rock ratio and the isotopic evolution of fluid during fluid-rock interaction, we used a stable isotope balance

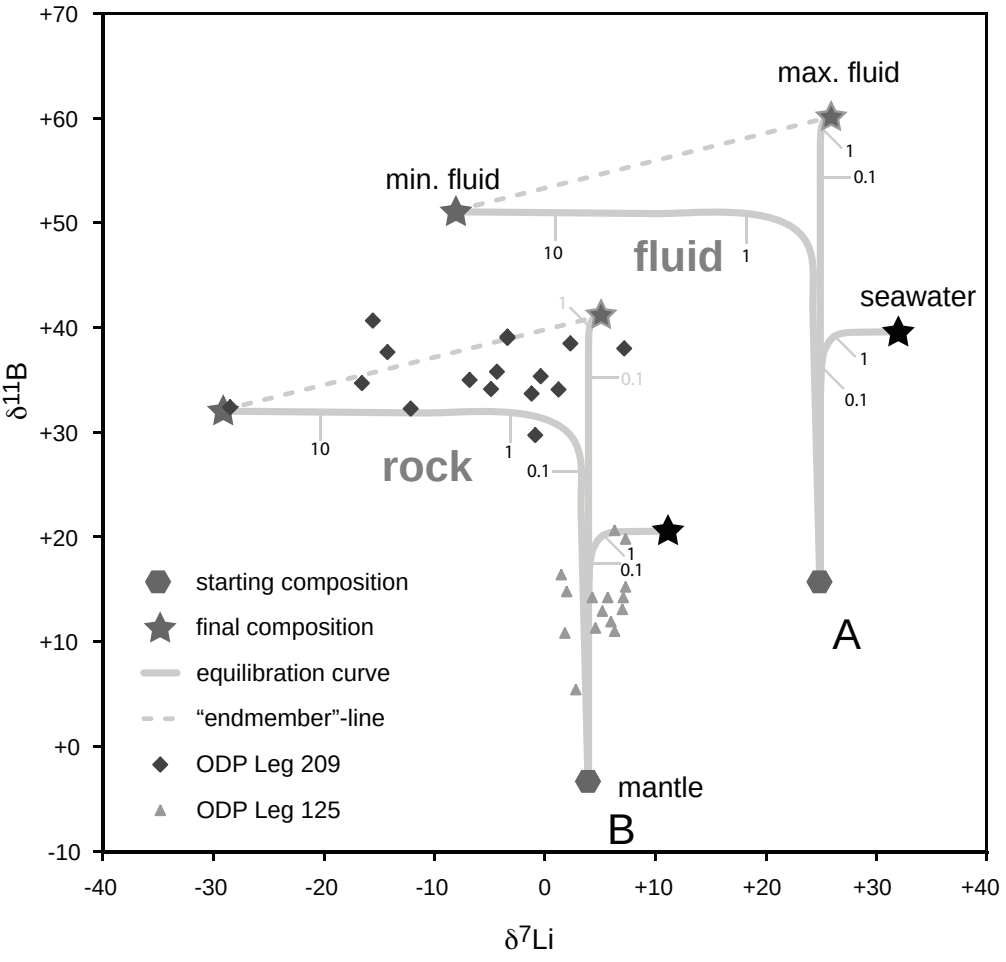

Fig. 3.6. $\delta^{7}Li$ versus $\delta^{11}B$ diagram showing the data points of ODP Leg 209 and ODP Leg 125 (Benton et al., 2001; Benton et al., 2004). Lines correspond to modelled fluid-rock interaction using the equation of Pennisi et al. (2000). They show the evolution of $\delta^{7}Li$ and $\delta^{11}B$ in fluid (A) and co-existing rock (B) at different water/rock ratios. Input values are reported in Table 2; 'min. fluid' and 'max. fluid' curves correspond to minimal and maximal fluid values from Fig. 3.5 to explain ODP Leg 209 dataset (e.g. for $\delta^{7}Li$ initial fluid: +26 and -8 ‰).

equation (EQ2; after Pennisi et al., 2000), which is a derivative of EQ1, solved for final fluid composition, assuming $\delta_r^f = \delta_w^f - \Delta$.

$$\delta_w^f = \frac{N * \delta_w^i + \frac{C_r}{C_w} * (\delta_r^i + \Delta_{w-r})}{N + C_r / C_w} \qquad \text{(EQ 2)}$$

Input values and results are reported in Table 2. Applying this equation to the Li and B isotopic system shows that already low values of N lead to near final fluid composition for $\delta^{11}B$, while $\delta^{7}Li$ requires higher N (Table 2 and Fig. 3.6). The range produced from minimal and maximal fluid composition (input values from Fig. 3.5.B and C cover most of the data points measured at ODP Leg 209, while seafloor weathering (equilibrium with seawater) leads to lighter $\delta^{11}B$ and heavier $\delta^{7}Li$ (Fig. 3.6). Data from ODP Leg 125 (Mariana fore arc, Benton et al., 2001; Benton et al., 2004) are probably not derivates of similar fluid evolution processes, as high serpentinization is not coherent with low N (Fig. 3.6).

3.8. Implications for the global B and Li cycle

Our data have potential impact on the issue of light element recycling and isotope fractionation in subduction zones. The $\delta^{11}B$ and $\delta^{7}Li$ obtained on the samples from ODP Leg 209 are the heaviest and the lightest, respectively, found so far for serpentinized peridotites from the oceanic domain. Subduction of oceanic mantle with such features could potentially control the composition of slab fluids, particularly in cases where magmatic oceanic crust is largely absent. Subduction and dehydration of oceanic crust should produce slab fluids that have heavy $\delta^{11}B$ and $\delta^{7}Li$ and high B (and Li) concentrations. In contrast, fluids released from a subducting ODP Leg 209-type mantle should probably have considerably lighter $\delta^{7}Li$ and heavier $\delta^{11}B$, very low Li and variably high B concentrations. Even if there is magmatic crust, the B isotopic composition of serpentinized mantle should control the composition of slab fluids, as it is the principal carrier of B, especially if only its upper part is dehydrated (Vils et al., 2008). For Li, our study showed that the extremely light $\delta^{7}Li$ values are coupled to very low Li contents of serpentinites. Thus, it is unlikely that the extremely light $\delta^{7}Li$ as found in ODP Leg 209 serpentinites are transferred to slab fluids. Even a small fraction of magmatic or sedimentary crust would strongly dominate the Li budget (Vils et al., 2008).

An important question to ask is if oceanic mantle with B and Li element and isotope characteristics such as those encountered in ODP Leg 209 is likely to enter a subduction zone. As oceanic lithosphere moves away from the spreading center and cools, serpentinized peridotites may attain isotopic equilibrium with seawater if they have sufficient time. One argument in favor of this hypothesis may be that $\delta^{11}B$ of dredged serpentinites is lighter (+8.3 to +12.6‰; Spivack and Edmond, 1987) than that of drilled serpentinites from ODP 209. On the other hand, the slow reaction kinetics at such low temperatures could impede re-equilibration. Permeability experiments on peridotites showed that at 100°C, a 100m thick mantle column is completely serpentinized after 3 Ma, at 34°C only after ~160 Ma (MacDonald and Fyfe, 1985). Thus, given that the average age of an oceanic plate before being subducted is 75 Ma, it seems unlikely that low-temperature re-equilibration affects a considerable part of the serpentinized oceanic mantle.

Another point to consider is that serpentinization related to slab bending (Ranero et al., 2003) might influence the B and Li isotope characteristics of the serpentinized mantle. Serpentine and serpentinite formed at these conditions should have lighter $\delta^{11}B$ than ODP Leg 209 samples if they equilibrate with seawater at fairly low temperatures. However, plate bending and subsequent subduction are likely to be faster than re-equilibration of B and Li isotopes, given the low velocity of serpentinization at low temperatures. Unfortunately, there are no B and Li isotope data from this geodynamic setting. Serpentinized peridotites from the Mariana fore-arc mantle wedge show significant enrichment in ^{7}Li ($\delta^{7}Li$ of +10.3‰) and ^{11}B ($\delta^{11}B$ of +25.3‰), presumably due to reaction with subduction-related fluids (Benton et al., 2001; Benton et al., 2004). However, these data from a mantle wedge beneath the upper plate of a subduction zone cannot be compared to our data from ODP Leg 209. In a subduction scenario, the latter should represent the mantle of the lower plate which should a-priori not be exposed to

slab fluids. Concluding, more B and Li isotope data are needed to constrain the evolution of $\delta^{7}Li$ and $\delta^{11}B$ of the oceanic mantle with time.

CONCLUSIONS

1) Serpentinization of peridotite at ODP Leg 209 Sites 1272A and 1274A enriched the rock in B and ^{11}B and depleted it in Li and ^{7}Li. Serpentinization thus led to a considerable fractionation of B and Li isotopes.

2) The ODP Leg 209 rocks and the fluids calculated to be in equilibrium with them have the heaviest $\delta^{11}B$ and the lightest $\delta^{7}Li$ reported so far. The peridotites were neither serpentinized by weathering under seafloor conditions nor exposed to the latter after serpentinization. Most likely, serpentinization was not a single-stage process, but a continuous process of fluid-rock interaction, with the original seawater changing its B, $\delta^{11}B$, Li and $\delta^{7}Li$ signature upon reaction.

3) Moderate water/rock ratios (~39) calculated from the Sr isotopic composition of the samples imply an infinite rock reservoir, but limited seawater availability. Low water/rock ratios (~1) already lead to near-final $\delta^{11}B$ composition of the rock, while $\delta^{7}Li$ is modified considerably only at higher water/rock ratios. This suggests that B exchange during serpentinization is faster and easier than Li exchange.

4) There is a fair chance that extremely heavy $\delta^{11}B$ in serpentinized oceanic mantle can be transported into subduction zones, as the B budget of the plate is dominated by serpentinites. On the contrary, extremely light $\delta^{7}Li$ in the oceanic mantle is unlikely to survive as the Li budget is dominated by the oceanic crust, even at small fractions

ACKNOWLEDGMENTS

The authors would like to thank Arjan Dijkstra, Chiara Boschi, Andrea Dini and Othmar Müntener for fruitful discussion, which helped to improve the manuscript. We also like to thank Soodabeh Durali-Müller for technical support in the chemistry laboratory (University of Frankfurt). This research used samples provided by the Ocean Drilling Program (ODP). ODP is sponsored by the U.S. National Science Foundation (NSF) and participating countries under management of Joint Oceanographic Institutions (JOI), Inc. This study was supported by the Swiss national foundation Grant 200021-10361.

APPENDIX: Model parameters used for Figure 3.5

For $\delta^{11}B$, we use a combined fractionation factor (as for Fig. 3.4), considering the equilibrium fractionation between $B(OH)_3$ and $B(OH)_4^-$ in a fluid and the fractionation between $B(OH)_4^-$ (aq) and silicates (Liu and Tossell, 2005, and reported in appendix Table 1). For B and Li it is assumed that no further isotope fractionation takes place when the adsorbed species are integrated into the mineral lattice (Palmer and Swihart, 1996). For B, we calculate the $\delta^{11}B$ evolution in fluid and rock as a function of temperature at constant pH (8.2; Fig. 3.5.A) and as a function of pH at constant temperature (200°C; Fig. 3.5.B). For Li, we use a minimum fractionation of -4‰ (Chan et al., 1992) which was established for weathering of basalt on the ocean floor. Further on, we apply a maximum fractionation of -21‰ (Vigier et al., 2008), assuming the Li isotope fractionation between seawater and serpentine is similar to that between seawater and missing phase in the ocean.

For B, the fluid evolution model is based on the assumption of equilibrium between the two dissolved B isotopes (^{10}B and ^{11}B) in the fluid. As B is removed from the solution by reaction with the rock, the tetrahedral form is preferentially adsorbed on the mineral surface and later integrated into the lattice, according to the fractionation between $B(OH)_4$ (aq) and BO_4 in silicates (Liu and Tossell, 2005). If no isotopic fractionation between $B(OH)_4$ and BO_4 occurs, the adsorbed B has the same isotopic signature as the dissolved tetrahedral species. As re-equilibration between dissolved and adsorbed B occurs, the isotopic ratio of the total adsorbed B is at any time equal to that of the dissolved tetrahedral species plus the mineral fractionation. With proceeding fluid-rock interaction, the fraction of ^{11}B in the fluid increases as ^{10}B prefers tetrahedral coordination. A rock reacting with an evolved fluid that has already lost large parts of its B will thus have much heavier $\delta^{11}B$ than a rock reacting with virtually unchanged seawater.

Li in aqueous solutions is highly hydrated and usually assumes tetrahedral coordination (Olsher, 1991). It was shown that during low-temperature weathering of soils, surface water preferentially removes ^{7}Li (Pistiner and Henderson, 2003). Seafloor weathering leads to a fractionation $\Delta^{7}Li_{rock\text{-}seawater\text{-}}$ of -4‰ (Chan et al., 1992; Chan et al., 1993). As shown by Vils et al. (2008), Li is leached during serpentinization at ODP Leg 209, thus the $\delta^{7}Li$ of the co-existing fluid becomes lighter (Fig. 3.5.C).

Appendix Table 1 Model parameters for Figure 3.4 (from Liu and

T (°C)	25	60	300
α $B(OH)_3$-$B(OH)_4$	1.027	1.024	1.011
α $B(OH)_4$ - BO_4 (in silicate)	1.0137	1.0121	1.0056
α $B(OH)_3$-BO_4 (min-sw pH 7)	1.0408	1.0367	1.0188
Δ min-sw pH 7	-40.8	-36.7	-18.8
Δ min-sw pH 10	-13.7	-12.1	-5.6
Δ min- sw pH 8	-36.7	-29.5	-16
Δ $B(OH)_3$-$B(OH)_4$ in sw	-27	-24	-11

sw seawater; min mineral; Δ fraction; α fractionation factor

Supplementary Table 1 Standard measurements

	$^{11}B/^{10}B$ measured	±2SD	$^{11}B/^{10}B$ corrected	$\delta^{11}B$ [‰]
NIST SRM 951	4.0518	0.0015	4.0434	-0.05
(without chemistry)	4.0501	0.0008	4.0417	-0.48
	4.0524	0.0013	4.044	0.1
	4.0521	0.0012	4.0437	0.03
	4.0518	0.0014	4.0434	-0.05
Average	***4.0516***	***0.0016***	***4.0433***	***-0.09***
NIST SRM 951	4.0509	0.0014	4.0425	-0.27
(through full rock chemistry)	4.0523	0.0014	4.0439	0.08
	4.052	0.0014	4.0436	0
	4.0522	0.0018	4.0438	0.05
	4.0507	0.0025	4.0423	-0.32
	4.0534	0.0016	4.0450	0.35
	4.0521	0.0008	4.0437	0.02
	4.0524	0.0018	4.0440	0.1
Average	***4.0520***	***0.0016***	***4.0436***	
	$^{87}Sr/^{86}Sr$	$\pm2\sigma_{mean}$	±2SD	
NIST SRM 987	0.710236	0.00001		
	0.710240	0.000008		
	0.710246	0.000008		
	0.710241	0.000008		
	0.710248	0.000011		
	0.710255	0.000009		
Average	***0.710244***		***0.000012***	
	$^{7}Li/^{6}Li$	$\pm2\sigma_{mean}$	±2SD	
JB-2	5.8	0.1		
	4.5	0.5		
	4.8	0.9		
	4.9	1.1		
	4.8	0.6		
	5.0	0.4		
	4.8	0.7		
	5.3	0.5		
Average	***5.0***		***0.8***	

REFERENCES

Albarède F, Michard A, Minister JF, Michard G, 1981. $^{87}Sr/^{86}Sr$ ratio in hydrothermal water and deposits from the East Pacific Rise at 21°N. Earth and Planetary Science Letters 55, 229-236.

Alt JC, Shanks III WC, Bach W, Paulick H, Garrido CJ, Beaudoin G, 2007. Hydrohtermal alteration and microbial sulfate reduction in peridotite and gabbro exposed by detachement faulting at the mid-Atlantic ridge, 15°20'N (ODP Leg 209): A sulfur and oxygene isotope study. Geochemistry Geophysics Geosystems 8, 1-22.

Bach W, Garrido CJ, Paulick H, Harvey J, Rosner M, 2004. Seawater-peridotite interactions: First insights from ODP Leg 209, MAR 15°N. Geochemistry Geophysics Geosystems 5, 1-22.

Benton LD, Ryan JG, Savov IP, 2004. Lithium abundance and isotopic systematics of forearc serpentinites, Conical Seamount, Mariana forearc: Insights into the mechanics of slab-mantle exchange during subduction. Geochemistry Geophysics Geosystems 5, 1-14.

Benton LD, Ryan JG, Tera F, 2001. Boron isotope systematics of slab fluids as inferred from a serpentine seamount, Mariana forearc. Earth and Planetary Science Letters 187, 273-282.

Bonatti E, Lawrence J, Morandi N, 1984. Serpentinization of oceanic peridotites: temperature dependence of mineralogy and boron content. Earth and Planetary Science Letters 70, 88-94.

Boschi C, 2006. Building Lost City: serpentinization, mass transfer and fluid flow in an oceanic core complex. PhD-thesis ETH Zürich.

Boschi C, Dini A, Früh-Green G, Kelley DS, 2008. Isotopic and element exchange during serpentinization and metasomatism at the Atlantis Massif (MAR 30°N): Insights from B and Sr isotope data. Geochimica et Cosmochimica Acta 72, 1801-1823.

Bouman C, Elliott T, Vroon PZ, 2004. Lithium inputs to subduction zones. Chemical Geology 212, 59-79.

Brooker, R. A., James, R. H., and Blundy, J. D., 2004. Trace elements and Li isotope systematics in Zabargad peridotites: Evidence of ancient subduction processes in the Red Sea mantle. Chemical Geology 212, 179-204.

Cannat M, 1993. Emplacement of mantle rocks in the seafloor at mid-ocean ridges. Journal of Geophysical Research 98, 4163-4172.

Catanzaro EJ, Champion CE, Garner EL, G. M, Sappenfield KM, Shields KM, 1970. Boric acid: Isotopic and assay standard reference materials. US Nat. Bur. Standards Spec. Publ. 260-17,70 pp

Chan LH, Edmond J, Thompson G, 1993. A lithium isotope study of hot springs and metabasalts from mid-ocean ridge hydrothermal systems. Journal of Geophysical Research 98,9653-9659.

Chan LH, Edmond J, Thompson G, Gillis KM, 1992. Lithium isotopic composition of submarine basalts: Implications for the lithium cycle in the oceans. Earth and Planetary Science Letters 108, 151-160.

Davies AC, Bickel MJ, Teagle DAH, 2003. Imbalance in the oceanic strontium budget. Earth and Planetary Science Letters 211, 173-187.

Decitre S, Deloule E, Reisberg L, James R, Agrinier P, Mével C, 2002. Behavior of Li and its isotopes during serpentinization of oceanic peridotites. Geochemistry Geophysics Geosystems 3.

Delacour A, Früh-Green G, Frank M, Gutjahr M, Kelley DS, 2008. Sr- and Nd-isotope geochemistry of the Atlantis Massif (30°N, MAR): Implications for fluid fluxes and lithospheric heterogeneity. Geochimica et Cosmochimica Acta 254, 19-35.

Douville E, Charlou JL, Oelkers EH, Bienvenu P, Jove Colon CF, Donval JP, Fouquet Y, Prieur D, Appriou P, 2002. The rainbow vent fluids (36°14'N, MAR): The influence of ultramafic rocks and phase separation on trace metal content in mid-Atlantic ridge hydrothermal fluids. Chemical Geology 184, 37-48.

Edmond J, Measures C, McDuff RE, Chan LH, Collier R, Grant B, Gordon LI, Corliss JB, 1979. Ridge crest hydrothermal activity and the balance of The major and minor elements in the ocean: the Galapagos data. Earth and Planetary Science Letters 46, 1-18.

Elliott T, Jeffcoate A, Bouman C, 2004. The terrestrial Li isotope cycle: Light-weight constraints on manle convection. Earth and Planetary Science Letters 220, 231-245.

Escartin J, Mével C, MacLeod CJ, McCaig AM, 2003. Constraints on deformation conditions and the origin of oceanic detachments: The mid-Atlantic ridge core complex at 15°45'N. Geochemistry Geophysics Geosystems 4, 1-37.

Flesch G, Anderson AR, Svec HJ, 1973. A secondary isotopic standard for $^{6}Li/^{7}Li$ determinations. International Journal of Mass Spectrometry and Ion Physics 12, 265-272.

Foustoukos DI, James RH, Berndt ME, Seyfried Jr. WE, 2004. Lithium isotopic systematics of hydrothermal vent fluids at the Main Endeavour Field, Northern Juan de Fuca Ridge. Chemical Geology 212, 17-26.

Foustoukos DI, Savov IP, Janecky DR, 2008. Chemical and isotopic constaints on water/rock interactions at the Lost City hydrothermal field, 30°N mid-Atlantic ridge. Geochimica et Cosmochimica Acta 72, 5457-5474.

Frost BR, Beard JS, 2007. On silica activity and serpentinization. Journal of Petrology 48, 1351-1368.

Godard M, Lagabrielle Y, Alard O, Harvey J, 2008. Geochemistry of the highly depleted peridotites drilled at ODP Sites 1272 and 1274 (Fiffteen-Twenty Fracture Zone, mid-Atlantic ridge): Implications for mantle dynamics beneath a slow spreading ridge. Earth and Planetary Science Letters 267, 410-425.

Hart SR, Blusztajn J, Dick HJB, Meyer PS, Muehlenbachs K, 1999. The fingerprint of seawater circulation in a 500-meter section of ocean crust gabbros. Geochimica et Cosmochimica Acta 63, 4059-4080.

Hemming NG, Reeder RJ, N. HG, 1995. Mineral-fluid partitioning and isotopic fractionation of boron in synthetic calcium carbonate. Geochimica et Cosmochimica Acta 59, 371-379.

Huh Y, Chan LH, Zhang L, Edmond J, 1998. Lithium and its isotopes in major world rivers: Implications for weathering and the oceanic budget. Geochimica et Cosmochimica Acta 62, 2039-2051.

Ishikawa A, Nakamura E, 1992. Boron isotope geochemistry of the oceanic crust from DSDP/ODP Hole 504B. Geochimica et Cosmochimica Acta 56, 1633-1639.

Ishikawa T, Nakamura E, 1993. Boron isotope systematics of marine sediments. Earth and Planetary Science Letters 117, 567-580.

Kakihana H, Kotaka M, 1977. Equilibrium constants for boron isotope-exchange reactions. Bulletin Res. Lab. Nucl. React 2, 1-12.

Kelemen PB, Kikawa E, Miller DJ, 2004. Proceedings of the Ocean Drilling Program. Preliminary Report Leg 209

Kelemen PB, Kikawa E, Miller DJ, 2007. Proc. ODP, Sci. Results, vol 209. College Station, TX (Ocean Drilling Program)

Kelley DS, Karson JA, Blackman DK, Früh-Green G, Butterfield DA, Lilley MD, Olson EJ, Schrenk MO, Roe K, Lebon GT, Rivizzigno P, 2001. An off-axis hydrothermal field near the mid-Atlantic ridge at 30°N. Nature 412, 145-149.

Li YH, 1982. A brief discussion on the mean oceanic residence time of elements. Geochimica et Cosmochimica Acta 46, 2671-2675.

Liu Y, Tossell A, 2005. Ab initio molecular orbital calculations for boron isotope fractionations on boric acids and borates. Geochimica et Cosmochimica Acta 69,3995-4006

MacDonald AH, Fyfe WS, 1985. Rate of serpentinization in seafloor environments. Tectonophysics 116, 123-135..

McCaig AM, Cliff RA, Escartin J, Fallick AE, MacLeod CJ, 2007. Oceanic detachment faults focus very large volumes of black smoker fluids. Geology 35, 935-938.

McCulloch M, Gregory RT, Wasserburg GJ, Taylor HPJ, 1980. A neodymium, strontium and oxygen isotopic study of the Cretaceous Semail ophiolite and implications for the petrogenesis and seawater-hydrothermal alteration of oceanic crust. Earth and Planetary Science Letters 46, 201-211.

Mével C, 2003. Serpentinization of abyssal peridotites at mid-ocean ridges. Compte Rendus Geoscience 335, 825-852.

Michael PJ, Langmuir CH, Dick HJB, Snow JE, Goldstein SL, Graham DW, Lehnert K, Kurras G, Jokat W, Mühe R, Edmonds HN, 2003. Magmatic and amagmatic seafloor generation at the ultraslow-spreading Gakkel ridge, Arctic Ocean. Nature 423, 956-961.

Niu Y, 2004. Bulk-rock major and trace element compositions of abyssal peridotites: Implications for mantle melting, melt extraction and post-melting processes beneath mid-ocean ridges. Journal of Petrology 45, 2423-2458.

Olsher U, 1991. Coordination chemistry of lithium ion: A crystal molecular structure. Chemical Review 91, 137-164.

Palmer MR, 1991. Boron isotope systematics of hydrothermal fluids and tourmalines: A synthesis. Chemical Geology 94, 111-121.

Palmer MR, Edmond J, 1989. The strontium isotope budget of the modern ocean. Earth and Planetary Science Letters 92, 11-26.

Palmer MR, Spivack AJ, Edmond J, 1987. Temperature and pH controls over isotopic fractionation during adsorption of boron on marine clay. Geochimica et Cosmochimica Acta 51, 2319-2323.

Palmer MR, Swihart GH, 1996. Boron isotope geochemistry: an overview, vol 33. Mineralogical Society of America, Washington, D.C., pp 709-740.

Paulick H, Bach W, Godard M, De Hoog JCM, Suhr G, Harvey J, 2006. Geochemistry of abyssal peridotites (mid-Atlantic ridges, 15°20'N, ODP Leg 209): Implications for fluid/rock interaction in slow spreading environments. Chemical Geology 234, 179-210.

Pelletier L, 2008. The oceanic mantle as an important repository for the light elements Li, Be and B. PhD-Thesis. University of Neuchâtel.

Pennisi M, Leeman WP, Tonarini S, Pennisi A, Nabelek PI, 2000. Boron, Sr, O and H isotope geochemistry of groundwaters from Mt. Etna (Sicily) - hydrologic implications. Geochimica et Cosmochimica Acta 64, 961-974.

Pistiner JS, Henderson GM, 2003. Lithium-isotope fractionation during continental weathering processes. Earth and Planetary Science Letters 214, 327-339.

Pokrovsky O. S., Schott J. and Castillo A, 2005. Kinetics of brucite dissolution at 25°C in the presence of organic and inorganic ligands and divalent metals. Geochimica et Cosmochimica Acta 69, 905–918.

Quinby-Hunt MS, Turekian KK, 1983. Distribution of elements in seawater. EOS 64,130-132

Rehkamper M, Hofmann AW, 1997. Recycled ocean crust and sediment in Indian Ocean

MORB. Earth and Planetary Science Letters 147, 93-106.

Ryan JG, Langmuir CH, 1987. The systematics of lithium abundances in young volcanic rock. Geochimica et Cosmochimica Acta 51, 1727-1741.

Salters VJM, Stracke A, 2004. Composition of the depleted mantle. Geochemistry Geophysics Geosystems 5, 1-27.

Savov IP, Ryan JG, D'Antonio M, Fryer P, 2007. Shallow slab fluid release across and along the Mariana arc-basin system: Insights from geochemistry of serpentinized peridotites from the Mariana Forearc. Journal of Geophysical Research 112.

Savov IP, Ryan JG, D'Antonio M, Kelley K, Mattie P, 2005. Geochemistry of serpentinized peridotites from the Mariana Forearc Conical Seamount, ODP Leg 125: Implications for the elemental recycling at subduction zones. Geochemistry Geophysics Geosystems 6, 1-24.

Schmidt K, Koschinsky A, Garbe-Schönberg D, de Carvalho LM, Seifert R, 2007. Geochemistry of hydrothermal fluids from the ultramafic-hosted Logatchev hydrothermal field, 15°N on the mid-Atlantic ridge: Temporal and spatial investigation. Chemical Geology 242, 1-21.

Seitz H-M, Brey GP, Lahaye Y, Durali S, Weyer S, 2004. Lithium isotopic signatures of peridotite xenoliths and isotopic fraction at high temperature between olivine and pyroxenes. Chemical Geology 212, 163-177.

Sen S, Stebbins JF, Hemming NG, Ghosh B, 1994. Coordination environments of B impurities in calcite and aragonite polymorphs: A ^{11}B MAS NMR study. American Mineralogist 79, 819-825.

Seyfried Jr. WE, Chen X, Chan LH, 1998. Trace element mobility and lithium isotope exchange during hydrothermal alteration of seafloor weathered basalt: An experimental study at 350°C, 500 bars. Geochimica et Cosmochimica Acta 62, 949-960.

Seyfried Jr. WE, Janecky DR, Mottl MJ, 1984. Alteration of the oceanic crust: Implications for geochemical cycles of lithium and boron. Geochimica et Cosmochimica Acta 48, 557-569.

Seyler M, Lorand J-P, Dick HJB, Drouin M, 2007. Pervasive melt percolation reactions in ultra-depleted refractory harzburgites at the mid-Atlantic ridge, 15°20'N: ODP Hole 1274A. Contributions to Mineralogy and Petrology 153, 303-319.

Simon L, Lécuyer C, Maréchal C, Coltice N, 2006. Modelling the geochemical cycle of boron: Implications for the long-term $\delta^{11}B$ evolution of seawater and oceanic crust. Chemical Geology 225, 61-76.

Smith HJ, Spivack AJ, Staudigel H, Hart SR, 1995. The boron isotopic composition of altered oceanic crust. Chemical Geology 126, 119-135.

Spivack AJ, Edmond J, 1987. Boron isotope exchange between seawater and oceanic crust. Geochimica et Cosmochimica Acta 51, 1033-1043.

Spooner ETC, Chapman HJ, Smewing JD, 1977. Strontium isotopic contamination and oxidation during ocean floor hydrothermal metamorphism of the ophiolitic rocks of the Troodos Massif, Cyprus. Geochimica et Cosmochimica Acta 41, 873-890.

Stein CA, Stein S, 1992. A model for the global variations in oceanic depth and heat flow with lithospheric age. Nature 359, 123-129.

Stein S, Stein CA, 1996. Thermo-mechanical evolution of oceanic lithosphere: Implications for the subduction process and deep earthquakes (overview). In: Bebout GE, Scholl DW, Kirby SH, Platt JP (eds) Subduction: top to bottom, vol 96. pp 1-17,

Suhr G, Kelemen PB, Paulick H, 2008. Microstructures in Hole 1274A peridotites, ODP Leg 209, mid-Atlantic ridge: Tracking the fate of melts percolation in periodotite as the lithosphere is intercepted. Geochemistry Geophysics Geosystems 9, 1-23.

Taylor HPJ, 1977. Water/rock interactions and the origin of H_20 in granitic batholiths. Journal of the Geological Society, London 133, 509-558.

Thompson G, Melson WG, 1970. Boron contents of serpentinites and metabasalts in the oceanic crust: Implications for the boron cycle in the oceans. Earth and Planetary Science Letters 8, 61-65.

Tomascak PB, 2004. Devolopments in the understandings and application of lithium isotopes in earth and planetary sciences. Reviews in Mineralogy and Geochemistry 55,153-195

Tomascak PB, Langmuir CH, Le Roux PJ, 2008. Lithium isotopes in global mid-ocean ridge basalts. Geochimica et Cosmochimica Acta 72, 1626-1637.

Tonarini S, Pennisi M, Adomi-Braccesi A, Dini A, Ferrara G, Gonflantini R, Wiedenbeck M, Gröning M, 2003. Intercomparison of boron isotope and concentration measurements. Part I: Selection, preparation and homogeneity tests of the intercomparison materia. Geostandards Newsletter 27, 21-39.

Vigier N, Decarreau A, Millot R, Carignan J, Petit S, France-Lanord C, 2008. Quantifying Li isotope fractionation during smectite formation and implications for the Li cycle. Geochimica et Cosmochimica Acta 72, 780-792.

Vils F, 2009. Light elements in oceanic and ophiolitic serpentinites. PhD-Thesis. University of Neuchâtel.

Vils F, Pelletier L, Kalt A, Müntener O, Ludwig T, 2008. The Lithium, Boron and Beryllium

content of serpentinized peridotites from ODP Leg 209 (Sites 1272A and 1274A): Implications for lithium and boron budgets of oceanic lithosphere. Geochimica et Cosmochimica Acta 72, 5475-5504.

Wunder B, Meixner A, Romer RL, Heinrich W, 2006. Temperature-dependent isotopic fractionation of lithium between clinopyroxene and high-pressure hydrous fluids. Contributions to Mineralogy and Petrology 151, 112-120.

You CF, Spivack AJ, Grieskes JM, Rosenbauer R, Bischoff JL, 1995. Experimental study of boron geochemistry: Implications for fluid processes in subduction zones. Geochimica et Cosmochimica Acta 59, 2435-2442.

Zhang L, Chan LH, Gieskes JM, 1998. Lithium isotope geochemistry of pore waters from Ocean Drilling Programm Sites 918 and 919, Irminger Basin. Geochimica et Cosmochimica Acta 62, 2437-2450.

Chapter IV

Contrasting behaviour of beryllium and lithium-boron during seafloor alteration and progressive metamorphism: a study on the Totalp, Platta and Malenco ophiolites

to be submitted to Geochimica et Cosmochimica Acta

ABSTRACT

The Totalp-Platta-Malenco transect in the Eastern Central Alps offers a unique opportunity to study the behaviour of Li, Be and B in ultramafic rocks in response to serpentinization and to progressive Alpine metamorphism. These units represent the remnants of a former ocean-continent transition that was intensely serpentinized during exposure on the Jurassic seafloor of the Ligurian Tethys. From north to the south, three classical isograde reactions (chrysotile + talc => antigorite; chrysotile => antigorite + brucite; chrysotile + tremolite => antigorite + diopside) have been used to quantify the evolution of the light element content of metamorphic minerals. We determined the Li, Be and B concentrations in major silicate minerals from the ultramafic bodies of Totalp, Platta and Malenco by secondary ion mass spectrometry. Mantle minerals have similar Be concentrations (e.g. <0.001 to 0.009 µg/g in olivine) as metamorphic minerals that replace the primary phases (e.g. <0.001 to 0.016 µg/g in serpentine). The Be mantle signature is thus neither erased during seafloor alteration nor by progressive metamorphism from prehnite-pumpellyite to epidote-amphibolite facies. In contrast, the Li and B inventories of metamorphic minerals reflect the chrysotile-to-antigorite transition. Both elements display higher concentrations in the low-temperature serpentine polymorph chrysotile (max. 156 µg/g Li, max. 318 µg/g B) than in antigorite (max. 0.11 µg/g Li, max. 12 µg/g B), indicating Li and B decrease during low temperature serpentine phase transitions in ultramafic rocks. This contrasting behaviour of the light elements is also reflected in the Li and B content of chlorite, which recrystallized during progressive Alpine metamorphism.

The Be content of primary mantle clinopyroxene in all peridotite massifs is much higher relative to clinopyroxene from the oceanic mantle, but similar to Be values from mantle xenoliths and subduction-related peridotite massifs. These data support previous hypothesis that the mantle rocks from the Eastern Central Alps have a subcontinental origin. We therefore conclude that Be behaves conservatively during prograde metamorphism of ultramafic rocks, at least at low-temperature, and thus retains the fingerprint of ancient igneous events in mantle peridotites.

4.1. Introduction

Fully hydrated peridotites represent the largest fluid reservoir along subduction zones, and deliver about 10 wt.% bulk fluid to sub-arc depth, where antigorite-breakdown occurs (Ulmer and Trommsdorff, 1995). Transformation of antigorite to olivine and orthopyroxene at depth liberates a mobile phase, which is partially recycled in back-arc volcanoes (e.g. Ryan et al., 1995; Ulmer and Trommsdorff, 1995). As dehydration reactions during prograde Alpine metamorphism record similar paths as during subduction (e.g. Evans and Trommsdorff, 1970; Scambelluri et al., 1995), mineral isograde in Alpine ophiolite bodies are on-land analogues for what is actively going on in the subduction zone factory, although some ophiolites are overprinted by retrograde metamorphism. In general, dehydration reactions favour release and removal of mobile elements from rocks into a fluid or liquid (e.g. Brenan et al., 1998).

Studies on light elements (Li, Be and B) added important information to the understanding of geological cycles and systems. By squeezing out serpentinites at 30 kbar and 750°C, Tenthorey and Hermann (2004) showed that serpentinites have a potential to release B at great depth. Systematic in-situ and whole rock studies on light elements in serpentinites confirmed an enrichment in B (Bonatti et al., 1984; Savov et al., 2005; Li and Lee, 2006; Pelletier et al., 2008b; Vils et al., 2008) and additionally showed depletion in Li (Pelletier et al., 2008b; Vils et al., 2008) compared to depleted mantle (Salters and Stracke, 2004), although depletion in Li is not as pronounced as B enrichment. In-situ measurements from dredged serpentinites from Hess Deep also showed high-temperature enrichment in Li during serpentinization (Decitre et al., 2002). In addition, studies on the $\delta^{11}B$ whole rock composition of drilled serpentinites from Atlantis massif and from ODP Leg 209 showed that enrichment in ^{11}B is probably related to interaction of evolved seawater with peridotites (Boschi et al., 2008; Vils et al., 2009).

Compared to B and Li, whole rock data on Be from peridotites are quite rare. Calculations of the Be content of the primitive mantle (0.054 or 0.068 µg/g; McDonough and Sun, 1995; Lyubetskaya and Korenaga, 2007) or the depleted mantle (0.025 µg/g; Salters and Stracke, 2004) constrain the low abundance of this element in the upper mantle. Recent analysis of fresh peridotites from the Pindos ophiolite (Greece) revealed whole rock Be contents below detection limit (<0.003 µg/g), with in-situ Be measurements in all minerals below 0.005 µg/g (except pargasite with 0.012 µg/g; Pelletier et al., 2008b). Dredged abyssal peridotites worldwide contain on average 0.044 µg/g Be (0.001 to 0.212 µg/g; Niu, 2004). Estimates based on in-situ secondary ion-mass spectrometry (SIMS) measurements of ODP Leg 209 samples documented a similarly low abundance of Be (average <0.003 µg/g; Vils et al., 2008). Seawater contains about 0.0002 ng/g Be (Li, 1982). Seawater alteration is therefore an unlikely process to enrich serpentinites in Be relative to peridotites. A higher Be content is reported in Mariana fore-arc samples (0.07 to 0.16 µg/g; Zanetti et al., 2006) and from peridotites interpreted as modified by slab fluids (0.213 to 0.01 µg/g; Brooker et al., 2004; Paquin et al., 2004; Scambelluri et al., 2006). Samples from the metamorphic Geisspfad ophiolite in central Switzerland display a weak Be enrichment along the contact with surrounding gneisses (Pelletier et al., 2008a).

Mineral-fluid partitioning experiments performed at 900 °C and 2.0 GPa indicated that Be is slightly compatible in clinopyroxene and micas (e.g. D_{Be} cpx/fluid = 1.8), but is incompatible in garnet or amphibole (e.g. grt/fluid = 0.0024; Brenan et al., 1998). Similar results were obtained from field studies on metamorphosed high-pressure oceanic crust. Be is highly incompatible in garnet, quartz, and talc, but compatible in phengite (e.g. D_{Be} tlc/fluid= 0.0324; D_{Be} phe/fluid =5.04; Marschall et al., 2006; Marschall et al., 2007).

In metasedimentary rocks from the Catalina schist (USA), B/Be ratio decreases (72 to 21) with increasing metamorphism (lawsonite-albite to epidote-amphibolite facies; Bebout et al., 1993). Metabasites from the same locality show a less pronounced decrease in B/Be ratio, but the latter are mostly lower than average altered oceanic crust (30, Bebout et al., 1993). Decrease in the B/Be ratio is related to preferential removal of B in H_2O-rich fluids during devolatilization reactions and, consequently, leads to high B/Be ratios in back-arc volcanoes (e.g. Bebout

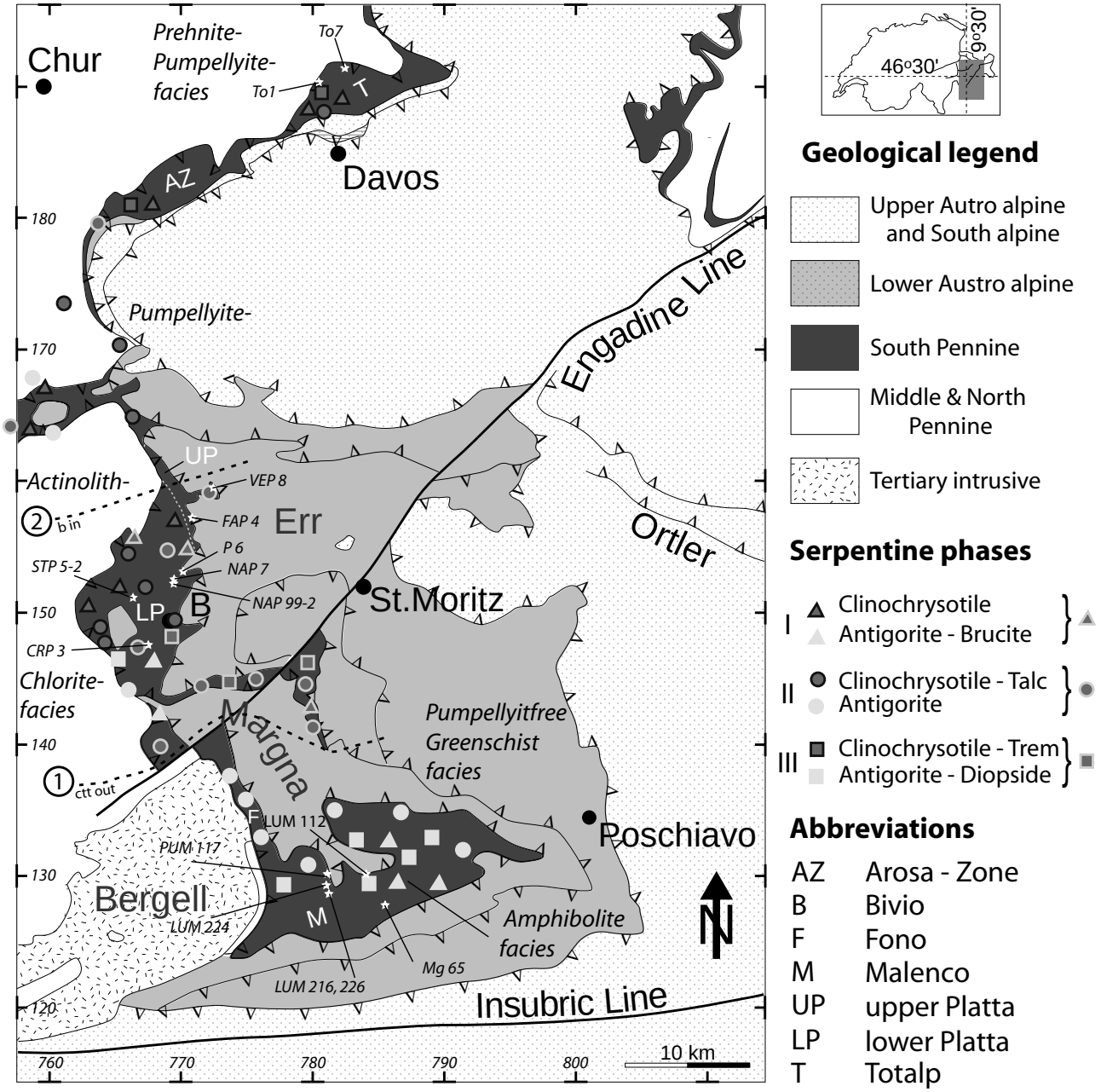

Fig. 4.1. Simplified geological map of the Davos-Malenco region (modified after Trommsdorff, 1983; Froitzheim et al., 1994; Ulmer and Trommsdorff, 1999; Desmurs et al., 2002) including serpentine type occurrence and metamorphic facies from Trommsdorff, 1983). Isograds are indicated: 1) end of reaction I-III (ctt out: clinochrysotile, talc and tremolite (trem) out); 2) start of reaction III with brucite in.

et al., 1993; Ryan et al., 1996; Bouvier et al., 2008).

Be measurements in sediments and pore water from ODP Sites 808, 671 and 672 showed that Be content in pore water increases around detachment faults, and potential Be mobilization during pore fluid expulsion upon sediment burial is suggested (You et al., 1994). The only high-T and high-P (850°C and 1.5 GPa) dehydration experiment on Be content in serpentinites was conducted by Tatsumi and Isoyama (1988). The starting material contained 12 to 59.2 µg/g Be. They showed that maximal 5% of the total Be can be mobilized during dehydration reactions in serpentinites. Such a low solubility is in line with in-situ measurements of Be and B in metamorphic rocks from the Franciscan complex and the Catalina schists and the higher concentration of Be in partially dehydrated veins (Domanik et al., 1993). Suspension experiments on biotite and albite

(Aldahan et al., 1999) demonstrate that Be solubility is pH-dependent at low temperature (25°C), a result that was later supported by studies on the distribution of Be between soil and river or seawaters (You et al., 1989).

In this paper we present Li, Be and B data from serpentinized peridotites from the Totalp, Platta and Malenco ophiolites, an area which represents an ocean-continent transition of the mid-Jurassic Piemonte Ligurian ocean. All samples presented here have been previously investigated in terms of whole rock and in-situ major and trace elements (Desmurs, 2001; Müntener et al., 2004; Müntener et al., 2009), allowing us to focus on the behaviour of the light elements. We analyzed in-situ major and light element contents of the different minerals by electron microprobe and secondary ion mass spectrometry (SIMS). We evaluated Li, Be and B data of the mantle minerals and of the metamorphic products and examined their significance for monitoring metamorphic and primary mantle processes. While Li and B are sensitive to metamorphic reactions we infer that the Be content remains conservative during the replacement of primary mantle minerals by their metamorphic counterparts. We discuss some implications this might have for the interpretation of exhumed peridotites and the mantle processes they record.

4.2. Geological setting

In the south-eastern part of the Swiss Alps (Eastern Central Alps), remnants of the Liguria-Piemonte segment of the Mesozoic Tethys are exposed. These ophiolite bodies belong to the Penninic nappes and form a ~60 km long N-S section, from Davos (CH) to the Valmalenco (I) area, along the boundary of the overlying Austroalpine nappes (Fig. 4.1). The ophiolites and the continental rocks of the Austroalpine nappes represent the southern part of the Alpine Tethys and the continental margin of the Adria (micro-) continent. In this study we will focus on three ophiolite bodies, from N to the S, Totalp, Platta and Malenco. Detailed petrographic studies along this transect showed progressive Alpine regional metamorphism from prehnite-pumpellyite facies in the north to greenschist facies in the south (Dietrich and Peters, 1971; Trommsdorff and Evans, 1974; Trommsdorff, 1983). In the north, chrysotile/lizardite is the dominant serpentine polymorph, with relict mantle minerals (Peters, 1963), while in the Platta nappe the transition from chrysotile to antigorite has been observed (Dietrich, 1969). In Val Malenco, antigorite is the stable serpentine polymorph (Trommsdorff and Evans, 1974) with rare, submicroscopic inclusions of chrysotile (Mellini, 1987). Mantle clinopyroxene can be found as relicts throughout these ophiolite bodies (Mellini, 1987; Müntener et al., 2004). At the contact between exhumed mantle and pelagic sediments, ophicarbonates were formed, in which calcite partially replaces serpentine (Bernoulli and Weissert, 1985; Früh-Green et al., 1990; Pozzorini and Früh-Green, 1996; Desmurs et al., 2001). $\delta^{18}O$ of ophicarbonates and serpentinites from the Totalp-Arosa zone not only confirmed that the degree of metamorphism increased towards the south, but also suggest that most of the serpentinization is related to interaction between seawater and peridotite (Früh-Green et al., 1990). In addition, increasing δD (from -120 to -42 ‰) and decreasing

Table 1 Sample locations and mineral content

		(CH-Koord)			mantle phases					preal. phases		oceanic phases			alpine met. phases				
Sample name	massif	x	y	type	ol	cpx	opx	spl	pg	trem	chl	serp	mgt	chl	di	atg	chl	Ref	accessories
To 1	To	780'425	190'200	serp lherzolite	x	x	x	x	-	x	(x)	x	x	x	-	-	(x)	-	FeNiS
To 7	To	782'325	191'200	serp lherzolite	x	x	x	x	-	-	(x)	x	x	x	-	-	(x)	*1*	-
NAP 7	LP	769'500	153'005	serp lherzolite	-	x	-	x	-	-	-	x	x	x	-	-	(x)	*2*	FeNiS, An
NAP 99-2	LP	769'650	152'500	serp lherzolite	-	x	-	x	-	-	-	x	x	x	-	-	(x)	*2*	FeNiS
P 6	LP	770'120	153'310	serp lherzolite	-	x	-	x	-	-	-	x	x	-	x	-	-	-	-
CRP 3	LP	767'750	147'250	serp lherzolite	-	x	-	x	-	-	-	x	x	x	-	-	(x)	*2*	-
STP 5-2	LP	766'350	151'125	serp lherzolite	-	x	-	x	-	-	-	x	x	x	x	-	x	*1,2*	-
VEP 8	UP	772'625	159'675	serp lherzolite	-	x	-	x	-	-	-	x	x	-	-	-	-	*1,2*	FeNiS
FAP 4	UP	771'325	157'650	serp lherzolite	-	x	-	-	-	-	-	x	x	x	-	-	-	*1,2*	tit
Mg 65	MAL	785'760	127'850	serp lherzolite	x	x	-	-	-	-	-	-	-	-	x	x	x	*1*	cc, pv, FeNiS
L-Um 112-4	MAL	784'105	130'720	spl peridotite	x	x	x	x	x	x	x	-	-	-	-	-	-	*1,3*	tc
P-Um 117	MAL	781'460	130'110	serp lherzolite	x	x	-	-	-	-	-	-	x	-	x	x	x	*1*	-
L-Um 216-1	MAL	781'130	128'600	spl peridotite	x	-	-	x	x	x	x	(x)	-	-	-	x	-	*1,3*	cc
L-Um 216-2	MAL	781'130	128'600	spl peridotite	x	-	-	x	x	x	x	(x)	-	-	-	x	-	*1,3*	phl, FeNiS
L-Um 224	MAL	781'070	129'130	spl websterite	x	x	-	-	-	x	-	(x)	x	-	-	x	-	*3*	cc
L-Um 226	MAL	781'130	128'600	spl peridotite	x	x	x	x	x	x	x	-	-	-	-	-	-	*3*	-

1: Müntener et al., 2004; 2: Demurs 2001; 3: Müntener 1997; gran granular; ol olivine; cpx clinopyroxene; di: diopside; opx orthopyroxene; trem tremolite; spl spinel; mgt magnetite; serp chrysotie/lizardite; chl chlorite; an andradite, cc calcite; phl phlogopite; pg pargasite; tc talc, tit titanite, pv perovskite. crosses in parenthesis indicate that that origin is unclear

$\delta^{18}O$ (from +10 to +7.4 ‰) from the Totalp to the Malenco serpentinites reflect regional metamorphism, but some Malenco antigorites still contain an oceanic signature (Burkhard and O'Neil, 1988).

The ophiolites exposed in the Totalp, Platta, and Malenco units represent a type example of an ocean-continent transition zone (Manatschal and Müntener, 2009). The mantle rocks in these units are characterized by a largely serpentinized peridotite basement intruded and/or covered by small or moderate volumes of mafic rocks, and the lack of a "complete" ophiolite stratigraphy. The close association of serpentinite, diabase and radiolarites (known as the 'Steinmann trinity') was first described by Steinmann, 1905, for a historical perspective, see Bernoulli et al. (2003). Serpentinized peridotites in the Platta area are commonly overlain by ophicalcites, representing tectono-sedimentary breccias related to mantle exhumation (Desmurs et al., 2001). In the Eastern Central Alps extensional allochthons of continental basement rocks and their pre- and syn-rift sedimentary cover locally overlie the exhumed mantle rocks (Manatschal and Nievergelt, 1997). The serpentinized mantle rocks are in places stratigraphically overlain by Jurassic radiolarites indicating that they must have been uplifted from mantle depth to the sea floor in Mesozoic times. On the other hand, field evidence showed that the mantle rocks in Val Malenco represent a fragment of subcontinental mantle in Permian times, welded to the lower crust by a tholeiitic gabbro intrusion (Müntener and Hermann, 1996). Radiometric age determinations (U-Pb on zircons) showed that crystallization of the gabbro and partial melting of the lower crust were coeval and of Permian age (Hansmann et al., 2001; Hermann and Rubatto, 2003). There is thus evidence that some of the mantle exposed on the seafloor in Mesozoic times has a subcontinental origin.

In the following, we describe rock occurrence from N to the S within the three ophiolite bodies. The northernmost massif, the Totalp ophiolite (TO) consists of serpentinite, pyroxenite (rare garnet-pyroxenite), diabase, ophicarbonates and pelagic sediments (Peters, 1963). Regional metamorphism overprinted the Totalp peridotite along the contact zones with the surrounding gneisses (e.g. formation of prehnite-bearing assemblages; Peters, 1963). Detailed mapping, mineralogical and petrographical studies and a stratigraphic description are published in Peters (1963).

The intermediate ophiolite massif, the Platta nappe, is divided in two subunits, the lower Platta (LP) and upper Platta (UP) units (Cornelius, 1932; Dietrich, 1970; Desmurs, 2001; Desmurs et al., 2002). The LP consists of basalts, gabbros, serpentinized mantle, sedimentary rocks and extensional allochthons. The UP (NW part of the Platta nappe) contains basalts, serpentinized mantle, sediments and extensional allochthons. The UP unit probably originated closer towards the continental margin than the LP unit. Preserved spinel foliation and parallel pyroxenite bands indicate equilibration within the spinel stability field (Desmurs, 2001). The LP (closer to the ocean) is mostly less deformed and pyroxenite-poor (Desmurs, 2001). Detailed geological maps and a stratigraphic description are given by Dietrich (1970).

South of the Engadine Line, the Malenco (MAL) ophiolite body is composed of gabbros, dunites, spinel-peridotites, pyroxenites, rodingites (mafic dikes) and ophicarbonates (Müntener and Hermann, 1996). During Alpine metamorphism, the Malenco nappe recrystallized under epidote-amphibolite facies conditions (0.5 to 0.7 GPa and 450 to 500°C; Guntli and Liniger, 1989; Hermann, 1997). In the late Tertiary, the Western part of the Val Malenco complex was intruded by the Bregaglia intrusion (tonalite and granodiorite). Related contact metamorphism led to a partial amphibolite facies overprint (e.g. Trommsdorff and Evans, 1972; Burkhard and O'Neil, 1988). Antigorite is the only serpentine phase found in the MAL area, although submicroscopic chrysotile occurrences are found (Mellini, 1987). A detailed map and cross sections are published by Montrasio et al. (2005) and commented by Trommsdorff et al. (2005).

4.3. Analytical techniques

Major and light element analyses follow the same procedure and machine set-up as previously described by Vils et al. (2008). The major element compositions of olivine, clinopyroxene, orthopyroxene, spinel, magnetite, amphibole, chlorite and serpentine minerals (Appendix A) were determined by electron microprobe analysis (EPMA) using a JEOL JXA-8200 (University of Bern,

Switzerland). An accelerating potential of 15 kV, a beam current of 20 nA and counting times of 30 s for Si, Al, Mg and Na and 20 s for the other elements were used. Minerals and synthetic oxides were used as standards. Samples were analyzed with a spot size of approximately 1 µm (see Vils et al., 2008 for details about serpentine analysis).

Li, B and Be were analyzed in-situ on polished thin sections by Secondary Ion Mass Spectrometry (SIMS) using a modified Cameca IMS 3f ion microprobe at the Mineralogical Institute of Heidelberg, Germany. A 14.5 keV/ 20 nA $^{16}O^-$ primary beam with ~30 µm diameter and acceleration to a nominal energy of 4.5 keV for the positive secondary ions was used. Secondary ^{7}Li, ^{9}Be, ^{11}B and ^{30}Si ions were collected applying the energy filtering method using an offset of 75 eV at a mass resolution of ~1030 (m/Δm, 10%) and a nominal imaged field of 25 mm. Secondary ion intensities were normalized to the count rates of ^{30}Si and calibrated against the NIST SRM610 glass reference material using the concentrations (preferred averages) reported in Pearce et al. (1997); the accuracy is estimated to be < 20% for Li and < 10% for Be and B (Ottolini et al., 1993). Li, B and Be concentrations were quantified using the SiO2 values of the corresponding EPMA analysis. The setup chosen and the background lead to a detection limit (critical value) of 1.4 ng/g (Li), 1.0 ng/g (Be) and 2.6 ng/g (B; Currie, 1968; Marschall and Ludwig, 2004).

Due to the generally low concentration levels of Li, Be and B in mantle rocks, contamination during sample preparation and handling is always problematic, particularly for B (Shaw et al., 1988). Careful sample preparation is thus a necessary prerequisite for accurate analyses. The standard protocol established by Marschall and Ludwig (2004) was used to prepare the thin sections for this study at the Geological Institute of Neuchâtel resulting in B contamination levels of <2 ng/g. Li contamination is typically 50 times less than for B, and Be does not show any sign of contamination.

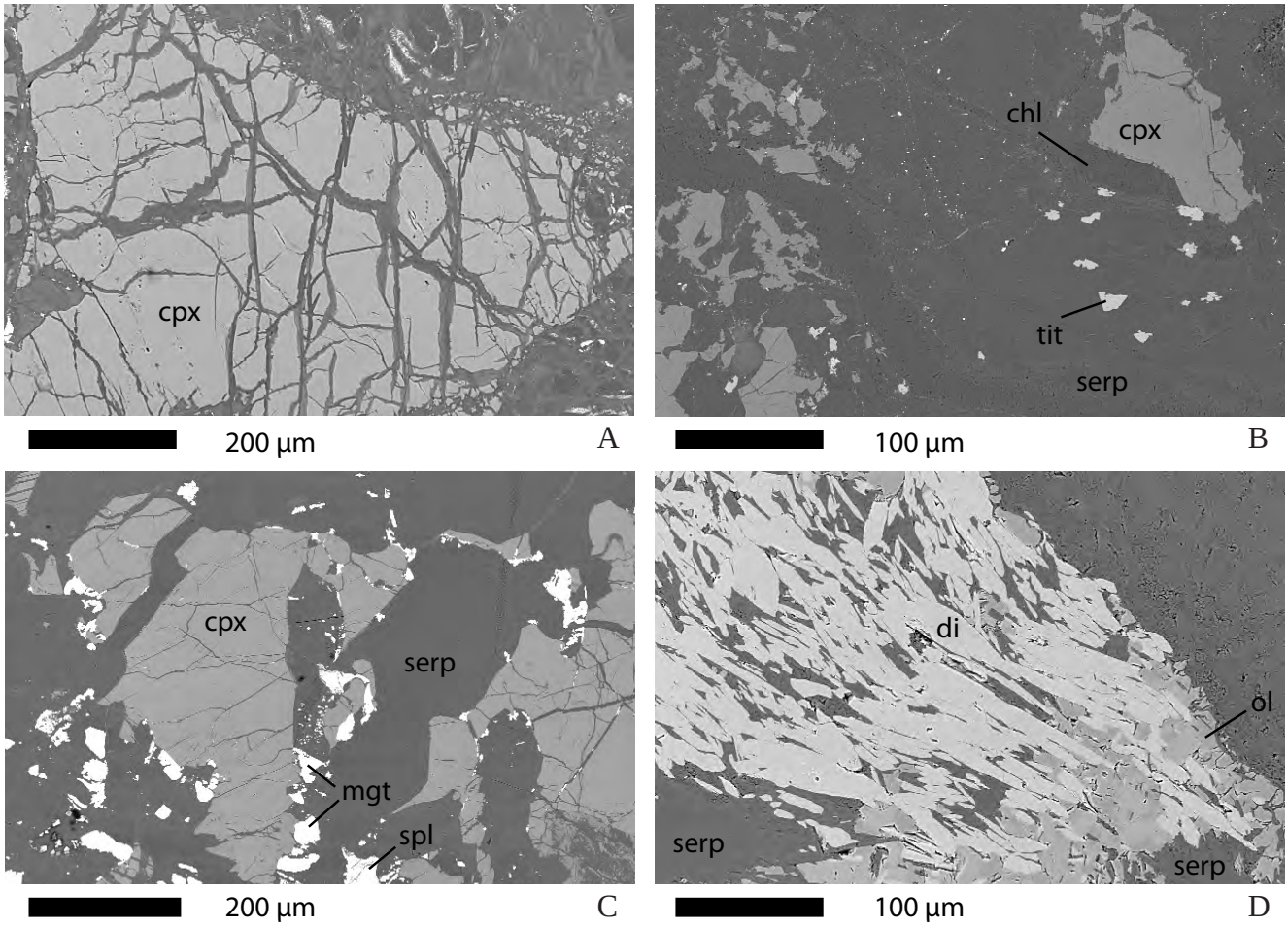

Fig. 4.2: Backscattered images of some studied samples, illustrating the textural difference between the massifs. A) sample To1 B) sample fap4 C) sample crp3 D) samples pum 117 (cpx clinopyroxene, di alpine diopside, ol olivine, tit titanite, serp serpentine, chl chlorite, spl spinel, mgt magnetite).

4.4. Sample characteristics

Mineral compositions and investigated rock types are summarized in Table 1. All samples are partially to completely altered with estimated serpentinization degrees of 20 to 95% (Fig. 4.2). The texture is mostly porphyroclastic. Only sample P 6 has a mylonitic texture with 'augen'-like, elongated pyroxene porphyroclasts. Clinopyroxene (cpx) occurs throughout the samples (except sample L-Um 216). Cpx in sample P-Um 117 is Alpine metamorphic diopside crystallized in elongated clusters within a vein (Fig. 4.2). Mantle olivine (ol) and orthopyroxene (opx) are commonly found in the Totalp and Malenco region, but very rare in the Platta ultramafic rocks. Opx and cpx contain exsolution lamellae of the complementary pyroxene. Ti-rich primary amphiboles and tremolite are commonly found in Totalp and Malenco samples. Talc, phlogopite and a nickel-iron-sulfide occur are accessory phases in some samples. Magnetite is usually associated with serpentine, while primary Cr-spinel can be found in relatively unaltered peridotites and in some strongly serpentinized samples. Serpentine (serp) and chlorite are the most common secondary phases formed after mantle phases. In the samples studied chrysotile is the serpentine phase occurring in the TO, UP and LP massif, while antigorite occurs in the MAL massif. Serpentine forms pseudomorphic textures after opx (bastite) and ol (meshes; using nomenclature after Wicks and Whittaker, 1977), rare serpentine veins are also present. Veins of calcite occur in samples Mg 65, L-Um 224 and L-Um 216-2. Chlorite occurs throughout the samples. Two different chlorite formation events are postulated, one prealpine and the other (Müntener et al., 2000), although separation of the two is not trivial. Andradite (hydrogarnet) was identified in sample NAP 7, titanite was found in sample FAP 4 and perovskite in sample MG 65. In general the microtextures suggest that ol is primarily replaced by serp, while opx is often partially or completely replaced by talc in Malenco samples. Metamorphic tremolite is usually replacing primary cpx, but might also occur as coronas around opx (for details, see Müntener et al., 2000 and Desmurs et al., 2001).

4.5. Mineral chemistry

Mineral compositions are listed in Appendix A. Here we summarized the most important results.

4.5.1 Mantle phases

Olivine from MAL has Mg# ranging from 0.86 to 0.91. This overlaps with olivine from TO (average 0.89). NiO contents vary between 0.17 and 0.37 wt% (MAL), 0.17 and 0.27 wt% (TO) respectively. Our samples from LP and UP contain no ol (Table 1).

Orthopyroxenes found in 4 samples and show variations in Al_2O_3 (2.52 to 4.19 wt%) and SiO_2 content (54.9 to 56.8 wt%). CaO content is low (0.25 to 0.48 wt%). Mg# ranges from 0.90 to 0.91, similar to olivine.

Mantle clinopyroxene (cpx) and Alpine metamorphic diposide occur throughout the three massifs (Table 1). The Mg# of mantle cpx varies between 0.90 to 0.92. CaO contents range from 20.5 to 24.0 wt% and Al_2O_3 varies between 1.74 and 6.75 wt%. Alpine diopside, in contrast, has Mg# varying between 0.91 and 0.97 and Al_2O_3 ranging from 0.03 to 0.87 wt%.

Spinel grains often display holly leave structures and may be Al- or Cr-rich (Müntener, 1997; Desmurs, 2001). Al-rich spinel is found only in the MAL and TOT ophiolite.

Two types of amphiboles occur throughout the three massifs, a Ti-rich amphibole (Ti-pargasite or kaersutite) and a Mg-hornblende to tremolitic amphibole (Appendix A). Ti-pargasite contains 0.48 to 5.87 wt% TiO_2 and Mg# varies between 0.89 and 0.91 %. In tremolite the Mg# ranges from 0.94 to 0.96 %. TiO_2 content is much lower than that of Ti-pargasite (0.03 to 0.25 wt%). Cr_2O_3 content varies between 0.08 and 0.51 wt%.

4.5.2 Metamorphic phases

The most abundant metamorphic formed phases are serpentine and chlorite (Table 1). They are often intergrown and could not be analysed separately. In order to distinguish an analysis comprising mostly serpentine from one representing mainly chlorite, a maximum of 4 wt% Al_2O_3 for serpentine was used. Serpentine minerals have variable SiO_2 (38.68 and 42.57 wt%), and FeO ranges from 3.07 to 8.66 wt%. Al_2O_3 varies between 0.10 and 2.82 wt%. Chlorite has variable Al_2O_3

content ranging (from 12.01 to 17.54 wt%) and SiO_2 (from 32.03 to 35.18 wt%). TiO_2 and Cr_2O_3 contents are below detection limit. As additional oxide, magnetite is common within the studied samples. Some less abundant minerals have not been analysed by EMP (calcite, an iron-nickel sulfide), and others have rarely been analysed (titanite, phlogopite talc and andratite). Titanite contains 32.25 wt% TiO_2 and 31.41 wt% SiO_2. Phlogopite contains high amounts of TiO_2 (average 1.35 wt%). Talc is rich in Cl (3.42 wt%). Andradite contains 35.29 wt% SiO_2.

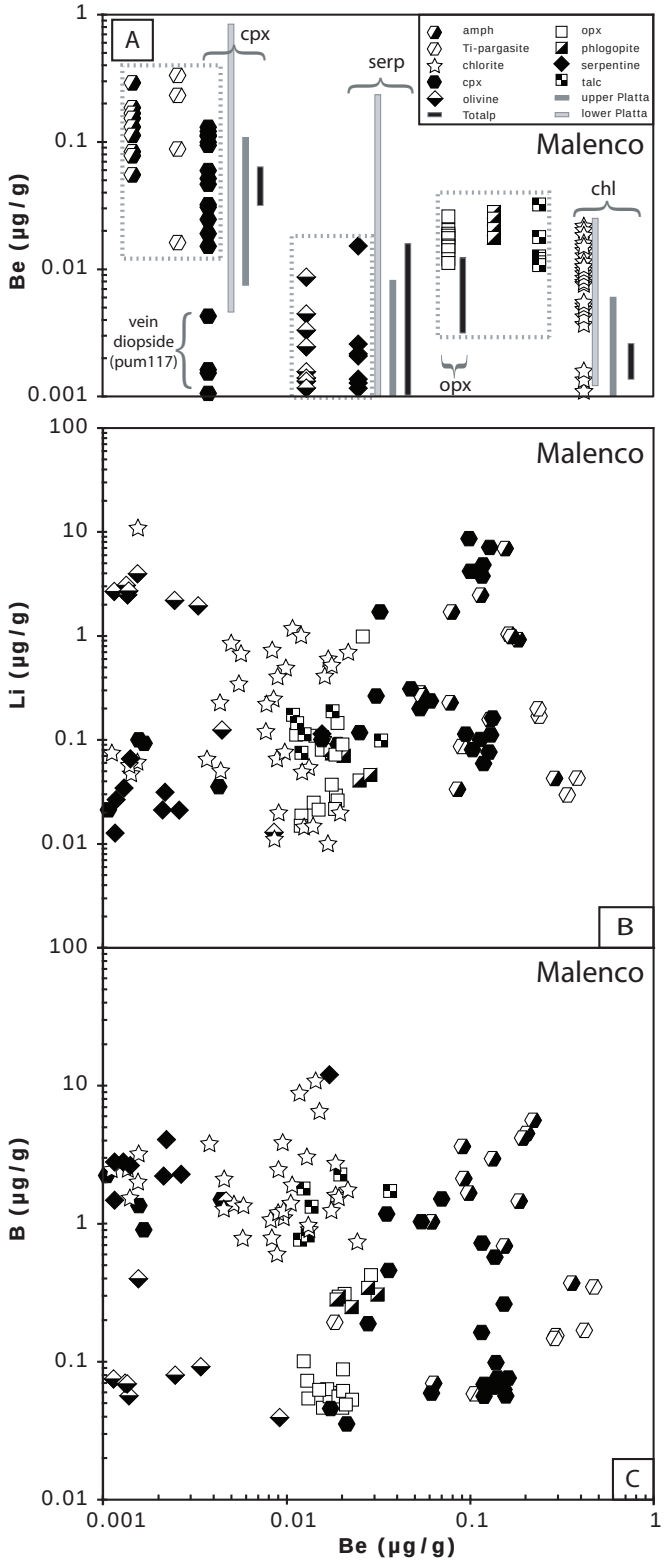

Fig. 4.3. A) Be-content of the different mineral phases occurring in the Malenco massif. Additionally mineral data from the Totalp and Plata massif are added if available. B) Li versus Be diagram and C) and B versus Be-diagram.

4.6. Light elements

As Pelletier et al. (2008a) could show for the Geisspfad ophiolite in the Alps, fluids from country rock influence the light element content in an ophiolite body only within the outermost 100 to 150 m. In order to avoid

Fig. 4.4. Transect from Platta to Malenco ophiolite, plotting Li (A), Be (B) and B (C) data of chlorites.

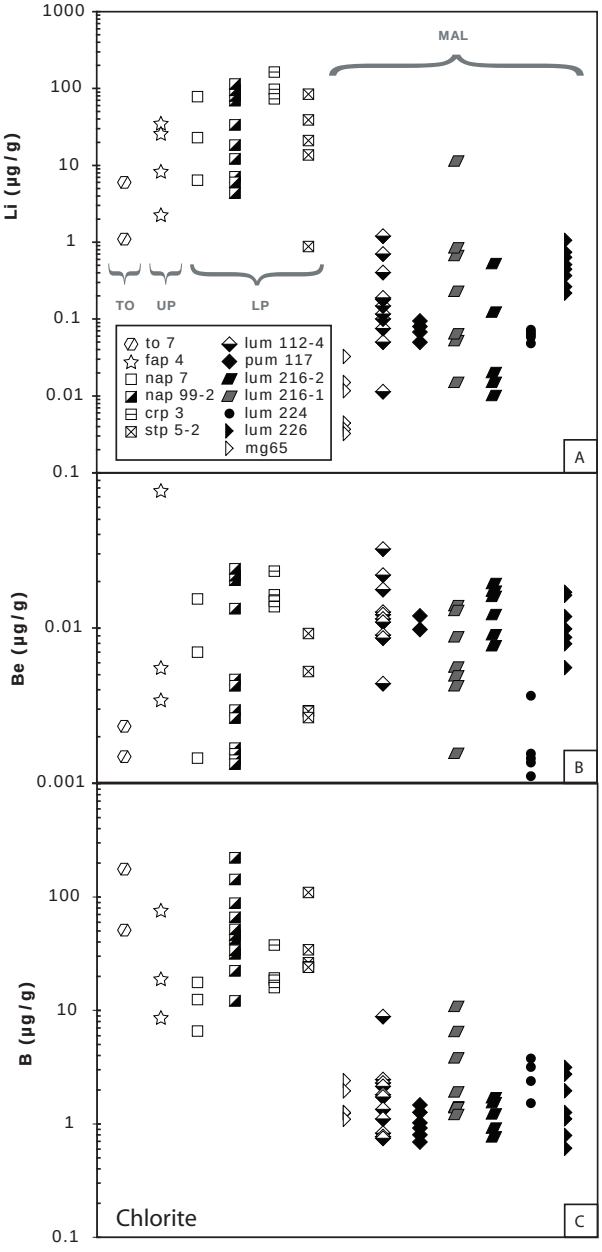

Table 2: SIMS analyses of olivine, orthopyroxene, tremolite, Ti-pargasite, phlogopite

	Sample	Li (µg/g)	2 sigma (µg/g)	Be (µg/g)	2 sigma (µg/g)	B (µg/g)	2 sigma (µg/g)
	Olivine						
TO	to1c2ol1	1.563	0.051	b.d.l.	-	0.050	0.010
TO	to1c2ol7	1.609	0.045	b.d.l.	-	0.042	0.014
TO	to1c2ol1	1.456	0.043	b.d.l.	-	0.042	0.009
TO	to7c2ol4	1.837	0.058	b.d.l.	-	0.075	0.018
TO	to7c2ol1	1.811	0.070	0.001	0.001	0.069	0.015
TO	to7c2ol6	1.751	0.031	b.d.l.	-	0.057	0.009
MAL	lum112c3ol2	1.509	0.232	b.d.l.	-	0.104	0.006
MAL	lum117c2tr9	0.124	0.016	0.004	0.006	1.461	0.058
MAL	lum216-1c1ol1	1.335	0.059	b.d.l.	-	0.049	0.015
MAL	lum216-c1-ol1	1.139	0.042	b.d.l.	-	0.107	0.028
MAL	lum216-c2-ol1	1.244	0.046	b.d.l.	-	0.154	0.042
MAL	lum216-c2-ol5	1.091	0.061	b.d.l.	-	0.173	0.019
MAL	lum216_2c3ol6	3.043	0.102	0.001	0.001	0.070	0.013
MAL	lum216_2c1ol1	2.362	0.238	0.001	0.001	0.063	0.022
MAL	lum216_2c1ol7	2.700	0.061	0.001	0.001	0.074	0.016
MAL	lum216_2c1ol8	2.826	0.117	b.d.l.	-	0.068	0.024
MAL	lum216_2c1ol5	2.679	0.082	0.001	0.002	0.057	0.021
MAL	lum216_2c1ol4	2.556	0.099	0.001	0.002	0.070	0.011
MAL	lum216_2c3col10	2.650	0.083	b.d.l.	-	0.071	0.015
MAL	lum216_2c4ol3	2.154	0.052	0.002	0.003	0.080	0.023
MAL	lum216_2c4ol2	2.450	0.064	b.d.l.	-	0.095	0.030
MAL	lum216_2c4ol4	2.886	0.096	b.d.l.	-	0.084	0.021
MAL	lum216_2c3sol3	2.754	0.063	b.d.l.	-	0.097	0.028
MAL	lum226c1ol2	0.013	0.004	0.009	0.002	0.039	0.008
MAL	lum226c1ol3	0.198	0.018	b.d.l.	-	0.054	0.016
MAL	lum226c4ol3	1.847	0.036	b.d.l.	-	0.073	0.019
MAL	lum226c1ol1	1.959	0.058	0.003	0.002	0.092	0.016
MAL	mg65c4ol1	0.882	0.041	b.d.l.	-	2.044	0.075
MAL	lum224c1ol2	3.865	0.075	b.d.l.	-	0.103	0.029
MAL	lum224c2ol1	3.997	0.039	0.002	0.001	0.396	0.033
MAL	lum224c2ol9	4.974	0.114	b.d.l.	-	0.175	0.026
MAL	lum224c2ol2	1.279	0.052	b.d.l.	-	0.545	0.044
	Orthopyroxene						
TO	to1c2op3	0.494	0.020	0.005	0.001	0.304	0.035
TO	to1c2op5	0.218	0.008	0.007	0.001	1.135	0.077
TO	to1c2op1	0.341	0.027	0.007	0.002	0.129	0.020
TO	to1c2op4	0.775	0.044	0.006	0.002	1.674	0.154
TO	to1c1op4	0.158	0.012	0.006	0.002	0.034	0.008
TO	to7c1ol2	0.121	0.020	0.003	0.002	0.022	0.008
TO	to7c1ol4	0.257	0.017	0.007	0.002	0.029	0.010
TO	to7c1ol1	0.115	0.008	0.006	0.003	0.140	0.021
TO	to7c2op2	0.170	0.020	0.011	0.003	0.421	0.044
TO	to7c2op4	0.848	0.101	0.010	0.004	0.538	0.056
MAL	lum112c3ol3	0.112	0.002	0.012	0.010	0.101	0.013
MAL	lum112c1op1	0.073	0.009	0.019	0.001	0.059	0.011
MAL	lum112c1op3	0.110	0.007	0.016	0.004	0.059	0.010
MAL	lum112c1ol7	0.081	0.003	0.016	0.003	0.055	0.001
MAL	lum112c1op8	0.110	0.011	0.015	0.001	0.046	0.013
MAL	lum112c2op4	0.145	0.040	0.019	0.004	0.309	0.008
MAL	lum112c2op7	0.036	0.004	0.018	0.003	0.056	0.003
MAL	lum112c2op1	0.090	0.005	0.020	0.005	0.051	0.002
MAL	lum226c1op1	0.029	0.005	0.019	0.004	0.088	0.018
MAL	lum226c1op5	0.026	0.006	0.019	0.004	0.048	0.012
MAL	lum226c1op10	0.015	0.003	0.012	0.003	0.072	0.019
MAL	lum226c3op1	0.019	0.003	0.012	0.003	0.054	0.018
MAL	lum226c3op3	0.025	0.007	0.014	0.004	0.061	0.020
MAL	lum226c3ol2	0.997	0.054	0.026	0.003	0.420	0.052
MAL	lum226c3op5	0.022	0.005	0.018	0.004	0.047	0.007
MAL	lum226c3ol3	0.021	0.005	0.015	0.003	0.062	0.009
	Tremolite						
MAL	lum112c1cp4a	0.266	0.015	0.055	0.005	0.068	0.007
MAL	lum216_2c3sr5	0.283	0.112	0.054	0.210	1.014	0.308
MAL	lum216_2c3sr5	0.283	0.112	0.054	0.210	1.014	0.308
MAL	lum216-1c1am1	7.081	0.138	0.154	0.011	1.464	0.068
MAL	lum216-1c1am1	7.081	0.138	0.154	0.011	1.464	0.068
MAL	lum216-1c1am3	1.710	0.083	0.080	0.007	2.160	0.190
MAL	lum216-1c1am3	1.710	0.083	0.080	0.007	2.160	0.190
MAL	lum216-c1-am3xx	2.456	0.049	0.113	0.010	2.928	0.092
MAL	lum216-c1-am3xx	2.456	0.049	0.113	0.010	2.928	0.092
MAL	lum216-c2-am1	0.033	0.011	0.084	0.012	1.673	0.107
MAL	lum216-c2-am1	0.033	0.011	0.084	0.012	1.673	0.107
MAL	lum216-c2-am5	0.227	0.021	0.078	0.010	3.617	0.293
MAL	lum216-c2-am5	0.227	0.021	0.078	0.010	3.617	0.293
MAL	lum224c3ol2 (am)	0.989	0.060	0.165	0.017	4.364	0.190
MAL	lum224c3ol2 (am)	0.989	0.060	0.165	0.017	4.364	0.190
MAL	lum224c3ol3 (am)	1.019	0.030	0.161	0.011	4.170	0.130
MAL	lum224c3ol3 (am)	1.019	0.030	0.161	0.011	4.170	0.130
MAL	lum224c3ol4 (am)	0.902	0.039	0.184	0.015	5.406	0.145
MAL	lum224c3ol4 (am)	0.902	0.039	0.184	0.015	5.406	0.145
MAL	lum226c3am1+2	0.043	0.004	0.289	0.017	0.367	0.034
MAL	lum226c3am1+2	0.043	0.004	0.289	0.017	0.367	0.034
MAL	lum226c4am2	0.043	0.011	0.379	0.029	0.353	0.048
MAL	mg65c4orgcp3	0.158	0.016	0.130	0.010	0.685	0.032
	Ti-pargasite						
MAL	lum112c2cp3	0.175	0.013	0.238	0.015	0.154	0.014
MAL	lum112c2cp4	0.198	0.018	0.235	0.028	0.149	0.018
MAL	lum216_2c3cp2	0.030	0.005	0.337	0.012	0.169	0.017
MAL	lum226c3cp1	0.087	0.010	0.090	0.008	0.059	0.018
MAL	mg65c4cp8	0.094	0.012	0.017	0.004	0.192	0.020
	Phlogopite						
MAL	lum216_2c3amph2	0.041	0.013	0.025	0.007	0.342	0.067
MAL	lum216_2c3amph1	0.069	0.011	0.020	0.004	0.249	0.034
MAL	lum216_2c3amph3	0.047	0.010	0.028	0.004	0.306	0.058
MAL	lum216_2c3amph5a	0.078	0.009	0.017	0.004	0.288	0.034
MAL	lum216_2c3amph5b	0.076	0.009	0.018	0.004	0.294	0.043

any influence of the country rocks or the Bergaglia intrusion all analysed samples were chosen carefully (Fig. 4.1). Li, Be and B concentrations of mantle and metamorphic phases are listed in Tables 2, 3, 4 and 5, and are displayed in Figs. 4.3 to 4.7. Be concentration within all studied minerals of the three ophiolites ranges from below detection limit (<0.001) to 0.898 µg/g (Fig. 4.3). Be is highest in clinopyroxenes and amphiboles and lowest in olivine, serpentine and chlorite. Within one mineral type no major difference in Be concentration occurs (Fig. 4.3), while Li and B concentrations vary between the three massifs (e.g. chlorite Fig. 4.4 or serpentine in Fig. 4.5).

Light element concentrations in olivine from the Totalp peridotite massif ranges from 1.45 to 1.83 µg/g for Li, is <0.001 for Be and from 0.04 to 0.07 µg/g for B. In the Malenco massif, olivine displays more than two orders of magnitude variation in the Li content, varying between 0.01 and 4.97 µg/g, and similar results are obtained for B (0.04 to 1.46 µg/g). Be varies between <0.001 and 0.009 µg/g.

Average light element contents of orthopyroxene from the Totalp and Malenco massifs (0.21 µg/g (Li), 0.013 µg/g (Be) and 0.23 µg/g (B)) are generally lower than those of olivine. The variability of B concentrations is minimal over the two massifs, but the Li content is lower, and the Be content is higher in the Malenco massif (Li: average 0.11 µg/g, compared to average 0.35 µg/g; Be: average 0.0167 µg/g compared to average to 0.0068 µg/g, respectively).

Clinopyroxenes from the TO massif have Li content ranging from 0.25 to 1.89 µg/g, the Be content varies between 0.03 and 0.06 µg/g and B content ranging from 0.04 to 2.13 µg/g. Clinopyroxene from the Upper Platta unit has Li concentrations varying between 0.17 and 13.68 µg/g, Be between 0.008 and 0.099 µg/g and B concentrations between 0.04 and 110.89 µg/g. Lower Platta

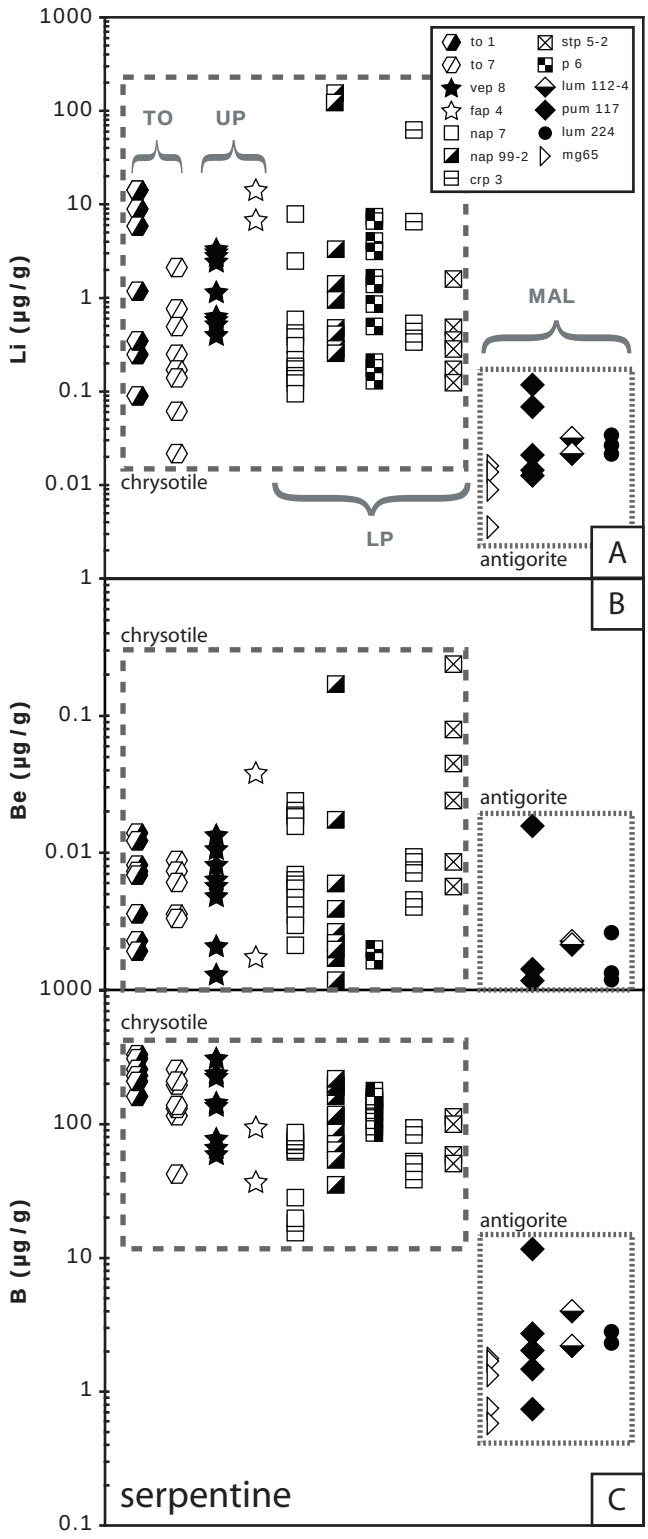

Fig. 4.5. Transect from Platta to Malenco ophiolite, plotting Li (A), Be (B) and B (C) data of serpentine.

clinopyroxene have Li concentrations ranging from 0.12 to 4.47 µg/g, Be concentrations varying from 0.005 to 0.89 µg/g and B concentrations varying between 0.03 and 41.56 µg/g. Malenco clinopyroxene contains 0.01- 8.70 µg/g Li, less than 0.13 µg/g Be and 0.04-3.21 µg/g B.

The two amphiboles occurring in the MAL massif have a distinct light element signal. Tremolite displays highly variable Li and B concentrations (Li: 0.03 to 7.08 µg/g; B: 0.07 to 5.41 µg/g) and Be concentrations up to 0.29 µg/g (Table 2). Ti-pargasite on the contrary is more homogeneous and has low Li and B contents (Li: 0.03 to 0.20 µg/g; B: 0.06 to 0.19 µg/g), while the Be content is similar (0.02 to 0.34 µg/g).

Chlorites have highly variable Be concentrations from <0.001 to 0.078 µg/g. TO, LP and UP show higher Li (>0.87 µg/g), higher B (>6.48 µg/g) content and similar variation in Be concentration compare to MAL (Fig. 4.4). MAL samples are much lower in Li (down to 0.003 µg/g) and B (down to 0.59 µg/g) compared to the other massifs.

Serpentines in the Malenco ultramafic rocks have Li concentrations below 0.12 µg/g (0.003 to 0.12 µg/g), while in the Platta and Totalp ultamafic rocks, Li reaches values up to 156.86 µg/g (Fig. 4.5). Be content is similar in all three massifs, varying between <0.001 and 0.237 µg/g-concentration is generally high in the Totalp peridotite (<0.001 to 0.014 µg/g), the upper Platta (0.001 to 0.039 µg/g) and the lower Platta unit (<0.001 to 0.237 µg/g) compared to antigorite serpentine from Malenco, ranging from <0.001 to 0.016 µg/g.

Andradite from LP (NAP 7) contains 12.48 µg/g Li, 0.009 µg/g Be and 35.80 µg/g B based on a single analyse. Phlogopite has Li content varying between 0.04 and 0.08 µg/g, Be ranging from 0.017 to 0.028 µg/g and B varying between 0.25 and 0.34 µg/g.

4.7. Discussion

4.7.1 Influence of prograde metamorphism on Be

Comparing Be contents of different Ca-phases (tremolite-pargasite-cpx) within the MAL massif reveals that they have similar Be concentrations, with exception of vein diopside (Fig. 4.3). A similar behaviour is observed with for the Mg-phases (opx-tlc-phl and ol-serp). Comparing TO, LP, UP and MAL similar Be concentrations for cpx, opx, serp and chl were measured (Fig. 4.3, Tables 2-4). Thus the data seems to indicate that the Be content does not vary with increasing

Table 3: SIMS analyses of clinopyroxenes

	Sample	Li (µg/g)	2 sigma (µg/g)	Be (µg/g)	2 sigma (µg/g)	B (µg/g)	2 sigma (µg/g)		Sample	Li (µg/g)	2 sigma (µg/g)	Be (µg/g)	2 sigma (µg/g)	B (µg/g)	2 (
TO	to1c2cp3	0.355	0.020	0.041	0.005	0.037	0.010	UP	vep8c2cp1	1.057	0.025	0.054	0.005	0.044	
TO	to1c2cp5	0.512	0.020	0.052	0.005	0.110	0.014	UP	vep8c2cp4	0.902	0.050	0.054	0.005	0.092	
TO	to1c2cp2	0.525	0.023	0.046	0.008	0.255	0.033	UP	vep8c4op4	1.355	0.043	0.052	0.007	0.041	
TO	to1c1cp3	0.824	0.033	0.051	0.006	0.091	0.020	UP	vep8c4cp1	1.859	0.051	0.057	0.005	0.046	
TO	to1c1cp4	0.249	0.014	0.034	0.004	1.021	0.048	UP	vep8c4op2	0.799	0.036	0.057	0.005	0.171	
TO	to7c4cp2	1.326	0.024	0.048	0.008	0.055	0.014	UP	vep8c4cp7	0.907	0.042	0.057	0.006	0.045	
TO	to7c4cp4	1.372	0.052	0.049	0.008	0.697	0.054	UP	vep8c4cp3	0.841	0.035	0.064	0.007	0.049	
TO	to7c1cp1	1.389	0.064	0.047	0.007	2.134	0.091	UP	vep8c4cp2	1.619	0.055	0.053	0.008	0.044	
TO	to7c1cp4	1.892	0.052	0.048	0.004	0.325	0.053	UP	fap4c2cp1	69.504	1.289	0.075	0.010	110.891	
TO	to7c1cp12	1.206	0.057	0.043	0.005	0.054	0.015	UP	fap4c2cp2	5.077	0.124	0.008	0.003	98.820	
TO	to7c1cp9	0.976	0.037	0.061	0.008	0.073	0.014	UP	fap4c2cp5	1.239	0.036	0.104	0.011	0.485	
LP	nap7c1cp1	1.762	0.061	0.125	0.010	0.995	0.061	UP	fap4c3cp2	2.300	0.116	0.104	0.007	0.686	
LP	nap7c1cp5	1.357	0.041	0.122	0.007	0.617	0.039	UP	fap4c4cp9	1.732	0.034	0.100	0.009	1.490	
LP	nap7c1cp8	1.789	0.046	0.122	0.007	0.136	0.020	MAL	lum112c1cp5a	0.204	0.014	0.052	0.007	0.059	
LP	nap7c3cp2	2.536	0.058	0.146	0.008	4.195	0.093	MAL	lum112c1cp5	0.091	0.006	0.019	0.002	0.036	
LP	nap7c3cp8	2.249	0.051	0.114	0.012	6.096	0.171	MAL	lum112c1cp2	0.102	0.010	0.016	0.003	0.046	
LP	napc2cp1	1.942	0.031	0.131	0.005	1.803	0.091	MAL	lum117c1tr5	0.455	0.118	0.082	0.037	3.207	
LP	napc3cp3	1.412	0.049	0.140	0.010	2.324	0.126	MAL	lum117c3tr8	0.091	0.029	0.013	0.015	2.369	
LP	napc5cp7	1.547	0.141	0.182	0.069	0.199	0.076	MAL	lum117c1tr1	4.003	0.648	b.d.l.	-	1.636	
LP	napc5cp1	0.321	0.016	0.627	0.019	25.523	0.301	MAL	lum117c1tr2	0.313	0.116	0.047	0.033	1.030	
LP	napc5cp9	0.171	0.005	0.898	0.023	29.121	0.328	MAL	lum117c3tr3	0.022	0.004	0.001	0.001	2.236	
LP	nap99-2c5cp4	1.559	0.039	0.129	0.005	0.653	0.051	MAL	lum117c3tr9	0.014	0.004	0.001	0.001	1.543	
LP	nap99-2c5cp8	1.527	0.044	0.131	0.015	0.218	0.032	MAL	lum117c2tr3	0.095	0.014	0.002	0.001	0.901	
LP	nap99-2c5cp10	1.606	0.051	0.109	0.009	0.422	0.042	MAL	lum117c2tr6	0.017	0.003	b.d.l.	-	0.876	
LP	nap99-2c4cp1	0.808	0.028	0.115	0.020	41.560	0.832	MAL	lum117c2tr5	0.077	0.007	b.d.l.	-	1.162	
LP	nap99-2c4cp11	1.552	0.031	0.123	0.014	3.672	0.272	MAL	lum117c2tr2	0.240	0.024	0.060	0.004	1.521	
LP	nap99-2c4cp8	2.427	0.051	0.136	0.022	6.632	0.199	MAL	lum117c2tr2a	0.267	0.035	0.031	0.005	1.170	
LP	nap99-2c1cp9	1.724	0.062	0.127	0.016	1.041	0.116	MAL	lum117c2tr1	3.971	0.386	0.114	0.007	0.580	
LP	nap99-2c3cp4	1.549	0.023	0.126	0.005	0.150	0.022	MAL	lum117c2sr6	0.101	0.015	0.002	0.002	1.377	
LP	nap99-2c3cp2	1.485	0.051	0.103	0.012	0.120	0.021	MAL	lum226c1cp10	0.061	0.012	0.116	0.010	0.099	
LP	nap99-2c4cp9	0.498	0.026	0.071	0.011	18.204	0.340	MAL	lum226c4cp3	0.101	0.010	0.112	0.015	0.065	
LP	nap99-2c5cp7	1.951	0.027	0.123	0.014	2.422	0.085	MAL	lum226c4cp1	0.168	0.013	0.133	0.010	0.075	
LP	crp3c7cp2	2.888	0.143	0.070	0.013	2.480	0.130	MAL	lum226c3cp4	0.082	0.011	0.101	0.007	0.069	
LP	crp3c1cp9	4.470	0.098	0.105	0.011	2.569	0.211	MAL	lum226c1cp6	0.115	0.011	0.097	0.014	0.162	
LP	crp3c1cp6	0.964	0.036	0.085	0.008	0.032	0.014	MAL	lum226c1cp9	0.112	0.019	0.128	0.015	0.058	
LP	crp3c1cp1	1.621	0.067	0.077	0.008	0.445	0.061	MAL	lum226c1cp1	0.076	0.012	0.125	0.015	0.063	
LP	crp3c8cp5	1.001	0.054	0.107	0.012	0.129	0.021	MAL	lum224c2cp1	4.221	0.096	0.100	0.010	0.057	
LP	crp3c8cp1	1.107	0.051	0.084	0.005	0.207	0.018	MAL	lum224c2cp3	4.790	0.107	0.117	0.008	0.076	
LP	crp3c7cp1	1.922	0.058	0.099	0.013	0.087	0.025	MAL	lum224c2cp5	7.091	0.141	0.126	0.009	0.262	
LP	crp3c7cp2-5	1.595	0.067	0.305	0.019	28.622	0.318	MAL	lum224c2cp6	8.699	0.105	0.098	0.014	0.717	
LP	crp3c7cp2-4	0.386	0.030	0.137	0.013	5.721	0.249	MAL	mg65c4cp5	0.036	0.005	0.004	0.001	1.483	
LP	crp3c7cp2-1	0.402	0.029	0.201	0.019	22.827	0.356	MAL	mg65c4cp4	1.734	0.057	0.032	0.003	0.463	
LP	crp3c8cp6	1.298	0.023	0.092	0.011	3.483	0.127	MAL	mg65c3cp4	0.070	0.009	0.047	0.007	0.637	
LP	stp5-2c3cp2	1.356	0.044	0.522	0.020	34.148	0.500	MAL	mg65c5cpx3	0.118	0.012	0.025	0.004	0.187	
LP	stp5-2c3cp1	1.151	0.043	0.494	0.028	34.565	0.270	MAL	p6C2cp1	0.989	0.028	0.011	0.006	25.493	
LP	stp5-2c2cp2	1.514	0.036	0.139	0.011	0.533	0.055	MAL	p6C2cp2	1.199	0.044	0.008	0.004	24.947	
LP	stp5-2c2cp1	1.649	0.064	0.102	0.010	0.187	0.027	MAL	p6C4cp4	0.938	0.035	0.188	0.016	22.873	
LP	stp5-2c4cp3	0.154	0.016	0.312	0.021	18.102	0.281	MAL	p6C4cp3	0.756	0.032	0.005	0.004	11.675	
LP	stp5-2c4cp2	0.116	0.012	0.443	0.029	37.919	2.091	MAL	p6C4cp1b	1.009	0.036	0.068	0.010	20.898	
LP	stp5-2c4cp5	2.334	0.066	0.120	0.006	2.991	0.132	MAL	p6C4cp2	0.433	0.012	0.022	0.007	11.150	
LP	stp5-2c4cp1	1.490	0.059	0.138	0.011	2.362	0.183								
LP	stp5-2c2cp3	1.372	0.045	0.139	0.010	1.321	0.081								

metamorphic grade.

Our findings are in general consistent with previous studies on the behaviour of light elements. Li, Be and B are regarded as fluid mobile (Brenan et al., 1998) and are thus expected to be enriched in the extracted fluids during prograde metamorphism, with the consequence that primary minerals should display slightly higher light element concentration compared to secondary minerals. In-situ measurements by inductively coupled plasma emission spectrometry on minerals from the Catalina schists showed that Be is not fluid-mobile within a subduction zone, as primary minerals and secondary minerals formed under high-grade metamorphism have similar Be concentration Bebout et al. (1993). On the other hand limited Be mobility at high-grade metamorphism was suggested by Domanik et al. (1993). The findings of the latter are also in line with the experiments of Tatsumi and Isoyama (1988).

We infer that Be concentrations within mantle minerals is thus probably following a two-stage process: (A) at low T and P and common fluid compositions, any phase transformation related to serpentinization keeps mineral Be content stable suggesting limited mobility of Be during low-temperature alteration. (B) at high-temperature (850-900°C) and pressure (1.5-2.0 GPa), as experiments suggest (Tatsumi and Isoyama, 1988; Brenan et al., 1998), Be displays some mobile behaviour and can therefore be slightly enriched within the mantle wedge or subcontinental mantle.

The MAL ophiolite preserved a complex history preserved in minerals formed under mantle conditions to Alpine metamorphism (Müntener, 1997). Mantle relicts are olivine, clinopyroxene, orthopyroxene, spinel and Ti-pargasite. During exhumation of the peridotites retrograde hydration reactions at elevated temperature formed talc, chromite, chlorite, Mg-hornblende to Na-rich tremolite (Müntener et al. 2000). Brucite, ilmenite, magnetite, chlorite and serpentine minerals such as chrysotile and lizardite formed during low temperature alteration of the ultramafic rocks on the seafloor. During Alpine convergence, progressive metamorphism

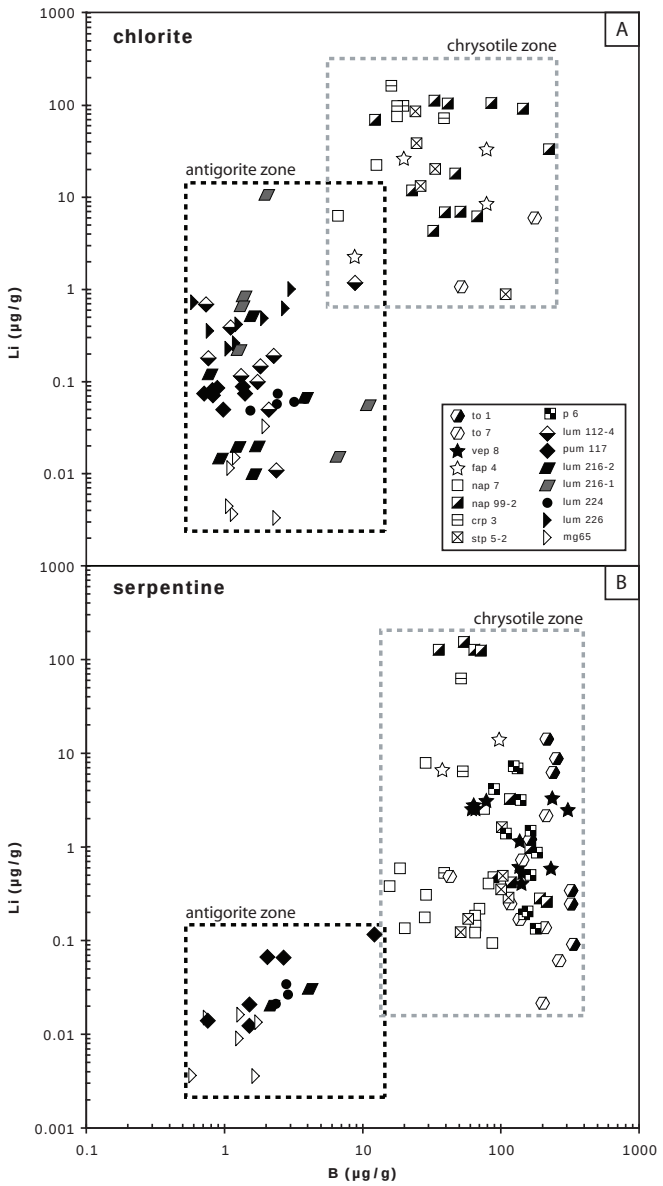

Fig. 4.6. Li versus Be diagram of chlorites (A) and serpentine (B).

of serpentinite formed epidote-amphibolite facies paragenesis in the Malenco ultramafic rocks consisting of antigorite, chlorite, magnetite, Ti-clinohumite, olivine and diopside (Trommsdorff, 1983; Guntli and Liniger, 1989; Hermann, 1997).

In terms of light elements, the transformation from primary to metamorphic phases is monitored to a certain extent by minerals of 'similar' chemistry: olivine transforms into serpentine (mesh texture in serpentine), tremolite transforms into metamorphic diopside. Chlorite on the contrary, can be formed at the expense of all primary phases as long as an Al-rich phase is present (e.g. spinel).

Fig. 4.3 illustrates dehydration reactions and loss of light elements related to increasing metamorphism, with respect to Li and B. In contrast, Be displays a conservative behaviour. Minerals formed during alpine metamorphism have Be concentrations similar to primary minerals (e.g. ol similar to serp). Mineral analyses from the other massifs follow the same trend (Fig. 4.3), thus indicating that Be concentrations of metamorphic minerals largely reflect the compositions of the primary minerals.

4.7.2 Mirroring serpentine transformation from N to S

During subduction of oceanic mantle, prograde metamorphism changes serpentinites first from lizardite/chrysotile-rich assemblage to antigorite schists and ends with antigorite breakdown and formation of a metamorphic rock with olivine, orthopyroxene and chlorite (metaharzburgite, e.g. Trommsdorff et al., 1998). Prograde metamorphism in Alpine serpentinites generally follows a lower pressure path, but is a natural laboratory to study such phase transformations. From TO to MAL, the metamorphic conditions change from prehnite-pumpellyite to epidote-amphibolite facies (Fig. 4.1). The serpentine mineral from N to S changes from chrysotile to antigorite and follows three major mineral reactions in the MSH/CMSH-system: chrysotile => antigorite + brucite (I), chrysotile + talc => antigorite (II) and chrysotile + tremolite => antigorite + diopside (III; Fig 4.1). From N to S the change from chrysotile to antigorite is gradual and the Platta unit is considered as a reaction transition zone, although our studied samples contain only chrysotile. In MAL, antigorite is the main serpentine mineral (Peretti, 1988), while TO is dominated by chrysotile (Peters, 1963). Two additional reactions might occur as well within the studied rocks and influence the available fluid budget: chrysotile => antigorite+ forsterite + H_2O (IV) and brucite + chrysotile => forsterite + H_2O (V; Evans et al., 1976). However, these reactions IV and V are probably irrelevant in our case, since reaction I completely consumed chrysotile.

The Be variability of mantle minerals is similar in the two massifs (TO and MAL) varying between <0.001 and 0.016 µg/g, and prograde Alpine metamorphism did not modify the primary mineral Be content (Fig. 4.3). Oceanic chrysotile/lizardite (<0.001 to 0.080 µg/g, ODP Leg 209; Vils et al., 2008) and ophiolitic antigorite (e.g. <0.001 to

Table 4: SIMS analyses of serpentine

Sample	Li (µg/g)	2 sigma (µg/g)	Be (µg/g)	2 sigma (µg/g)	B (µg/g)	2 sigma (µg/g)
Serpentine						
to1c2sr1	0.256	0.014	0.007	1.652	325.282	3.253
to1c2sr5	0.092	0.011	0.014	1.788	327.166	1.178
to1c2sr8	14.347	0.189	0.007	1.346	213.297	0.768
to1c2sr12	8.948	0.082	0.008	2.440	250.767	1.154
to1c2sr1	6.226	0.524	0.002	0.728	231.753	8.992
to1c2sr4	1.190	0.044	0.002	1.347	161.903	1.943
to1c2sr7	0.354	0.030	0.004	0.002	318.205	1.622
to1c1sr1	9.036	0.089	0.012	2.082	246.887	1.037
to7c4sr4	0.253	0.020	0.003	0.001	116.694	1.421
to7c4sr2	0.062	0.009	0.006	0.003	259.096	1.332
to7c4sr1	0.140	0.022	0.007	0.003	202.364	1.493
to7c1sr2	2.170	0.093	0.009	0.003	210.209	0.727
to7c2sr10	0.754	0.037	0.006	0.002	140.537	0.919
to7c1sr3	0.497	0.034	b.d.l.	-	42.263	0.636
to7c1sr5	0.022	0.005	0.009	0.002	198.305	0.892
to7c4sr9	0.172	0.014	0.004	0.002	135.232	1.755
nap7c1sr1	7.987	0.532	0.006	0.002	28.501	0.744
nap7c1sr10	0.179	0.019	0.005	0.002	27.970	0.276
nap7c1sr12	0.315	0.025	0.004	0.002	28.456	0.640
nap7c1sr2	0.190	0.011	0.016	0.003	63.310	0.843
nap7c1sr3	0.221	0.012	0.006	0.001	69.540	1.200
nap7c1sr8	0.139	0.019	0.004	0.002	19.898	0.236
nap7c3sr6	0.126	0.013	0.007	0.001	63.533	0.404
nap7c3sr7	0.148	0.007	0.006	0.003	64.975	0.495
nap7c2sr11	0.096	0.006	0.020	0.004	85.505	0.516
nap7c2sr5	0.386	0.025	0.003	0.001	15.527	0.442
nap7c2sr8	0.604	0.031	0.002	0.002	18.429	1.120
nap7c2sr9	0.096	0.010	0.018	0.003	85.622	0.550
nap7c5sr1	0.420	0.022	0.024	0.003	80.168	0.455
nap7c5sr5	2.550	0.228	0.019	0.016	74.477	1.646
nap99-2c1sr8	0.477	0.025	0.002	0.001	86.902	0.998
nap99-2c1sr9	0.420	0.022	b.d.l.	-	117.254	0.116
nap99-2c3sr5	0.285	0.016	0.002	0.001	188.268	0.836
nap99-2c5sr3	3.374	0.120	0.001	0.002	115.346	0.722
nap99-2c5sr7	0.263	0.015	0.002	0.002	211.746	3.274
nap99-2c5sr8	0.996	0.035	0.003	0.003	162.666	0.911
nap99-2c1sr1	156.859	2.814	0.004	0.002	53.836	0.825
nap99-2c1sr2	125.295	2.245	0.004	0.003	70.187	1.867
nap99-2c1sr5	128.519	0.792	0.006	0.002	35.066	0.320
nap99-2c1sr6	127.968	1.761	0.017	0.003	63.363	1.661
stp5-2c2sr1	0.123	0.013	0.006	0.001	50.545	0.568
stp5-2c2sr2	0.172	0.020	0.008	0.002	57.999	0.581
stp5-2c4sr3	0.352	0.026	0.078	0.007	100.968	0.717
stp5-2c4sr1	0.289	0.019	0.024	0.006	112.847	0.907
stp5-2c4sr2	0.485	0.024	0.044	0.008	102.141	1.083
stp5-2c4sr4	1.603	0.030	0.237	0.013	100.952	0.533

Sample	Li (µg/g)	2 sigma (µg/g)	Be (µg/g)	2 sigma (µg/g)	B (µg/g)	2 sigma (µg/g)
crp3c1sr2	6.527	0.128	0.004	0.002	52.624	0.657
crp3c1sr1	63.306	1.394	0.007	0.002	50.727	0.673
crp3c8sr2	0.372	0.028	0.009	0.002	82.320	0.831
crp3c7sr1	0.541	0.033	0.004	0.002	38.460	0.688
crp3c8sr3	0.344	0.019	0.009	0.002	93.345	0.491
vep8c2sr5	0.532	0.017	0.006	0.001	140.856	1.023
vep8c2sr7	0.595	0.038	0.013	0.003	227.419	1.292
vep8c2sr4	2.480	0.112	0.010	0.003	302.069	4.005
vep8c2sr1	3.324	0.127	0.013	0.003	232.693	1.941
vep8c2sr11	2.740	0.115	0.001	0.001	63.268	2.298
vep8c2sr12	3.186	0.058	0.002	0.001	76.228	1.674
vep8c2sr13	0.406	0.023	0.006	0.001	141.450	0.603
vep8c4sr3	2.565	0.076	0.001	0.001	60.973	0.721
vep8c4sr1	2.599	0.065	0.001	0.001	64.779	0.637
vep8c4sr10	0.625	0.021	0.008	0.002	136.107	1.328
vep8c4sr14	1.149	0.030	0.005	0.001	135.596	1.546
fap4c2sr12	6.963	0.116	0.039	0.001	37.351	0.959
fap4c2sr3	14.536	0.620	0.002	0.002	96.331	1.000
lum117c1sr3	0.068	0.033	b.d.l.	-	2.017	0.189
lum117c1sr7	0.117	0.036	0.016	0.013	11.969	1.489
lum117c2sr8	0.014	0.008	0.001	0.001	0.759	0.078
lum117c3sr4	0.067	0.005	0.001	0.001	2.663	0.064
lum117c3sr5	0.021	0.003	0.001	0.001	1.527	0.061
lUM117c3tsr9	0.013	0.002	0.001	0.001	1.483	0.038
lum216_2c4sr9	0.021	0.004	0.002	0.001	2.229	0.126
lum216_2c4sr8	0.032	0.005	0.002	0.001	4.085	0.128
lum224c1sr1	0.027	0.005	0.001	0.001	2.830	0.179
lum224c1sr7	0.035	0.014	0.001	0.001	2.790	0.105
lum224c1sr9	0.021	0.003	0.003	0.001	2.298	0.162
mg65c4sr13	0.004	0.002	0.000	0.001	1.648	0.045
mg65c4sr8	0.013	0.005	0.001	0.000	1.733	0.092
mg65c4orgsr8	0.016	0.006	b.d.l.	-	0.745	0.144
mg65c4orgsr10	0.016	0.004	0.001	0.001	1.291	0.164
mg65c5sr2	0.004	0.002	b.d.l.	-	0.579	0.034
mg65c4orgsr5	0.009	0.003	b.d.l.	-	1.263	0.049
p6C2sr7	1.473	0.119	b.d.l.	-	107.576	2.130
p6C2sr1	0.137	0.017	0.002	0.002	177.177	1.414
p6C2sr6	0.198	0.008	b.d.l.	-	145.154	0.912
p6C4sr6	7.562	0.118	b.d.l.	-	122.437	0.803
p6C2sr5	1.523	0.106	0.002	0.001	160.607	0.723
p6C2sr9	1.674	0.044	0.001	0.001	97.902	1.255
p6C4sr7	0.512	0.025	0.002	0.002	144.421	0.471
p6C4sr8	7.118	0.102	b.d.l.	-	130.287	0.698
p6C4sr9	3.307	0.072	b.d.l.	-	137.064	0.606
p6C4sr1	0.523	0.016	b.d.l.	-	163.307	0.585
p6C4sr3	0.895	0.023	0.001	0.001	179.130	0.838
p6C4sr5	0.211	0.015	b.d.l.	-	153.816	1.335
p6C4sr4	4.214	0.131	b.d.l.	-	88.500	0.789

0.040 µg/g; Marschall, 2005; Pelletier et al., 2008a) contain similar concentrations of Be, compared to our data. However, in the Mariana forearc, higher Be concentrations up to 0.070 to 0.160 µg/g for serpentinized harzburgites are reported (Zanetti et al., 2006). Some serpentinized mud volcanoes are currently venting, and geochemical investigation of these fluids suggests dehydration reactions in the subducted Pacific plate as a source of elevated Be contents (e.g. Mottl et al., 2003; Mottl et al., 2004). Thus the elevated Be concentration reported for Mariana forearc is related to the liberated fluid release as well as the original mantle composition.

Comparing chrysotile from the TO, LP and UP to antigorite from MAL, reveals relatively high Li and B content in TO, LP and UP compared to MAL (Fig. 4.6). The sharp drop of Li and B concentrations seems to be related to the complete transformation of chrysotile into antigorite (Reaction I-III completed, Fig. 4.1). The stoichiometry of the mineral reactions in a simplified CMSH-system indicates that the transformation is conservative with respect to H_2O (see reactions I-III), e.g. no fluid is added or released. Electron microprobe analyses of serpentine revealed that the mineral structure of chrysotile and antigorite accommodates considerable amounts of FeO_{tot}^{2+} (up to 0.33 wt%; Appendix A). A second, important observation is that modal magnetite increases from LP and UP to the MAL ophiolite. Therefore, redox-reactions with water liberation are very likely to take place during transition from chrysotile to antigorite (e.g. Fe-serp + O_2 => mgt + SiO_2 + H_2O; VI). As B and Li are both fluid-mobile (e.g. Brenan et al., 1998), both elements would be enriched in the fluid phase and in precipitating minerals.

Although partition coefficients reported for amphiboles (e.g. amphibole/fluid 0.016 B; Brenan et al., 1998) might suggest that the latter are a sink for the Li and B lost during chrysotile-antigorite transformation, low abundance of amphiboles in the MAL massif does not compensate the whole rock budget. On the other hand, brucite formed by reaction I might be a sink for B (estimated to 60 µg/g at Hess Deep; Plas, 1997; Früh-Green et al., 2004), but brucite is known to occur only rarely within the studied massifs (Trommsdorff and Evans, 1974). Diopside on

the contrary is not known to incorporate high amount of B (max. 13 µg/g, Neumann et al., 2002; Neumann et al., 2004; see also Fig. 4.), so metamorphic diopside is not a sink either. Therefore, to incorporate the ~100 µg/g B in newly formed brucite or diopside seems very unlikely. Additionally, pore-fluid measurements of the Mariana fore-arc mud-serpentinites showed B content ranging from 1.98 to 42.90 µg/g and Li content < 0.11 µg/g, with higher B and lower Li concentration at the bottom (Mottl et al., 2003). Compared to the pore fluids, serpentinites from Mariana fore-arc (brucite containing) have higher Li concentrations (1.59 to 18.9 µg/g) and similar B concentrations (6.8 to 57.5 µg/g; Benton et al., 2001; Benton et al., 2004; Savov et al., 2007). Savov et al. (2007) proposed that dehydration at the onset of subduction leads to loss of B (80%) and Li (9%) from the oceanic plate. Such a process is in line with the high B content of pore fluids and serpentine mud at the Mariana fore-arc.

Investigations of chrysotile/lizardite from oceanic peridotites showed that B is highly enriched and Li highly depleted compared to primary phases (e.g. up to 138 µg/g (B) in serp, 2.39 µg/g (B) in cpx at ODP Leg 209 respectively; Vils et al., 2008). Chrysotile from TO, LP and UP shows B and Li concentrations that are very similar to those of serpentine from oceanic environments (Fig. 4.6). In-situ measurements of light elements in antigorite from metamorphic environments have been conducted before (Scambelluri et al., 2004; Marschall, 2005; Pelletier et al., 2008a). In general, they agreed that antigorite contains up to 39 µg/g B. Additionally, Scambelluri et al. (2004) studied the B and Li composition in serpentine on the subduction path, comparing samples from different localities under different P-T conditions. High-pressure metamorphism decreased the amount of B and lowered Li in antigorite (e.g. 26 – 200 µg/g B in chrysotile and 9.5 - 39.8 µg/g B in antigorite; Scambelluri et al., 2004). Antigorite from the MAL massif also has considerably lower B and Li content than chrysotile from TO, LP and UP (Fig. 4.5). Thus we propose that the phase transition from chrysotile to antigorite leads to a change in the light element content of the latter (Fig. 4.5) and the observed loss of Li and B seems related to increasing metamorphism (Fig. 4.5).

In addition, increase of pressure and temperature leads to an increase of structural equilibrium in antigorite (e.g. less crystal defects, increasing crystal size and increasing structural homogeneity) and shortens the lattice parameter a (Mellini, 1987, Padron-Navarta et al., 2008). Regional metamorphic MAL antigorites have such short a-wavelenghts (m=17; Mellini, 1987). A similar response of the crystal structure

Table 5: SIMS analyses of chlorite

	Sample	Li (µg/g)	2 sigma (µg/g)	Be (µg/g)	2 sigma (µg/g)	B (µg/g)	2 sigma (µg/g)
TO	to7c2sr1	5.911	0.184	0.002	0.001	172.824	1.258
TO	to7c2sr3	1.079	0.056	0.001	0.002	50.819	0.632
LP	nap7c5sr6	76.737	1.484	0.015	0.008	17.490	0.650
LP	nap7c2xx3	22.687	1.566	0.007	0.002	12.551	0.174
LP	nap7c2xx1a	6.258	0.236	0.001	0.001	6.482	0.060
LP	nap99-2c5xx1	4.310	0.115	0.002	0.002	31.861	0.514
LP	nap99-2c1sr12	106.363	0.796	0.023	0.004	84.986	0.357
LP	nap99-2c1sr13	111.725	0.476	0.013	0.003	32.729	1.661
LP	nap99-2c3sr2	12.036	0.489	0.002	0.002	22.398	0.520
LP	nap99-2c4sr10	6.151	0.347	0.001	0.002	66.769	0.433
LP	nap99-2c4sr5	18.133	0.306	0.003	0.002	45.799	0.358
LP	nap99-2c4sr7	6.830	0.343	0.001	0.001	50.505	0.451
LP	nap99-2c4sr8	103.266	4.182	0.003	0.002	40.737	0.942
LP	nap99-2c5sr5	90.482	0.945	0.024	0.008	143.111	1.428
LP	nap99-2c5xx3	6.822	0.636	0.005	0.002	39.152	0.765
LP	nap99-2c3sr1	68.911	1.494	0.004	0.002	12.040	0.277
LP	nap99-2c5xx6	32.950	0.648	0.020	0.005	220.618	2.312
LP	crp3c7sr3	97.416	1.274	0.016	0.004	19.185	0.614
LP	crp3c7sr4	98.033	1.002	0.015	0.005	18.268	0.363
LP	crp3c1sr6	163.892	0.947	0.023	0.004	15.969	0.310
LP	crp3c1sr5	73.408	0.391	0.014	0.003	38.301	0.381
LP	stp5-2c3sr5	38.516	1.176	0.003	0.002	24.377	0.460
LP	stp5-2c3sr3	13.384	0.526	0.003	0.001	25.833	0.683
LP	stp5-2c3sr4	20.454	4.002	0.003	0.001	33.479	1.084
LP	stp5-2c3sr7	0.879	0.039	0.009	0.003	107.300	0.680
LP	stp5-2c3sr2	84.101	3.122	0.005	0.002	23.978	0.494
UP	fap4c2sr13	26.559	0.364	0.006	0.002	19.625	0.339
UP	fap4c2sr8	2.345	0.055	0.078	0.006	8.670	0.232
UP	fap4c3sr13	8.545	0.116	b.d.l.	-	77.624	0.959
UP	fap4c3sr3	35.023	0.620	0.003	0.002	77.511	1.000
MAL	lum112c1sr5	0.393	0.040	0.009	0.001	1.109	0.051
MAL	lum112c3sr4	0.050	0.004	0.004	0.001	2.117	0.490
MAL	lum112c1sr1	0.691	0.055	0.022	0.003	0.729	0.027
MAL	lum112c3sr7	0.011	0.001	0.008	0.001	2.401	0.166
MAL	lum112c1xx7	1.171	0.057	0.011	0.002	8.731	0.211
MAL	lum112c1sr6	0.115	0.005	0.012	0.002	1.319	0.032
MAL	lum112c3sr5	0.075	0.005	0.012	0.001	0.821	0.397
MAL	lum112c3sr6	0.190	0.028	0.018	0.004	2.263	0.039
MAL	lum112c3sr9	0.178	0.016	0.011	0.000	0.758	0.038
MAL	lum112c2sr6	0.100	0.015	0.032	0.006	1.729	0.216
MAL	lum112c2sr2	0.147	0.018	0.011	0.002	1.800	0.059

	Sample	Li (µg/g)	2 sigma (µg/g)	Be (µg/g)	2 sigma (µg/g)	B (µg/g)	2 sigr (µg/g
MAL	lum117c1sr4	0.050	0.031	0.012	0.015	0.969	0.1
MAL	lum117c1sr4a	0.076	0.031	0.010	0.009	1.398	0.2
MAL	lum117c1sr5	0.088	0.062	b.d.l.	-	1.334	0.3
MAL	lum117c2sr1	0.071	0.007	b.d.l.	-	0.820	0.0
MAL	lum117c2sr2	0.074	0.010	b.d.l.	-	0.717	0.0
MAL	lum117c2sr4	0.085	0.006	b.d.l.	-	0.874	0.0
MAL	lum117c2sr5	0.079	0.007	b.d.l.	-	0.820	0.0
MAL	lum216_2c3sr7	0.521	0.030	0.017	0.003	1.551	0.1
MAL	lum216_2c1sr1	0.015	0.003	0.012	0.003	0.911	0.1
MAL	lum216_2c1sr6	0.020	0.006	0.019	0.003	1.706	0.1
MAL	lum216_2c1sr5	0.010	0.005	0.017	0.004	1.575	0.0
MAL	lum216_2c1sr4	0.020	0.006	0.009	0.002	1.227	0.1
MAL	lum216_2c3sr1	0.121	0.007	0.008	0.002	0.777	0.0
MAL	lum226c1sr3	0.411	0.039	0.016	0.005	1.237	0.0
MAL	lum226c1sr4	0.603	0.029	0.017	0.004	2.706	0.2
MAL	lum226c4sr1	0.712	0.059	0.008	0.004	0.594	0.0
MAL	lum226c4sr3	0.221	0.012	0.008	0.003	1.062	0.0
MAL	lum226c3sr2	1.010	0.042	0.012	0.003	3.040	0.2
MAL	lum226c3sr4	0.343	0.026	0.005	0.002	0.771	0.0
MAL	lum226c3sr1	0.480	0.020	0.010	0.004	1.901	0.0
MAL	lum226c1sr2	0.249	0.017	0.008	0.003	1.204	0.0
MAL	lum216-1c1cl2	10.939	0.107	0.002	0.001	1.987	0.1
MAL	lum216-1c1sr1	0.839	0.032	0.005	0.002	1.394	0.0
MAL	lum216-1c1sr12	0.066	0.012	0.009	0.002	3.853	0.1
MAL	lum216-1c1sr2	0.671	0.031	0.006	0.003	1.349	0.0
MAL	lum216-1c1sr3	0.226	0.022	0.004	0.002	1.248	0.0
MAL	lum216-c1-sr11	0.054	0.018	0.013	0.005	10.858	0.7
MAL	lum216-c2-cl1	0.015	0.006	0.014	0.004	6.517	0.5
MAL	lum224c2sr10	0.060	0.011	0.002	0.002	3.182	0.1
MAL	lum224c2sr2	0.074	0.011	0.001	0.001	2.407	0.1
MAL	lum224c2sr5	0.049	0.009	0.001	0.001	1.530	0.1
MAL	lum224c2sr7	0.065	0.015	0.004	0.002	3.790	0.2
MAL	lum224c2sr8	0.057	0.007	0.001	0.001	2.377	0.1
MAL	MG65c4sr2	0.015	0.004	b.d.l.	-	1.197	0.2
MAL	MG65c3sr8	0.003	0.002	b.d.l.	-	2.349	0.1
MAL	MG65c3sr2	0.004	0.001	b.d.l.	-	1.158	0.0
MAL	MG65c5sr3	0.004	0.001	b.d.l.	-	1.061	0.0
MAL	MG65c5sr17	0.011	0.004	b.d.l.	-	1.085	0.1
MAL	MG65c5sr1	0.032	0.004	b.d.l.	-	1.944	0.1

of lizardite, chrysotile and clinochlore with respect to changing pressure and temperature has been reported (e.g. Mellini and Zanazzi, 1989; Welch and Marshall, 2001; Mizukami et al., 2007). It might be argued that not only phase transformation from chrysotile to antigorite controls the Li and B content of the serpentine, but also the internal order of the tetraheadral and octaheadral layers.

4.7.3 Low temperature chlorite transformation

In ultramafic rocks, chlorite is stable over a wide P-T range, ending with the chlorite breakdown reactions in the amphibolite facies (chl -> spl + ol + opx; or chl + trem -> opx + cpx; Grove et al., 2006). At low P-T conditions, especially during weathering, chlorite can transform into clay minerals (e.g. Rabenhorst et al., 1982; Lee et al., 2003; Hseu et al., 2007). In addition, chlorites can form mixed-layer sheet silicates (e.g. integrating smectite or serpentine layers into chlorite layers; Reynolds, 1988).

Chlorite from the Geisspfad ophiolite shows a large variation in Be concentrations from <0.001 to 0.223 µg/g (Pelletier et al., 2008a). The average Be concentration in chlorite from all studied ultramafic bodies (0.009 µg/g, this study) are similar to the average content of the Geisspfad body (0.014 µg/g) supporting the previously made statement that Be shows little variability during transformation of primary to metamorphic minerals (see 'section 4.7.2').

Chlorite from the TO, LP and UP massifs has higher Li and higher B content than chlorite from the MAL massif, similar to serpentine (Fig. 4.6). Chlorite in alpine serpentinites shows low Li (0.03 to 1.55 µg/g) and low B content (0.69 to 3.12 µg/g; Pelletier et al., 2008a). Measurements on ocean floor occurrences are rare (4.40 µg/g Li, 1.80 µg/g B; Erro Tobbio, Scambelluri et al., 2004; 0.40 and 0.53 µg/g Li; 0.97 and 0.85 µg/g B; ODP Leg 209, Vils et al., 2008). Chlorite in HP ultramafic rocks from the Betic Cordillera have moderate Li contents (0.12 to 0.32µg/g) and B content varying between 1.70 and 4.60 µg/g (Scambelluri et al., 2004).

Reported B concentrations from chlorite from oceanic (max. 0.97 µg/g; Vils et al., 2008) and high-pressure ultramafic rocks (max. 4.60 µg/g; Scambelluri et al., 2004) are low compared to oceanic serpentine (max. 139 µg/g; e.g. Pelletier et al., 2008b; Vils et al., 2008). To sum up, chlorite from the TO, LP and UP massifs contains high amounts of Li and B compared to literature data (Fig. 4.4). In general B substitutes in silicates for Al and Si and Li for Mg or Fe. As chlorite is mostly composed of Si, Al and Mg, their concentrations in chlorites are high and favour any Li and B substitution into the crystal lattice.

For Li, such incorporation in chlorite is known and high enrichments occur (e.g. Pelletier et al., 2008a). For B, such processes are not reported. As clay minerals tend to contain high amounts of B (e.g. up to 230 µg/g for pelagic clay; Li 1982), high B concentration in TO, LP and UP might be related to transformation of chlorites into interstratified two-component chlorite-clay minerals. Assuming average B concentrations of pelagic clay minerals and maximum B concentration reported for chlorite (4.60 µg/g; Scambelluri et al., 2004), a 1:1, two-component chlorite-clay mineral could contain up to 120 µg/g B, which is similar to measured B concentrations in chlorites from TO, LP and UP. Nevertheless as serpentine and chlorite are often intergrown, such a signal could also be related to mixed ion probe analyses.

As previous discussed, the internal order of serpentine minerals probably plays an important role for the Li and B concentrations (section '4.7.2'). The similarity in the crystallographic structure of chlorite with serpentine suggests a similar dependence over the pressure-temperature range investigated. As increasing P and T leads to an increasing ordering of the serpentine structure, a similar process might be operative for chlorite. In line with this hypothesis are the reported chlorite values of the Betic Cordillera (Scambelluri et al., 2004), as they occur around similar high ordered antigorites (m=17; Padron-Navarta et al., 2008) as observed in the MAL massif (m=17; Mellini, 1987). These chlorites have similar Li (0.12 to 0.32 µg/g) and B (1.7 to 4.6 µg/g) concentration as reported in Table 5 for MAL massif.

So far the response of lattice parameters of chlorite during prograde metamorphism is poorly constrained. The systematic change of Li and B in chlorite during prograde metamorphism might be related to three process: (a) mixed analyses of chlorite with

serpentine or clay (interlayer or intergrown); (b) P-T related crystal structural change, where a higher 'order' is achieved with higher P-T; or (c) or a mixture of the two described processes.

4.7.4 Oceanic or subcontinental mantle?

A good chemical fingerprint for the origin of clinopyroxene in mantle peridotite might be the light elements concentrations, since oceanic mantle cpx is low in Li (0.104-0.204 µg/g), low in Be (<0.001 µg/g) and low in B (0.007-0.014 µg/g; Pelletier et al., 2008b). Late-stage metasomatic events can crystallize Li-rich clinopyroxenes in oceanic mantle (e.g. 0.44 to 5.41 µg/g, Pelletier et al., 2008b; Vils et al., 2008). Studies on xenoliths showed that subcontinental mantle differs geochemically from oceanic mantle, and clinopyroxenes have distinct light element concentrations. Subcontinental clinopyroxene has higher Be concentrations (0.02-3.90µg/g; Neumann et al., 2002; Neumann et al., 2004; Kaeser et al., 2007; Kaliwoda et al., 2008) than oceanic mantle and both are variable in B and Li (Fig. 4.7). It is known that during any metsomatic event, Li is enriched compared to B (e.g. Fiorentini and Beresford, 2008), or Li within clinopyroxene and olivine are in disequilibrium as proposed by Seitz and Woodland (2000). For Be, this is in line with the experimental data of Tatsumi and Isoyama (1988), where at 1.5 GPa and 850°C peridotite loose up to 5 % in initial Be. Such an extraction should increase the Be concentration available within the mantle wedge. For B, high mobility during mineral-melt interactions leads to a preferable enrichment of B in the melt and thus in metasomatised phases.

Clinopyroxenes from the TO, LP, UP and MAL massifs are enriched in Be, B and Li compared to DM or oceanic mantle (Fig. 4.7). Exceptions are alpine metamorphic diopsides from sample Pum117, Mg65 and Lum112 (reaction III, Fig. 4.1, 4.2). In general, reported clinopyroxenes are primary mantle phases. Comparing primary minerals from TO, UP, LP and MAL (Fig. 4.3) show that there is no change in Be concentration, although the reported massifs represent different metamorphic degrees (Fig. 4.1). Thus, alpine metamorphism has no influence on the Be composition of the clinopyroxenes. Further on, Ca-phases are enriched in Be compared to the other minerals (Fig. 4.3) and might act as a sink for Be during alpine metamorphism. Over the 3 massifs there is no change in cpx Be concentration (Fig. 4.3) and there is little evidence that Alpine metamorphism lead to Be enrichment. Thus, the consistent Be signature of mantle clinopyroxene from TO to MAL suggests that the Be signal is still of primary

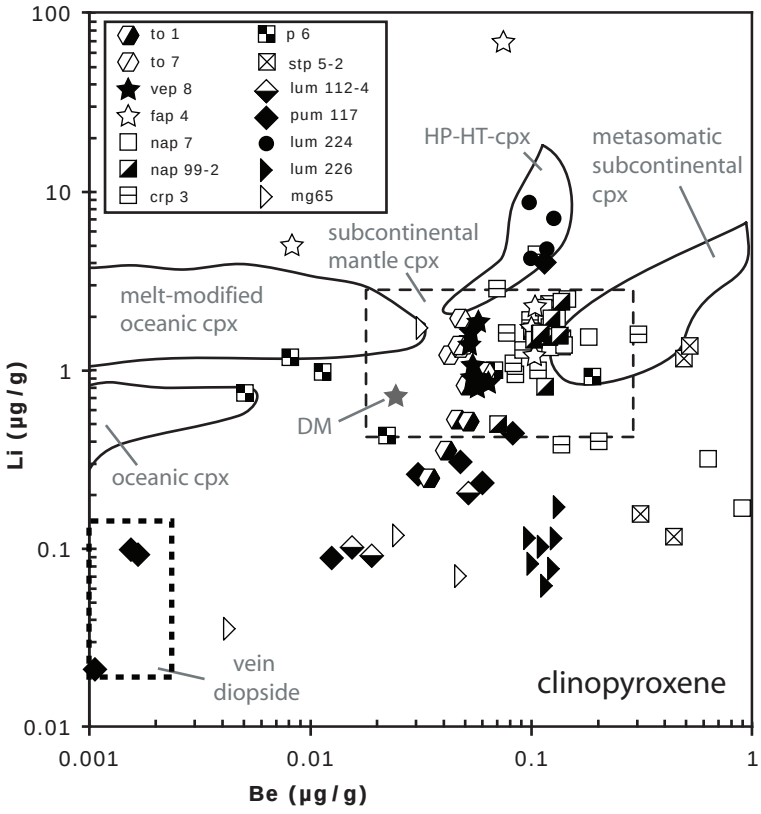

Fig. 7: Li versus Be diagram of clinopyroxenes from the four ophiolite massifs (to: TO; vep, fap: UP; nap, p, stp, crp: LP; lum, mg: MAL). Additionally, range of subcontinental mantle and oceanic mantle are shown for comparison, as well as depleted mantle value (DM Salters and Stracke, 2004; oceanic cpx Pelletier et al., 2008b; melt-modified oceanic cpx Vils et al., 2008; HP-HT cpx Paquin et al., 2004; Scambelluri et al., 2006; subcontinental mantle Neumann et al., 2002; Neumann et al., 2004; Kaeser et al., 2007; Kaliwoda et al., 2008; metasomatic subcontinental mantle Kaeser et al., 2007).

origin. Comparing our data with literature data from xenoliths and other peridotite massifs show similar concentrations of Be (Fig. 4.7) and thus supports previous proposals that the TO-MAL transect is essentially composed of subcontinental mantle that was later exposed on the Tethyan ocean floor (e.g. Desmurs, 2001; Desmurs et al., 2002; Manatschal and Müntener, 2009; Müntener et al., 2009).

4.7.5 Implications for the Li and B recycling within the subduction zone

Serpentinization is the key process in enriching B in the oceanic plate and controls the input budget to the subduction zone factory (e.g. Scambelluri et al., 2004; Tenthorey and Hermann, 2004; Savov et al., 2005; Vils et al., 2008). Li budget on the contrary is rather dominated by the basalts and the sedimentary cover (e.g. Vils et al., 2008).

Prior to plate bending, the B budget of the oceanic plate is mainly dominated by serpentinites (Vils et al., 2008) and plate bending probably increases the serpentinizated volume. Dehydration reactions of the sedimentary layer in the accretionary prism should even enhance that signal. Chrysotile breakdown follows in the early stage of subduction and liberates a considerable amount of B and Li into the mantle wedge during phase transition to antigorite (as shown by the TO-MAL transect). Although antigorite breakdown is an important source for water to depth (Ulmer and Trommsdorff, 1995), lower whole rock Li and B concentrations are available as prior chrysotile breakdown. Thus B might be additionally liberated at depth, but serpentine still contains one order of magnitude more B than depleted mantle (0.06 µg/g; Salters and Stracke, 2004). Modelling of water release in subduction zone settings assumes that dehydration reactions of serpentinites are only related to antigorite breakdown (e.g. Rüpke et al., 2004). As previously discussed during the chrysotile breakdown potentially water is released (see 'section 4.7.2'), thus such small water circulations might influence strongly the elemental budget for fluid-mobile elements prior to antigorite breakdown. Observed change in B concentration with increasing slab depth (Ryan et al., 1995), might also reflect the different dehydration reactions, but further investigation is needed. What so ever the detailed dehydration reactions in the slab are, it is important to state, that B enrichment related to serpentinite of the mantle wedge occurs.

4.8. Conclusions and summary

1) As mantle and secondary mineral pairs in the Malenco ophiolite have similar Be compositions, Be seems to behave rather conservative in ultramafic systems with respect to fluid mobility, at least to temperatures up to to 450°C.

2) Due to dehydration reactions during prograde metamorphism, the mineralogical change from chrysotile to antigorite leads to Li and B loss within the serpentine minerals. The dehydration reaction concurs with a change in total B and Li that is stored in serpentine. The lower content of Li and B in antigorite has a considerable impact on element cycling, as at antigorite breakdown, two orders of magnitude lesser amount of Li and B could potentially be released into the mantle wedge.

3) During oceanic alteration, low temperature clay mineral formation leads to an increase of B within chlorites. As prograde metamorphism occur, retransformation of the clay-layers into chlorites lower the B and Li considerably.

4) Clinopyroxenes of all three massifs have high Be content compared to clinopyroxene remnants for oceanic crust. As change in Be concentrations related to metamorphism, spongy mineral behaviour or external fluids could be excluded. Similar values for clinopyroxene are reported for subcontinental mantle. This observation is in line with the proposed subcontinental origin of the three massifs.

ACKNOWLEDGMENTS

Platta samples are provided by Laurent Desmurs. Funding for this research was provided by the Swiss National Science Foundation (Grant 200021-10361 and Grant 200021-103479/1). We would like to thank Alfons Berger and Julien Allaz (Bern, Switzerland) and Thomas Ludwig (Heidelberg, Germany) for technical support at their microprobe / SIMS. Discussions with Arjan Dijkstra and Sonja Pabst helped to improve the manuscript.

REFERENCES

Aldahan, A., Haiping, Y., and Possnert, G., 1999. Distribution of beryllium between solution and minerals (biotite and albite) under atmospheric conditions and variable pH. Chemical Geology 156, 209-229.

Bebout, G. E., Ryan, J. G., and Leeman, W. P., 1993. B-Be systematics in subduction-related metamorphic rocks: Characterization of the subducted component. Geochimica et Cosmochimica Acta 57, 2227-2237.

Benton, L. D., Ryan, J. G., and Savov, I. P., 2004. Lithium abundance and isotopic systematics of forearc serpentinites, Conical Seamount, Mariana forearc: Insights into the mechanics of slab-mantle exchange during subduction. Geochemistry Geophysics Geosystems 5, 1-14.

Benton, L. D., Ryan, J. G., and Tera, F., 2001. Boron isotope systematics of slab fluids as inferred from a serpentine seamount, Mariana forearc. Earth and Planetary Science Letters 187, 273-282.

Bernoulli, D., Manatschal, G., Desmurs, L., and Müntener, O., 2003. Where did Gustav Steinmann see the trinity? Back to the roots of Alpine ophiolite concept. In: Dilek, Y. and Newcomb, S. (Eds.), Ophiolite concept and the evolution of geological thought. Geological society of America; special paper 373, 93-110.

Bernoulli, D. and Weissert, H., 1985. A transform margin in the Mesozoic Tethys: Evidence from the Swiss Alps. Geologische Rundschau 74, 665-679.

Bonatti, E., Lawrence, J., and Morandi, N., 1984. Serpentinization of oceanic peridotites: Temperature dependence of mineralogy and boron content. Earth and Planetary Science Letters 70, 88-94.

Boschi, C., Dini, A., Früh-Green, G., and Kelley, D. S., 2008. Isotopic and element exchange during serpentinization and metasomatism at the Atlantis massif (MAR 30°N): Insights from B and Sr isotope data. Geochimica et Cosmochimica Acta 72, 1801-1823.

Bouvier, A.-S., Métrich, N., and Deloule, E., 2008. Slab-derived fluids in the magma sources of St. Vincent (Lesser Antilles Arc): Volatile and light element imprints. Journal of Petrology 49, 1427-1448.

Brenan, J. M., Neroda, E., Lundstrom, C. C., Shaw, H. F., Ryerson, G. F. J., and Phinney, D. L., 1998. Behaviour of boron, beryllium and lithium during melting and crystallization: Constraints from mineral-melt partitioning experiments. Geochimica et Cosmochimica Acta 62, 2129-2141.

Brooker, R. A., James, R. H., and Blundy, J. D., 2004. Trace elements and Li isotope systematics in Zabargad peridotites: Evidence of ancient subduction processes in the Red Sea mantle. Chemical Geology 212, 179-204.

Burkhard, D. J. M. and O'Neil, J. R., 1988. Contrasting serpentinization processes in the Eastern Central Alps. Contributions to Mineralogy and Petrology 99, 498-506.

Cornelius, H. P., 1932. Geologische Karte der Err-Julier Gruppe 1:25'000. Schweizerische Geologische Kommission.

Currie, L. A., 1968. Limits for qualitative detection and quantitative determination. Analytical Chemistry 40, 586-593.

Decitre, S., Deloule, E., Reisberg, L., James, R., Agrinier, P., and Mével, C., 2002. Behavior of Li and its isotopes during serpentinization of oceanic peridotites. Geochemistry Geophysics Geosystems 3.

Desmurs, L., 2001. Mantle evolution and magmatism in an evolving ocean-continent transition: the Platta nape, eastern Switzerland. Ph. D. thesis, Swiss Federal Institute of Technology Zurich.

Desmurs, L., Manatschal, G., and Bernoulli, D., 2001. The Steinmann Trinity revisited: Mantle exhumation and magmatism along an ocean-continent transition: the Platta nappe, eastern Switzerland. Geological Society, London, Special Publications 187, 235-266.

Desmurs, L., Müntener, O., and Manatschal, G., 2002. Onset of magmatic accretion within a magma-poor rifted margin: A case study from the Platta ocean-continent transition, eastern Switzerland. Contributions to Mineralogy and Petrology 144, 365-382.

Dietrich, V., 1969. Die Ophiolithe des Oberhalbsteins (Graubünden) und das Ophiolithmaterial der ostschweizerischen Molasseablagerungen, ein petrographischer Vergleich. H.Lange and Cie AG, Bern, Switzerland.

Dietrich, V., 1970. Die Stratigraphie der Platta-Decke. Eclogae Geologica Helvetia 633, 631-671.

Dietrich, V. and Peters, T., 1971. Regionale Verteilung der Mg-Phyllosilikate in den Serpentiniten des Oberhalbsteins. Schweizerische Mineralogische und Petrographische Mitteilungen 51, 329-348.

Domanik, K. J., Hervig, R. L., and Peacock, S. M., 1993. Beryllium and boron in subduction zone minerals: An ion microprobe study. Geochimica et Cosmochimica Acta 57, 4997-5010.

Evans, B., Johannes, W., Oterdoom, H., and Trommsdorff, V., 1976. Stability of chrysotile and antigorite in the serpentinite multisystem. Schweizerische Mineralogische und Petrographische Mitteilungen 56, 79-93.

Evans, B. and Trommsdorff, V., 1970. Regional metamorphism of ultramafic rocks in the Central Alps: Parageneses in the system CaO-MgO-SiO_2-H_2O. Schweizerische Mineralogische und Petrographische Mitteilungen 50, 481-42.

Fiorentini, M. L. and Beresford, S. W., 2008. Role of volatiles and metasomatized subcontinental lithospheric mantle in the genesis of magmatic Ni–Cu–PGE mineralization: Insights from in-situ H, Li, B analyses of hydromagmatic phases from the Valmaggia ultramafic pipe, Ivrea-Verbano Zone (NW Italy). Terra nova 20, 333-340.

Froitzheim, N., Schmid, S. M., and Conti, P., 1994. Repeated change from crustal shortening to orogen-parallel extension in the Austroalpine units of Graubünden. Eclogae Geologica Helvetia 89, 81-110.

Früh-Green, G., Connolly, J. A. D., Plas, A., Kelly, D. S., and Grobéty, B., 2004. Serpentinization of oceanic peridotites: Implications for geochemical cycles and biological activity, The subseafloor biosphere at mid-ocean ridges. American Geophysical Union.

Früh-Green, G., Weissert, H., and Bernoulli, D., 1990. A multiple fluid history recorded in Alpine ophiolites. Journal of the Geological Society, London 147, 959-970.

Grove, T. L., Chatterjee, N., Parman, S. W., and Médard, E., 2006. The influence of H_2O on mantle wedge melting. Earth and Planetary Science Letters 249, 74-89.

Guntli, P. and Liniger, M., 1989. Metamorphose in der Margna-Decke im Bereich Piz da la Margna und Piz Fedoz (Oberengadin). Schweizerische Mineralogische und Petrographische Mitteilungen 69, 289-301.

Hansmann, W., Müntener, O., and Hermann, J., 2001. U-Pb zircon geochronology of a tholeiitic intrusion and associated migmatites at a continental crust-mantle transition, Val Malenco, Italy. Schweizerische Mineralogische und Petrographische Mitteilungen 81, 239-255.

Hermann, J., 1997. The Braccia gabbro (Malenco, Alps): Permian intrusion at the crust to mantle interface and Jurassic exhumation during rifting. Ph.D. thesis, Swiss Federal Institute of Technology.

Hermann, J. and Rubatto, D., 2003. Relating zircon and monazite domains to garnet growth zones: Age and duration of granulite facies metamorphism in the Val Malenco lower crust. Journal of Metamorphic Geology 21, 833-852.

Hseu, Z. V., Tsai, H., Hsi, H. C., and Chen, Y. C., 2007. Weathering sequences of clay minerals in soils along a serpentinitic toposequence. Clay and Clay Minerals 55, 389-401.

Kaeser, B., Kalt, A., and Ludwig, T., 2007. Li, Be, and B abundances in minerals of peridotite xenoliths from Marsabit (Kenya): Disequilibrium processes and implications for subduction zone signatures. Geochemistry Geophysics Geosystems 8, 1-25.

Kaliwoda, M., Ludwig, T., and Altherr, P. D. R., 2008. A new SIMS study of Li, Be, B and δ^7Li in mantle xenoliths from Harrat Uwayrid (Saudi Arabia). Lithos 106, 261-279.

Lee, B. D., Sears, S. K., Graham, R. C., Amrhein, C., and Vali, H., 2003. Secondary mineral genesis from chlorite and serpentine in an ultramafic soil toposequence. Soil Science Society of America Journal 67, 1309-1317.

Li, Y. H., 1982. A brief discussion on the mean oceanic residence time of elements. Geochimica et Cosmochimica Acta 46, 2671-2675.

Li, Z.-X. A. and Lee, C.-T. A., 2006. Geochemical investigation of serpentinized oceanic lithospheric mantle in the Feather River Ophiolite, California: Implications for the recycling rate of water by subduction. Chemical Geology 235, 161-185.

Lyubetskaya, T. and Korenaga, J., 2007. Chemical composition of Earth's primitive mantle and its variance: 1. Method and results. Journal of Geophysical Research 112.

Manatschal, G. and Müntener, O., 2009. A type sequence across an ancient magma-poor ocean-continent transition: The example of the western Alpine Tethys ophiolites. Tectonophysics 458, 1-8.

Manatschal, G. and Nievergelt, P., 1997. A continent ocean transition recorded in the Err and Platta napes (eastern Switzerland). Eclogae Geologica Helvetia 90, 3-27.

Marschall, H., Altherr, P. D. R., and Rüpke, L. H., 2007. Squeezing out the slab-modelling the release of Li, Be and B during progressive high-pressure metamorphism. Chemical Geology 239, 323-335.

Marschall, H., Altherr, R., Ludwig, T., Kalt, A., Gméling, K., and Kasztovszky, Z., 2006. Partitioning and budget of Li, Be and B in high-pressure metamorphic rocks. Geochimica et Cosmochimica Acta 70, 4750-4769.

Marschall, H. R., 2005. Lithium, beryllium and boron in high-pressure metamorphic rocks from Syros (Greece), Ph. D. thesis, Ruprecht-Karls Universität.

Marschall, H. R. and Ludwig, T., 2004. The low-boron contest. Minimising surface contamination and analysing boron concentration at the ng/g-level by secondary ion mass spectrometry. Mineralogy and Petrology 81, 265-278.

McDonough, W. F. and Sun, S.-S., 1995. The composition of the Earth. Chemical Geology 120, 223-253.

Mellini, M., 1987. Antigorite polysomatism: Behaviour during progressive metamorphism. Contributions to Mineralogy and Petrology 97, 147-155.

Mellini, M. and Zanazzi, P. F., 1989. Effects of pressure on the structure of lizardite-1T. European Journal of Mineralogy 1, 13-19.

Mizukami, T., Kagi, H., Wallis, S. R., and Fukura, S., 2007. Pressure-induced change in the compressional behavior of the O-H bond in

chrysotile: A Raman high-pressure study up to 4.5 GPa. American Mineralogist 92, 1456-1463.

Montrasio, A., Trommsdorff, V., Hermann, J., Müntener, O., and Spillmann, P., 2005. Carta Geologica della Valmalenco. Supplement to Schweizerische Mineralogische und Petrographische Mitteilungen 85.

Mottl, M. J., Komor, S. C., Fryer, P., and Moyer, C. L., 2003. Deep-slab fluids fuel extremophilic Archaea on a Mariana forearc serpentinite mud volcano: Ocean Drilling Progam Leg 195. Geochemistry Geophysics Geosystems 4, 1-14.

Mottl, M. J., Wheat, G. C., Fryer, P., Gharib, J., and Martin, J. B., 2004. Chemistry of springs across the Mariana forearc shows progressive devolatilization of the subducting plate. Geochimica et Cosmochimica Acta 68, 4915-4933.

Müntener, O., 1997. The Malenco peridotites (Alps): Petrology and geochemistry of subcontinental mantle and Jurassic exhumation during rifting. Ph. D. thesis, Swiss Federal Institute of Technology Zurich.

Müntener, O. and Hermann, J., 1996. The Val Malenco lower crust-upper mantle complex and its field relations (Italian Alps). Schweizerische Mineralogische und Petrographische Mitteilungen 76, 475-500.

Müntener, O., Hermann, J., and Trommsdorff, V., 2000. Cooling history and exhumation of lower-crustal granulite and upper mantle (Malenco, Eastern Central Alps). Journal of Petrology 41, 175-200.

Müntener, O., Manatschal, G., Desmurs, L., and Pettke, T., 2009. Consequences of melt infiltration in the peridotite basement on 'magma-poor' passive margins: Implications for the generation of 'anomalous' oceanic crust. Journal of Petrology in prep.

Müntener, O., Pettke, T., Desmurs, L., Meier, M., and Schaltegger, U., 2004. Refertilization of mantle peridotite in embryonic ocean basins: trace element and Nd isotopic evidence and implications for crust-mantle relationships. Earth and Planetary Science Letters 221, 293-308.

Neumann, E.-R., Griffin, W. L., Pearson, N. J., and O'Reilly, S. Y., 2004. The evolution of the upper mantle beneath the Canary Islands: Information from trace elements and Sr isotope ratios in minerals in mantle xenoliths. Journal of Petrology 45, 2573-2612.

Neumann, E.-R., Wulff-Pedersen, E., Pearson, N. J., and Spencer, E. A., 2002. Mantle xenoliths from Tenerife (Canary Islands): Evidence for reactions between mantel peridiotites and silicic carbonatite melts inducing metasomatism. Journal of Petrology 43, 825-857.

Niu, Y., 2004. Bulk-rock major and trace element compositions of abyssal peridotites: Implications for mantle melting, melt extraction and post-melting processes beneath mid-ocean ridges. Journal of Petrology 45, 2423-2458.

Ottolini, L., Bottazzi, P., and Vannucci, R., 1993. Quantification of lithium, beryllium and boron in silicates by secondary ion mass spectrometry using conventional energy filtering. Analytical Chemistry 65, 1960-1968.

Padron-Navarta, J. A., Lopez Sanchez-Vizcaino, V., Garrido, C. J., Gomez-Pugnaire, M. T., Jabaloy, A., Capitani, G. C., and Mellini, M., 2008. Highly ordered antigorite from Cerro del Almirez HP-HT serpentinites, SE Spain. Contributions to Mineralogy and Petrology 156, 679-688.

Paquin, J., Altherr, R., and Ludwig, T., 2004. Li-Be-B systematics in the ultrahigh-pressure garnet peridotite from Alpe Arami (Central Swiss Alps): Implications for slap-to-mantle transfer. Earth and Planetary Science Letters 218, 507-519.

Pearce, N., Perkins, W. T., Westgate, J. A., Gorton, M. P., Jackson, S. E., Neal, C. R., and Chenery, S. P., 1997. A compilation of new and published major and trace element data for NIST SRM 610 and NIST SRM 612 glass reference materials. Geostandards Newsletter 21, 115-144.

Pelletier, L., Müntener, O., Kalt, A., Vennemann, T. W., and Belgya, T., 2008a. Emplacement of ultramafic rocks into the continental crust monitored by light and other trace elements: An example from the Geisspfad body (Swiss-Italian Alps). Chemical Geology 255, 143-159.

Pelletier, L., Vils, F., Kalt, A., and Gméling, K., 2008b. Li, B and Be contents of harzburgites from the Dramala Complex (Pindos ophiolite, Greece): Evidence for a MOR-type mantle in a supra-subduction zone environment. Journal of Petrology 49, 2043-2080.

Peretti, A., 1988. Occurrence and stabilities of opaque minerals in the Malenco serpentinite (Sondrio, Northern Italy). Ph.D. thesis, Swiss Federal Institute of Technology Zurich (ETHZ).

Peters, T., 1963. Mineralogie und Petrographie des Totalpserpentins bei Davos. Schweizerische Mineralogische und Petrographische Mitteilungen 43, 529-684.

Plas, A., 1997. Petrologic and stable isotope constraints on fluid-rock interaction, serpentinization and alteration of oceanic ultramafic rocks, Ph.D. thesis, Swiss Federal Institute of Technology Zurich (ETHZ).

Pozzorini, D. and Früh-Green, G., 1996. Stable isotope systematics of the Ventina ophicarbonate zone, Bergell contact aureole. Schweizerische Mineralogische und Petrographische Mitteilungen 76, 549-564.

Rabenhorst, M. C., Foss, J. E., and Fanning, D. S., 1982. Genesis of Maryland soils formed from serpentinite. Soil Science Society of America Journal 46, 607-616.

Reynolds, R. C., 1988. Mixed layer chlorite minerals. In: Bailey, S. W. (Ed.), Hydrous phyllosilicates (exclusive of micas). Mineralogical society of America, Michigan. Chapter 15.

Rüpke, L. H., Morgan, P. J., Hort, M., and Connolly, J. A. D., 2004. Serpentine and the subduction zone water cycle. Earth and Planetary Science Letters 223, 17-34.

Ryan, J. G., Leeman, W. P., Morris, J., and Langmuir, C. H., 1996. The boron systematics of intraplate lavas: Implications for the crust and mantle evolution. Geochimica et Cosmochimica Acta 60, 415-422.

Ryan, J. G., Morris, J., Tera, F., Leeman, W. P., and Tsvetkov, A., 1995. Cross-Arc geochemical variations in the Kurile Arc as a function of slab. Science 270, 625-627.

Salters, V. J. M. and Stracke, A., 2004. Composition of the depleted mantle. Geochemistry Geophysics Geosystems 5, 1-27.

Savov, I. P., Ryan, J. G., D'Antonio, M., and Fryer, P., 2007. Shallow slab fluid release across and along the Mariana arc-basin system: Insights from geochemistry of serpentinized peridotites from the Mariana fore-arc. Journal of Geophysical Research 112.

Savov, I. P., Ryan, J. G., D'Antonio, M., Kelley, K., and Mattie, P., 2005. Geochemistry of serpentinized peridotites from the Mariana fore-arc Conical Seamount, ODP Leg 125: Implications for the elemental recycling at subduction zones. Geochemistry Geophysics Geosystems 6, 1-24.

Scambelluri, M., Hermann, J., Morten, L., and Rampone, E., 2006. Melt- versus fluid-induced metasomatism in spinel to garnet wedge peridotites (Ulten Zone, Eastern Italian Alps): Clues from trace element and Li abundances. Contributions to Mineralogy and Petrology 151, 372-394.

Scambelluri, M., Müntener, O., Hermann, J., Piccardo, G. B., and Trommsdorff, V., 1995. Subduction of water into the mantle: History of an Alpine peridotite. Geology 23, 459-462.

Scambelluri, M., Müntener, O., Ottolini, L., Pettke, T., and Vannucci, R., 2004. The fate of B, Cl and Li in the subducted oceanic mantle and in the antigorite breakdown fluids. Earth and Planetary Science Letters 222, 217-234.

Seitz, H.-M. and Woodland, A. B., 2000. The distribution of lithium in peridotitic and pyroxenitic mantle lithologies - an indicator of magmatic and metasomatic processes. Chemical Geology 166, 47-64.

Shaw, D. M., Higgins, M. D., Hinton, R. W., Truscott, M. G., and Middleton, T. A., 1988. Boron in chondritic meteorites. Geochimica et Cosmochimica Acta 52, 2311-2319.

Steinmann, G., 1905. Geologische Beobachtungen in den Alpen. II. Die schardtsche Ueberfaltungstheorie und die geologische Bedeutung der Tiefseeabsätze und der ophiolitischen Massengesteine. Berichte der naturforschenden Gesellschaft zu Freiburg i.B. 16, 18-67.

Takahashi, E., Uto, K., and Schilling, J. G., 1987. Primary magma compositions and Mg/Fe ratios of their mantle residues along mid-Atlantic ridge 29°N to 73°N. Technical Report ISEI, Okayama University Ser. A, 1-14.

Tatsumi, Y. and Isoyama, H., 1988. Transportation of beryllium with H_2O at high pressures: Implication for magma genesis in subduction zones. Geophysical Research Letters 15, 180-183.

Tenthorey, E. and Hermann, J., 2004. Composition of fluids during serpentinite breakdown in subduction zones: Evidence for limited boron mobility. Geology 32, 865-868.

Trommsdorff, V., 1983. Metamorphose magnesiumreicher Gesteine: Kritischer Vergleich von Natur, Experiment und thermodynamischer Datenbasis. Fortschritte der Mineralogie 61, 238-308.

Trommsdorff, V. and Evans, B., 1972. Progressive metamorphism of antigorite schists in the Bergell tonalite aureole (Italy). American Journal of Science 272.

Trommsdorff, V. and Evans, B., 1974. Alpine metamorphism of peridotitic rocks. Schweizerische Mineralogische und Petrographische Mitteilungen 54.

Trommsdorff, V., López Sánchez-Vizcaín, V., Gómez-Pugnaire, M. T., and Müntener, O., 1998. High pressure breakdown of antigorite to spinifex-textured olivine and orthopyroxene, SE Spain. Contributions to Mineralogy and Petrology 132, 139-148.

Trommsdorff, V., Montrasio, A., Hermann, J., Müntener, O., Spillmann, P., and Gieré, R., 2005. The geological map of Valmalenco. Schweizerische Mineralogische und Petrographische Mitteilungen 85, 1-13.

Ulmer, P. and Trommsdorff, V., 1995. Serpentine stability to mantle depths and subduction-related magmatism. Science 268, 858-861.

Ulmer, P. and Trommsdorff, V., 1999. Phase relations of hydrous mantle subducting to 300 km, mantle petrology: Field observations and high pressure experimentation. The Geochemical Society. Special pub. 6, 259-281.

Vils, F., Pelletier, L., Kalt, A., Müntener, O., and Ludwig, T., 2008. The lithium, boron and beryllium content of serpentinized peridotites from ODP Leg 209 (Sites 1272A and 1274A): Implications for lithium and boron budgets of oceanic lithosphere. Geochimica et Cosmochimica Acta 72, 5475-5504.

Vils, F., Tonarini, S., Seitz, H.-M., and Kalt, A., 2009. Boron, Lithium and Strontium isotopes as tracers of seawater-serpentinite interaction at mid-Atlantic ridge, ODP Leg 209. Earth and

Planetary Science Letters submitted.
Welch, M. D. and Marshall, W. G., 2001. High-pressure behavior of clinochlore. American Mineralogist 86, 1380-1386.
Wicks, F. J. and Whittaker, E. J. W., 1977. Serpentine textures and serpentinization. Canadian Mineralogist 15, 459-488.
You, C. F., Lee, T., and Li, Y. H., 1989. The partition of Be between soil and water. Chemical Geology 77, 105-118.
You, C. F., Morris, J., Gieskes, J. M., Rosenbauer, R., Zheng, S. H., Xu, X., Ku, T. L., and Bischoff, J. L., 1994. Mobilization of beryllium in the sedimentary column at convergent margins. Geochimica et Cosmochimica Acta 58, 4887-4897.
Zanetti, A., D'Antonio, M., Spadea, P., Raffone, N., and Vannucci, R., 2006. Petrogenesis of mantle peridotites from the Izu-Bonin-Mariana (IBM) Forearc. Ofioliti 31, 189-206.

ANNEX A.1 Electron microprobe analysis of major element in olivine (normalized to four oxygens)

	To7	(n=2)	TO1	(n=4)	MG65	(n=2)	LUM 224	(n=18)	LUM 216-1	(n=6)	Lum 216-2	(n=3)	Lum 112	(n=4)	Lum 226	(n=3)	PUM117	(n=5)
	average	stdev	average	stdev	average	stdev	average	stdev	average	stdev	average	stdev	average	stdev	average	stdev	average	stdev
SiO_2	41.02	0.24	40.53	0.12	39.18	0.28	40.63	0.19	40.44	0.20	40.94	0.21	41.10	0.08	41.10	0.10	40.88	0.21
TiO_2	0.00	0.00	0.02	0.03	0.00	0.00	0.01	0.01	0.03	0.03	0.00	0.00	0.03	0.03	0.00	0.01	0.14	0.11
Cr_2O_3	0.01	0.01	0.01	0.01	0.00	0.01	0.03	0.04	0.01	0.02	0.04	0.04	0.01	0.02	0.00	0.01	0.04	0.03
Al_2O_3	0.01	0.02	0.03	0.05	0.04	0.04	0.00	0.00	0.01	0.01	0.00	0.00	0.00	0.01	0.01	0.00	0.01	0.01
FeO	10.66	0.05	10.39	0.17	13.80	0.15	12.85	0.44	9.27	0.38	11.10	0.30	9.79	0.48	10.81	0.07	7.95	0.39
MnO	0.08	0.00	0.15	0.06	0.50	0.03	0.17	0.02	0.12	0.05	0.11	0.01	0.15	0.06	0.11	0.01	0.36	0.09
NiO	0.27	0.02	0.17	0.19	0.17	0.00	0.25	0.03	0.37	0.03	0.25	0.03	0.36	0.02	0.29	0.01	0.35	0.02
MgO	49.15	0.40	48.68	0.26	44.90	0.56	47.14	0.40	49.09	0.38	49.13	0.07	49.67	0.27	49.20	0.07	50.17	0.32
CaO	0.02	0.00	0.02	0.00	0.11	0.08	0.01	0.01	0.02	0.01	0.01	0.01	0.01	0.00	0.02	0.02	0.04	0.01
Na_2O	0.01	0.01	0.01	0.01	0.01	0.01	0.00	0.00	0.01	0.01	0.00	0.00	0.00	0.00	0.01	0.01	0.01	0.01
K2O	0.01	0.00	0.00	0.01	0.00	0.00	0.00	0.00	0.00	0.00	0.00	0.00	0.00	0.00	0.00	0.00	0.00	0.00
ZnO	0.01	0.01	0.00	0.00	0.00	0.00	0.02	0.01	0.00	0.00	0.02	0.01	0.02	0.01	0.00	0.00	0.01	0.01
Total	**101.25**	**0.58**	**100.00**	**0.20**	**98.70**	**0.67**	**101.12**	**0.59**	**99.36**	**0.48**	**101.61**	**0.49**	**101.14**	**0.23**	**101.54**	**0.16**	**99.95**	**0.69**
Si	0.996	0.000	0.996	0.001	0.993	0.001	0.999	0.003	0.996	0.001	0.992	0.001	0.996	0.002	0.996	0.002	0.996	0.003
Ti	0.000	0.000	0.000	0.001	0.000	0.000	0.000	0.000	0.001	0.001	0.000	0.000	0.001	0.000	0.000	0.000	0.002	0.002
Cr	0.000	0.000	0.000	0.000	0.000	0.000	0.001	0.001	0.000	0.000	0.001	0.001	0.000	0.000	0.000	0.000	0.001	0.001
Al	0.000	0.000	0.001	0.001	0.001	0.001	0.000	0.000	0.000	0.000	0.000	0.000	0.000	0.000	0.000	0.000	0.000	0.000
Fe	0.216	0.002	0.213	0.004	0.292	0.006	0.264	0.009	0.191	0.008	0.225	0.005	0.198	0.010	0.219	0.001	0.162	0.007
Mn	0.002	0.000	0.003	0.001	0.011	0.001	0.004	0.000	0.003	0.001	0.002	0.000	0.003	0.001	0.002	0.000	0.007	0.002
Ni	0.005	0.000	0.003	0.004	0.003	0.000	0.005	0.001	0.007	0.001	0.005	0.001	0.007	0.000	0.006	0.000	0.007	0.000
Mg	1.779	0.003	1.782	0.006	1.696	0.007	1.727	0.010	1.802	0.008	1.774	0.005	1.794	0.010	1.776	0.001	1.822	0.007
Ca	0.001	0.000	0.001	0.000	0.003	0.002	0.000	0.000	0.000	0.000	0.000	0.000	0.000	0.000	0.000	0.000	0.001	0.000
Na	0.000	0.000	0.000	0.000	0.000	0.000	0.000	0.000	0.000	0.001	0.000	0.000	0.000	0.000	0.000	0.000	0.000	0.001
K	0.000	0.000	0.000	0.000	0.000	0.000	0.000	0.000	0.000	0.000	0.000	0.000	0.000	0.000	0.000	0.000	0.000	0.000
Add Ele	0.000	0.000	0.000	0.000	0.000	0.000	0.000	0.000	0.000	0.000	0.000	0.000	0.000	0.000	0.000	0.000	0.000	0.000
Total	**3.000**	**0.000**	**3.000**	**0.000**	**3.000**	**0.000**	**3.000**	**0.000**	**3.000**	**0.000**	**3.000**	**0.000**	**3.000**	**0.000**	**3.000**	**0.000**	**3.000**	**0.000**
Total Cation	3.003	0.001	3.003	0.001	3.005	0.001	3.001	0.002	3.003	0.001	3.006	0.001	3.002	0.002	3.003	0.002	3.001	0.002
xMg	0.888	0.001	0.889	0.003	0.845	0.003	0.863	0.005	0.899	0.004	0.884	0.002	0.895	0.005	0.886	0.001	0.910	0.003

ANNEX A.2 Electronmicroprobe analysis of major element in clinopyroxene (normalized to six oxygens)

	mantle clinopyroxenes																				oceanic/ metamorphic diopside									
sample	TO1	(n=3)	to7	(n=6)	FAP 4	(n=11)	Vep 8	(n=7)	CRP 3	(n=9)	NAP 99	(n=9)	NAP7	(n=9)	Lum 112	(n=4)	LUM 224	(n=6)	LUM 226	(n=5)	P-UM117	(n=13)	MG65	(n=9)	P 6	(n=9)	crp 3	(n=3)	Nap 99	(n=2)
	average	stdev	average	stdev	average	stdev	average	stdev	average	stdev	average	stdev	average	stdev	average	stdev	average	stdev	average	stdev	average	stdev	average	stdev	average	stdev	average	stdev	average	stdev
SiO2	51.70	0.24	53.01	0.39	52.35	0.41	53.19	0.26	52.63	0.54	53.30	1.17	54.40	1.72	53.00	0.27	52.77	1.54	53.19	0.24	54.91	1.39	55.95	0.34	55.07	0.36	55.377	0.443	55.49	0.03
TiO2	0.62	0.05	0.29	0.03	0.62	0.07	0.40	0.03	0.35	0.05	0.49	0.28	0.33	0.36	0.81	0.03	0.19	0.08	0.28	0.03	0.47	1.04	0.02	0.03	0.09	0.05	0.064	0.046	0.03	0.01
Cr2O3	0.60	0.19	0.63	0.20	0.41	0.09	1.18	0.14	1.01	0.11	0.631	0.373	0.42	0.51	1.12	0.11	0.84	0.35	0.83	0.08	0.12	0.22	0.03	0.06	0.32	0.08	0.045	0.054	0.134	0.123
Al2O3	5.73	0.36	6.44	0.75	6.75	0.55	6.29	0.32	3.79	0.70	2.924	1.702	1.74	2.18	5.29	0.05	5.28	1.28	5.85	0.30	0.87	1.99	0.04	0.07	0.21	0.10	0.030	0.007	0.048	0.042
Fe2O3	1.04	0.28	0.08	0.20	0.16	0.14	0.02	0.03	0.30	0.22	0.262	0.380	0.06	0.11	0.60	0.43	1.03	1.66	0.12	0.16	0.21	0.26	0.02	0.07	0.15	0.15	0.000	0.000	0.130	0.184
FeO	1.43	0.33	2.42	0.18	2.85	0.17	2.41	0.12	2.70	0.23	2.587	0.571	2.33	0.40	1.63	0.29	1.65	0.83	2.33	0.29	0.88	0.68	1.31	0.08	1.69	0.20	2.887	1.166	1.533	0.047
MnO	0.02	0.02	0.03	0.02	0.09	0.04	0.09	0.03	0.01	0.01	0.054	0.054	0.13	0.08	0.09	0.05	0.04	0.04	0.02	0.02	0.06	0.05	0.07	0.03	0.12	0.05	0.167	0.097	0.072	0.030
NiO	0.07	0.04	0.02	0.02	0.03	0.03	0.02	0.02	0.03	0.01	0.036	0.019	0.01	0.01	0.05	0.02	0.03	0.03	0.03	0.02	0.02	0.02	0.02	0.03	0.02	0.02	0.013	0.015	0.052	0.028
MgO	14.60	0.48	14.45	0.44	15.01	0.49	14.99	0.49	16.10	0.46	16.525	0.766	17.29	0.93	14.93	0.10	15.54	1.87	14.51	0.14	17.67	1.14	17.84	0.11	17.75	0.21	16.697	0.735	17.670	0.198
CaO	21.73	0.26	21.45	0.25	21.14	0.26	20.47	0.55	22.67	0.44	23.284	1.280	24.00	1.33	21.58	0.16	20.81	1.75	21.13	0.61	25.04	1.54	25.78	0.19	25.05	0.27	25.710	0.229	25.730	0.325
Na2O	1.50	0.03	1.66	0.16	1.36	0.14	1.79	0.10	0.58	0.06	0.431	0.245	0.26	0.28	1.71	0.04	1.58	0.51	1.81	0.19	0.31	0.57	0.08	0.04	0.06	0.01	0.024	0.010	0.032	0.013
K2O	0.01	0.01	0.01	0.01	0.00	0.00	0.00	0.00	0.00	0.01	0.002	0.002	0.00	0.00	0.00	0.00	0.01	0.02	0.01	0.01	0.01	0.01	0.00	0.00	0.00	0.01	0.002	0.003	0.005	0.001
Add Ox	0.00	0.00	0.02	0.02	0.00	0.01	0.00	0.01	0.02	0.03	0.185	0.173	0.01	0.01	0.00	0.01	0.02	0.01	0.01	0.01	0.01	0.01	0.00	0.01	0.01	0.01	0.005	0.008	0.079	0.112
Total	**99.04**	**0.38**	**100.51**	**0.40**	**100.77**	**0.28**	**100.85**	**0.15**	**100.20**	**0.30**	**#####**	**0.383**	**100.99**	**0.30**	**100.81**	**0.15**	**99.77**	**0.87**	**100.13**	**0.32**	**100.58**	**0.67**	**101.18**	**0.58**	**100.54**	**0.57**	**101.02**	**0.148**	**101.01**	**0.202**
Si	1.890	0.008	1.907	0.016	1.880	0.014	1.905	0.008	1.912	0.016	1.93	0.04	1.958	0.056	1.904	0.011	1.909	0.042	1.920	0.007	1.977	0.055	2.005	0.004	1.990	0.005	2.00	0.00	2.00	0.00
Ti	0.017	0.001	0.008	0.001	0.017	0.002	0.011	0.001	0.010	0.001	0.01	0.01	0.009	0.010	0.022	0.001	0.005	0.002	0.008	0.001	0.013	0.028	0.001	0.001	0.002	0.001	0.00	0.00	0.00	0.00
Cr	0.017	0.006	0.018	0.006	0.012	0.002	0.033	0.004	0.029	0.003	0.02	0.01	0.012	0.015	0.032	0.003	0.024	0.010	0.024	0.002	0.003	0.006	0.001	0.002	0.009	0.002	0.00	0.00	0.00	0.00
Al	0.247	0.015	0.273	0.031	0.286	0.023	0.266	0.014	0.162	0.030	0.12	0.07	0.074	0.093	0.224	0.002	0.225	0.054	0.249	0.012	0.037	0.084	0.002	0.003	0.009	0.004	0.00	0.00	0.00	0.00
Fe3+	0.029	0.008	0.002	0.005	0.004	0.004	0.000	0.001	0.008	0.006	0.01	0.01	0.002	0.003	0.016	0.012	0.028	0.046	0.003	0.004	0.006	0.007	0.001	0.002	0.004	0.004	0.00	0.00	0.00	0.00
Fe2+	0.044	0.010	0.073	0.006	0.086	0.005	0.072	0.004	0.082	0.007	0.08	0.02	0.070	0.012	0.049	0.009	0.050	0.025	0.070	0.009	0.027	0.020	0.039	0.002	0.051	0.006	0.09	0.04	0.05	0.00
Mn	0.001	0.001	0.001	0.001	0.003	0.001	0.003	0.001	0.000	0.000	0.00	0.00	0.004	0.002	0.003	0.002	0.001	0.001	0.001	0.001	0.002	0.002	0.002	0.001	0.004	0.002	0.01	0.00	0.00	0.00
Ni	0.002	0.001	0.001	0.001	0.001	0.001	0.001	0.001	0.001	0.000	0.00	0.00	0.000	0.000	0.002	0.001	0.001	0.001	0.001	0.001	0.001	0.001	0.001	0.001	0.001	0.001	0.00	0.00	0.00	0.00
Mg	0.796	0.025	0.775	0.025	0.804	0.026	0.800	0.024	0.872	0.024	0.89	0.04	0.927	0.047	0.799	0.005	0.838	0.107	0.781	0.006	0.948	0.064	0.953	0.005	0.956	0.009	0.90	0.03	0.95	0.01
Ca	0.851	0.011	0.826	0.009	0.813	0.011	0.785	0.022	0.882	0.016	0.90	0.05	0.925	0.048	0.831	0.005	0.806	0.063	0.817	0.026	0.966	0.062	0.990	0.006	0.970	0.009	1.00	0.00	0.99	0.01
Na	0.107	0.002	0.116	0.011	0.095	0.010	0.124	0.007	0.041	0.004	0.03	0.02	0.018	0.020	0.119	0.003	0.111	0.035	0.127	0.013	0.022	0.039	0.005	0.003	0.004	0.001	0.00	0.00	0.00	0.00
K	0.001	0.001	0.000	0.000	0.000	0.000	0.000	0.000	0.000	0.000	0.00	0.00	0.000	0.000	0.000	0.000	0.001	0.001	0.001	0.000	0.000	0.001	0.000	0.000	0.000	0.000	0.00	0.00	0.00	0.00
Add El	0.000	0.000	0.000	0.001	0.000	0.000	0.000	0.000	0.001	0.001	0.00	0.00	0.000	0.000	0.000	0.000	0.000	0.000	0.000	0.000	0.000	0.000	0.000	0.000	0.000	0.000	0.00	0.00	0.00	0.00
Total	4.000	0.000	4.000	0.000	4.000	0.000	4.000	0.000	4.000	0.000	4.00	0.00	4.000	0.000	4.000	0.000	4.000	0.000	4.000	0.000	4.000	0.000	4.000	0.000	4.000	0.000	4.00	0.00	4.00	0.00
Total Cations	4.010	0.003	3.998	0.003	4.001	0.002	3.998	0.002	4.002	0.003	0.919	0.019	4.000	0.002	4.004	0.007	4.011	0.022	4.000	0.003	4.001	0.003	3.997	0.002	4.000	0.003	4.00	0.00	0.95	0.01
xMg(Fetot)	0.917	0.006	0.912	0.005	0.899	0.005	0.917	0.003	0.088	0.016	4.00	0.00	0.928	0.016	0.924	0.004	0.916	0.011	0.914	0.009	0.966	0.025	0.960	0.003	0.945	0.009	0.91	0.04	4.00	0.00

ANNEX A.3 Electronmicroprobe analysis of major element in orthopyroxene (normalized to six oxygens)

	To7	(n=3)	TO1	(n=3)	Lum 112-4	(n=11)	Lum 226	(n=3)
	average	stdev	average	stdev	average	stdev	average	stdev
SIO2	56.60	0.19	54.91	0.71	55.71	0.21	56.80	0.95
TIO2	0.05	0.01	0.13	0.01	0.25	0.05	0.03	0.03
Cr2O3	0.18	0.08	0.22	0.05	0.55	0.08	0.17	0.11
AL2O3	3.14	0.38	4.19	0.53	3.88	0.20	2.52	1.64
Fe2O3	0.19	0.19	0.40	0.11	0.16	0.16	0.30	0.27
FEO	6.89	0.31	6.80	0.06	5.62	0.23	6.75	0.54
MNO	0.11	0.02	0.09	0.07	0.14	0.05	0.10	0.02
NiO	0.04	0.01	0.08	0.07	0.09	0.02	0.05	0.02
MGO	33.73	0.29	32.56	0.48	33.73	0.20	33.99	0.60
CAO	0.27	0.03	0.42	0.04	0.48	0.16	0.25	0.06
NA2O	0.04	0.01	0.05	0.02	0.05	0.02	0.02	0.02
K2O	0.02	0.01	0.01	0.01	0.00	0.00	0.00	0.00
Add Ox	0.00	0.00	0.00	0.00	0.00	0.01	0.01	0.01
Total	**101.24**	**0.31**	**99.85**	**0.77**	**100.66**	**0.47**	**101.00**	**0.18**
Si	1.93	0.01	1.90	0.01	1.91	0.01	1.94	0.03
Ti	0.00	0.00	0.00	0.00	0.01	0.00	0.00	0.00
Cr	0.00	0.00	0.01	0.00	0.01	0.00	0.00	0.00
Al	0.13	0.02	0.17	0.02	0.16	0.01	0.10	0.07
Fe3+	0.00	0.00	0.01	0.00	0.00	0.00	0.01	0.01
Fe2+	0.20	0.01	0.20	0.00	0.16	0.01	0.19	0.02
Mn	0.00	0.00	0.00	0.00	0.00	0.00	0.00	0.00
Ni	0.00	0.00	0.00	0.00	0.00	0.00	0.00	0.00
Mg	1.72	0.01	1.68	0.01	1.72	0.01	1.73	0.03
Ca	0.01	0.00	0.02	0.00	0.02	0.01	0.01	0.00
Na	0.00	0.00	0.00	0.00	0.00	0.00	0.00	0.00
K	0.00	0.00	0.00	0.00	0.00	0.00	0.00	0.00
Add El	0.00	0.00	0.00	0.00	0.00	0.00	0.00	0.00
Total	4.00	0.00	4.00	0.00	4.00	0.00	4.00	0.00
Total cations	4.001	0.002	4.003	0.001	4.001	0.002	4.002	0.003
xMg(Fetot)	0.895	0.004	0.890	0.003	0.912	0.002	0.896	0.005

ANNEX A.4 Electronmicroprobe analysis of major element in tremolite (normalized to 23 oxygens and 2OH)

	LUM 224	(n=12)	LUM 216-2	(n=3)	Lum 216-1	(n=14)	LUm112	(n=5)	LUM 226	(n=12)
	average	stdev	average	stdev	average	stdev	average	stdev	average	stdev
SiO2	56.64	0.67	52.18	1.40	57.67	0.64	56.08	1.75	54.08	4.08
TiO2	0.03	0.02	0.15	0.13	0.01	0.01	0.25	0.26	0.10	0.13
Cr2O3	0.12	0.11	0.08	0.03	0.19	0.12	0.50	0.37	0.51	0.32
Al2O3	1.47	0.37	2.99	0.47	0.66	0.40	2.64	1.48	3.77	3.37
Fe2O3	0.00	0.00	0.00	0.00	0.00	0.00	0.00	0.00	0.00	0.00
FeO	2.32	0.62	2.65	1.00	1.87	0.23	3.38	2.33	2.28	0.90
MnO	0.04	0.03	0.06	0.05	0.05	0.02	0.07	0.03	0.02	0.02
NiO	0.05	0.02	0.10	0.04	0.06	0.03	0.08	0.01	0.06	0.02
MgO	23.22	0.24	26.35	3.24	24.63	2.73	27.69	5.89	24.19	3.12
CaO	11.57	0.40	9.71	1.58	11.20	3.23	7.58	6.54	11.49	2.26
Na2O	2.37	0.25	0.65	0.18	0.89	0.29	0.73	0.78	1.25	0.88
K2O	0.10	0.03	0.04	0.02	0.03	0.01	0.02	0.02	0.03	0.01
Add ox	0.00	0.01	0.00	0.00	0.01	0.02	0.00	0.00	0.01	0.02
H2O	2.28	0.01	2.17	0.04	2.28	0.01	2.30	0.08	2.24	0.07
F	0.00	0.00	0.00	0.00	0.00	0.00	0.00	0.00	0.00	0.00
Cl	0.00	0.00	0.20	0.12	0.04	0.04	0.13	0.10	0.15	0.09
Total	100.21	0.50	97.33	0.79	99.60	0.54	101.46	1.47	100.18	2.11
F,Cl=O	0.00	0.00	0.04	0.03	0.01	0.01	0.03	0.02	0.03	0.02
Total	**100.21**	**0.50**	**97.28**	**0.82**	**99.59**	**0.54**	**101.43**	**1.48**	**100.14**	**2.11**
Si	7.441	0.068	7.058	0.211	7.551	0.053	7.222	0.250	7.112	0.422
Ti	0.003	0.001	0.016	0.014	0.001	0.001	0.025	0.026	0.010	0.014
Cr	0.012	0.011	0.009	0.003	0.020	0.012	0.051	0.039	0.053	0.034
Al	0.228	0.058	0.477	0.077	0.102	0.061	0.401	0.227	0.594	0.542
Fe3+	0.000	0.000	0.000	0.000	0.000	0.000	0.000	0.000	0.000	0.000
Fe2+	0.255	0.069	0.299	0.112	0.205	0.026	0.359	0.241	0.253	0.104
Mn	0.004	0.003	0.007	0.005	0.005	0.002	0.008	0.003	0.002	0.002
Ni	0.006	0.003	0.011	0.004	0.006	0.003	0.008	0.001	0.006	0.002
Mg	4.547	0.049	5.310	0.633	4.804	0.497	5.295	1.000	4.738	0.540
Ca	1.628	0.056	1.408	0.233	1.574	0.454	1.062	0.919	1.619	0.319
Na	0.605	0.065	0.169	0.046	0.227	0.074	0.185	0.199	0.322	0.235
K	0.017	0.006	0.006	0.003	0.005	0.002	0.003	0.003	0.005	0.002
Add El	0.001	0.001	0.000	0.000	0.003	0.004	0.000	0.000	0.002	0.004
H	2.000	0.000	1.955	0.028	1.990	0.009	1.972	0.022	1.966	0.020
F	0.000	0.000	0.000	0.000	0.000	0.000	0.000	0.000	0.000	0.000
Cl	0.000	0.000	0.045	0.028	0.010	0.009	0.028	0.022	0.034	0.020
Total Cations	14.746	0.056	14.771	0.215	14.502	0.051	14.621	0.117	14.717	0.232
xMg(Fetot)	0.947	0.013	0.948	0.012	0.959	0.006	0.941	0.028	0.949	0.020

Electronmicroprobe analysis of major element in Ti-pargasite (normalized to 23 oxygens and 2OH)

	LUM 226	(n=5)	LUM 216-2	(n=2)	lum 216-1	(n=2)	LUm112	(n=3)
	average	stdev	average	stdev	average	stdev	average	stdev
SiO2	43.85	0.45	42.15	0.16	44.89	0.25	43.47	0.19
TiO2	1.46	0.22	9.57	0.16	0.48	0.06	5.87	0.88
Cr2O3	1.05	0.07	0.98	0.05	1.27	0.12	1.12	0.07
Al2O3	13.92	0.73	14.23	0.45	12.35	0.09	14.68	0.10
Fe2O3	0.00	0.00	0.00	0.00	0.00	0.00	0.00	0.00
FeO	3.69	0.41	3.71	0.01	3.24	0.60	3.22	0.07
MnO	0.00	0.01	0.07	0.06	0.00	0.00	0.06	0.04
NiO	0.06	0.02	0.10	0.02	0.05	0.06	0.10	0.02
MgO	17.45	0.70	16.71	0.05	18.96	0.27	17.33	0.30
CaO	12.00	0.22	11.06	0.08	11.91	0.03	11.66	0.05
Na2O	3.36	0.19	3.56	0.28	3.72	0.02	3.82	0.32
K2O	0.01	0.01	1.21	0.05	0.04	0.00	0.53	0.08
Add ox	0.00	0.01	0.00	0.00	0.00	0.00	0.00	0.00
H2O	2.18	0.01	2.06	0.06	2.17	0.01	2.19	0.06
F	0.00	0.00	0.00	0.00	0.00	0.00	0.00	0.00
Cl	0.05	0.04	0.98	0.17	0.12	0.03	0.40	0.23
Total	99.09	0.34	106.37	0.43	99.18	0.90	104.44	0.33
F,Cl=O	0.01	0.01	0.22	0.04	0.03	0.01	0.09	0.05
Total	**99.08**	**0.34**	**106.15**	**0.47**	**99.15**	**0.90**	**104.36**	**0.29**
Si	5.991	0.050	5.480	0.014	6.125	0.005	5.684	0.033
Ti	0.150	0.023	0.936	0.009	0.050	0.006	0.577	0.086
Cr	0.113	0.007	0.100	0.004	0.137	0.013	0.116	0.007
Al	2.242	0.119	2.180	0.054	1.986	0.027	2.263	0.018
Fe3+	0.000	0.000	0.000	0.000	0.000	0.000	0.000	0.000
Fe2+	0.422	0.048	0.403	0.001	0.369	0.066	0.352	0.007
Mn	0.000	0.001	0.007	0.006	0.000	0.000	0.006	0.005
Ni	0.006	0.002	0.011	0.002	0.005	0.006	0.010	0.003
Mg	3.554	0.135	3.237	0.030	3.856	0.030	3.378	0.060
Ca	1.757	0.033	1.541	0.022	1.741	0.015	1.634	0.006
Na	0.889	0.051	0.898	0.077	0.983	0.012	0.968	0.081
K	0.002	0.001	0.201	0.007	0.007	0.001	0.088	0.013
Add El	0.001	0.001	0.000	0.000	0.000	0.000	0.000	0.000
H	1.987	0.010	1.784	0.039	1.972	0.007	1.912	0.051
F	0.000	0.000	0.000	0.000	0.000	0.000	0.000	0.000
Cl	0.013	0.010	0.216	0.039	0.028	0.007	0.088	0.051
Total Cations	15.127	0.015	14.994	0.060	15.259	0.026	15.077	0.080
xMg(Fetot)	0.894	0.014	0.889	0.001	0.913	0.014	0.906	0.002

ANNEX A.5 Electronmicroprobe analysis of major element in serpentine (normalized to nine oxygens)

	to1	(n=7)	CRP 3	(n=5)	NAP7	(n=3)	nap 99	(n=2)	P-UM 117	(n=30)	lum 216-1	(n=9)	lum 216-2	(n=1)	Lum 224	(n=14)	Mg 65	(n=24)
	average	stdev	average	stdev	average	stdev	average	stdev	average	stdev	average	stdev	average	stdev	average	stdev	average	stdev
Si	1.921	0.029	1.939	0.066	1.940	0.025	1.927	0.030	1.966	0.018	1.899133	0.136581	1.924		1.993	0.022	1.961	0.029
Ti	0.002	0.001	0.002	0.003	0.001	0.001	0.004	0.000	0.003	0.002	0.00018	0.000216	0.000		0.000	0.000	0.001	0.001
Cr	0.003	0.004	0.009	0.013	0.005	0.004	0.013	0.008	0.010	0.006	0.001	0.003	0.002		0.004	0.004	0.010	0.004
Al	0.156	0.054	0.111	0.120	0.114	0.051	0.125	0.048	0.147	0.020	0.006	0.015	0.114		0.139	0.037	0.155	0.024
Fe2+	0.195	0.061	0.167	0.034	0.214	0.015	0.277	0.020	0.120	0.007	0.358	0.184	0.178		0.184	0.017	0.189	0.033
Mn	0.004	0.002	0.002	0.001	0.003	0.001	0.004	0.003	0.002	0.002	0.005	0.004	0.004		0.001	0.001	0.003	0.003
Ni	0.008	0.009	0.003	0.001	0.001	0.001	0.004	0.000	0.005	0.001	0.007	0.004	0.006		0.005	0.001	0.002	0.001
Mg	2.698	0.025	2.759	0.085	2.715	0.017	2.639	0.002	2.696	0.013	2.815	0.416	2.786		2.606	0.032	2.630	0.052
Ca	0.010	0.001	0.004	0.002	0.004	0.001	0.004	0.005	0.001	0.001	0.002	0.001	0.003		0.001	0.001	0.004	0.011
Na	0.000	0.001	0.000	0.000	0.001	0.002	0.001	0.002	0.004	0.001	0.001	0.001	0.001		0.002	0.001	0.000	0.001
K	0.001	0.001	0.000	0.000	0.000	0.000	0.002	0.002	0.000	0.001	0.001	0.001	0.001		0.000	0.000	0.000	0.000
Add El	0.000	0.000	0.001	0.001	0.001	0.001	0.000	0.000	0.000	0.001	0.001	0.001	0.000		0.001	0.001	0.000	0.000
H	3.969	0.007	3.996	0.002	3.955	0.052	3.968	0.022	3.999	0.001	3.994	0.005	3.828		3.999	0.001	3.999	0.001
F	0.000	0.000	0.000	0.000	0.000	0.000	0.000	0.000	0.000	0.000	0.000	0.000	0.013		0.000	0.000	0.000	0.000
Cl	0.031	0.007	0.004	0.002	0.045	0.052	0.032	0.022	0.001	0.001	0.006	0.005	0.159		0.001	0.001	0.001	0.001
Total Cations	**4.998**	**0.024**	**4.998**	**0.004**	**4.999**	**0.002**	**5.001**	**0.004**	**4.955**	**0.007**	**5.097**	**0.137**	**5.018**		**4.936**	**0.011**	**4.956**	**0.035**
SiO2	39.09	1.04	41.59	1.63	40.64	0.63	39.55	0.28	42.00	0.57	38.68556	2.09937	39.16		42.57	0.68	41.98	0.89
TiO2	0.06	0.03	0.07	0.07	0.04	0.02	0.11	0.00	0.08	0.05	0.00	0.01	0.00		0.01	0.01	0.01	0.01
Cr2O3	0.08	0.09	0.25	0.35	0.12	0.10	0.33	0.22	0.28	0.16	0.03	0.08	0.05		0.10	0.12	0.26	0.11
Al2O3	2.70	0.93	2.02	2.15	2.02	0.91	2.19	0.85	2.66	0.38	0.10	0.26	1.97		2.53	0.68	2.82	0.43
FeO	4.73	1.41	4.28	0.85	5.37	0.40	6.80	0.44	3.07	0.19	8.66	4.25	4.32		4.70	0.43	4.84	0.84
MnO	0.11	0.06	0.04	0.02	0.06	0.04	0.10	0.08	0.05	0.04	0.11	0.10	0.09		0.03	0.01	0.08	0.07
NiO	0.21	0.22	0.08	0.02	0.02	0.02	0.11	0.01	0.14	0.01	0.18	0.10	0.15		0.12	0.02	0.05	0.03
MgO	36.83	0.85	39.71	1.46	38.16	0.36	36.33	0.34	38.65	0.38	38.65	6.49	38.04		37.35	0.56	37.76	0.78
CaO	0.19	0.03	0.08	0.03	0.08	0.02	0.08	0.09	0.02	0.02	0.04	0.02	0.05		0.03	0.02	0.08	0.22
Na2O	0.00	0.01	0.00	0.00	0.01	0.02	0.01	0.02	0.05	0.02	0.01	0.01	0.01		0.03	0.01	0.01	0.01
K2O	0.01	0.01	0.01	0.00	0.00	0.00	0.03	0.04	0.01	0.01	0.01	0.01	0.01		0.00	0.01	0.00	0.00
Add ox	0.00	0.00	0.01	0.01	0.01	0.01	0.00	0.00	0.00	0.01	0.02	0.02	0.00		0.02	0.02	0.00	0.01
H2O	12.11	0.23	12.85	0.12	12.42	0.23	12.21	0.04	12.81	0.13	12.22	0.40	11.68		12.81	0.10	12.83	0.13
F	0.00	0.00	0.00	0.00	0.00	0.00	0.00	0.00	0.00	0.00	0.00	0.00	0.09		0.00	0.00	0.00	0.00
Cl	0.37	0.08	0.05	0.02	0.56	0.63	0.39	0.27	0.01	0.02	0.07	0.06	1.91		0.02	0.02	0.01	0.02
Total	96.48	1.11	101.04	0.68	99.52	0.22	98.24	0.89	99.83	1.00	98.79	2.80	97.52		100.30	0.76	100.74	1.11
F,Cl=O	0.08	0.02	0.01	0.01	0.13	0.14	0.09	0.06	0.00	0.00	0.01	0.01	0.47		0.00	0.00	0.00	0.00
Total	**96.40**	**1.13**	**101.03**	**0.68**	**99.39**	**0.35**	**98.16**	**0.82**	**99.82**	**1.00**	**98.78**	**2.81**	**97.06**		**100.29**	**0.76**	**100.74**	**1.11**
Ratios and Site activities																		
xMg(Fe2+)	0.933	0.020	0.943	0.013	0.927	0.004	0.905	0.006348	0.957	0.002	0.883	0.069	0.940		0.934	0.006	0.933	0.010
xMg(Fetot)	0.933	0.020	0.943	0.013	0.927	0.004	0.905	0.006348	0.957	0.002	0.883	0.069	0.940		0.934	0.006	0.933	0.010
SumCAT	4.998	0.024	4.998	0.004	4.999	0.002	5.001	0.004013	4.955	0.007	5.097	0.137	5.018		4.936	0.011	4.956	0.035

ANNEX A.6 Electronmicroprobe analysis of major element in chlorite (normalized to nine oxygens)

chlorite	to7 average	(n=2) stdev	vep8c2sr9 n=1	crp 3 average	(n=7) stdev	nap99 average	(n=28) stdev	p6 average	(n=6) stdev	lum 112 average	(n=9) stdev	lum 216-2 average	(n=10) stdev	lum 226 average	(n=16) stdev
Si	1.636	0.056	1.641	1.645	0.071	1.582	0.092	1.837	0.037	1.523	0.035	1.618	0.076	1.535	0.037
Ti	0.000	0.001	0.002	0.000	0.000	0.000	0.000	0.003	0.002	0.003	0.003	0.000	0.000	0.001	0.001
Cr	0.000	0.000	0.013	0.002	0.001	0.003	0.003	0.026	0.012	0.055	0.024	0.072	0.042	0.028	0.019
Al	0.709	0.059	0.752	0.827	0.131	0.905	0.174	0.323	0.054	0.935	0.066	0.725	0.166	0.975	0.059
Fe2+	0.089	0.009	0.232	0.130	0.010	0.218	0.044	0.195	0.027	0.109	0.008	0.126	0.015	0.107	0.007
Mn	0.000	0.000	0.004	0.002	0.001	0.004	0.002	0.005	0.002	0.001	0.001	0.000	0.000	0.000	0.000
Ni	0.003	0.001	0.001	0.001	0.001	0.001	0.001	0.006	0.001	0.006	0.001	0.005	0.001	0.005	0.001
Mg	2.565	0.017	2.308	2.317	0.066	2.231	0.099	2.583	0.045	2.342	0.038	2.434	0.061	2.304	0.069
Ca	0.005	0.002	0.020	0.015	0.003	0.004	0.003	0.005	0.002	0.002	0.001	0.001	0.001	0.001	0.001
Na	0.001	0.000	0.001	0.001	0.001	0.001	0.001	0.001	0.001	0.002	0.001	0.001	0.001	0.012	0.024
K	0.000	0.000	0.001	0.001	0.000	0.001	0.001	0.000	0.000	0.002	0.002	0.000	0.000	0.002	0.002
Add El	0.000	0.000	0.000	0.001	0.002	0.010	0.016	0.002	0.003	0.000	0.000	0.001	0.001	0.000	0.000
H	3.954	0.020	3.994	3.999	0.001	3.981	0.039	3.994	0.004	3.995	0.002	3.998	0.002	3.996	0.003
F	0.000	0.000	0.00	0.000	0.000	0.000	0.000	0.000	0.000	0.000	0.000	0.000	0.000	0.000	0.000
Cl	0.046	0.020	0.01	0.001	0.001	0.019	0.039	0.006	0.004	0.005	0.002	0.002	0.002	0.004	0.003
Total Catior	**5.010**	**0.027**	**4.98**	**4.941**	**0.010**	**4.960**	**0.013**	**4.985**	**0.023**	**4.980**	**0.008**	**4.984**	**0.016**	**4.969**	**0.016**
SiO2	34.52	1.32	34.20	35.18	1.52	33.05	1.88	38.79	0.80	32.03	0.96	33.90	1.44	32.56	0.88
TiO2	0.01	0.02	0.04	0.01	0.01	0.01	0.01	0.07	0.07	0.07	0.08	0.01	0.01	0.02	0.02
Cr2O3	0.00	0.00	0.35	0.04	0.04	0.07	0.07	0.69	0.33	1.47	0.63	1.90	1.12	0.74	0.52
Al2O3	12.70	1.01	13.29	15.00	2.38	16.06	3.12	5.79	0.98	16.67	1.15	12.90	3.04	17.54	1.09
FeO	2.25	0.21	5.79	3.33	0.26	5.43	1.07	4.92	0.66	2.74	0.18	3.17	0.38	2.71	0.17
MnO	0.01	0.01	0.10	0.06	0.02	0.09	0.04	0.12	0.04	0.03	0.03	0.00	0.00	0.00	0.01
NiO	0.08	0.02	0.03	0.03	0.01	0.04	0.04	0.15	0.03	0.16	0.02	0.13	0.03	0.14	0.03
MgO	36.32	0.10	32.27	33.24	0.96	31.28	1.41	36.58	0.58	33.03	0.72	34.22	0.77	32.78	0.88
CaO	0.11	0.04	0.39	0.30	0.07	0.08	0.07	0.10	0.03	0.04	0.02	0.02	0.01	0.03	0.02
Na2O	0.01	0.00	0.01	0.01	0.01	0.01	0.01	0.01	0.01	0.02	0.01	0.01	0.01	0.13	0.27
K2O	0.00	0.00	0.02	0.02	0.01	0.02	0.01	0.01	0.01	0.03	0.03	0.01	0.00	0.03	0.03
Add ox	0.00	0.00	0.00	0.02	0.02	0.15	0.23	0.03	0.04	0.00	0.01	0.01	0.01	0.00	0.00
H2O	12.51	0.11	12.48	12.82	0.03	12.47	0.20	12.64	0.07	12.59	0.14	12.56	0.08	12.71	0.11
F	0.00	0.00	0.00	0.00	0.00	0.00	0.00	0.00	0.00	0.00	0.00	0.00	0.00	0.00	0.00
Cl	0.57	0.24	0.08	0.01	0.01	0.24	0.47	0.08	0.05	0.06	0.03	0.03	0.02	0.05	0.03
Total	99.09	0.08	99.05	100.04	0.31	98.98	0.68	99.98	0.44	98.95	0.96	98.87	0.58	99.44	0.83
F,Cl=O	0.13	0.06	0.018	0.00	0.00	0.05	0.11	0.02	0.01	0.01	0.01	0.01	0.01	0.01	0.01
Total	**98.96**	**0.03**	**99.028**	**100.04**	**0.31**	**98.93**	**0.69**	**99.96**	**0.44**	**98.94**	**0.96**	**98.86**	**0.58**	**99.43**	**0.83**

Chapter V

Ultramafic glasses fused on Ir-strip heater

FOREWORD

The following chapter deals with experiments conducted on an iridium strip-heater at the University of Neuchâtel. Prior to the described experiments on metabasic rocks, an other series of experiments with ultramafic rocks with the same aim and scopes were conducted.

In a first approach, direct quenching of ultramafic rocks on the strip heater was tried (see thesis of Laure Pelletier, 2008 (UniNe) for more details). Instead of forming a homogenous glass, the quenched ultramafic melts formed spinifex textures, segregating an olivine and an orthopyroxene glass. As element distribution is not homogenous, spinifex glasses cannot be used to analyze light element concentration.

In a second try, quartz was added to the ultramafic samples to increase silica content. This changes the type of melt from ultramafic to mafic, where olivine is not stable. Although we used ultra pure-silica (once foreseen to be a computer chip), ion probe analyses revealed high B contamination, with respect to expected values. A sample containing no B (<0.05 µg/g) had a corrected whole-rock value of 17.6 µg/g (on average) after quartz addition. As original silica B concentration is not exactly known (IC-MPS analyses revealed 68 ng/g B in the used quartz), decision was taken to conduct a series of experiments on metabasalts, as no quartz has to be added. These additional experiments should show us if there is any B contamination during sample and glass preparation and, additionally, the behavior of Li, Be and B on heating time and temperature can be studied. Our results on metabasalts from Syros islands (Greece) are presented in the following chapter (chapter 5).

Chapter V

Iridium-strip heater glass pellets: Effects of fusion temperature and time on Li, Be and B content

to be submitted to Geochemical Standards Newsletter

ABSTRACT

To solve a broad range of geochemical problems, precise and accurate whole rock and trace element analyses are required. Especially in the case of low abundant elements like Li, Be and B, which are widely used as tracers of alteration, subduction and recycling processes in the Earth, this is a critical issue. For in-situ mineral measurements of these elements, secondary ion mass spectrometry (SIMS) is probably the most sensitive and most accurate. A method that allows to analyse whole rock light element concentrations using SIMS would be extremely powerful and would dramatically increase sample throughput. However, a method to measure whole rock contents of all three light elements together is missing so far.

An Iridium-strip heater provides a flux free method to fuse directly homogeneous glass pellets from powdered rocks. These pellets can be investigated for major and light elements using microbeam (electron, ion or laser) methods. We have conducted experiments under different fusion temperatures (1500-1800°C) and time (30-240 s) on selected samples representing a wide variety of Li (0.91 to 56.5 µg/g), Be (0.24 to 3.5 µg/g) and B content (2.18 to 12 µg/g). We studied the behaviour of the three elements with respect to the different compositions, fusion time and temperature.

Homogeneity within the fused glasses is generally reached under the studied conditions for most elements. Electron microprobe measures and element distribution maps confirm this homogeneity. Light element measurements showed homogeneous behaviour for Li and Be (RSD of 3%, 6% respectively), but B is significantly less homogeneous (average RSD of 31%). Heating time dependent loss of Li, Be and B occurs throughout all studied samples, but Be and Li loss is always within analytical errors of the used methods (generally <10%). Significant B loss during fusion is found in almost every sample. In general, B is showing highly volatile behaviour, and at 1800°C most B has evaporated. Clearly, flux-less preparation of whole rock glasses is not a viable method for B analysis because of its volatility, but the method is well-suited for Li and Be.

5.1. Introduction

The "very low atomic mass elements" (Li, Be and B) have low abundance in most terrestrial rocks. An increasing number of studies have shown that Li, Be and B contents are key tracers of geochemical processes. For example, Li in back-arc lavas is a proxy for slab depth (e.g. Moriguti and Nakamura, 1998), ^{10}Be is used to constrain exposure ages of erratic blocks (e.g. Phillips et al., 2006) and B is preferentially incorporated in serpentinites in oceanic or subduction zone settings (e.g. Benton et al., 2001; Vils et al., 2008). To be able to analyze these elements accurately, precisely, and efficiently is therefore of high interest to the geochemical society.

Measuring whole rock composition in a quick and precise way has always been a challenge within geology, and to analyze the light elements is even more difficult. B contamination is quite common (e.g. Shaw et al., 1988) and measures avoiding it are proposed by Marschall and Ludwig (2004). One of the most used and quickest techniques for whole rock major and minor element analyses is X-ray fluorescence (XRF). As lithium-tetra-borate is used as a flux to lower melting points and to homogenize the samples, measurements of Li and B on the fused glasses are not possible. Be on the contrary is quite often measured (e.g. Paulick et al., 2006) and is accurate. Subsequent laser-ablation conductively coupled mass-spectrometry (LA-ICPMS) measurements on the XRF glasses allow the precise analysis of trace element concentrations (Günther et al., 2001), but can cause long-lasting Li and B contamination of the ICPMS components. An additional limitation of the preparation of XRF glasses is that one needs a relatively big sample mass (typically 1.5 g).

Nicholls (1974) first described direct, flux-less fusion of whole rock powders to form glasses with a strip heater. He found that analysis of international standards for major elements by electron microprobe (EMP) analysis led to a good agreement with recommended values, and homogeneity occurred within the samples. Accuracy of direct fusion combined with LA-ICPMS and EMP-measurements was shown by Fedorowich et al. (1993). Most elements were within 20% of the recommended values and precision ranged from 5 to 15% (Fedorowich et al., 1993).

First accuracy measurements by Ottolini et al. (1993a) on glass-pellets from a strip heater showed that SIMS is a useful method to analyze Li, Be and B in-situ even in low quantities and that NIST 610 is a useful standard to calibrate over a wide spectrum of light element concentration (for more details, see 'analytical part'). Based on NIST 610, studies on a wide variety of fields followed, e.g., studies of disequilibrium processes in

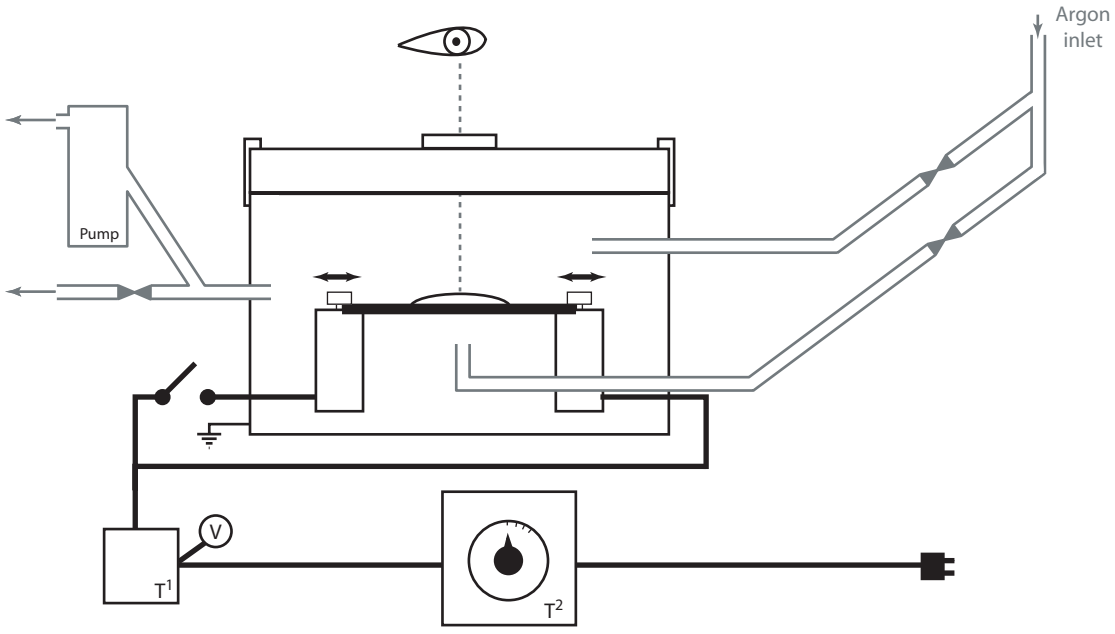

Fig. 5.1. Schematic diagram of the Ir-strip heater and the connected devises at the University of Neuchâtel (modified after Nicholls, 1974; Stoll et al., 2008). Figure not to scale, however chamber diameter is 32cm. T1: adjustable transformer 1 (220V to 12V); T2: transformer 2 (12V to 0-12V).

xenoliths (Kaeser et al., 2007), measurements of B concentrations in foraminifera (Spivack et al., 1993), and analysis of Be behaviour during prograde Alpine metamorphism (Vils, 2009). New developments in analysis techniques allow even in-situ isotopic measurements in minerals with low light element abundances (e.g. δ^7Li in olivine, Jeffcoate et al., 2007; δ^{11}B in serpentine, Pabst et al., 2008). This makes SIMS a quick, precise, and accurate method for light element measurements.

So far several studies used Ir-strip heaters to prepare glass pellets from whole rocks powders (e.g. Bottazzi et al., 1991; Ottolini et al., 1992; Ottolini et al., 1993b; Ottolini et al., 1993a) and analysed light element concentrations on these pellets. Le Fèvre and Ottlini (2006) proposed glass fusing in a graphite capsule as a possible method to produce Li and B standards for SIMS analyses, but so far the dataset is limited. Moreover, a systematic methodological study that looks into the behaviour of all three light elements during strip heater fusion is missing. The aim of this study is to show the light element behaviour on the Ir-strip heater under different temperature conditions and different heating times. Moreover, we discuss the limitations and problems in using Ir-strip heater glass pellets for light element studies.

5.2. Sample description

For this study, we used well-characterized samples from the island of Syros (Greece, Table 1). The samples were collected by H. Marschall near Kampos and are high-pressure metamorphosed equivalents of an ancient oceanic crust (e.g. Seck et al., 1996). The geological setting is well described in Marschall (2005). The treated samples are metabasites (Sy304, Sy342), eclogites (Sy323, Sy324, Sy411) and plagiogranites (Sy415). SiO_2 content varies from 45 to 70 wt% and Mg# (Mg# = 100*Mg/(Mg+Fe)) from 18 to 53. Detailed descriptions and chemical compositions can be found in Marschall (2005); Marschall et al. (2006). Samples contain a wide variety of light element concentrations (Li 5.6-72.3 µg/g, Be 0.5-3.5 µg/g, B 2.2-12 µg/g). Whole rock analyses of B have previously been conducted with PGAA and the precision of the published values is <1.3% (Marschall et al., 2005). Li and Be whole rock data are from wet chemistry ICP-AES and have an precision of ~20% (Marschall, 2005). The same powders as in Marschall (2005) have been used to avoid any additional contamination related to milling procedure or within-sample heterogeneity.

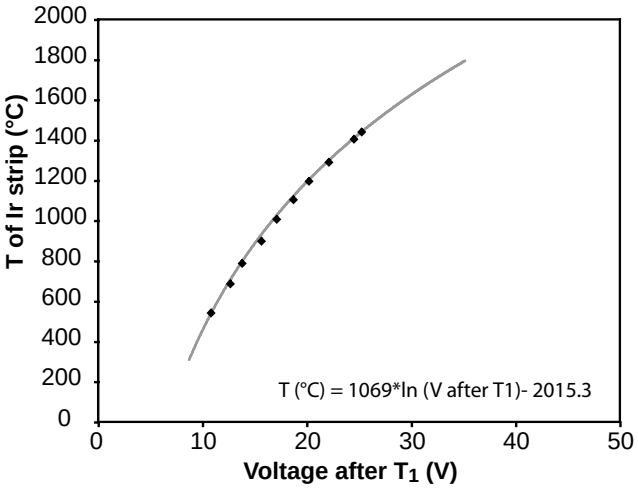

Fig. 5.2. Calibration curve obtained by pyrometer measurements on an Ir-strip during heating.

5.3. Experimental and analytical procedure

For our experiments, we designed and built an Ir-strip heater based on Nicholls (1974), but with some key modifications (Fig. 5.1). The major modification is the placing of the Ir-strip heating element within a steel-chamber. This allows the control of the fusion

Table 1: Studied samples from Syros (Greece) and chemical composition after Marschall, 2005

Sample	rock	SiO_2	xMg	Li	Li		Be	B	H_20
methode		*XRF*	*XRF*	*ICP-OES*	*ICPMS*	*2 sigma*	*ICP-MS*	*PGNAA*	*XRF*
SY304	metabasic	45.74	53.8	7.75	n.a.	-	0.46	12	3.17
SY342	metabasic	55.21	49.3	27.4	29.95	0.75	1	4.92	1.5
SY323	eclogite	45.35	44.8	45.8	42.02	0.44	2.1	4.77	0.78
SY324	eclogite	46.85	50.6	56.5	n.a.	-	2.2	2.18	0.7
SY411	eclogite	49.39	54.7	72.3	n.a.	-	2.9	3.8	0.5
SY415	meta-plagiogranite	70.32	17.9	5.62	5.27	0.05	3.5	10.6	0.68
SY347	serpentinites	41.41	90.8	0.91	1.34	0.05	0.24	5.52	12.12
SY429	serpentinites	45.03	87.5	2.81	2.49	0.09	0.47	11.3	9.75

environment and potentially reduces the loss of volatile elements. Additionally, a controlled atmosphere, argon environment within the chamber inhibits oxidation of the treated samples. Our design follows the previously described Ir-strip heaters in Nehring et al. (2008); Stoll et al. (2008). A 4 cm x 0.8 cm strip (0.15-0.17 mm thick) is wedged between two copper energetic poles to use the energy resistance to heat the strip. To suppress oxidation and loss of volatile elements (e.g. B, Li or Na) the Ir-strip heater is placed in a chamber and prior to fusion flooded with technical argon. A porthole in the top lid with a quartz glass window and covered with a removable dark welding glass allows the inspection of the sample material during fusion (Fig. 5.1). An IRCON Modline 2 pyrometer was used to calibrate the temperature in the centre of the Ir-strip without sample material between 800 and 1400°C, depending on the voltage measured at the first transformer. The following equation can be used to calculate the temperature at the Ir-strip heater at the University of Neuchâtel: T [°C]= 1069*ln([V] after T_1) - 2015.3 (Fig. 5.2). Measured temperature precision is in the range of ±25°C, but the error on the temperature is probably in the range of 50°C at temperatures above 1400°C, where the relation between voltage and temperature is extrapolated.

Only low amounts of sample material (3-11 µg) were used to fuse on the strip. Heating time on the strip ranged from 30 to 240s and temperature ranged from 1500° to 1800°C (Table 2). Fusion temperature was controlled by measuring the voltage after the first transformer (T_1) and are given in Table 2. After fusion, melt was quenched by swiching off the power with simultaneous switch on of an argon jet over the sample (Fig. 5.1). Tests with the pyrometer had shown that the strip cooled down to a temperature below 800°C well within a second, while Stoll et al. (2008) also showed that complete freezing occurs after <1s. For analytical procedure the glass pellets were embedded within evapoxy. To avoid any glass rim contamination due to the strip or surface heterogeneity, samples were polished and analyses were done on the flat surface. Quantitative major-element analyses of the glass pellets were determined using an electron microprobe (EMP; Jeol JXA-8200) at the University of Bern. A wave length dispersive mode with 15kV accelerating voltage and a beam current of 10 nA was used. Counting time for each element was 20s (30s for Si and Al, background 10s) with a defocused beam of 10 µm to minimize Na and K volatilization and matrix effects. Natural silicates and oxides have been used for standardization.

Li, B and Be were analyzed in-situ by Secondary Ion Mass Spectrometry (SIMS) using a modified Cameca IMS 3f ion microprobe at the Mineralogical Institute of Heidelberg, Germany, using the same machine setup as described in Vils et al. (2008). A 14.5keV/20nA $^{16}O^-$ primary beam with ~30 µm diameter and acceleration to a nominal energy of 4.5 keV for the positive

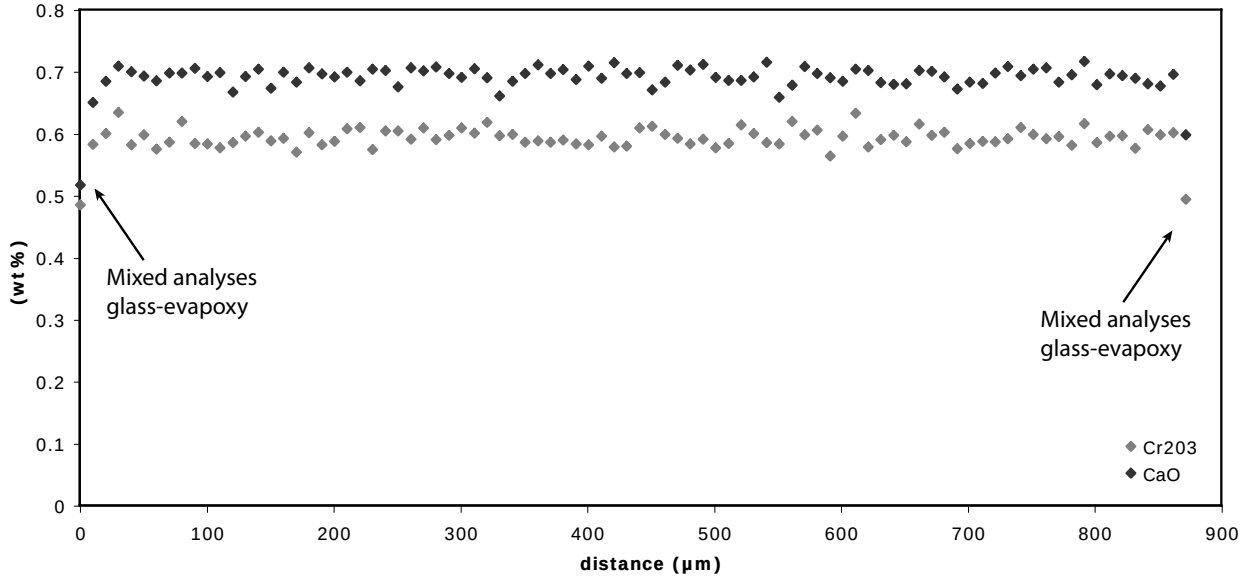

Fig. 5.3. Electron-microprobe profile through a glass, showing the homogeneity over a glass.

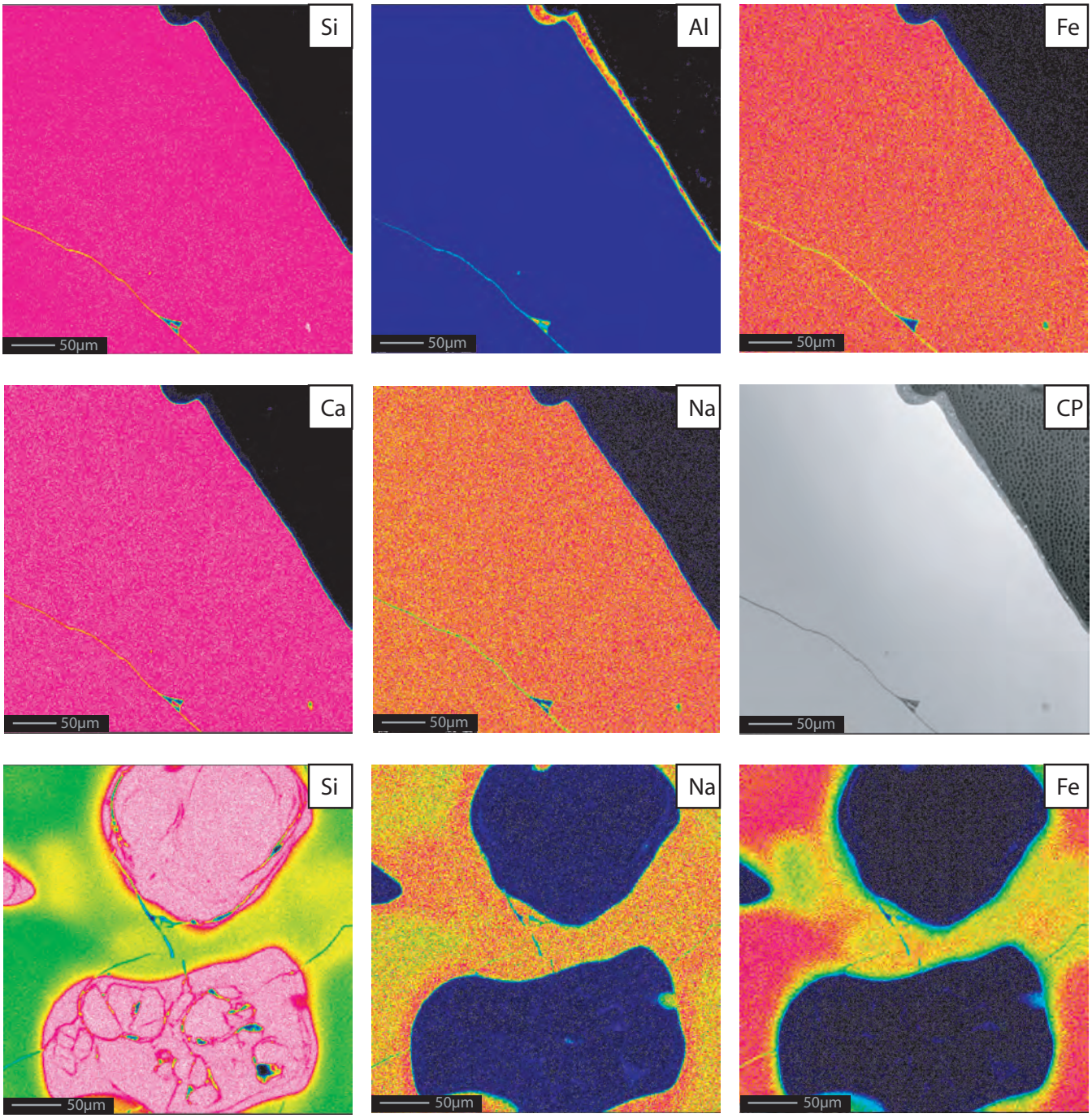

Fig. 5.4. Element distribution images of glass 15 & 25 and back-scattered images showing major element homogeneity and heterogeneity of the studied samples.

secondary ions was used. Secondary ^{7}Li, ^{9}Be, ^{11}B and ^{30}Si ions were collected applying the energy filtering method using an offset of 75 eV at a mass resolution of ~1030 (m/Δm, 10%) and a nominal imaged field of 25 mm. Secondary ion intensities were normalized to the count rates of ^{30}Si and calibrated against the NIST SRM610 glass reference material using the concentrations (preferred averages) reported in Pearce et al. (1997); the accuracy is estimated to be < 20% for Li and < 10% for Be and B (Ottolini et al., 1993a). Li, B and Be concentrations were quantified using the SiO_2 values of the corresponding EMP analysis. One single analysis comprised 10 cycles for each isotope with integration times of 8 s/cycle for Li, 16 s/cycle for Be and B, and 2 s/cycle for Si. The chosen setup and the background lead to a detection limit (critical value) of 1.4 ng/g (Li), 1.0 ng/g (Be) and 2.6 ng/g (B) (Currie, 1968; Marschall and Ludwig, 2004).

Due to the generally low concentration levels of Li, Be and B in mantle rocks, contamination during sample preparation and handling is always problematic, particularly for B (Shaw et al., 1988). Careful sample preparation is thus a necessary prerequisite for accurate analyses (see Marschall and Ludwig, 2004 for details). At the beginning of each SIMS analysis, a presputtering of ~400 s was applied to eliminate the potential rest of surface contamination. Additionally the imaged field was set smaller than the primary beam diameter (applying field aperture #2, d=750 µm) to suppress contaminating secondary ions from the crater edges (Benninghoven et al., 1987). Following the procedure described by Marschall and Ludwig (2004), the B contamination level is <2 ng/g. Li contamination is typically ~50 times lesser than for B, and Be does not show any sign of contamination.

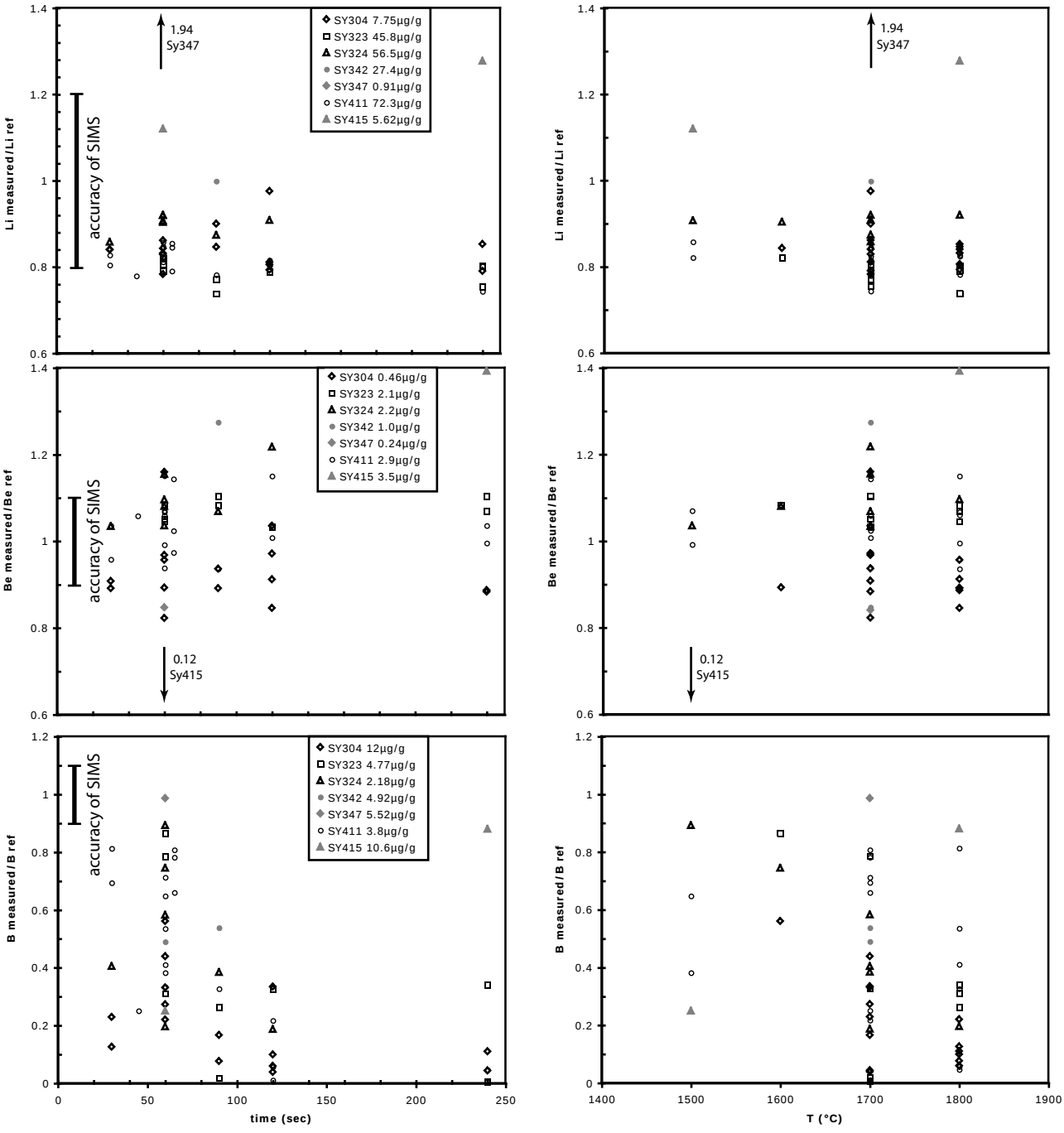

Fig. 5.5a. Measured light element/reference value versus time and temperature (reference values after Marschall, 2005; Table 1). Accuracy of SIMS-analyses indicated, showing range of analytical error.

Table 2: Experimental conditions on the stripheater

glass	Sample	Time	T		voltage T1		glass	Sample	Time	T		voltage T1	
	SYXXX	*(s)*	*(°C)*		*(V)*			*SYXXX*	*(s)*	*(°C)*		*(V)*	
1	411	60	1700		33.6	h	44	411	60	1600		29.1	p
2	323	60	1700		33.6	h	45	323	60	1600		29.2	
3	324	60	1700		33.8	h	46	323	60	1800		35.3	h
4	304	60	1700		33.6	h	47	324	60	1800		35.6	h
5	415	60	1700		33.6	p	48	411	60	1800		35.6	h
6	342	60	1700		33.6	p	49	411	30	1800		35.8	
7	323	90	1700			h	50	411	240	1800		35.4	h
8	323	120	1700		34.1	h	51	411	120	1800		35.6	
9	323	240	1700		34.3	h	52	411	90	1800		34.9	h
10	324	90	1700			h	53	411	120	1800	air	35.8	h
11	324	120	1700		33.6	h	54	411	60	1800	air	36	h
12	324	30	1700		33.6	h	55	304	60	1800	air	36.1	h
13	411	90	1700		33.5		56	304	120	1800	air	36.2	h
14	411	120	1700		33.5	h	57	304	60	1800		36.3	h
15	411	30	1700		33.4		58	304	90	1800		36.4	h
16	411	240	1700		33.5	h	59	304	30	1800		36.2	h
17	304	90	1700		33.5	h	60	304	120	1800		36.2	h
18	304	30	1700		33.4	h	61	304	240	1800		36.6	
19	304	120	1700		33.5	h	62	342	90	1800		36.6	p
20	304	240	1700		33.6		63	342	120	1800		36.7	p
21	415	90	1700		33.5	p	64	342	60	1800		36.4	
22	415	120	1700		33.6	p	64A	342	240	1800		36.4	p
23	415	30	1700		33.8	p	65	323	120	1800		36.6	
24	342	90	1700		33.6		66	323	240	1800		36.6	h
25	342	30	1700		33.7		67	323	90	1800		35.9	h
26	342	120	1700		33.7	p	68	415	60	1800		36.3	p
27	411	60	1700	air	34.1		69	415	120	1800		36.9	p
28	411	120	1700	air	34.1		70	415	30	1800		36.5	p
29	304	60	1700	air	34.3		71	415	240	1800		36.4	
30	304	120	1700	air	34.3	h	72	411	stepA	1700			xx
31	415	60	1500		34.2	h	73	411	step B	1700			h
32	411	45	1700		34.2	h	74	411	step C	1700			h
33	411	60	1500		27.2	h	75	304	stepA	1700			p
34	411	60	1500	b	27.4	h	76	304	step B	1700			p
35	323	60	1500		27.3	p	77	304	step C	1700			p
36	324	60	1500		27.3	h	78	304	60	1700		33.7	h
37	304	60	1500		27.4	p	79	304	60	1700		34	
38	415	60	1500		27.3	p	80	411	60	1700		34.1	h
39	342	60	1500		27.3	p	81	429	60	1700		34	h
40	342	60	1600		29.3	p	82	347	60	1700		34.1	h
41	415	60	1600		29.2	p							
42	304	60	1600		29.1								
43	324	60	1600		29.2	xx							

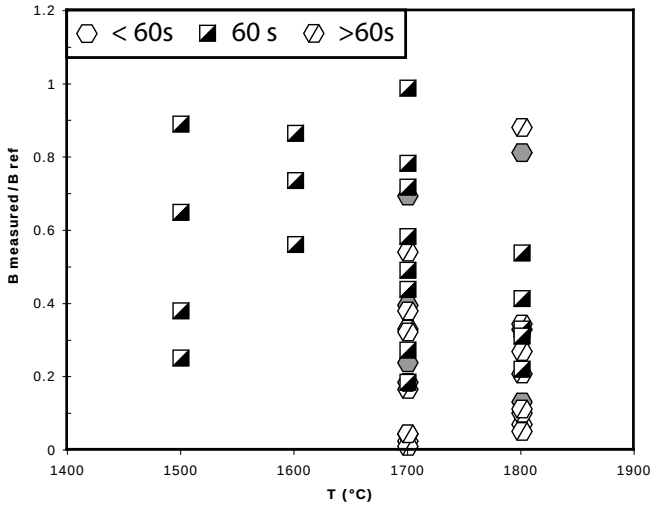

Fig. 5.5b. Measured light element/reference value versus temperature showing time dependency of the samples (reference values after Marschall, 2005; Table 1).

5.4. Results

Visual observation of the glasses has been conducted prior to any analytics, and heterogeneous samples have been excluded for further analyses. Overall microscopically determined heterogeneity was low. All experimental results are reported in Table 2, for homogeneous and heterogeneous samples. Average light element contents are reported in Table 3. In general, most experiments have been conducted under 1700°C as experience showed that, under these conditions, even spinels are dissolved into the glass phase. Some light element contents correspond to single analyses, thus minimal, maximal, and standard deviations are missing (Table 3). Mostly these points reflect heterogeneous glasses which are interesting in understanding low temperatures or low melting times, even if values can only be used as estimates.

Table 3: SIMS analyses of experimental glasses

average	Li	Be	B	min	Li	Be	B	max	Li	Be	B	STDEV	Li	Be	B	RSD	Li	Be	B
glass	*[µg/g]*	*[µg/g]*	*[µg/g]*		*[µg/g]*	*[µg/g]*	*[µg/g]*		*[µg/g]*	*[µg/g]*	*[µg/g]*		*[µg/g]*	*[µg/g]*	*[µg/g]*		*[%]*	*[%]*	*[%]*
1	38.529	2.437	3.747		38.111	2.408	3.281		38.938	2.453	4.342		0.464	0.020	0.440		1.205	0.811	11.744
2	36.888	2.207	3.745		35.930	2.161	2.989		38.154	2.280	4.099		1.043	0.051	0.511		2.828	2.308	13.630
3	51.986	2.542	1.271		50.667	2.482	1.186		53.654	2.627	1.460		1.252	0.061	0.127		2.407	2.412	9.996
4	6.678	0.534	3.272		6.274	0.445	0.752		7.097	0.665	5.577		0.406	0.097	1.974		6.076	18.256	60.325
5	7.457	5.915	11.280		7.010	5.252	8.399		7.779	6.506	15.388		0.399	0.630	3.653		5.355	10.655	32.387
6	22.448	1.137	1.024		21.847	0.915	0.451		22.901	1.340	1.565		0.521	0.174	0.554		2.319	15.280	54.104
7	35.333	2.319	0.086		34.938	2.244	0.081		35.521	2.368	0.092		0.267	0.054	0.005		0.755	2.324	5.449
8	36.104	2.169	1.556		35.334	2.155	1.148		36.549	2.180	1.881		0.541	0.011	0.334		1.497	0.489	21.460
9	34.562	2.317	0.022		33.079	2.296	0.010		35.860	2.342	0.037		1.143	0.021	0.012		3.307	0.908	53.461
10	49.388	2.351	0.839		47.865	2.243	0.610		50.639	2.413	1.233		1.183	0.080	0.283		2.394	3.412	33.780
11	51.334	2.680	0.408		50.148	2.519	0.207		52.825	2.740	0.778		1.108	0.107	0.258		2.159	4.003	63.113
12	48.476	2.276	0.883		47.258	2.142	0.448		49.404	2.335	1.265		0.934	0.090	0.432		1.926	3.968	48.911
14	58.976	2.924	0.042		56.658	2.859	0.019		60.713	3.018	0.057		1.662	0.056	0.016		2.819	1.926	37.216
15	58.138	3.004	2.636		56.696	2.880	1.675		59.248	3.063	5.189		0.916	0.079	1.289		1.575	2.641	48.894
16	53.763	3.005	0.022		49.966	2.905	0.014		56.956	3.044	0.030		2.936	0.067	0.008		5.460	2.219	34.738
17	6.971	0.431	1.992		6.835	0.416	1.774		7.060	0.452	2.224		0.097	0.015	0.196		1.391	3.469	9.832
18	6.510	0.418	2.751		6.375	0.394	1.745		6.674	0.457	4.281		0.145	0.028	1.123		2.228	6.597	40.812
19	7.557	0.476	0.462		7.140	0.460	0.417		8.026	0.498	0.489		0.445	0.020	0.040		5.888	4.147	8.614
19	6.031	0.437	0.124																
20	6.127	0.407	0.518		6.058	0.389	0.298		6.175	0.417	0.812		0.050	0.012	0.246		0.809	2.939	47.474
24	27.363	1.275	2.646		26.386	1.005	1.722		28.188	1.500	3.495		0.793	0.260	0.828		2.898	20.367	31.289
25	22.852	0.917	1.645																
26	22.301	0.992	1.232																
27	58.699	3.337	1.269		56.659	3.317	0.640		60.287	3.371	2.348		1.596	0.024	0.760		2.718	0.706	59.848
28	58.058	2.992	0.826		55.987	2.901	0.388		59.761	3.135	1.274		1.731	0.103	0.366		2.982	3.442	44.295
29	6.067	0.445	5.262		5.902	0.429	3.914		6.307	0.462	6.081		0.194	0.016	0.958		3.199	3.686	18.199
30	6.286	0.447	4.007		6.194	0.433	3.271		6.443	0.458	4.558		0.136	0.013	0.663		2.166	2.818	16.551
30	6.532	0.453	2.848																
31	6.295	0.426	2.653		6.218	0.408	1.804		6.343	0.440	3.727		0.043	0.012	0.758		0.689	2.887	28.554
32	56.332	3.070	0.954		53.938	2.825	0.384		57.356	3.351	1.537		1.607	0.272	0.612		2.853	8.871	64.149
33	59.386	2.877	2.461		57.187	2.697	2.178		62.516	2.999	2.742		2.455	0.134	0.245		4.133	4.664	9.936
34	62.010	3.103	1.452		61.372	2.928	1.016		62.556	3.304	2.137		0.513	0.155	0.519		0.827	4.984	35.723
35	34.876	2.353	2.077																
36	51.264	2.278	1.945		50.426	2.147	1.647		52.081	2.389	2.499		0.635	0.091	0.325		1.238	4.001	16.725
37	6.193	0.398	7.560		5.629	0.333	3.336		6.477	0.465	12.279		0.385	0.070	4.313		6.216	17.664	57.051
39	23.722	0.706	1.732		20.478	0.409	0.964		26.747	0.937	2.537		3.444	0.219	0.686		14.518	31.028	39.606
42	6.531	0.411	6.728		6.345	0.390	6.263		6.756	0.467	7.114		0.169	0.037	0.354		2.593	9.104	5.265
43	51.081	2.378	1.623		48.960	2.183	1.257		52.437	2.576	1.869		1.625	0.218	0.270		3.180	9.148	16.619
43	50.667	2.321	1.834		49.504	2.134	1.731		51.962	2.532	1.916		1.084	0.209	0.080		2.139	9.022	4.356
44	57.491	3.036	2.472		56.127	2.672	2.381		60.171	3.669	2.603		3.351	0.632	0.294		5.830	20.801	11.890
45	37.611	2.275	4.125		36.430	2.100	2.393		39.077	2.390	6.115		1.093	0.125	1.697		2.906	5.486	41.131
46	36.203	2.196	1.480		35.910	2.148	1.289		36.825	2.267	1.700		0.423	0.055	0.169		1.168	2.485	11.404
47	51.971	2.412	0.428		51.356	2.337	0.236		52.522	2.478	0.701		0.533	0.058	0.204		1.025	2.398	47.587
48	61.263	3.074	1.559		60.555	2.978	0.677		61.797	3.335	2.275		0.592	0.174	0.738		0.967	5.677	47.361
49	59.810	2.778	3.089		59.276	2.711	1.723		60.332	2.839	4.757		0.481	0.060	1.378		0.804	2.170	44.611
50	57.945	2.887	0.176		56.268	2.793	0.066		59.919	2.996	0.278		1.612	0.095	0.092		2.782	3.281	51.916
52	56.516	2.715	1.241		54.526	2.656	0.911		57.426	2.772	1.490		1.338	0.047	0.276		2.368	1.749	22.269
53	58.127	3.335	0.213		57.334	3.311	0.185		59.140	3.384	0.234		0.748	0.033	0.020		1.287	1.000	9.551
54	59.588	3.095	2.034		57.865	2.977	0.963		61.099	3.339	2.910		1.646	0.165	0.803		2.763	5.320	39.488
56	6.146	0.419	0.714		5.987	0.390	0.339		6.428	0.440	1.037		0.203	0.021	0.352		3.311	5.015	49.393
57	6.444	0.440	2.639		6.187	0.434	1.662		6.605	0.450	3.730		0.187	0.007	1.054		2.902	1.513	39.931
58	6.559	0.410	0.920		6.442	0.385	0.825		6.680	0.436	1.019		0.134	0.026	0.085		2.044	6.312	9.196
59	6.510	0.410	1.512		6.413	0.385	1.389		6.599	0.420	1.718		0.092	0.017	0.143		1.417	4.039	9.489
59	6.468	0.406	5.190		6.274	0.384	2.715		6.602	0.431	6.876		0.149	0.021	1.768		2.300	5.090	34.069
60	6.245	0.389	1.193		6.062	0.375	0.868		6.524	0.400	1.810		0.223	0.011	0.422		3.572	2.751	35.401

average glass	n	Li [µg/g]	Be [µg/g]	B [µg/g]	min	Li [µg/g]	Be [µg/g]	B [µg/g]	max	Li [µg/g]	Be [µg/g]	B [µg/g]	STDEV	Li [µg/g]	Be [µg/g]	B [µg/g]	RSD	Li [%]	Be [%]	B [%]
57	4	6.444	0.440	2.639		6.187	0.434	1.662		6.605	0.450	3.730		0.187	0.007	1.054		2.902	1.513	39.931
58	4	6.559	0.410	0.920		6.442	0.385	0.825		6.680	0.436	1.019		0.134	0.026	0.085		2.044	6.312	9.196
59	4	6.510	0.410	1.512		6.413	0.385	1.389		6.599	0.420	1.718		0.092	0.017	0.143		1.417	4.039	9.489
60	4	6.245	0.389	1.193		6.062	0.375	0.868		6.524	0.400	1.810		0.223	0.011	0.422		3.572	2.751	35.401
61	4	6.607	0.408	1.319		6.452	0.392	0.947		6.864	0.430	2.054		0.179	0.017	0.509		2.703	4.116	38.607
66	4	36.742	2.246	1.622		36.324	2.233	1.349		37.128	2.260	1.848		0.329	0.011	0.222		0.894	0.496	13.695
67	3	33.807	2.273	1.255		33.377	2.240	0.421		34.189	2.301	2.273		0.408	0.031	0.940		1.206	1.346	74.858
71	4	7.178	4.875	9.331		6.001	4.270	4.791		7.640	5.205	12.003		0.790	0.438	3.167		11.008	8.994	33.941
72	4	61.780	3.317	2.970		56.680	3.123	2.481		65.473	3.606	3.640		4.329	0.226	0.485		7.007	6.820	16.325
73	4	57.145	2.970	3.068		54.638	2.588	2.438		59.866	3.103	4.644		2.622	0.255	1.059		4.588	8.579	34.532
74	4	61.111	2.824	2.507		58.601	2.626	1.829		63.027	2.952	3.524		1.842	0.149	0.723		3.015	5.269	28.835
78	5	6.423	0.378	3.970		6.173	0.357	2.988		6.955	0.400	4.680		0.312	0.019	0.703		4.860	4.985	17.703
80	4	59.596	2.722	2.707		56.735	2.502	1.923		66.443	2.802	3.927		4.599	0.146	0.863		7.718	5.378	31.871
81	4	59.530	2.897	2.378		57.537	2.736	2.215		60.924	3.001	2.727		1.473	0.114	0.239		2.474	3.937	10.052
82	3	1.770	0.203	2.703		1.626	0.189	2.595		1.897	0.215	2.866		0.136	0.013	0.144		7.695	6.406	5.309
86	1	1.892	0.263	8.603																
87	1	0.847	0.091	7.778																

5.5. Discussion

5.5.1 Homogeneity of the glass

Homogeneity of glass samples is important to validate any analytical measures, therefore all studied glasses have been investigated on the optical microscope to select homogeneous glasses prior to any analytical treatment (Table 2). Back-scattered images on the selected homogeneous samples show no elemental heterogeneity (Fig. 5.2). Additionally, measurements of transects on Ir-strip heater glasses revealed that major elements do not show any zonation across glasses classified as homogeneous after optical inspection (Fig. 5.3). As Nicholls (1974); Fedorowich et al. (1993) already stated, no heterogeneity with respect to major and rare Earth elements in strip heater glasses occurs. To illustrate this homogeneity, we conducted element-distribution maps. Fig. 5.4 shows such a map for sample SY411 (glass 15) on major elements for Si, Ca, Al, Mg and Fe. No visible structure with exception of cracks and dust on the surface is shown in the images (Fig. 5.4). Overall, studied glasses are homogeneous, even at the rim of a sample (Fig. 5.4). Heterogeneity of a sample is illustrated by mapping a quartz bearing glass (sample SY342; glass 25). The two quartz crystals are clearly visible and zonal heterogeneity is shown in the glass around the minerals (Fig. 5.4). Observations of random, pixel size heterogeneity in homogeneous glasses correspond thus to analytical uncertainties and not to chemical heterogeneity (Fig. 5.4).

Light element measures show partial homogeneity. Relative standard deviations (RSD) of repeated concentration measurements within the same glass reveal that Li has homogeneity within 5%. Be has a higher grade of heterogeneity within 14%. Degree of B homogeneity is low, as RSD is on average 31%. RSD of Li and Be are within the analytical error of the SIMS, and thus Li and Be measurements are considered to be homogeneous, as no variation in the RSD is observed within the studied samples. On the contrary, RSD of B measurements are higher than analytical error, and variation with temperature occurs. We therefore conclude that Li and Be are homogeneous distributed in the glasses and that B is slightly heterogeneous.

5.5.2 Behaviour of Li, Be and B compared to temperature and concentration

Most concerns about using any high-temperature heating methods are that volatile elements (e.g. H_2O, Li, Be and B) might be lost during glass pellets formation. The use of flux-fusion in XRF should decrease the loss of volatile trace elements, as lower temperature than melting temperature for pure rock can be used (~1100°C). Nevertheless, as heating for homogenisation is taking about an hour, all fluids disappear and significant amounts of light elements may also be lost during the XRF glass preparation. The strengths of direct fusion on Ir-strip heater are lower heating times and variable heating temperatures.

Studies of Stoll et al. (2008) revealed that major and trace elements are homogeneous for melting temperature ≥1500°C. They proposed 1600°C and 10s as an optimal experimental temperature, as homogeneity for major elements and REE occurs. These conditions are somehow contradictory to previous reported values (60-120s and >1650°C) to obtain homogeneous glasses by Fedorowich et al. (1993). Our experiments on different times and temperatures are shown in Fig. 5.5. Data have been normalized to the reference value (Table 1) and are presented with regards to fusion time and temperature (Fig. 5.5). Both Li and Be concentrations do not show any significant time and temperature dependency, in contrast to B. High volatile loss occurs in B with increasing heating time, regardless of the initial B concentration and heating temperature (Fig. 5.5). At lower temperature, it is expected that lower B loss occurs as less fluids escape. Nevertheless, this is not observed as high $B_{measured}/B_{reference}$ ratios over all temperatures occur and temperature does not seem to play a critical role (Fig. 5.5). However, sample SY415 has low H_2O content (0.68wt%) and at 240s and 1800°C high $B_{measured}/B_{reference}$ ratios are shown (Fig. 5.5). On the contrary, high B loss seem to occur at 1500°C and 60s for the same sample. We suggest that, even if not visible at microscope, heterogeneity within this experimental glass must occur to explain such low B concentrations. Not only temperature and time play a role in B loss, but probably also the volatiles available in the treated sample, as indicated by sample SY415. Although Li values are within the analytical error, some Li loss seems to occur, as the minimum $Li_{measured}/Li_{reference}$ ratio is slightly decreasing with time and temperature (e.g. 0.82 at 1500°C and 0.74 at 1800°C).

5.5.3 Accuracy of the data

The accuracy of a dataset gives information if precise measurements are in good agreement with previously published results, which are assumed accurate. SIMS measurements of glasses measured here are comparable to whole rock measurements with PGAA and ICP-AES (Marschall, 2005). The accuracy for Li is within the range of analytical error ±20%. Similar accuracy is observed for Be concentrations. On the contrary, B is acting as a highly volatile element as discussed above, and is highly depleted in higher temperatures compared to initial composition (Fig. 5.5). Therefore, B content of the studied samples is not accurate and B concentration measured on glass pellets formed on a strip heater or any heating related experiment have to be interpreted with caution. A promising solution to overcome the problem of B loss may be to place a Ir-strip heater within a pressure vessel (personal communication, Jörg Hermann), but this could not be tested in our set-up.

5.6. Conclusion

In general, the Ir-strip heater is a useful tool to acquire precise and accurate whole rock data. With respect to light elements, Li and Be measures revealed that over a wide range of temperature (1500-1800°C), fusion time (30-240s) and sample concentrations, the measured values are accurate and within the analytical error of other methods. B on the contrary showed highly volatile behaviour, which lead to low accuracy and low homogeneity of the studied samples. Moreover, combined analyses of Ir-strip heater flux free fusion and SIMS is rather fast (comparing to any wet chemistry method). Therefore a high samples throughput can be achieved.

ACKNOWLEDGMENTS

This research used samples provided by Horst Marschall. The authors would like to thank Angelika Kalt, Laure Pelletier, Marina Lazarov, Thomas Ludwig, Anne-Lise Jourdan and Horst Marschall for fruitful discussions, which helped to improve the manuscript. The authors appreciate the technical support by Thomas Ludwig for analyzing the light elements on the SIMS in Heidelberg. Additionally the authors would like to thank Hans-Michael Seitz and Erich Hellebrand for their tips, which helped to build the Ir-strip heater at the University of Neuchâtel. This study was supported by the Swiss national foundation Grant 200021-10361.

REFERENCES

Benninghoven, A., Rüdenauer, F. G., and Werner, H. W., 1987. Secondary ion mass spectrometry: Basic concepts, instrumental aspects, applications and trends. John Wiley & Sons, New York Chichester Brisbane Toronto Singapore.

Benton, L. D., Ryan, J. G., and Tera, F., 2001. Boron isotope systematics of slab fluids as inferred from a serpentine seamount, Mariana forearc. Earth and Planetary Science Letters 187, 273-282.

Bottazzi, P., Ottolini, L., and Vannucci, R., 1991. Determination of rare earth elements in sixteen silicate reference samples by secondary ion mass spectrometry using conventional energy filtering technique. Geostandards Newsletter 15, 51-57.

Currie, L. A., 1968. Limits for qualitative detection and quantitative determination. Analytical Chemistry 40, 586-593.

Fedorowich, J. S., Richards, J. P., Jain, J. C., Kerrich, R., and Fan, J., 1993. A rapid methode for REE and trace-element analysis using laser sampling ICP-MS on direct fusion whole-rock glasses. Chemical Geology 106, 229-249.

Günther, D., von Quadt, A., Wirz, R., Cousin, H., and Dietrich, V., 2001. Element analyses using laser ablation-inductively coupled plasma-mass spectrometry (LA-ICP-MS) of geological samples fused with $Li_2B_4O_7$ and calibrated without matrix-matched standards. Mikrochimica Acta 136.

Jeffcoate, A., Elliott, T., Kasemann, S. A., Ionov, D., Cooper, K., and Brooker, R. A., 2007. Li isotope fractionation in peridotites and mafic melts. Geochimica et Cosmochimica Acta 71, 22-218.

Kaeser, B., Kalt, A., and Ludwig, T., 2007. Li, Be, and B abundances in minerals of peridotite xenoliths from Marsabit (Kenya): Disequilibrium processes and implications for subduction zone signatures. Geochemistry Geophysics Geosystems 8, 1-25.

Le Fèvre, B. and Ottlini, L., 2006. Preparation of reference glasses for in-situ analysis of lithium and boron. Microchimica Acta 155, 189-194.

Marschall, H., Altherr, R., Ludwig, T., Kalt, A., Gméling, K., and Kasztovszky, Z., 2006. Partitioning and budget of Li, Be and B in high-pressure metamorphic rocks. Geochimica et Cosmochimica Acta 70, 4750-4769.

Marschall, H., Kasztovszky, Z., Gméling, K., and Altherr, R., 2005. Chemical analysis of high-pressure metamorphic rocks by PGNAA: Comparison with results from XRF and solution ICP-MS. Journal of Radioanalytical and Nuclear Chemistry 265, 339-348.

Marschall, H. R., 2005. Lithium, Beryllium and Boron in high-pressure metamorphic rocks from Syros (Greece). Ph.D. thesis, Ruprecht-Karls Universität.

Marschall, H. R. and Ludwig, T., 2004. The low-boron contest. Minimising surface contamination and analysing boron concentration at the ng/g-level by secondary ion mass spectrometry. Mineralogy and Petrology 81, 265-278.

Moriguti, T. and Nakamura, E., 1998. Across-arc variation of lithium isotopes in lavas and implications for crust/mantle recycling at subduction zones. Earth and Planetary Science Letters 163, 167-174.

Nehring, F., Jacob, D. E., Barth, M. G., and Foley, S. F., 2008. Laser-ablation ICPMS analysis of siliceous rock glasses fused on an iridium strip heater using MgO dilution. Microchimica Acta 160, 153-163.

Nicholls, I. A., 1974. A direct fusion method of preparing silicate rock glasses for energy-dispersive electron microprobe analysis. Chemical Geology 14, 151-157.

Ottolini, L., Bottazzi, P., and Vannucci, R., 1993a. Quantification of lithium, beryllium and boron in silicates by secondary ion mass spectrometry using conventional energy filtering. Analytical Chemistry 65, 1960-1968.

Ottolini, L., Bottazzi, P., and Vannucci, R., 1993b. Quantitative SIMS analyses of REEs in silicate minerals: Choice of the standard for natural and glassy matrix. Geological survey of Canada.

Ottolini, L., Bottazzi, P., Vannucci, R., and Oddone, M., 1992. An Ion Probe contribution to rare Earth element investigation of gabbro GOG-1 using Secondary Ion Mass Spectrometry. Geostandards Newsletter 16, 13-19.

Pabst, S., Zack, T., and Savov, I. P., 2008. B- and Li-rich fluid pulses in the Mariana mantle wedge. Geochimica et Cosmochimica Acta 72, A715.

Paulick, H., Bach, W., Godard, M., De Hoog, J. C. M., Suhr, G., and Harvey, J., 2006. Geochemistry of abyssal peridotites (mid-Atlantic ridges, 15°20'N, ODP Leg 209): Implications for fluid/rock interaction in slow spreading environments. Chemical Geology 234, 179-210.

Pearce, N., Perkins, W. T., Westgate, J. A., Gorton, M. P., Jackson, S. E., Neal, C. R., and Chenery, S. P., 1997. A compilation of new and published major and trace element data for NIST SRM 610 and NIST SRM 612 glass reference materials. Geostandards Newsletter 21, 115-144.

Phillips, W. M., Hall, A. M., Mottram, R., Fifield, K., and Sugden, D. E., 2006. Cosmogenic ^{10}Be and ^{26}Al exposure ages of tors and erratics, Cairngorm Mountains, Scotland: Timescales for the development of a classic landscape of selective linear glacial erosion. Geomorphology 73, 222-245.

Seck, H. A., Kötz, J., Okrusch, M., Seidel, E., and Stosch, H. G., 1996. Geochemistry of a meta-ophiolite suite: An association of metagabbros,

eclogites and glaucophanites on the island of Syros, Greece. European Journal of Mineralogy 8, 607-623.

Shaw, D. M., Higgins, M. D., Truscott, M. G., and Middleton, T. A., 1988. Boron contaminiation in polished thin sections of meteorites: Implications for the trace-elements studies by alpha-track image or ion microprobe. American Mineralogist 73, 894-900.

Spivack, A. J., You, C. F., and Smith, H. J., 1993. Foraminiferal boron isotope ratios as a proxy for surface ocean pH over the past 21 Myr. Nature 363, 149-151.

Stoll, B., Jochum, K. p., Herwig, K., Amini, M., Flanz, M., Kreuzburg, B., Kuzmin, D., Willbold, M., and Enzweiler, J., 2008. An automated iridium-strip heater for LA-ICP-MS bulk analysis of geological samples. Geostandards and Geoanalytical research 32, 5-26.

Vils, F., 2009. Light elements in oceanic and ophiolitic serpentinites. Ph.D. thesis, University of Neuchâtel.

Vils, F., Pelletier, L., Kalt, A., Müntener, O., and Ludwig, T., 2008. The lithium, boron and beryllium content of serpentinized peridotites from ODP Leg 209 (Sites 1272A and 1274A): Implications for lithium and boron budgets of oceanic lithosphere. Geochimica et Cosmochimica Acta 72, 5475-5504.

Chapter VI

Summary of conclusions, implications and perspectives

The light element systematics of oceanic mantle were poorly constrained before the SNF-project "The oceanic mantle as an important repository for the light elements Li, Be and B" started. In the last years, two PhD students (Laure Pelletier and Flurin Vils) tried to identify major processes and parameters involved in light element enrichments or depletions within oceanic mantle from different tectonic settings. During this project, high-standard scientific collaborations with scientists from Heidelberg (D), Frankfurt (D), Budapest (H), Bern (CH), Lausanne (CH) and Pisa (I) were developed, and data were collected. The main questions addressed in this thesis were:

What are the light element contents of oceanic peridotites? What are the light element contents of the minerals composing oceanic and ophiolitic peridotites? Which mineral phase(s) is/are the major carrier(s) of Li, Be or B?

What is the implication of serpentinization for the light element budget of a subduction zone? Does serpentinized mantle play a key role in light element recycling?

What is the influence of serpentinization on the isotopic composition of mantle peridotites? Does seawater deplete or enrich the rocks in Li, Be and B?

What does prograde metamorphism do to the light element composition of serpentinized oceanic mantle? Does antigorite contain the same amount of light elements as chrysotile?

Can Li, Be and B whole rock contents be measured on iridium-strip heater glass pellets? Is there loss or gain of light elements during sample preparation with an Ir-strip heater? What is the influence of heating time and temperature during direct fusion on the homogeneity of the samples?

In order to answer these questions, an in-situ and whole rock petrological and geochemical study based on major and light element concentrations was conducted, as well as multi-isotope analysis of boron, lithium and strontium. Serpentinites recovered from the mid-Atlantic ridge and from the Alps (Totalp, Platta and Malenco) were selected for these studies and the results were presented in the individual chapters of this thesis. These chapters are partially submitted or published in international peer-reviewed journals.

In general, serpentinization was identified to be the major process controlling light element contents of partially to completely serpentinized peridotites. However, some minor processes, serpentinizing fluid compositions, and the effect of serpentinization conditions (e.g. pH, T) are not yet fully understood and the project revealed further questions which may be solved in future research projects. In the following paragraphs, major results and conclusions are combined, discussed and generalised.

6.1 Summary of conclusions and comparison with literature

Whole rock

1. No methods to analyse whole rock concentrations of Li, Be and B together were available up to now. Thus, we tried to combine available in-situ analyses by ion probe with direct fusion of whole rock samples on an Ir-strip heater to develop a quick and routine protocol to measure these three elements. Experiments testing the accuracy and precision of this approach were conducted at 1500 to 1800°C and 30 to 240s. Optimum temperature and time conditions were identified as 1700°C and 60s heating time to obtain homogeneous glasses and dissolution of all mineral phases (e.g. spinel). Ion probe measurements revealed that loss of all three elements occurred, but Li and Be contents were within analytical error, whereas a significant loss of B was reported during the high-temperature experiments (at 1800°C). However, low H_2O concentration (0.68 µg/g) within one studied sample led to nearly no loss of B even at 1800°C.

2. In oceanic settings, B concentrations in serpentinized peridotites are high (e.g. Bonatti et al., 1984). Higher H_2O contents of serpentinites are associated with increased B contents (Fig. 6.1). The dependency of B on water contents reveals that serpentinization is the leading process enriching unaltered mantle rock with B. Li, on the other hand, becomes depleted with increasing H_2O content. Li and B whole rock compositions of the studied oceanic serpentinites therefore show an inverse correlation of Li and B concentrations (Fig. 6.1). Pindos and Vourinos serpentines have low B content and average Li concentration (Fig. 6.1). Such systematics may develop during serpentinization by a fluid depleted in B compared to seawater. Mariana fore-arc serpentinites are enriched in Li compared to oceanic serpentinites, probably as a result of dehydration reactions occurring in the underlying subduction zone. Ophiolitic serpentinites (Feather River and Geisspfad) have constant B concentrations, but vary highly in Li. In general, B in serpentinites is enriched compared to depleted mantle (DM) and Li shows variable behaviour. During low T serpentinization, Li and B behave complementary. Be, on the contrary, does not vary with changing H_2O concentration.

In-situ

3. In-situ light element analyses of primary

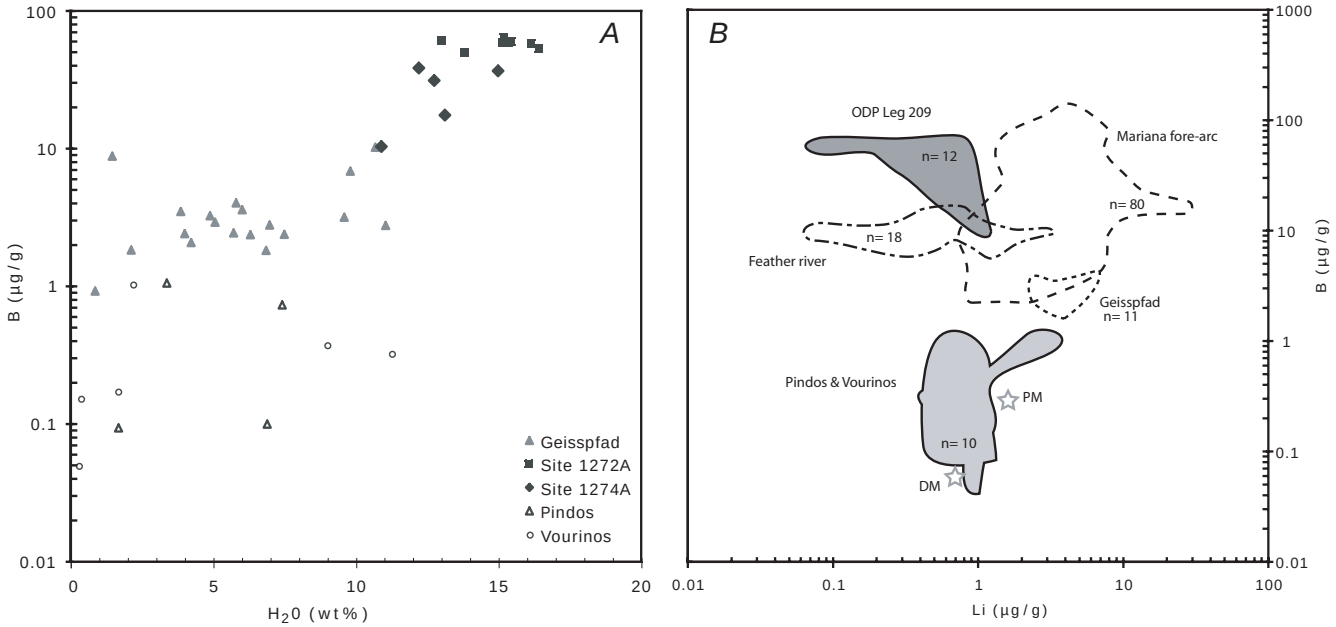

Fig. 6.1. A) PGAA analyses of whole rock samples from different localities showing B versus H_2O diagram. B content is increasing with increasing serpentinization of the rocks (higher H_2O). Data are from Pelletier (2008) and this study. B) Li versus B diagram, in grey contribution of this study. PM primitive mantle (McDonough and Sun, 1995); DM depleted mantle (Salters and Stracke, 2004); Mariana fore-arc (Benton et al. 2001; Benton et al. 2004; Savov et al. 2007); Geisspfad ophiolite (Pelletier et al. 2008a); ODP Leg 209 (Vils et al., 2008); Feather river (Li and Lee, 2006); Pindos and Vourinos ophiolites (Pelletier et al., 2008b; this study).

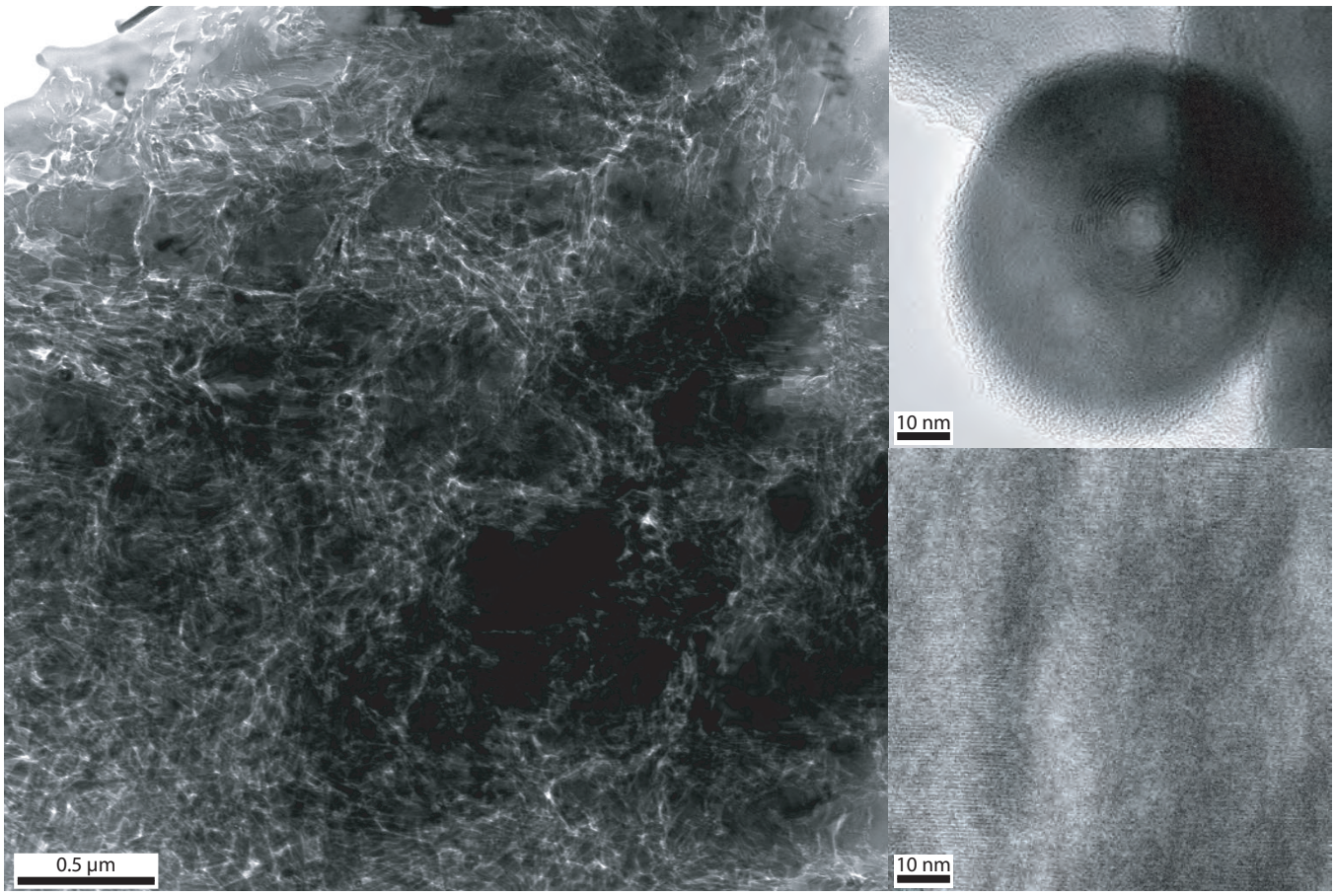

Fig. 6.2. TEM images of sample OD 28, showing A) chrysotile overgrowing lizardite; B) chrysotile single crystal structure; C) lizardite structure. A Philips CM20(0) TEM at the Institute of Microtechnology (University of Neuchâtel) was used.

phases (e.g. olivine) in serpentinized peridotites showed that in general Li, Be and B contents are low compared to secondary phases (e.g. serpentinite), but late-stage metasomatism increases the Li concentrations of clinopyroxenes (Fig. 2.9). Further on, Be contents in clinoproxenes formed in an oceanic setting differ from those clinopyroxenes formed in a subcontinental setting (Fig 4.6). This is important as it allows fingerprinting ancient igneous events in mantle peridotites. Overall, primary phases from oceanic and ophiolitic settings analyzed in this study are low in Li and B compared to secondary phases, while Be content is similar (e.g. Fig. 2.9 and 2.10).

4. In-situ analyses of serpentine are challenging, as grain size is mostly below ion probe spotsize (~12 µm). To assure that measured analyses are single-phase measurements and not a melange of different minerals, we conducted TEM analyses on different serpentine types in one ODP Leg 209 sample (Fig. 6.2). In bastite (formed after pyroxene) and mesh serpentine (after

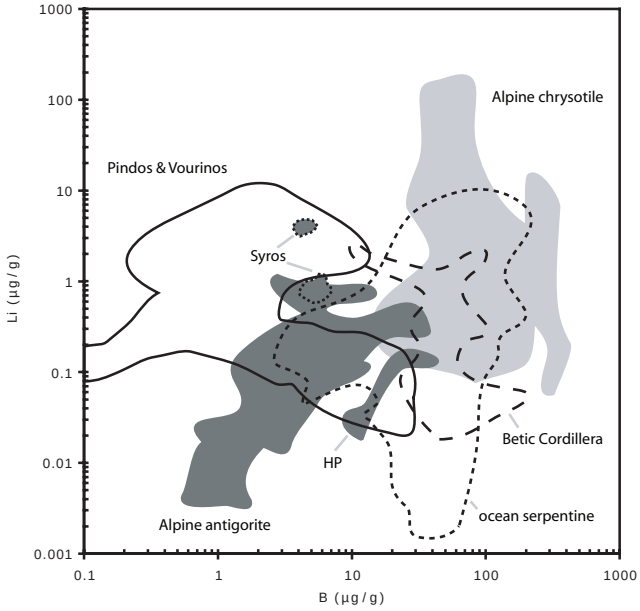

Fig. 6.3. Li versus B diagram of serpentine measurements. Alpine chrysotile consists of Totalp, Platta (this study); ocean serpentine field (ODP Leg 209); Alpine antigorite field consisting of Pfulwe, Geisspfad and Malenco (Marschall, 2005; Pelletier et al., 2008a; this thesis); Pindos and Vourinos (Pelletier et al., 2008; this thesis); Syros field after Marschall (2005); Betic Cordillera and HP (Erro-Tobbio) after Scambelluri et al. (2004).

olivine), chrysotile and lizardite occur. Low-temperature replacement of lizardite by chrysotile is recorded in bastite (Fig. 6.2). No other mineral phase was identified by TEM analysis. Additionally, measurements on several serpentinites by micro-Raman confirmed these observations, although high Li (>1µg/g) concentration in serpentine was attributed to incomplete serpentinization of the studied samples. Thus, ion probe measurements are assumed to represent mono-serpentine analyses, although probably composed of chrysotile and lizardite.

5. Serpentine (chrysotile) formed in the ocean is high in B and mostly lower in Li content than depleted mantle (0.7 µg/g Li, 0.06 µg/g B; Salters and Stracke, 2004; Fig. 6.3). Chrysotile occurring in Alpine settings has higher Li and similar B concentrations as chrysotile formed in the ocean. Antigorite measurements reveal that its B content is lower than that of serpentine formed in oceanic environments, but its Li content is variable. B loss thus occurred during prograde Alpine metamorphism. Overall, serpentine shows variability in Li and B concentrations, although different serpentinite types and formation environments can be distinguished.

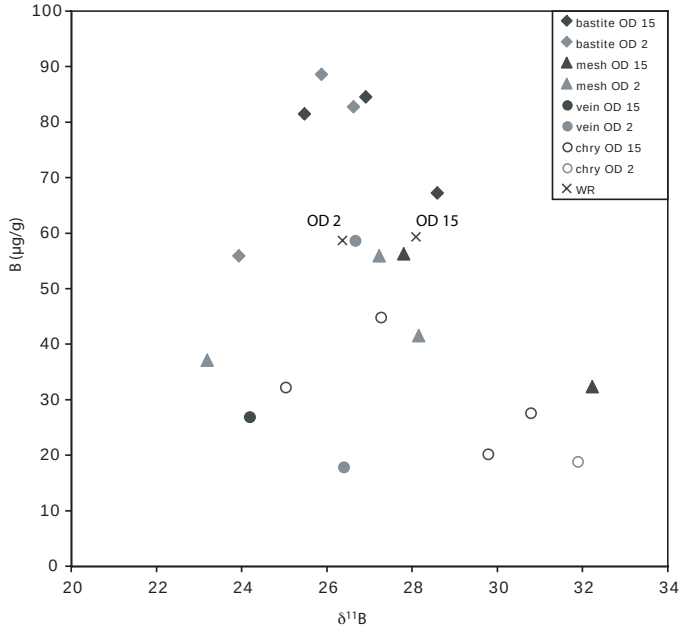

Fig. 6.4. Uncorrected in-situ measurements (ion probe) of $\delta^{11}B$ and B content on two ODP Leg 209 samples (OD 2 and OD 15) of different serpentine textures are shown in $\delta^{11}B$ versus B content diagram. Whole rock (WR) data are shown for reference (Vils et al., 2009), $\delta^{11}B$ data are corrected to SIMS-fractionation (-6‰).

Isotopes

6. $^{87}Sr/^{86}Sr$ whole rock analyses revealed ODP Leg 209 peridotites from the mid-Atlantic ridge were serpentinized at moderate water/rock ratios (average 39). Further on, this thesis reports the highest $\delta^{11}B$ and lowest $\delta^{7}Li$ measured so far in serpentinized peridotites (Fig. 3.6). This is in line with high B and low Li contents in these abyssal peridotites and supports the hypothesis that Li is leached out of the rock while B is enriched. Additionally, the fluid source of the high $\delta^{11}B$ and low $\delta^{7}Li$ signal is probably a seawater batch passing through the oceanic mantle, evolving during water-rock interactions with increasing volume passed. In-situ measurements of $\delta^{11}B$ in serpentine on two samples on the ion probe showed that $\delta^{11}B$ signal is dominated by serpentine (Fig. 6.4). This correlates with in-situ B measurements. As low sample numbers have been measured, no general conclusion can be drawn. Nevertheless, if we calculate an average of the measured phases (OD 2: +27.80‰ $\delta^{11}B$, 46.4 µg/g B and OD 15: +26.65‰ $\delta^{11}B$, 50.19 µg/g B, respectively), the calculated values are similar to the whole rock $\delta^{11}B$ and B measurements (Fig. 6.4).

6.2 Implications

During this project we could show that serpentinized mantle rocks are highly enriched in B and rather depleted in Li compared to the depleted mantle (DM). Be, on the other hand, seems immobile during serpentinization, as no enrichment in Be compared to DM was found. Further on, as Be has a very low abundances in mantle rocks and seawater, any enrichment/depletion is probably similar to the range of natural variations. During prograde metamorphism, on the other hand, phase transformation of serpentine extracts B and Li, while Be concentrations remain unaffected. During emplacement of an ophiolite body into the continental crust Li, Be and B concentrations of oceanic serpentinites can change by retrograde fluid flows (Pelletier, 2008). Obducted serpentinites, on the contrary, can keep oceanic signatures (e.g. Pindos (Pelletier, 2008) and Vourinos.

The main focus of this project was to quantify the light element input into subduction zones. Assuming that the isotopic and elemental composition found at ODP Leg 209 is representative for rocks entering a subduction

zone, subduction of seawater-altered oceanic lithosphere would have a major impact on the light element cycle within the subduction zone factory. Depth of serpentinization has been identified as a crucial parameter required to generate any fully quantitative model for the light elements contribution of the oceanic mantle during recycling and further research to quantify serpentinization is needed. Nevertheless, our results allow us to identify several processes regarding light elements occurrence in mantle rocks within the subduction zone. As Li is rather leached out of the rock and Be concentration is very low, the recycling within the subduction zone of Li and Be is dominated by the sediments and the mafic rocks and is not commented further on. The major implications for B element cycling in subduction zones are listed below, based on the results of this thesis and the thesis of Laure Pelletier (UNINE).

First, during serpentinization, B concentrations in mantle rocks are highly increasing (three orders of magnitudes), reaching contents similar to those of altered MORB and pelagic sediments. The results presented in Chapter 2 showed, that there is a difference between slow- and fast-spreading ridges. At slow- and fast-spreading ridges, the serpentinized mantle buffers the B budget of the oceanic plate, while at fast-spreading ridges the oceanic crust is controlling the Li budget. Although most of today's subducted ocean crust is of fast-spreading ridge type, the ancient Tethys was produced by slow-spreading ridges. Therefore, most serpentinites and metamorphosed oceanic crust exposed on-land are relicts of slow-spreading ridges, and their chemical signature should be similar to ODP Leg 209. Thus, B incorporated in serpentinites is an important reservoir possibly brought to depth within the subduction zone, and exposed rocks reflect processes related to slow-spreading ridges and subduction of the latter.

Second, the transformation of chrysotile to antigorite in Alpine ophiolites shows a B loss of one order of magnitude. The same reaction takes place within a subduction zone, and B is expelled. The chrysotile-antigorite transformation occurs at around 200°C, which is a condition rather found during the "early stage" of subduction. Thus, the expelled B is probably released by fluids into the accretionary prism or into the mantle wedge at shallow subduction.

Third, due to the chrysotile-antigorite transformation, a lesser amount of B is available at the antigorite-breakdown compared to the initial oceanic stage, but antigorite is still an important reservoir of B at these depths. The breakdown of antigorite liberates a fluid that probably ascends in the mantle wedge. B is mobile, hence it will be most likely be liberated into the fluid phase. This deserpentinization reaction is probably the reason why a change in B/Be ratio with increasing slab depth occurs in back-arc volcanoes (e.g. Bebout et al., 1993; Ryan et al., 1996; Bouvier et al., 2008).

Fourth, we measured the highest $\delta^{11}B$ values reported so far at ODP Leg 209. Assuming that these isotopic ratios are re-equilibrated neither in the ocean, nor during plate bending nor during the chrysotile-antigorite transformation, such a signal can be brought to depth. B isotopes in the fluid will probably follow a Rayleigh dehydration path, implying a decrease of $\delta^{11}B$ signal in the released fluids, accompanied by B loss in the rocks. In that way, a signal similar to what is found in today's OIB can be reached (e.g. Chaussidon and Marty, 1995; Turner et al., 2007. The $\delta^{11}B$ signal of ODP Leg 209 is associated with high B contents. Hence the released fluid should also be enriched in B (compared to DM) and as a result, this $\delta^{11}B$ signal would be transferred to surrounding rocks during dehydration or melting and modify considerably the isotopic composition of the mantle.

6.3 Further research topics

This thesis, together with the thesis of Laure Pelletier (2008, University of Neuchâtel), gives an overview on the light element systematics of serpentinized peridotites in different geological settings. Nevertheless, some questions still remain and others have been raised during the interpretation of accumulated data. Therefore, open questions are summarized and further research fields suggested below.

- Although our project covered a wide variety of different tectonic settings, not every serpentinization process (see Fig. 1.5) has been studied. Further research should focus on off-axis serpentinization, as this process is still poorly constrained.

New ocean drilling programs, the Nankai Trough Seismogenic Zone Experiment (NanTroSEIZE), where drilling through an oceanic plate into a subducted slab is planned, should reveal important information on dehydration processes during early subduction. Moreover, the light element studies of (pore-) fluids in drilled rocks from NanTroSEIZE will increase the knowledge about the light element cycle. Additionally, methods to trap diffusive fluids in accretionary prisms should be developed. The captured fluids should reveal additional information about dehydration processes during early subduction.

- Low-temperature interactions between the oceanic plate and seawater during residence in the ocean are not yet fully understood. Are seawater-rock interactions restricted to mid-ocean ridges, or is it an ongoing process? Does serpentinization occur off-ridge? How is serpentinization working during plate bending at the subduction zone? How does the fluid composition change through interaction with the oceanic mantle? Is there a chance to further enrich the oceanic plate in B with these processes?

- To understand the behaviour of light elements within subduction zones it is important to increase our knowledge on partition coefficients, in particular partition coefficients of minerals formed from antigorite breakdown as well as during antigorite formation. As Ulmer and Trommsdorff (1995) showed, antigorite is the possible water source to the mantle and therefore an important deliverer of mobile elements to the mantle wedge. Further on, recent geochemical investigations and modelling on ultramafic-hosted hydrothermal systems suggested that brucite probably plays a major role in the fluid emerging at such vent sites (Boschi, 2006; Foustoukos et al., 2008). Therefore a detailed study on light element compositions and fractionation factors between brucite and fluid, serpentine and clay minerals should clarify these issues.

- Studies of δ^7Li and δ^{11}B in serpentinites are few and the interaction of the two systems during serpentinization is still not clear. An increasing number of measurements on ophiolitic and oceanic serpentinites as well as fresh peridotites are needed to constrain whether light element concentrations in mantle rocks established within the ocean remain unchanged during subduction and metamorphism. Unpublished data from dredged serpentinites of the Vema fracture zone showed that with increasing age δ^{11}B decreases, approaching the equilibrium value between seawater and silicate rocks (+21‰; personal communication S. Tonarini). It is therefore not clear if an isotopic signal similar to that of ODP Leg 209 data is stable during residence in the ocean, or if equilibration to seawater occurs.

- In-situ isotopic work on mantle xenoliths suggested that Li diffuses fast within olivine and pyroxenes, and minerals show zoning profiles (e.g. Jeffcoate et al., 2007). No in-situ δ^{11}B, and only one in-situ δ^7Li study on serpentinites, is published to date. As Li is less abundant in serpentinites, in-situ δ^7Li work would be challenging and may not always be possible. B, on the contrary, is highly enriched, and in-situ work may be used to identify different serpentinization events or fluid origins. Work in progress at the University of Heidelberg by Sonja Pabst on mud volcanoes from the Mariana fore-arc will probably help to understand dehydration reactions and fluid mixing processes during early subduction.

- More experiments on the light element systematics of serpentine in low-temperature environments are needed to increase the understanding of natural observations and theoretical modelling. For example, it is known that B isotope compositions are pH-dependent. So far, Li isotopic compositions are assumed not to be pH-dependent. Comparison of Hess Deep and ODP Leg 209 samples reveals a different behaviour of Li fractionation at high and low temperature (Decitre et al., 2002; Vils et al., 2009) and pH-dependency should be considered as a potential key player for such behaviour.

REFERENCES

Agranier, A., Lee, C.-T. A., Li, X.-P., and Leeman, W. P., 2007. Fluid-mobile element budgets in serpentinized oceanic lithospheric mantle: Insights from B, As, Li, Pb, PGEs and Os isotopes in the Feather River Ophiolites, California. Chemical Geology 245, 230-241.

Bebout, G. E., Ryan, J. G., and Leeman, W. P., 1993. B-Be systemtics in subduction-related metamorphic rocks: Characterization of the subducted component. Geochimica et Cosmochimica Acta 57, 2227-2237.

Benton, L. D., Ryan, J. G., and Tera, F., 2001. Boron isotope systematics of slab fluids as inferred from a serpentine seamount, Mariana forearc. Earth and Planetary Science Letters 187, 273-282.

Benton, L. D., Ryan, J. G., and Savov, I. P., 2004. Lithium abundance and isotopic systematics of forearc serpentinites, Conical Seamount, Mariana forearc: Insights into the mechanics of slab-mantle exchange during subduction. Geochemistry Geophysics Geosystems 5, 1-14.

Bonatti E, Lawrence J, Morandi N, 1984. Serpentinization of oceanic peridotites: temperature dependence of mineralogy and boron content. Earth and Planetary Science Letters 70,88-94.

Boschi C, 2006. Building Lost City: Serpentinization, mass transfer and fluid flow in an oceanic core complex. Ph.D. thesis, Erdwissenschaften, ETH Zürich, Zurich.

Bouvier, A.-S., Métrich, N., and Deloule, E., 2008. Slab-derived fluids in the magma sources of St. Vincent (Lesser Antilles Arc): Volatile and light element imprints. Journal of Petrology 49, 1427-1448.

Chaussidon, M. and Marty, B., 1995. Primitive boron isotope composition of the mantle. Science 269, 383-386.

Decitre S, Deloule E, Reisberg L, James R, Agrinier P, Mével C, 2002. Behavior of Li and its isotopes during serpentinization of oceanic peridotites. Geochemistry Geophysics Geosystems 3.

Foustoukos DI, Savov IP, Janecky DR, 2008. Chemical and isotopic constaints on water/rock interactions at the Lost City hydrothermal field, 30°N Mid-Atlantic ridge. Geochimica et Cosmochimica Acta 72,5457-5474.

Jeffcoate A, Elliott T, Kasemann SA, Ionov D, Cooper K, Brooker RA, 2007. Li isotope fractionation in peridotites and mafic melts. Geochimica et Cosmochimica Acta 71,22-218.

Li, Z.-X. A. and Lee, C.-T. A., 2006. Geochemical investigation of serpentinized oceanic lithospheric mantle in the Feather River Ophiolite, California: Implications for the recycling rate of water by subduction. Chemical Geology 235, 161-185.

Marschall HR, 2005. Lithium, beryllium and boron in high-pressure metamorphic rocks from Syros (Greece). Ph.D. thesis, Ruprecht-Karls Universität, Heidelberg.

McDonough, W. F. and Sun, S.-S., 1995. The composition of the Earth. Chemical Geology 120, 223-253.

Pelletier, L., 2008. The oceanic mantle as an important repository for the light elements Li, Be and B. Ph.D. thesis, University of Neuchâtel.

Pelletier L, Vils F, Kalt A, Gméling K, 2008a. Li, B and Be contents of harzburgites from the Dramala Complex (Pindos ophiolite, Greece): Evidence for a MOR-type mantle in a supra-subduction zone environment Journal of Petrology 49, 2043-2080.

Pelletier, L., Müntener, O., Kalt, A., Vennemann, T. W., and Belgya, T., 2008b. Emplacement of ultramafic rocks into the continental crust monitored by light and other trace elements: An example from the Geisspfad body (Swiss-Italian Alps). Chemical Geology 255, 143-159.

Ryan, J. G., Leeman, W. P., Morris, J., and Langmuir, C. H., 1996. The boron systematics of intraplate lavas: Implications for the crust and mantle evolution. Geochimica et Cosmochimica Acta 60, 415-422.

Salters, V. J. M. and Stracke, A., 2004. Composition of the depleted mantle. Geochemistry Geophysics Geosystems 5, 1-27.

Savov, I. P., Ryan, J. G., D'Antonio, M., and Fryer, P., 2007. Shallow slab fluid release across and along the Mariana arc-basin system: Insights from geochemistry of serpentinized peridotites from the Mariana Forearc. Journal of Geophysical Research 112.

Scambelluri M, Müntener O, Ottolini L, Pettke T, Vannucci R, 2004. The fate of B, Cl and Li in the subducted oceanic mantle and in the antigorite breakdown fluids. Earth and Planetary Science Letters 222,217-234.

Turner, S., Tonarini, S., Bindeman, I., Leeman, W. P., and Schaefer, B. F., 2007. Boron and oxygen isotope evidence for recycling of subducted components over the past 2.5Gyr. Nature 447, 702-705.

Ulmer P, Trommsdorff V, 1995. Serpentine stability to mantle depths and subduction-related magmatism. Science 268,858-861.

Vils, F., Pelletier, L., Kalt, A., Müntener, O., and Ludwig, T., 2008. The lithium, boron and beryllium content of serpentinized peridotites from ODP Leg 209 (Sites 1272A and 1274A): Implications for lithium and boron budgets of oceanic lithosphere. Geochimica et Cosmochimica Acta 72, 5475-5504.

Vils F, Tonarini S, Seitz H-M, Kalt A, 2009. Boron, lithium and strontium isotopes as tracers of seawater-serpentinite interaction at Mid-Atlantic Ridge, ODP Leg 209. Earth and Planetary Science Letters submitted.

Appendix A

Additional sample descriptions

Before samples were measured on the EMP and on the SIMS, they were studied under the microscope and mostly also under the SEM, taking BSE images. In this appendix, I summarize the major mineral phases of each sample and document their occurrence with BSE images. The reported samples are from ODP Leg 209 (MAR; chapter II), Totalp (CH; chapter IV), Platta (CH; chapter IV), Malenco (I; chapter IV), Vourinos (GR; appendix B), Pindos (GR; Pelltier et al., 2008) and Cima di Gangnone (CH; appendix B).

Abbreviation	***mineral***
ol	*olivine*
cpx	*clinopyroxene*
opx	*orthopyroxene*
spl	*spinel*
mgt	*magnetite*
serp	*serpentine*
chry	*chrysotile*
ant	*antigorite*
chl	*chlorite*
amph	*amphibole*
mag	*magnesite*
il	*illmenite*

OD 2

ODP Leg 209

Depth: 61.75 m.b.s.f.
Minerals: ol, mgt, serp

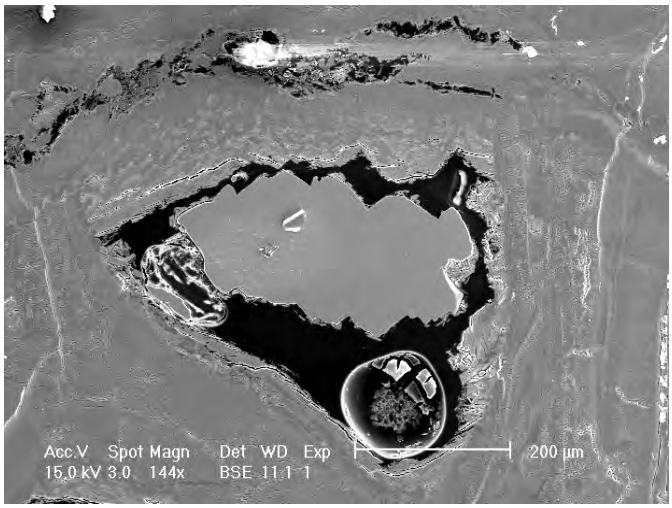

Ol grain surrounded by serpentine

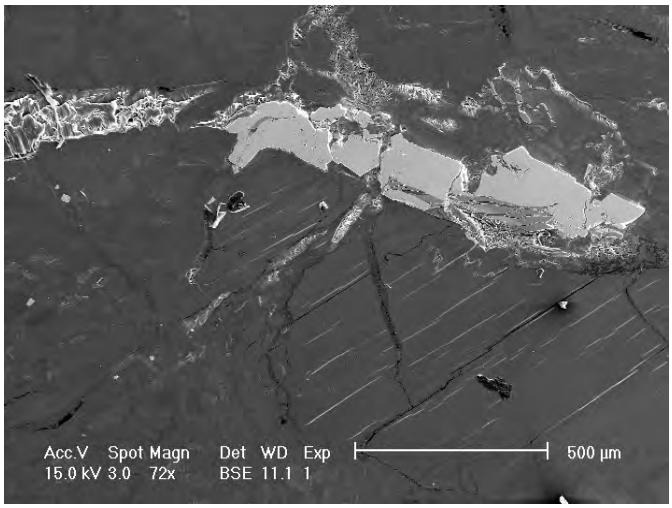

Mgt grain in serpentine; lower right, bastite structure with former clinopyroxenne lamellae

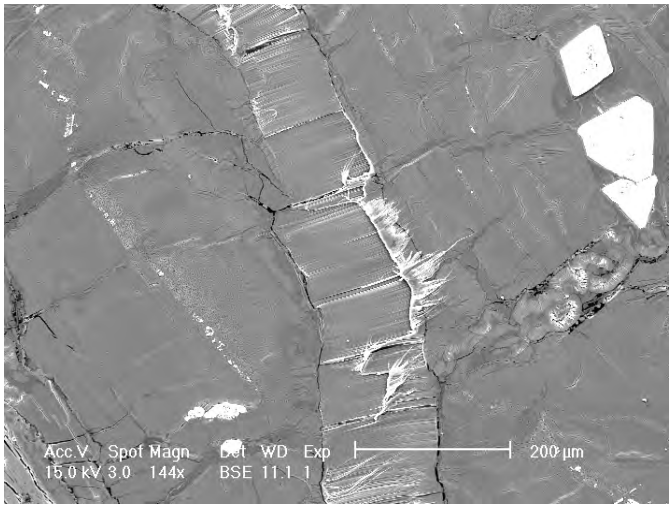

Chrysotile vein in serpentine matrix; top right: mgt crystals

Depth: 76.53 m.b.s.f.
Minerals: spl, mgt, serp

OD 6

ODP Leg 209

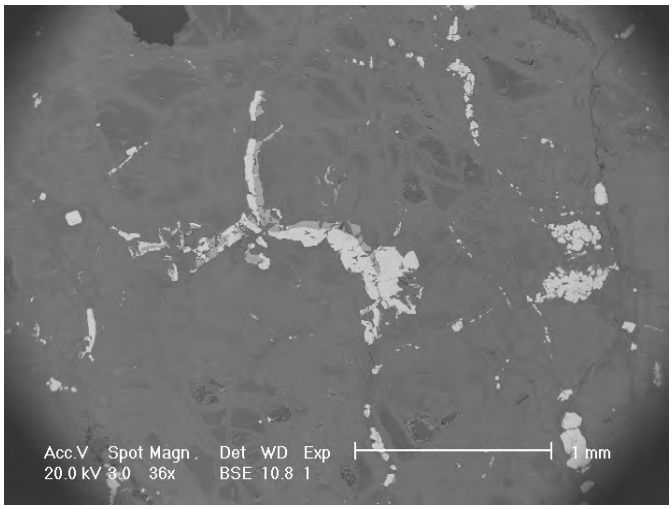

Overview image showing spl-mgt in serpentine matrix

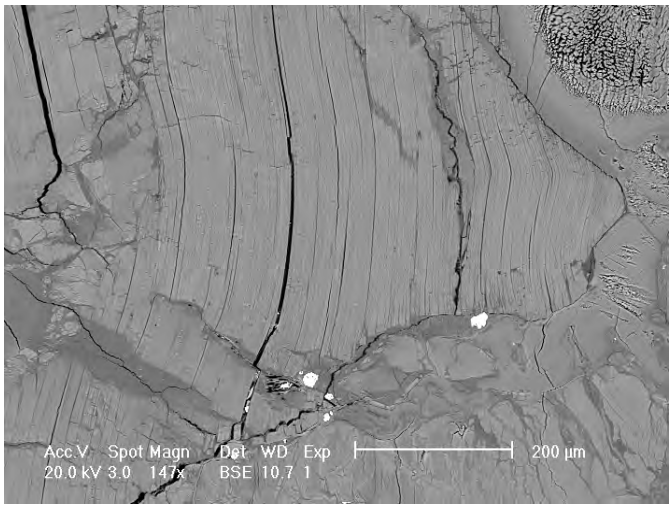

Lamellar bastite; top right: chrysotile

OD 7

ODP Leg 209

Depth: 80.18 m.b.s.f.
Minerals: spl, mgt, serp

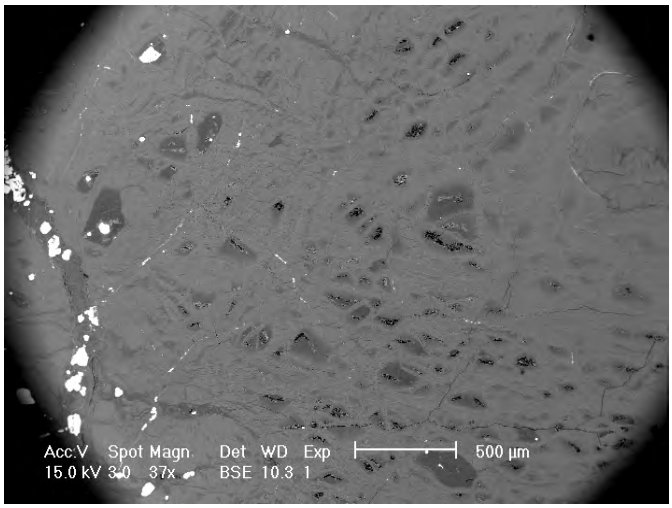

Overview showing serpentinization structures

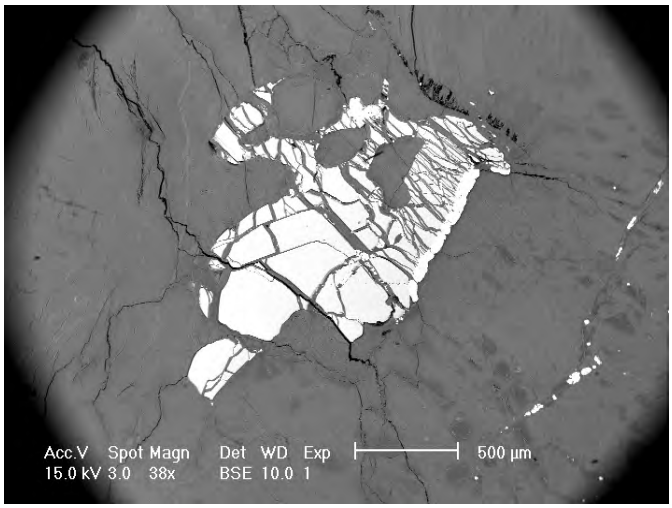

Spinel grain with mgt margin in serpentine matrix

Depth: 89.92 m.b.s.f.
Minerals: spl, mgt, serp

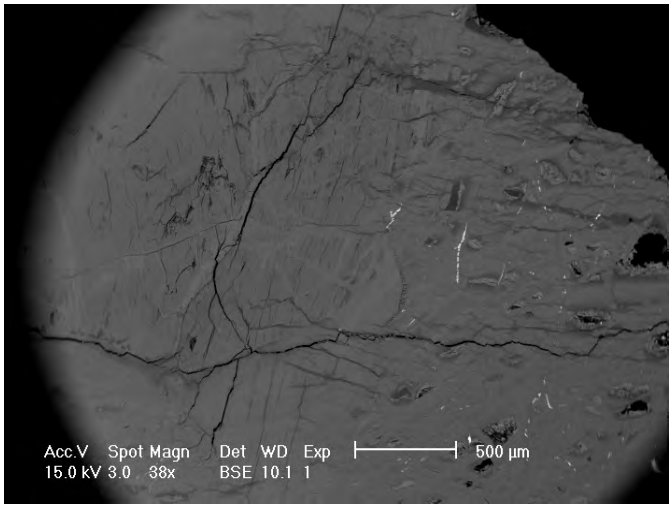

Serpentine matrix

OD 11

ODP Leg 209

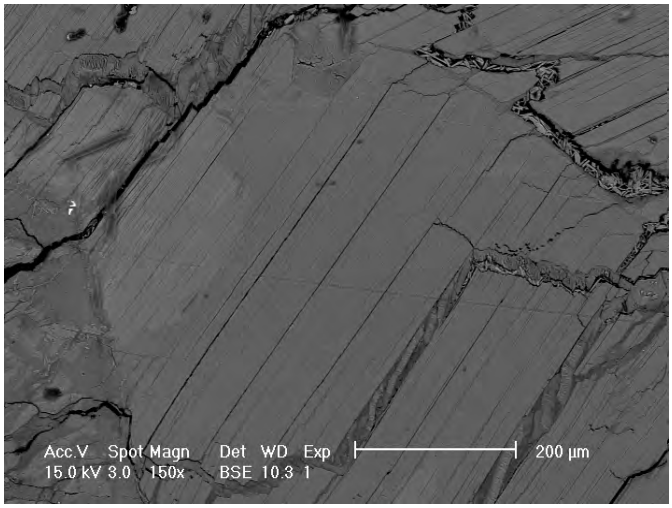

Bastite after opx with former cpx lamellae

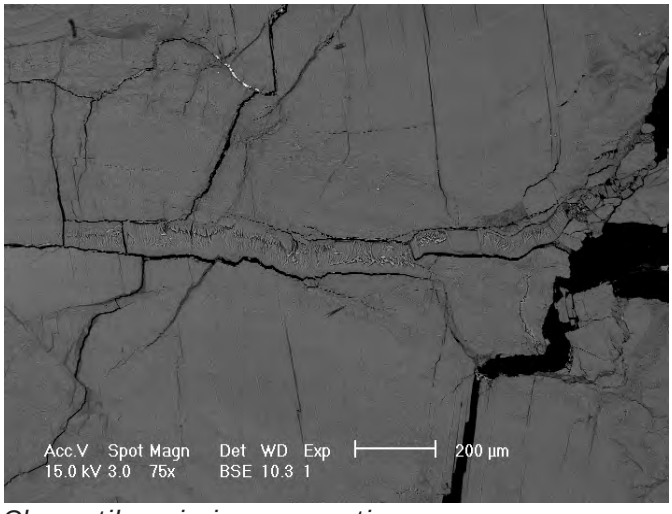

Chrysotile vein in serp matix

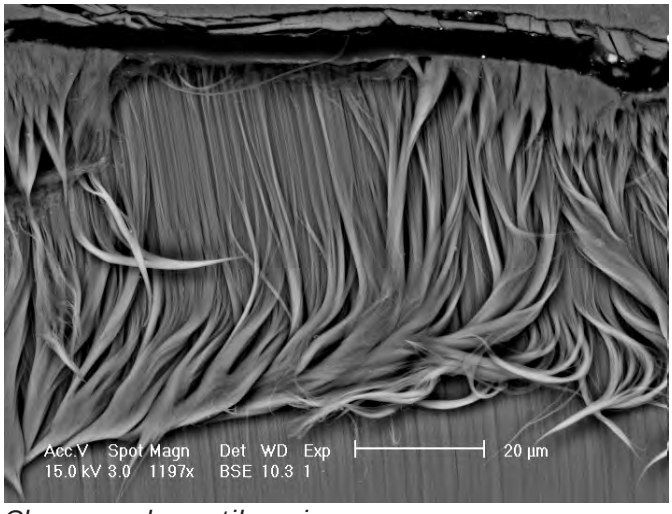

Close-up chrysotile vein

OD 15

ODP Leg 209

Depth: 99.85 m.b.s.f.
Minerals: mgt, spl, serp

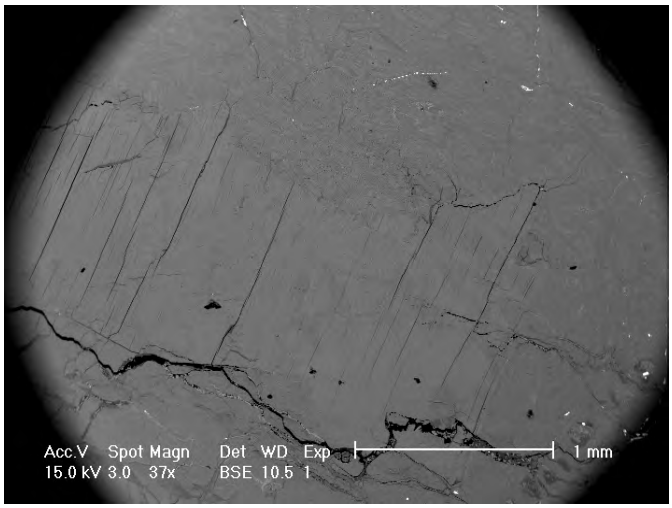

Overview of serpentine texture

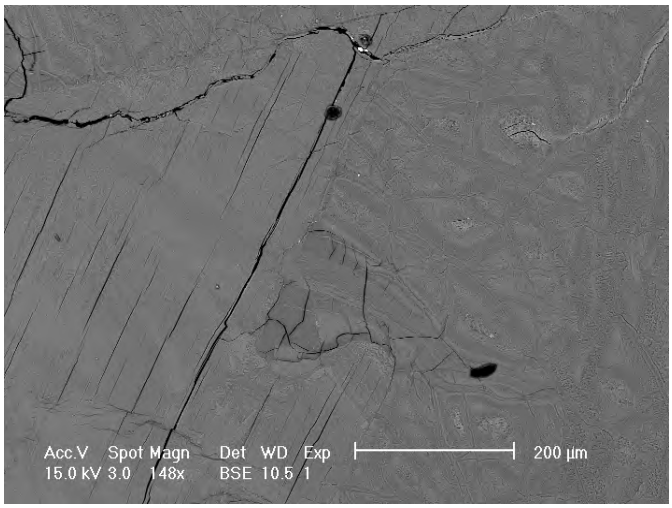

Serpentine texture of former opx (left) and olivine (right)

Depth: 110.19 m.b.s.f.
Minerals: spl, mgt, serp

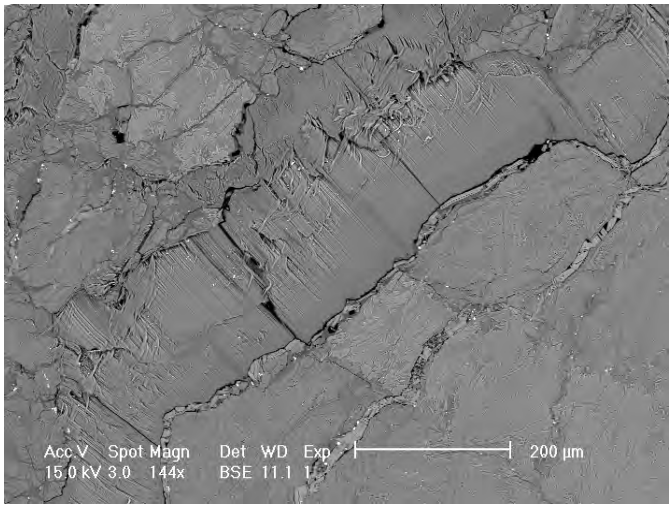

Chrysotile vein cross-cutting antigorite vein

OD 18

ODP Leg 209

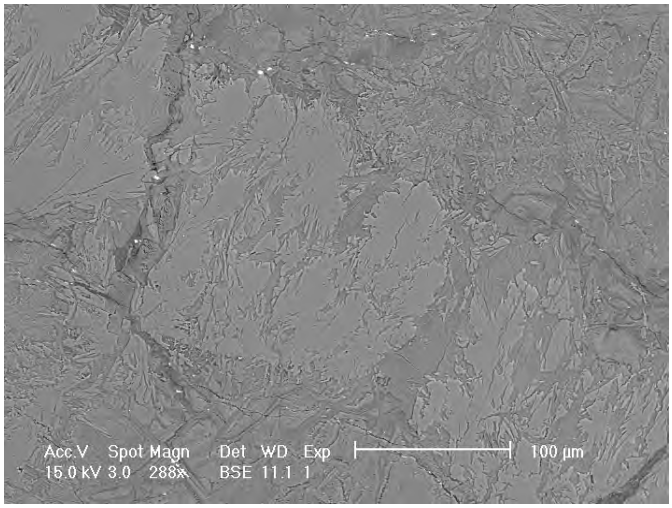

Flaky antigorite (determind by Micro-Raman, Pelletier, 2008)

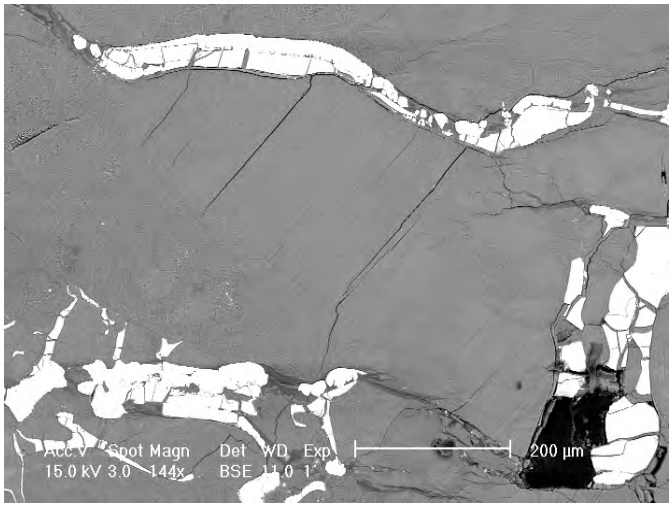

Bastite surrounded by magnetite

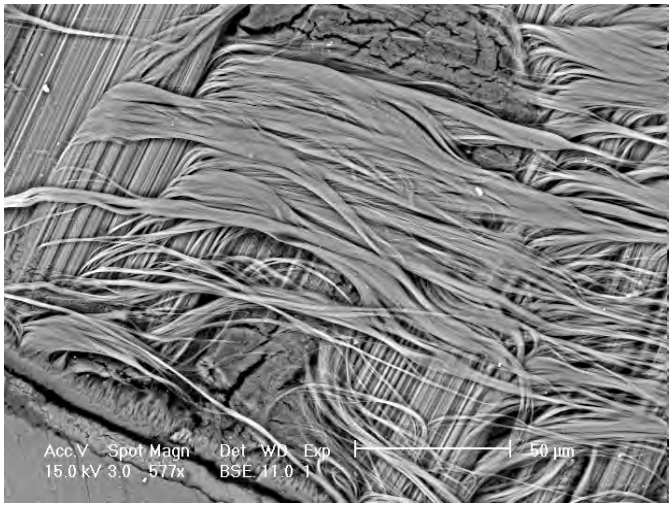

Chrysotile vein

OD 22

ODP Leg 209

Depth: 120.05 m.b.s.f.
Minerals: opx, mgt, spl, serp

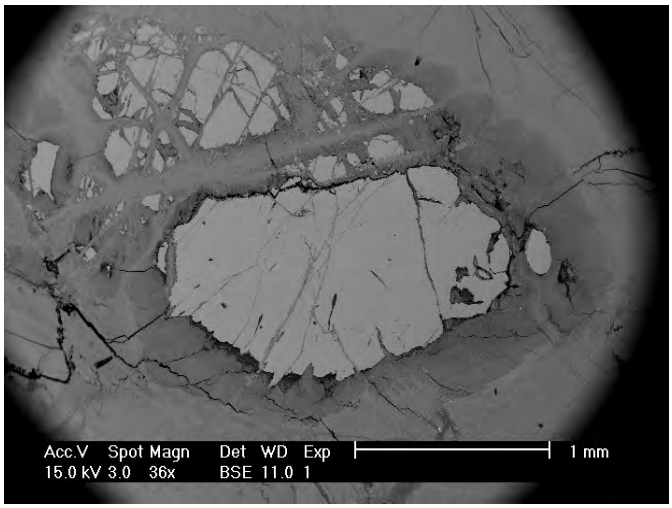

Opx in serpentine

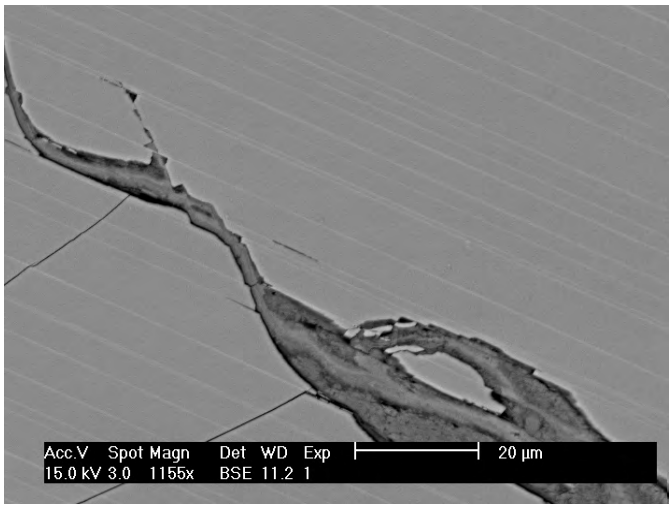

Cpx exsolution-lamellae in opx; serpentine vein cross-cutting the grain

Depth: 125.08 m.b.s.f.
Minerals: ol, opx, spl, mgt, serp

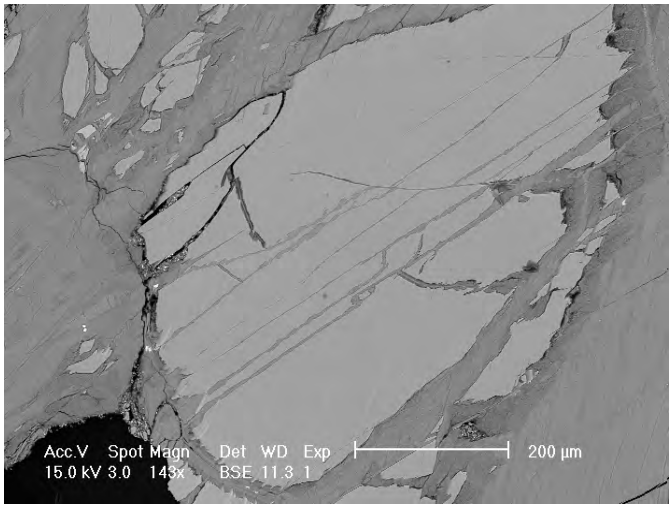

Opx grain in serpentine; small cpx grain upper part left

OD 26

ODP Leg 209

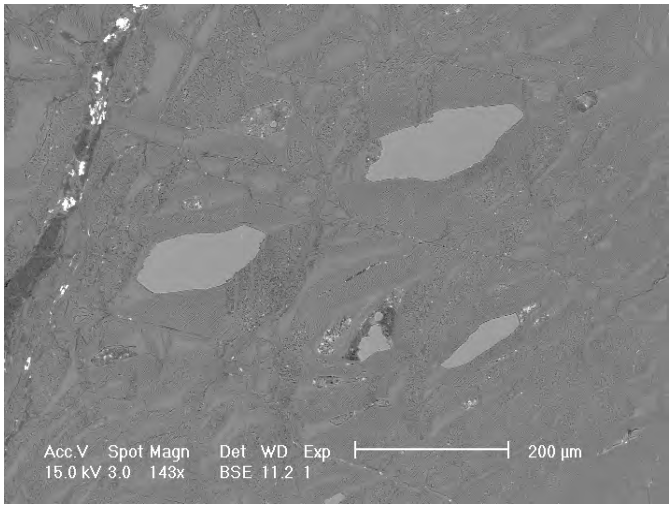

Ol in serpentine matrix

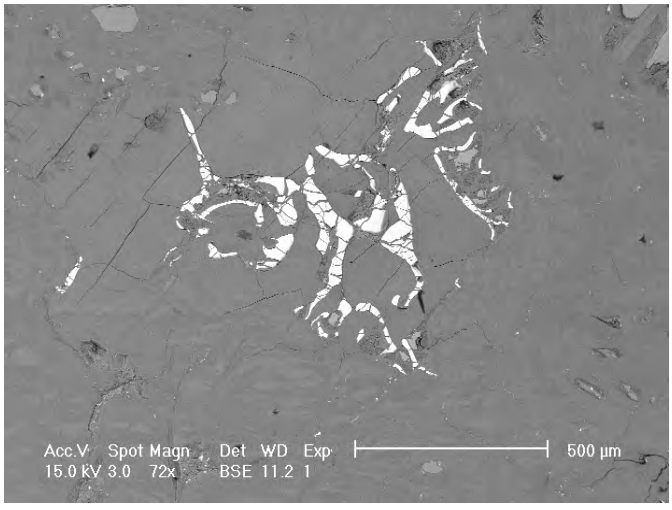

Mgt overgrowing former bastite (after opx)

OD 28

ODP Leg 209

Depth: 127.30 m.b.s.f.
Minerals: cpx, opx, ol, mgt, spl, serp

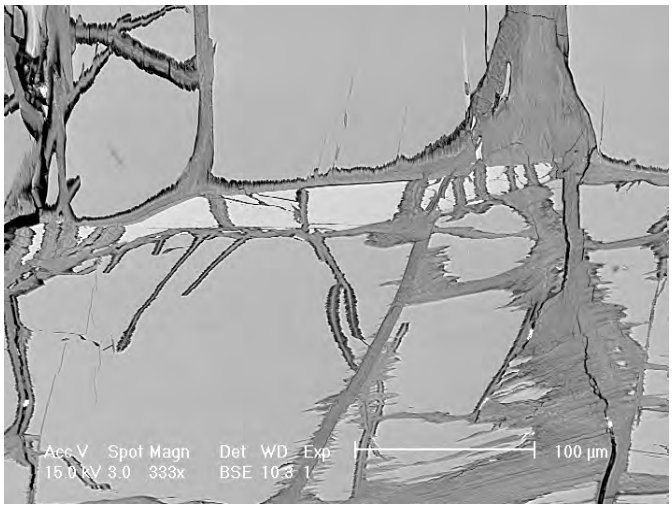

Elongated cpx grain between opx (with exsolution lamellae in serpentine

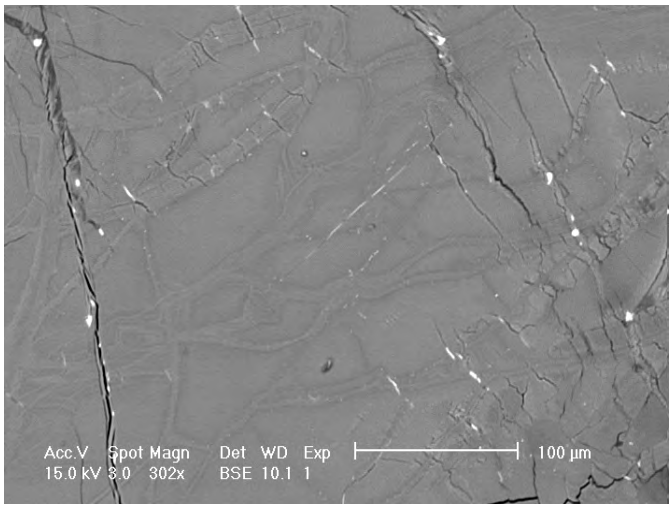

Serpentine matrix

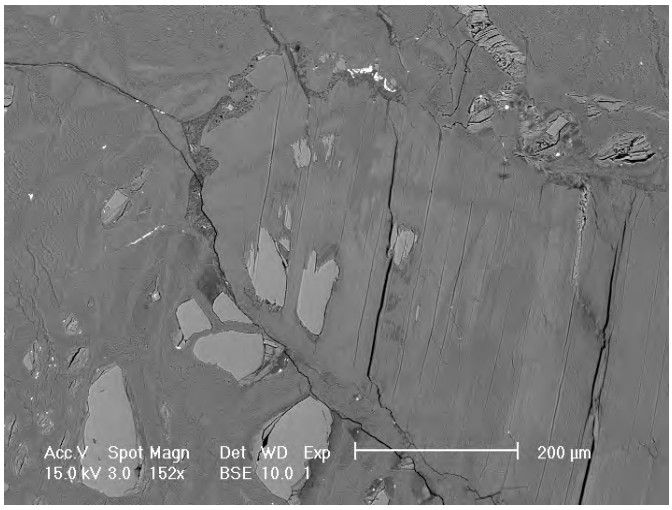

Bastite with small relicts of opx grains (in the middle)

Depth: 129.42 m.b.s.f.
Minerals: cpx, ol, opx, spl, mgt, serp

OD 29

ODP Leg 209

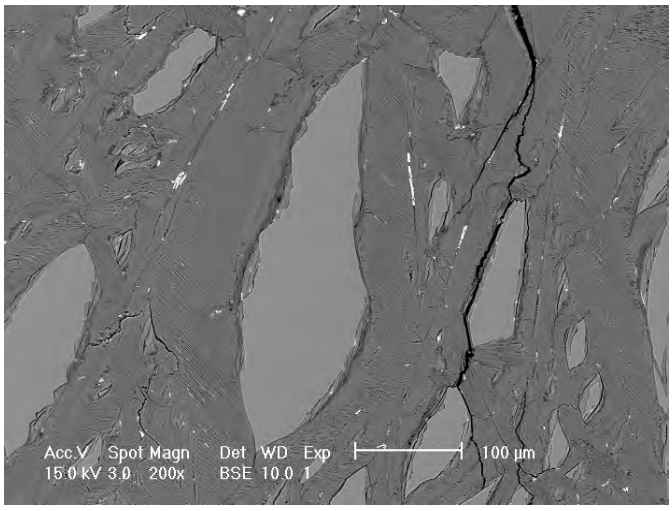

Ol in serpentine matrix

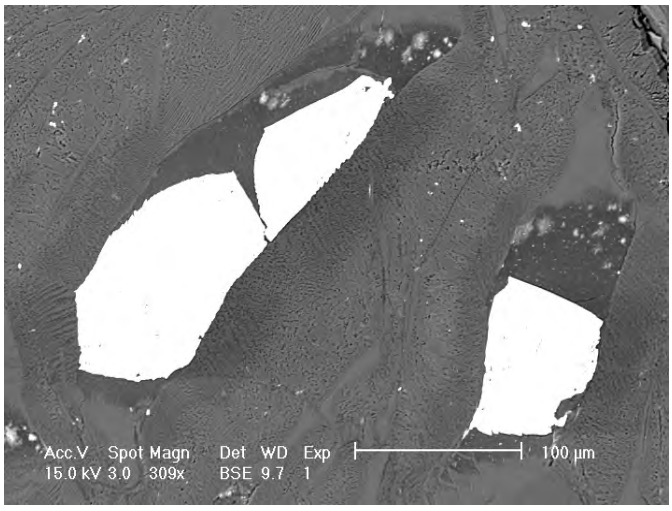

Mgt grains in serpentine matrix

OD 45

ODP Leg 209

Depth: 36.45 m.b.s.f. *Site 1274A*
Minerals: cpx, opx, ol, mgt, spl, serp

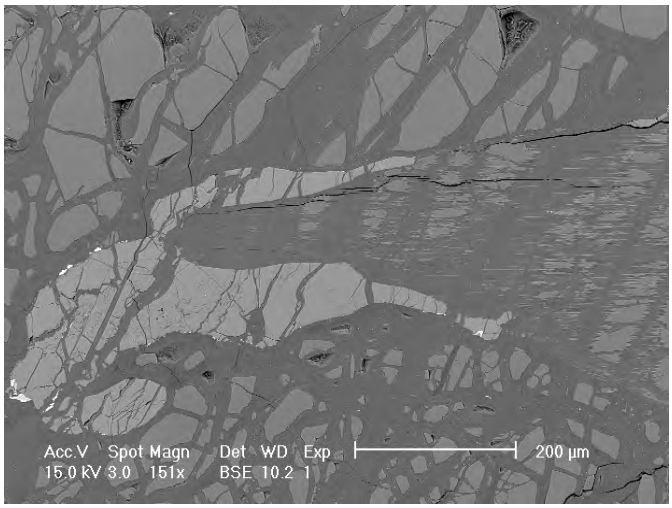

Cpx-grain surrounded by serp and ol

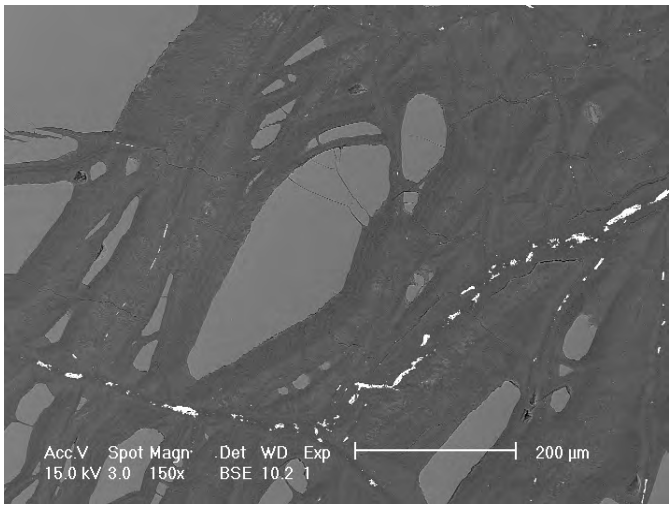

Ol in serpentine matrix

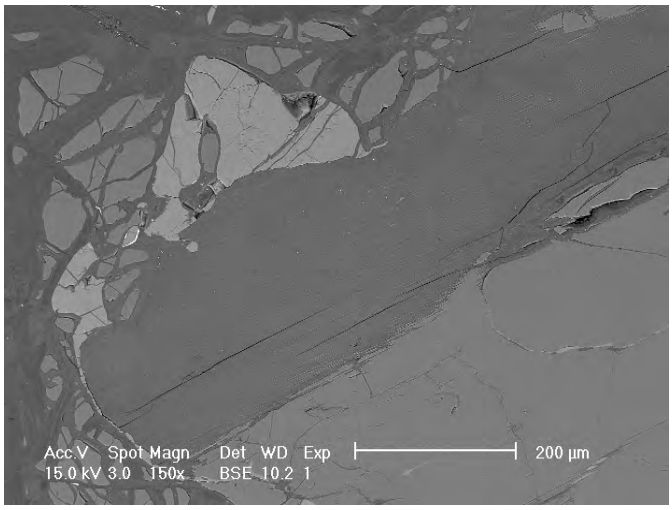

Cpx at the edge of a bastite; opx left over in the lower right corner

To 1

Totalp

Location: 780’425 / 190’200
Minerals: cpx, opx, ol, amph, spl, mgt, serp, chl

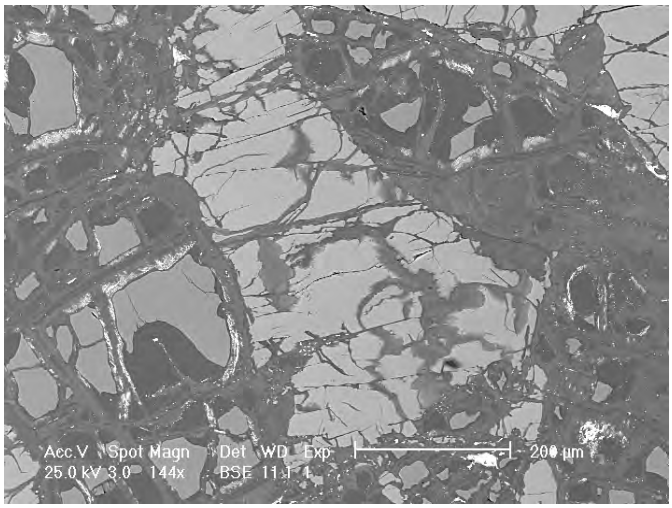

Cpx in serp surrounded by ol; darker spots are chl

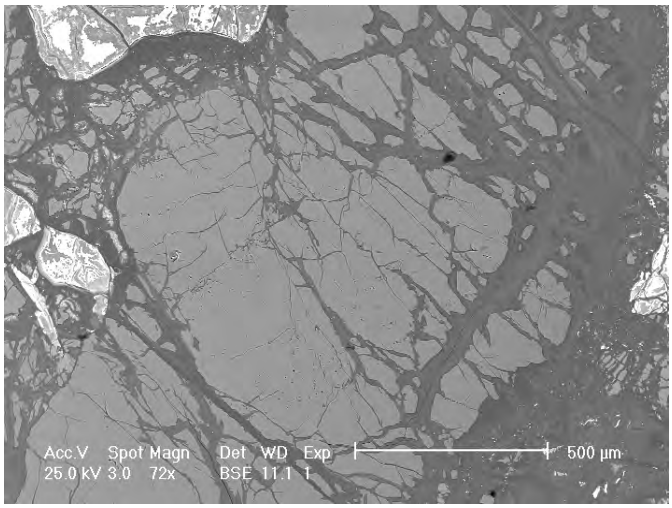

Large ol grain in serp; white phase is spl

Location: 782’325 / 191’200
Minerals: cpx, opx, ol, spl, mgt, serp, chl

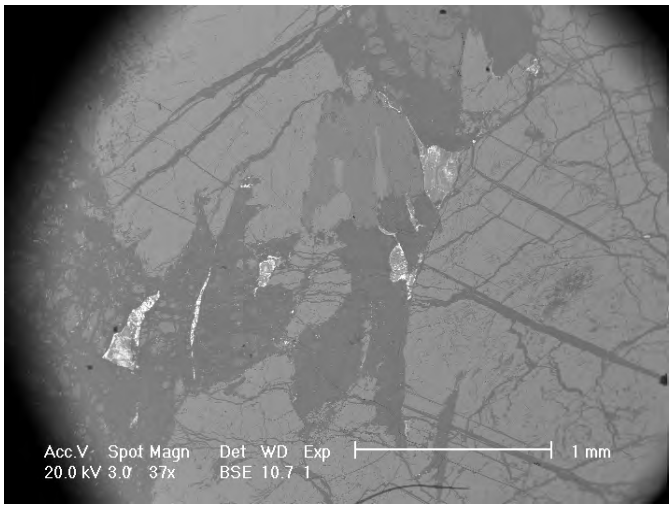

Cpx grains with opx and serp surrounding them

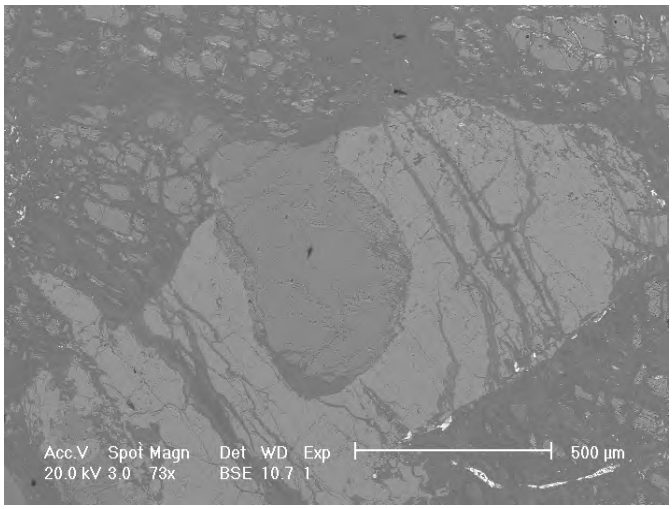

Cpx grain surrounding opx grain in serpentine

To 7

Totalp

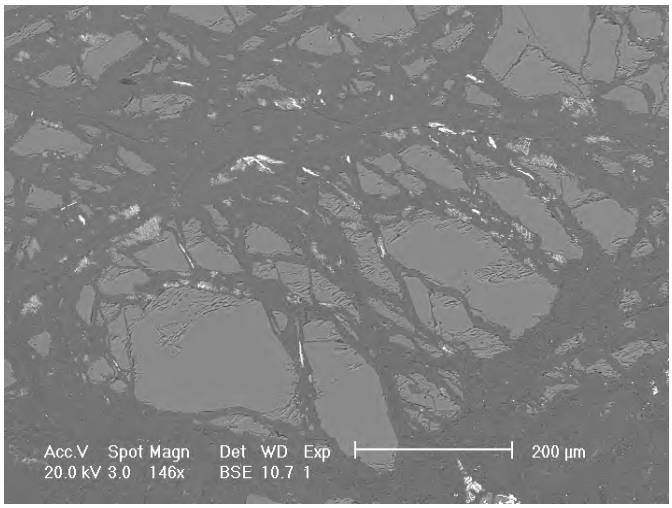

Ol grains in serpentine matrix

NAP 7

Lower Platta

Location: 769’500 / 153’005
Minerals: cpx, spl, mgt, serp, chl

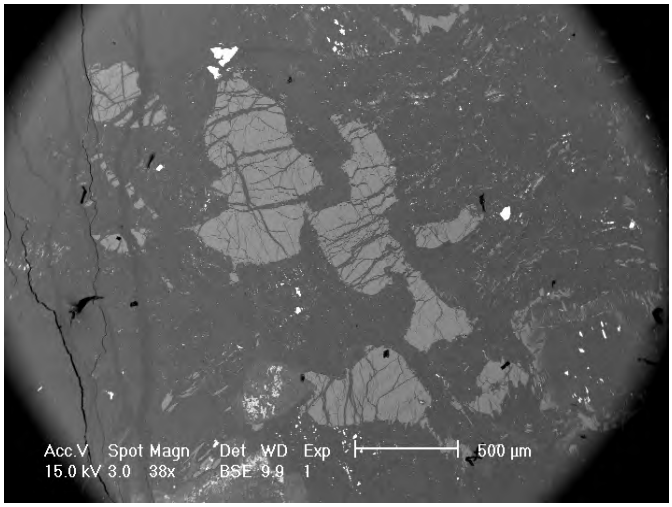

Overview with cpx and mgt in serpentine matrix

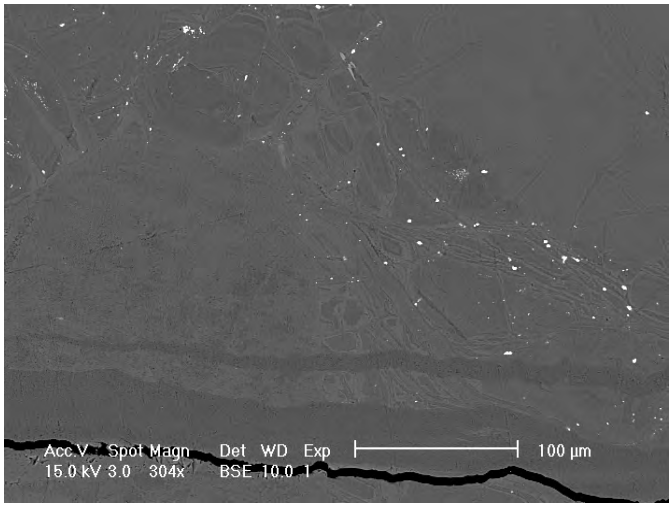

Serpentine texture, serp vein in the lower part

Location: 769’650 / 152’500
Minerals: cpx, spl, mgt, serp, chl

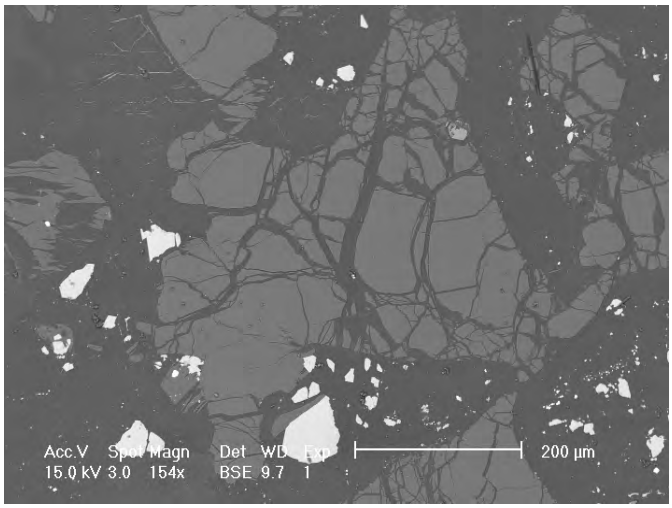

Ol grain in serp matrix; white mgt

NAP 99-2

Lower Platta

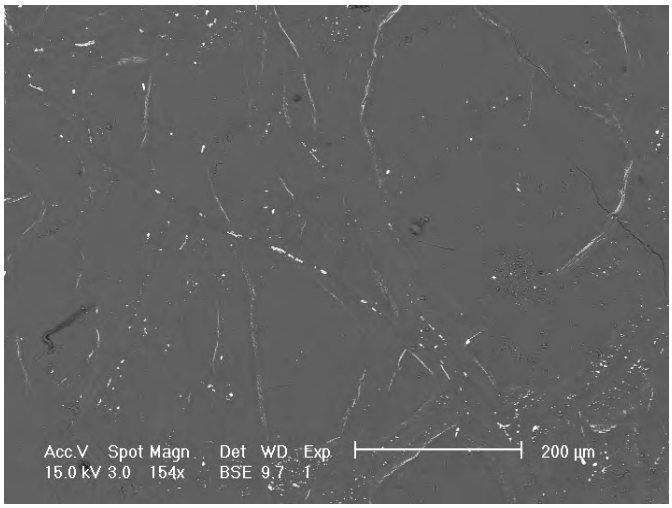

Serpentine texture

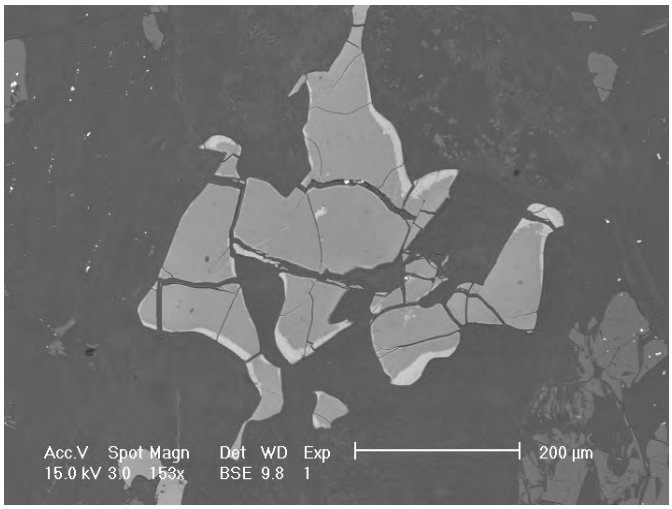

Spinel grain with mgt margin in serp

P 6

Lower Platta

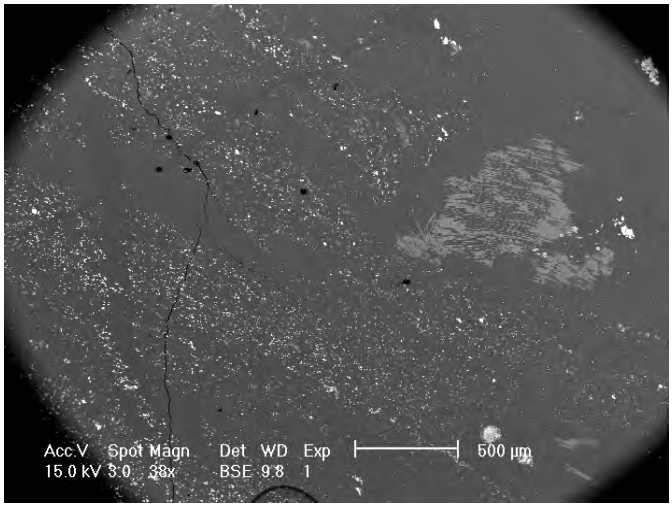

Overview with one cpx grain

Location: 770’120 / 153’310
Minerals: cpx, spl, mgt, serp

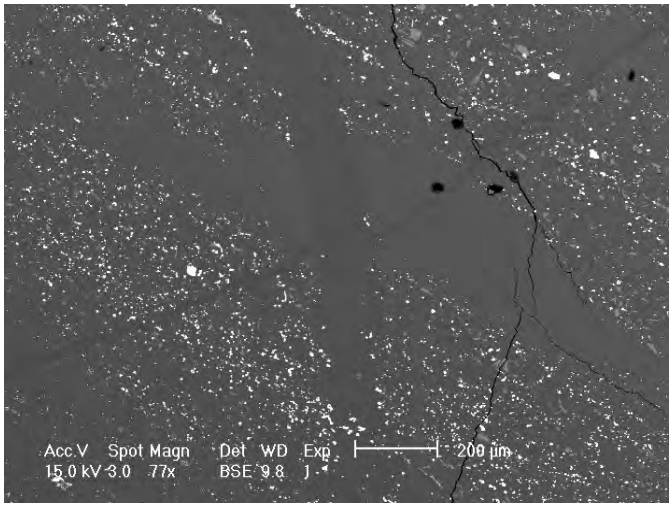

Fine-grained mgt in serpentine matrix; serp vein cross-cutting

Location: 767’750 / 147’250
Minerals: cpx, spl, mgt, serp, chl

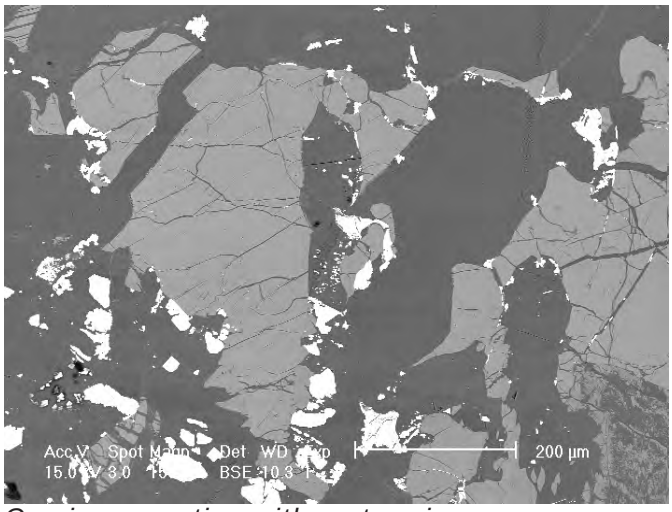

Opx in serpentine with mgt grains

CRP 3

Lower Platta

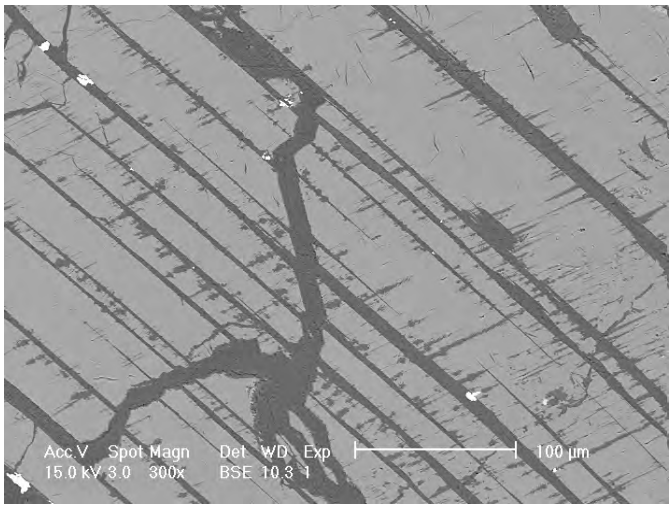

Former cpx lamellae (in opx), serpentinzed

STP 5-2

Lower Platta

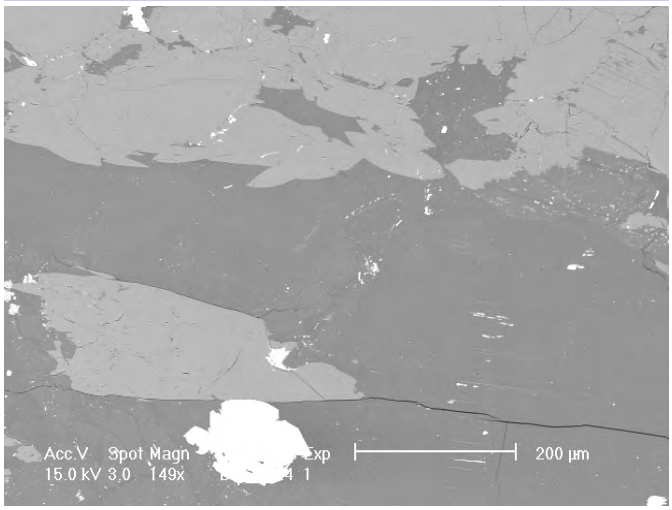

Cpx and mgt in serpentine matrix

Location: 766’350 / 151’125
Minerals: cpx, spl, mgt, serp, chl

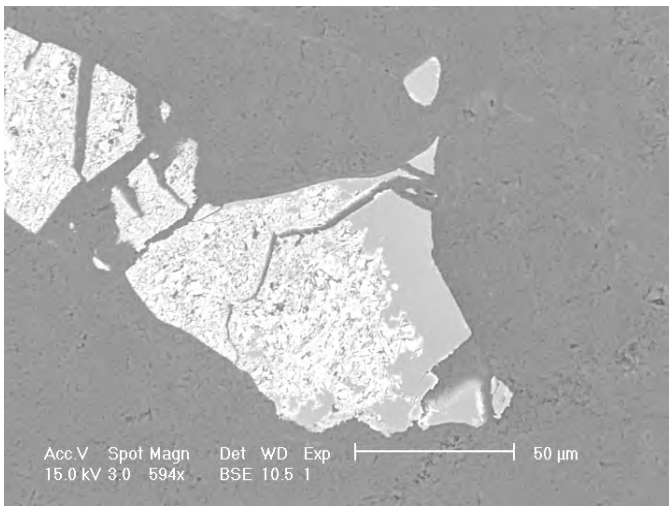

Spinel grain with mgt in serpentine

VEP 8

Upper Platta

Location: 772’625 / 159’675
Minerals: cpx, spl, mgt, serp, chl

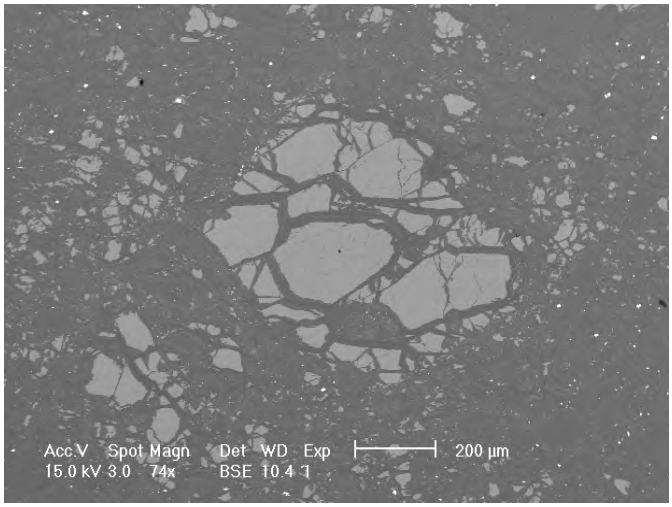

Ol grain in serpentine matrix

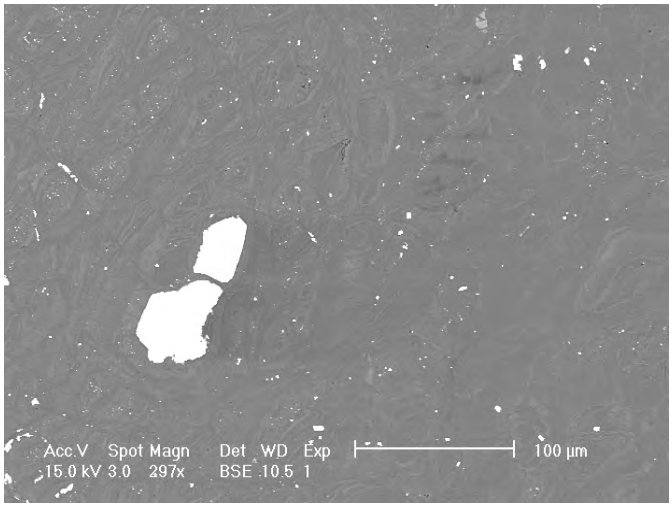

Mgt grain in serpentine matrix

Location: 771’325 / 157’650
Minerals: cpx, mgt, serp, chl

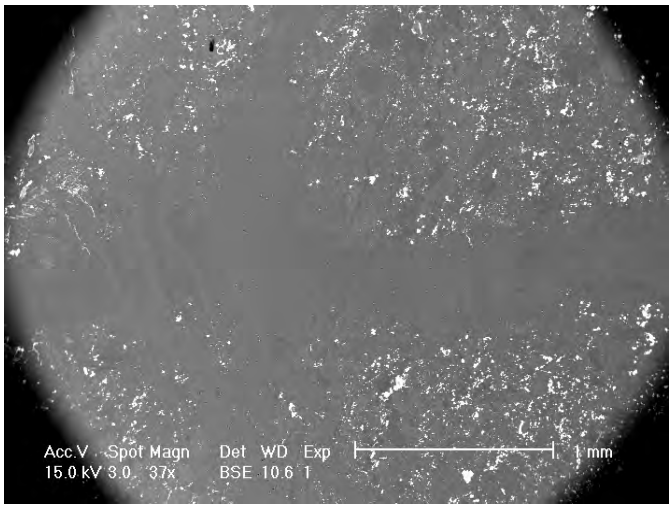

Overview, serpentine veins cross-cutting and mgt grains visible

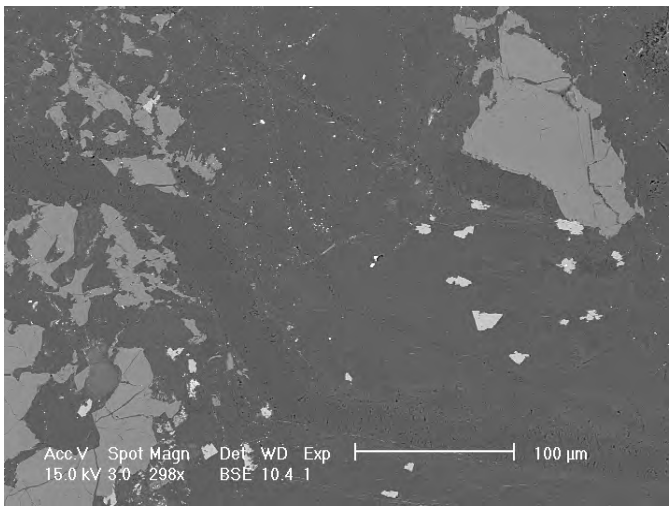

Cpx grains with mgt grains in serpentine matrix, serp vein crossing the section

FAP 4

Upper Platta

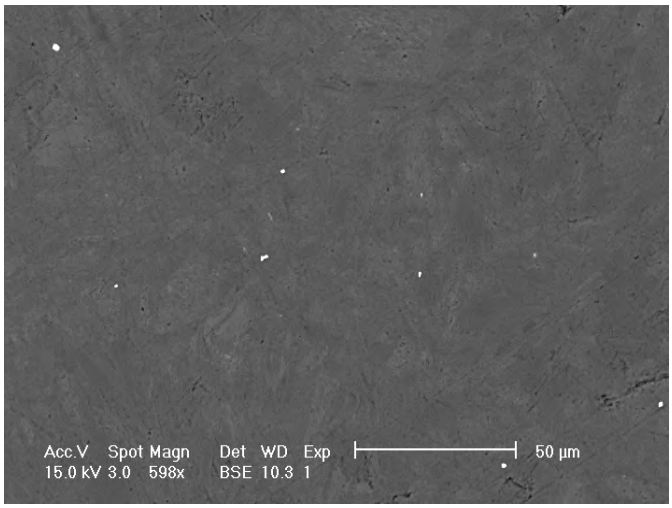

Serpentine texture

L-UM 112-4

Malenco

Location: 784’105 / 130’720
Minerals: cpx, opx, ol, amph, spl, chl

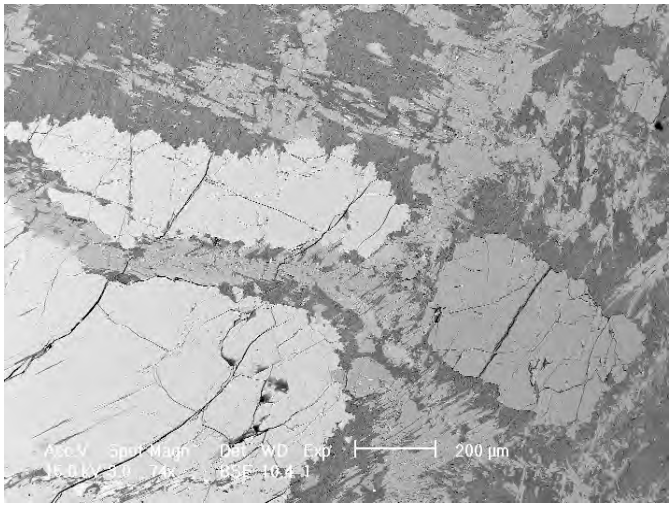

Cpx grains surrounded by amph, chl and ol

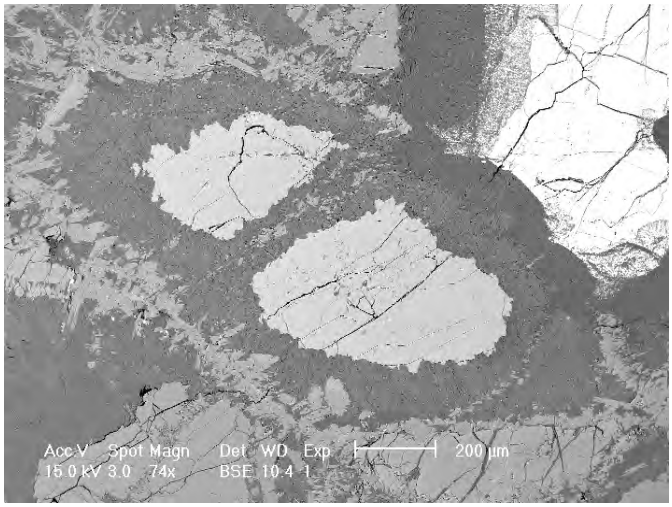

Two cpx- rains in chl; spl on the right

Location: 781’460 / 130’110
Minerals: cpx, ol, mgt, serp, chl

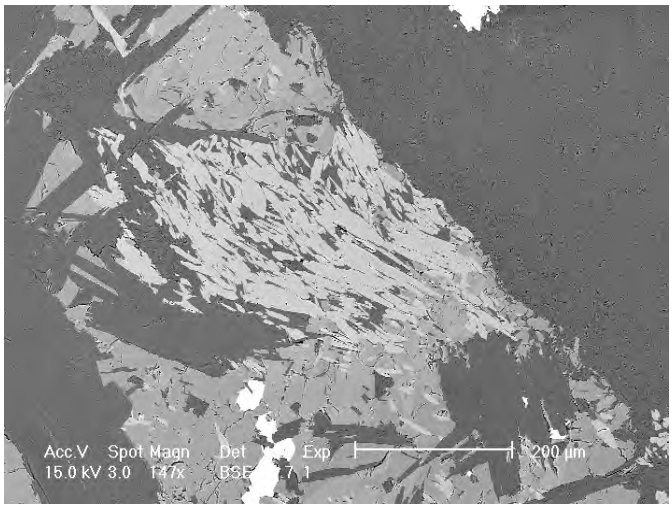

Vein diopside in serp-chl matrix surrounded by ol

P-UM 117

Malenco

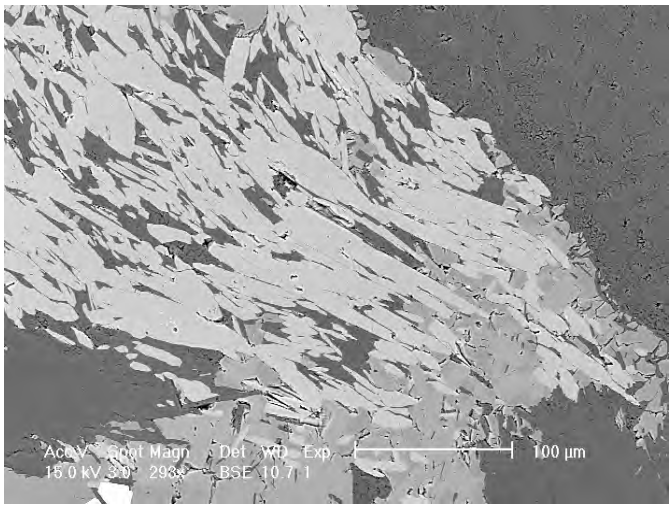

close-up of vein diopside

L-UM 224

Malenco

Location: 784’105 / 130’720
Minerals: cpx, ol, amph, spl, mgt, serp, chl

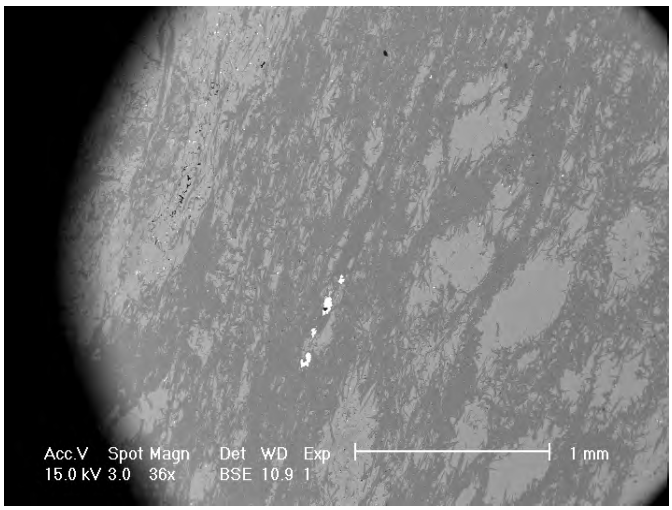

Sample texture overview

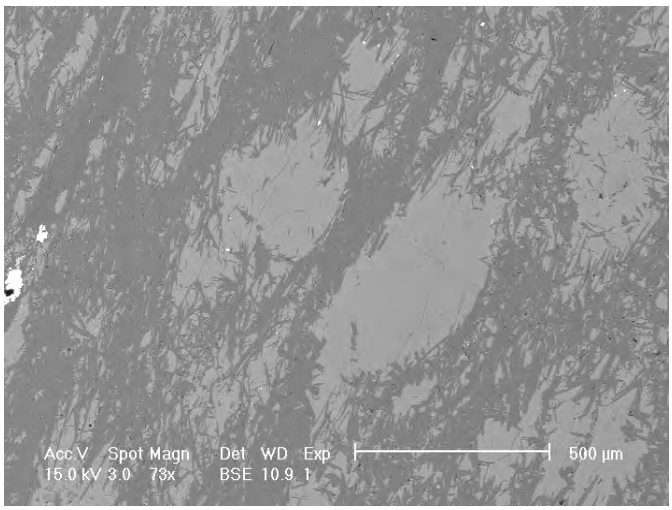

Ol grains in serpentine matrix

L-UM 216

Malenco

Location: 784’105 / 130’720
Minerals: opx, ol, amph, spl, serp, chl

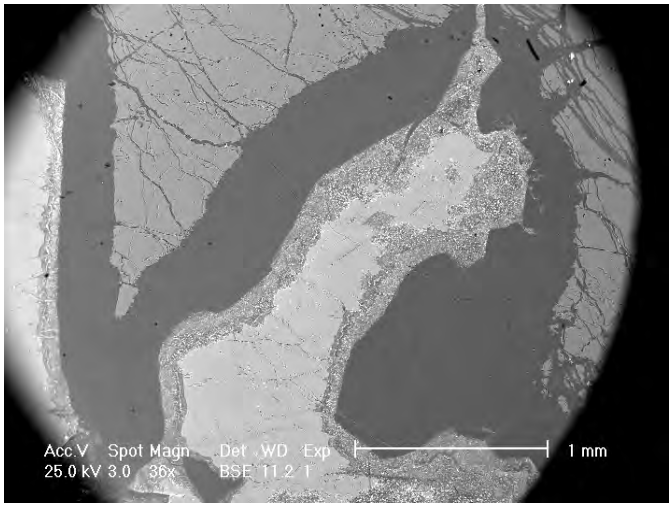

Overview of sample texture; whitish grain spl

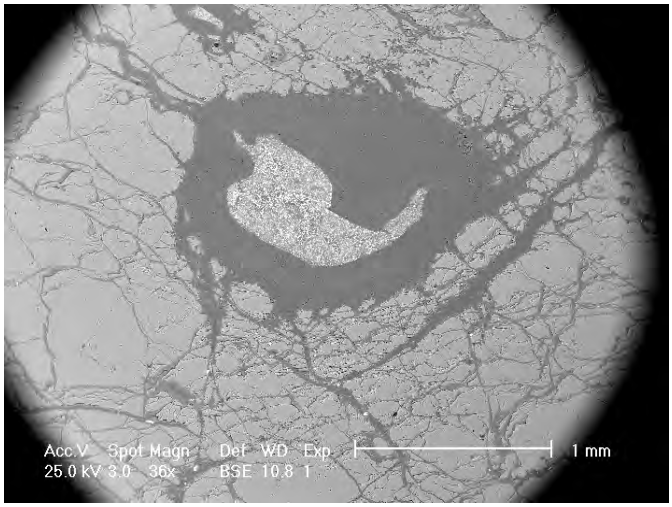

Spl grain in serp-chl amtrix surrounded by ol, opx and amph

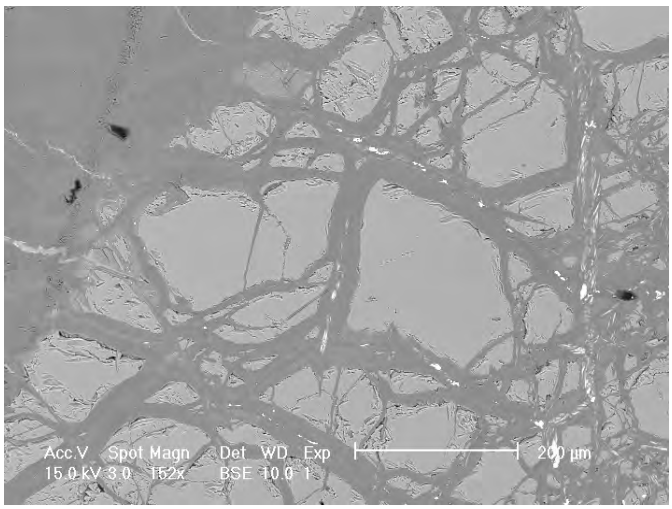

Ol-grains in serpentine

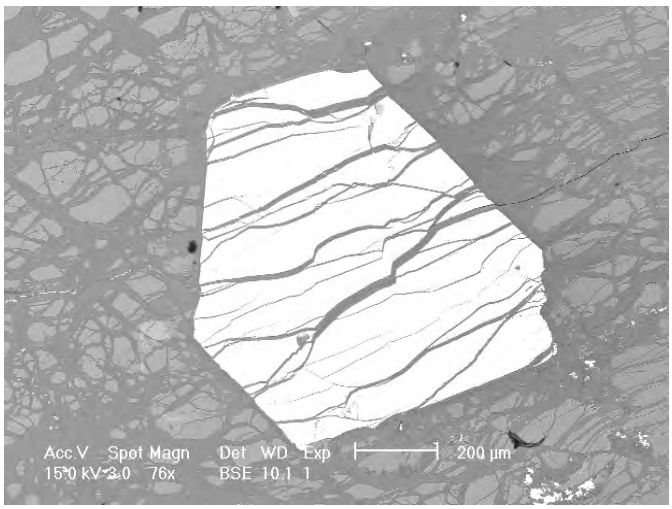

Mgt-grain in serpentine surrounded by ol

Location: 781’460 / 130’110
Minerals: cpx, opx, ol, trem, spl, chl

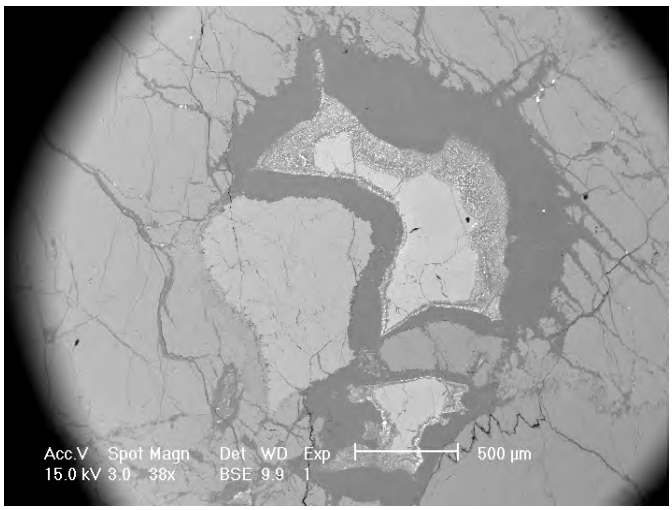

Overvies with spl surrounded serp-chl matrix; ol and cpx grains

L-UM 226

Malenco

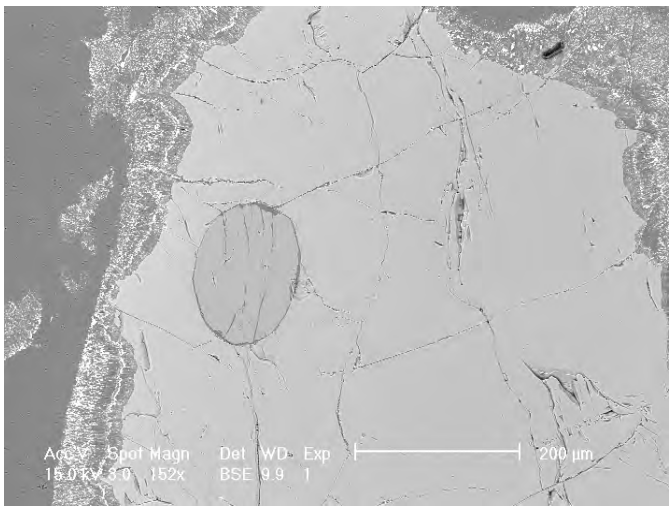

Ol-grain in cpx surrounded by serp

MG 65

Malenco

Location: 770’120 / 153’310
Minerals: mgt, serp, chl

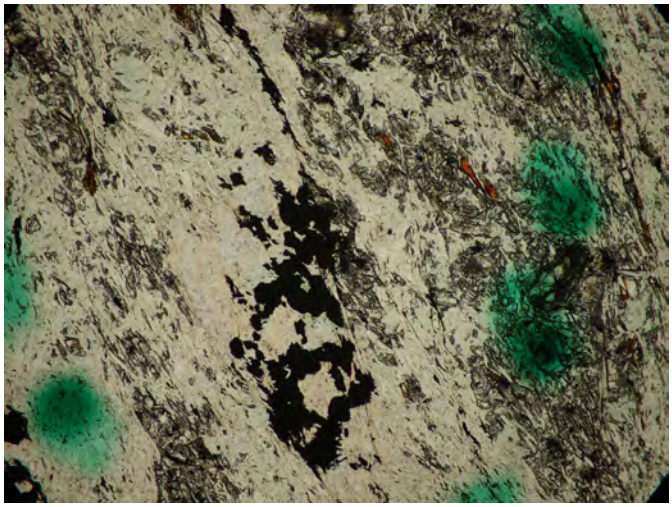

Fine-grained serpentine texture with mgt

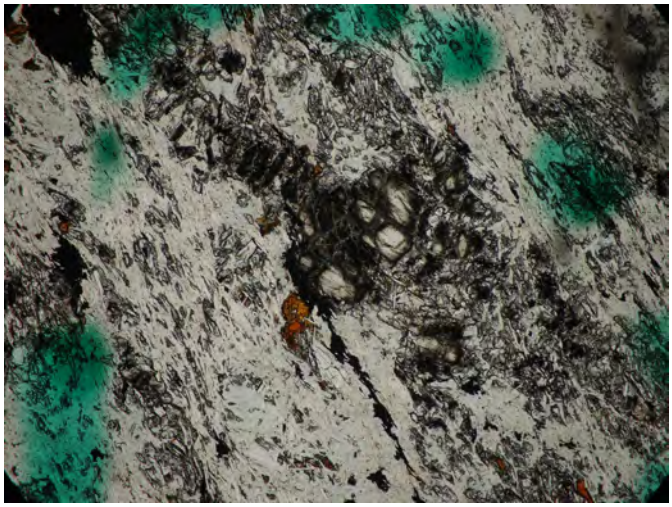

Fine grained serpentine texture with mgt

Vo 41

Vourinos

Location: 34T 560090 4447027
Minerals: cpx, opx, ol, spl, mgt, serp

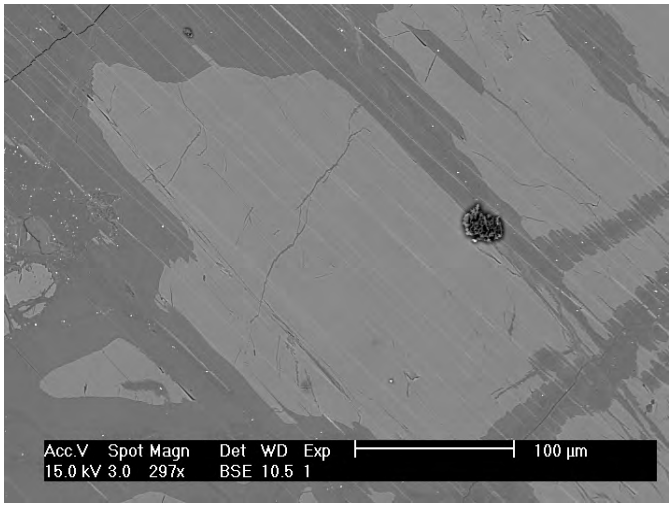

Opx with cpx exsolution lamellae serpentinized

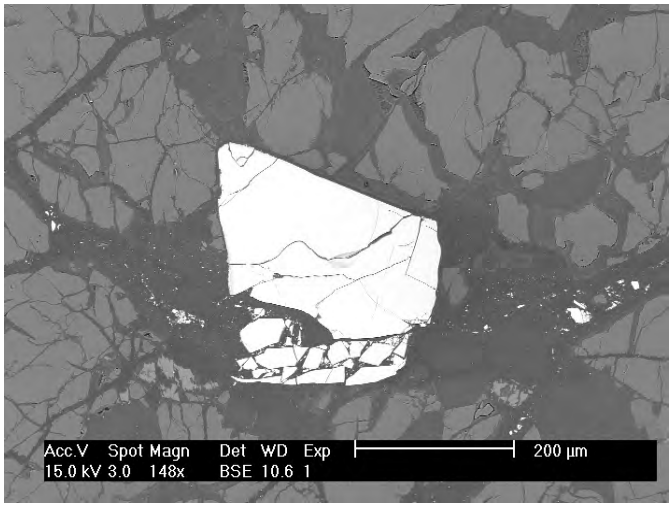

Mgt grain surrounded by ol and serp

Location: 34T 559160 4447499
Minerals: cpx, opx, ol, spl, mgt, serp

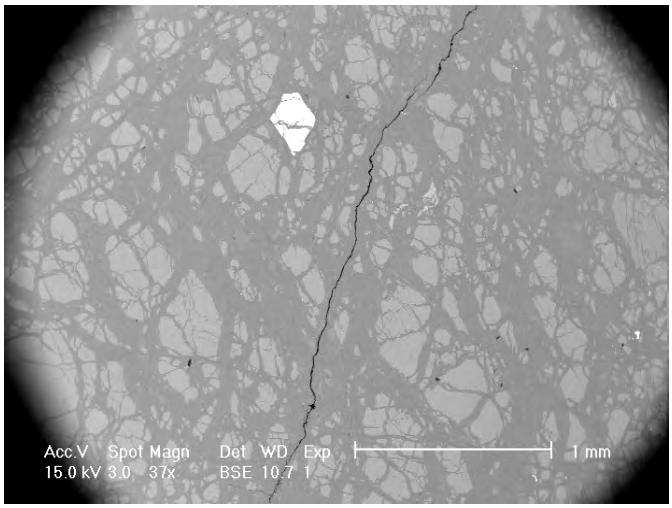

Overview with ol and mgt grains

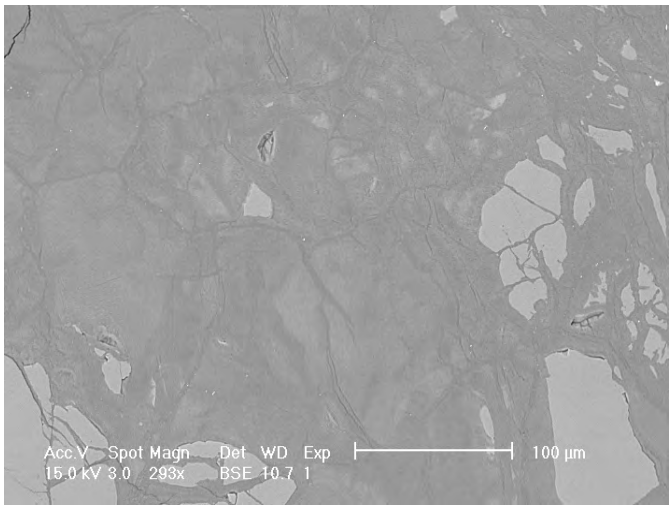

Serpentine texture with ol grains

Vo 43

Vourinos

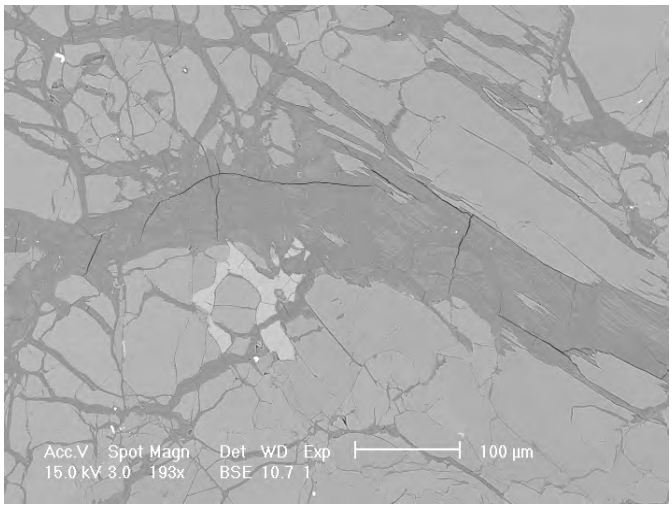

Interstitial cpx surrounded by ol, opx and serpentine vein

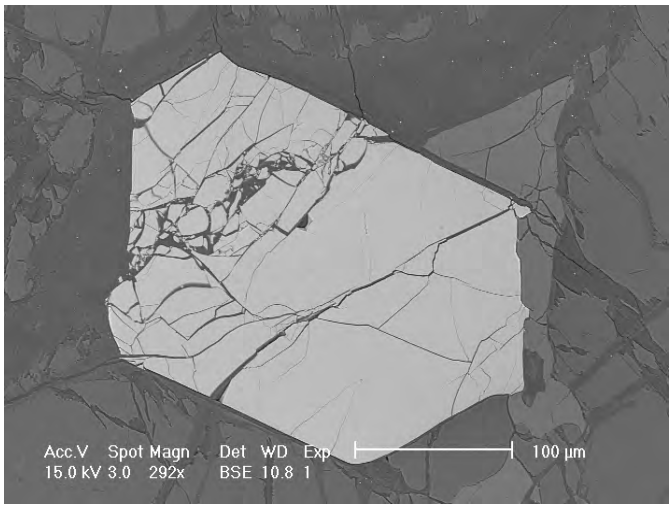

Spl grain with cpx (right) and ol

Vo 56

Vourinos

Location: 34T 565977 4433453
Minerals: cpx, opx, ol, spl, mgt, serp

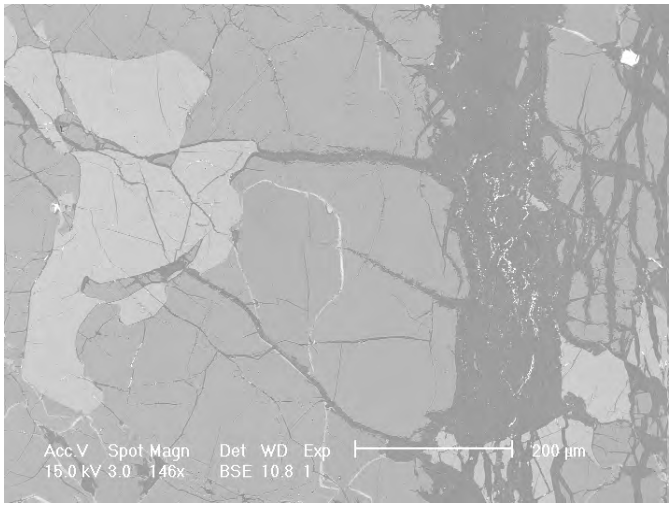

Interstitial cpx surrounded by opx, ol and serp

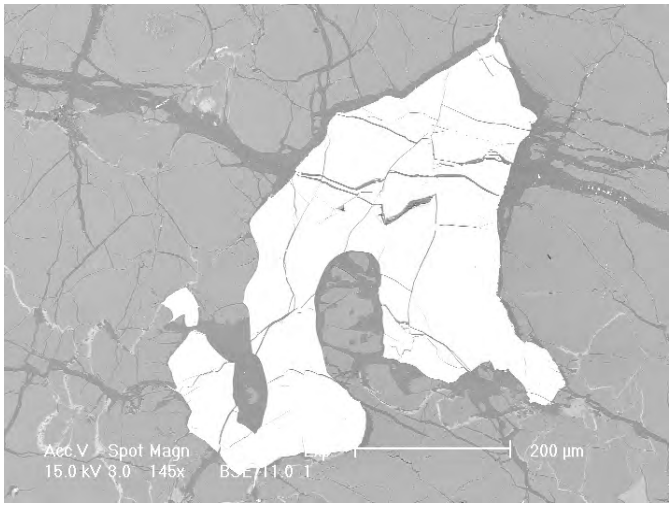

Spl grain surrounded by ol, opx and tinny cpx

Location: 34T 565977 4433453
Minerals: cpx, opx, ol, spl, serp

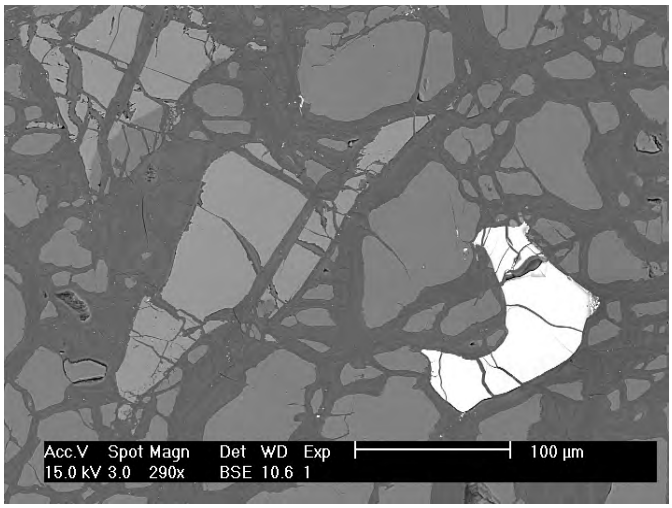

Cpx, ol and spl grains in serpentine

Vo 57

Vourinos

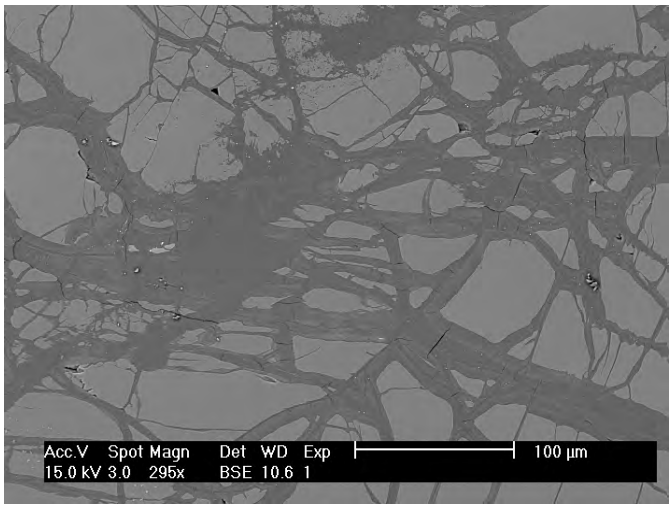

Ol grains in serpentine

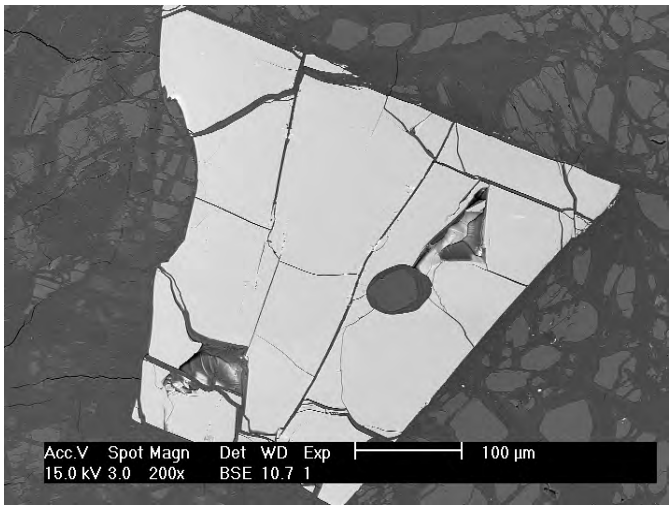

Spl grain surrounded by ol

Vo 67

Vourinos

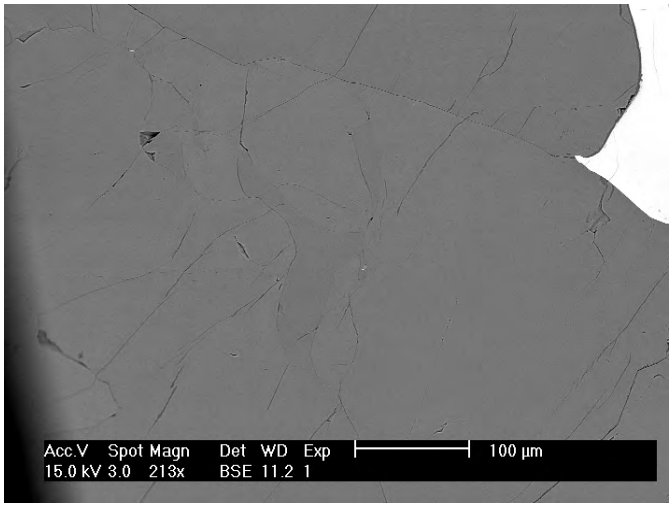

Spl grain surrounded by ol and opx grains

Location: 34T 553879 4443052
Minerals: cpx, opx, ol, spl, mgt, serp

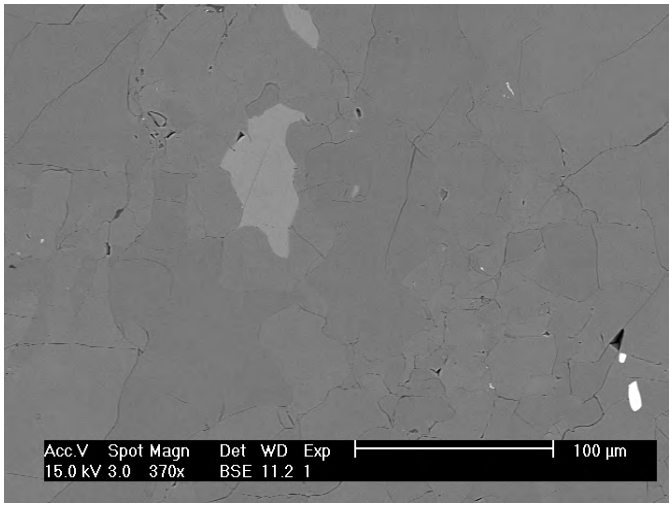

Interstial cpx and ol in opx

Location: 34S 518520 4415738
Minerals: cpx, opx, ol, spl, mgt, serp

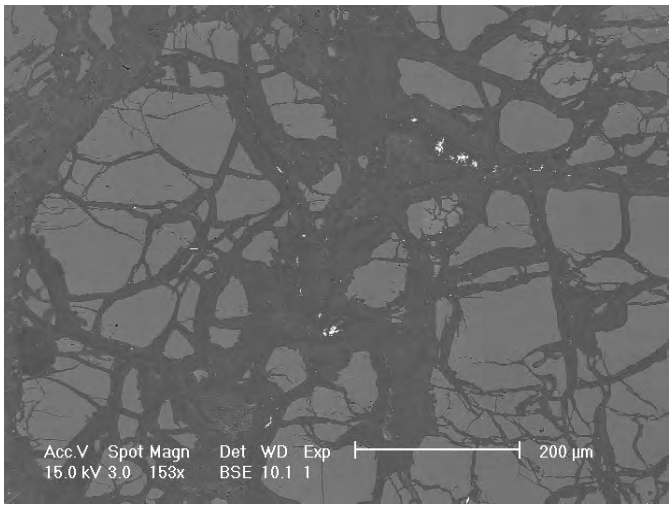

Ol grains in serpentine matrix

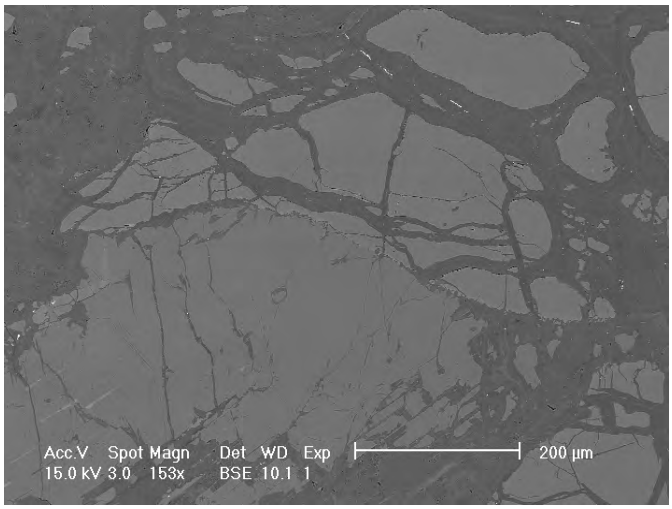

Ol and opx grains in serpentine matrix

P 6

Vourinos

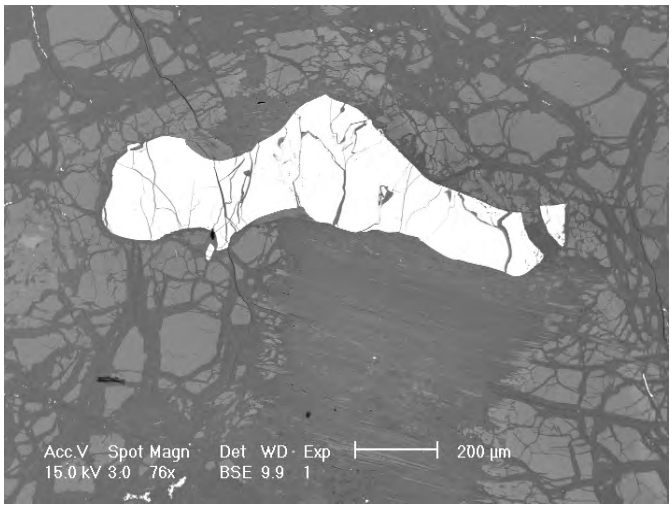

Spl grain surrounded by ol, opx, serp and cpx

CIG 1

Cima di Gagnone

Location: 708’900 / 132’450
Minerals: cpx, opx, ol, amph, garnet, il

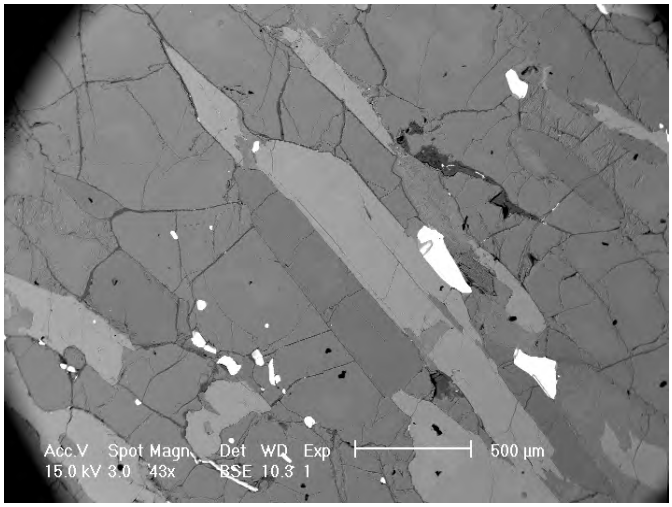

Textural overview

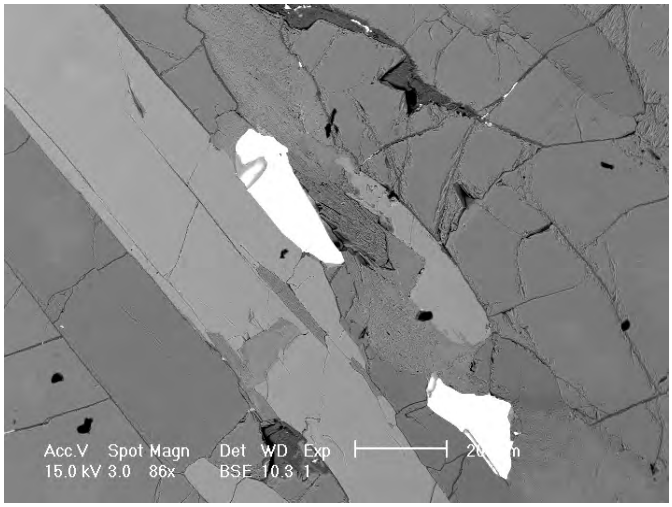

Cpx grain surrounded with garnet, il, opx and ol

Location: 707’700 / 131’750
Minerals: cpx, opx, ol, amph spl, il, chl, mag

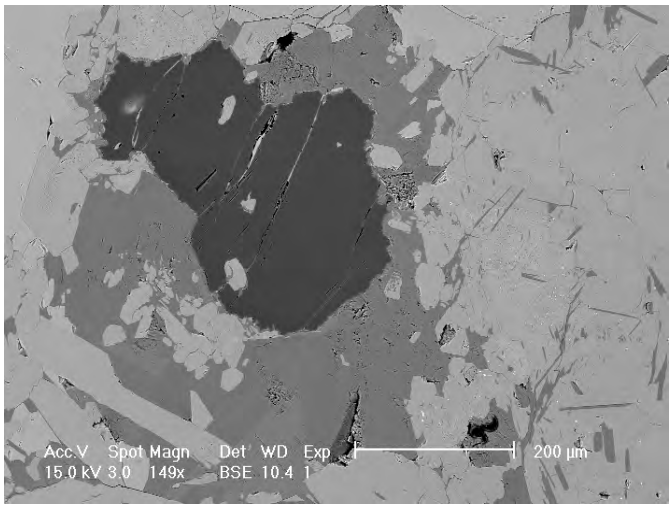

Mag (black) in chl matrix surrounded by amph, ol and opx

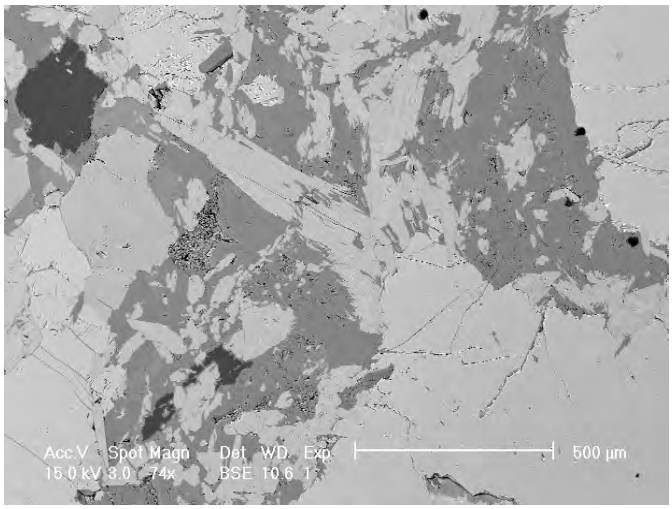

Amph grains in chl with mag, cpx, ol and opx

CIG 2

Cima di Gagnone

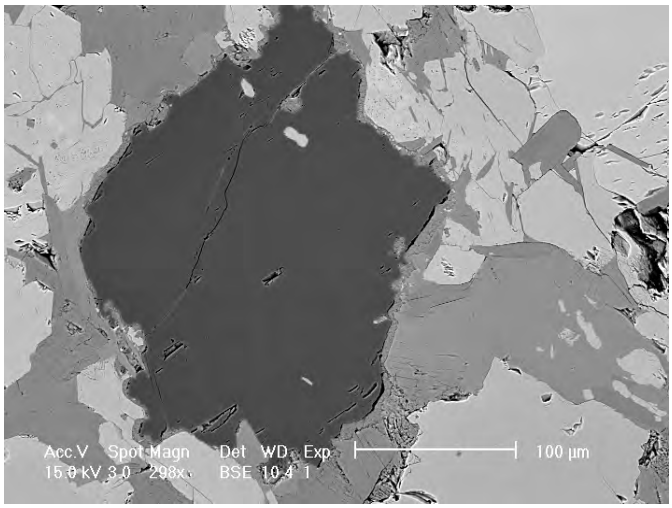

Mag in chlorite matrix around cpx and ol

CIG 1 — Cima di Gagnone

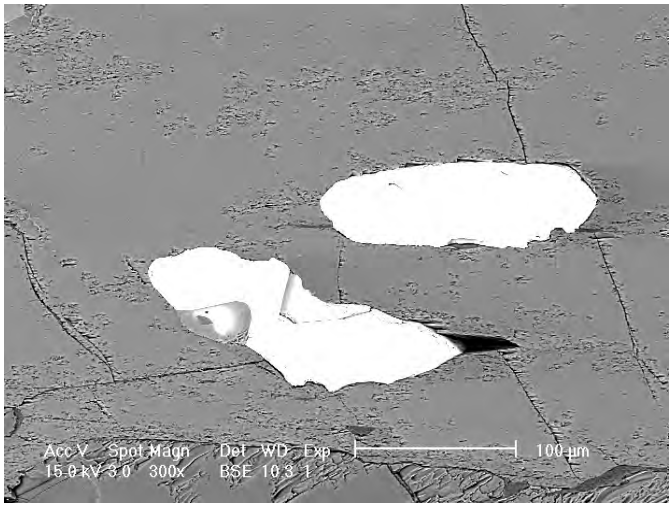

Two ilmenite grains within an amphibole grain

Location: 707'500 / 131'350
Minerals: opx, ol, amph spl, mgt, talc, mag

CIG 3 — Cima di Gagnone

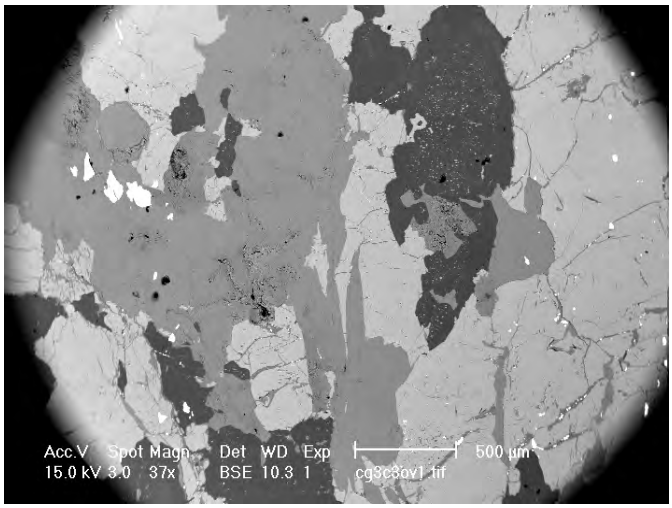

Textural overview

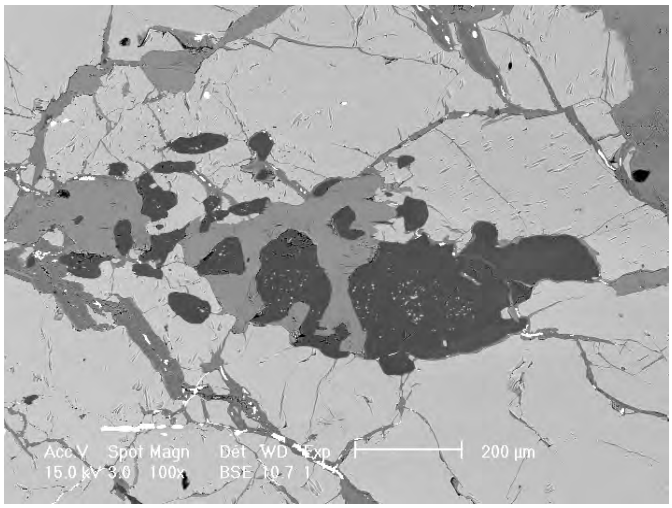

Ol grains enclosing mag and talc grains

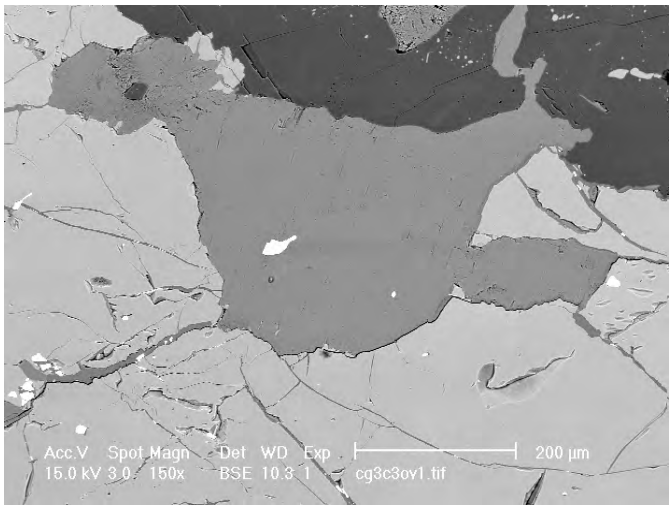

Talc grain surrounded by ol and mag

Appendix B

Additional Li, Be and B measurements

In the orientation phase at the beginning of the thesis, samples of ultramafic rocks from different geodynamic settings were studied. Then, work focused on ODP Leg 209 samples and on the transect Totalp-Platta-Malenco. This appendix contains light element (Li, Be and B) concentrations obtained by in-situ measurements of minerals from the Vourinos ophiolite (Greece) and the Cima di Gagnone ultramafic body (Swiss Alps). The Vourinos ophiolite, adjacent to the Pindos ophiolite (see Pelletier et al. 2008) represents non-metamorphic oceanic mantle and crust. The Cima di Gagnone ultramafic body represents hydrothermally altered, subducted oceanic mantle and crust, metamorphosed at high pressures and later retrogressed to different degrees. The analytical procedures are the same as described in chapter II of this thesis.

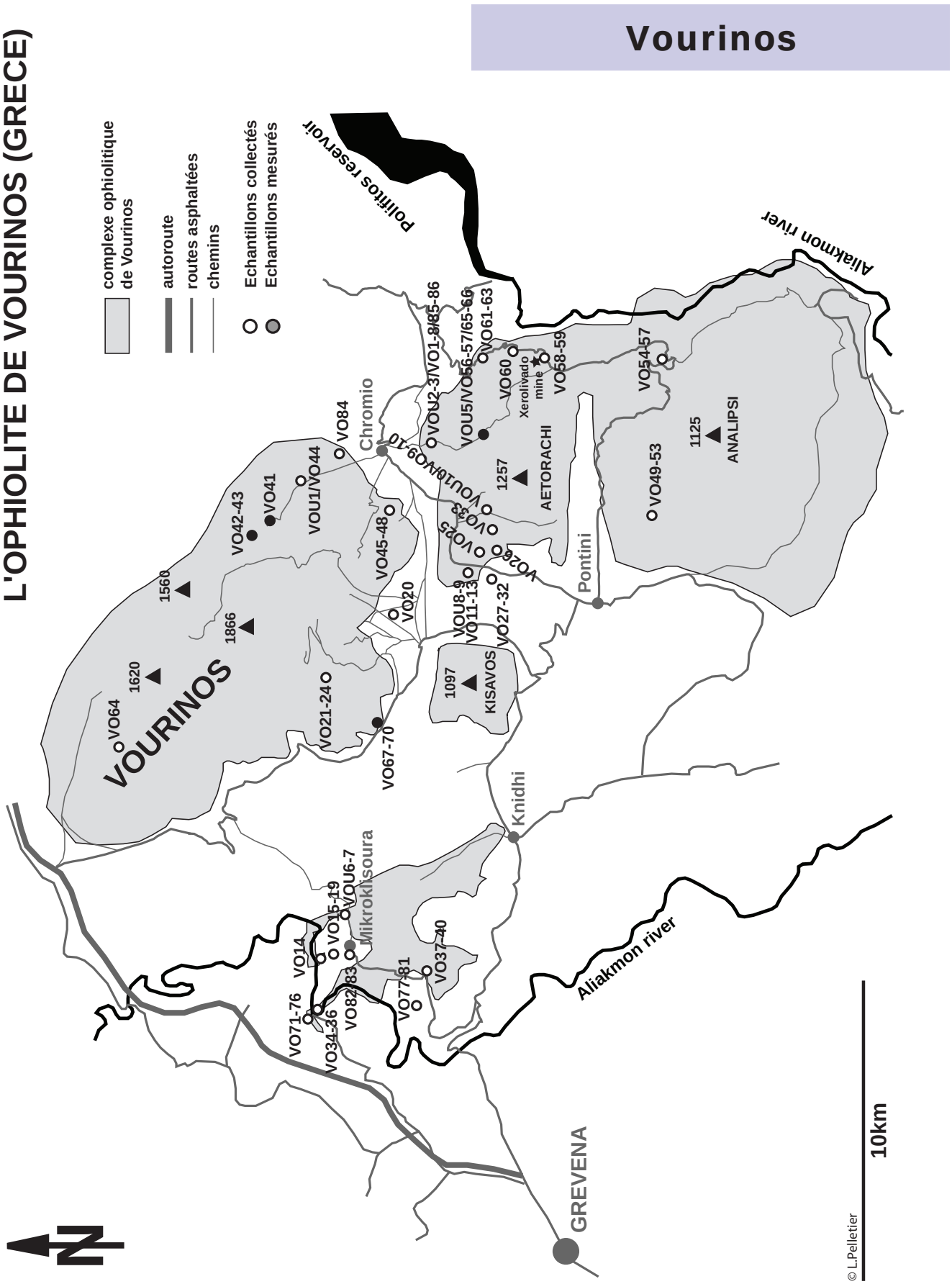

Fig. A.1. Simplified map of the Vourinos ophiolite with sample locations indicated.

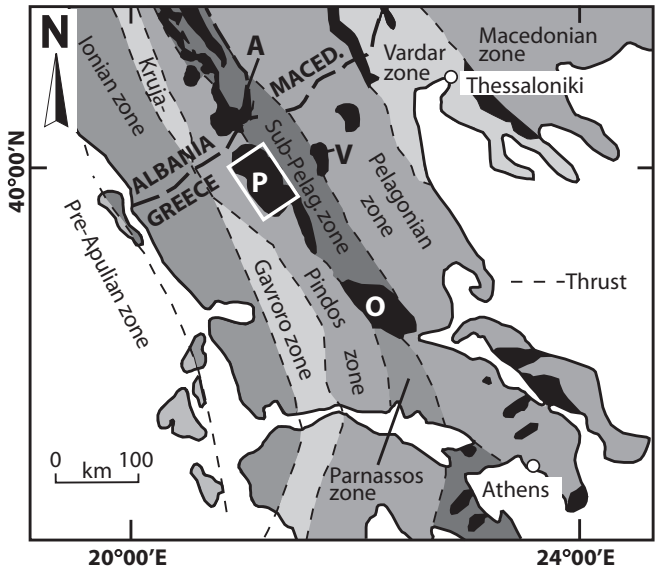

Fig. A.2. The Pindos ophiolite within the Hellenides, from Pelletier et al. (2008). P Pindos ophiolite; V Vourinos ophiolite; O Othris ophiolite; A Albanian ophiolites; Maced Macedonia; Sub-Pelag. zone Sub-Pelagonian zone.

Fig. A.3. Map of the Vourinos ophiolite and surrounding rocks showing the sample location (from Liati et al., 2004). 1: Triassic-Jurassic marbles; 2: peridodites and dunites; 3: ultramafic cummulates; 4: diorites, gabbros, plagiogranites; 5: basalts, dolerites; 6: Cretaceous limestones; 7: gneisses; 8: mélange; 9: sediments (late Jurassic-Oligocene).

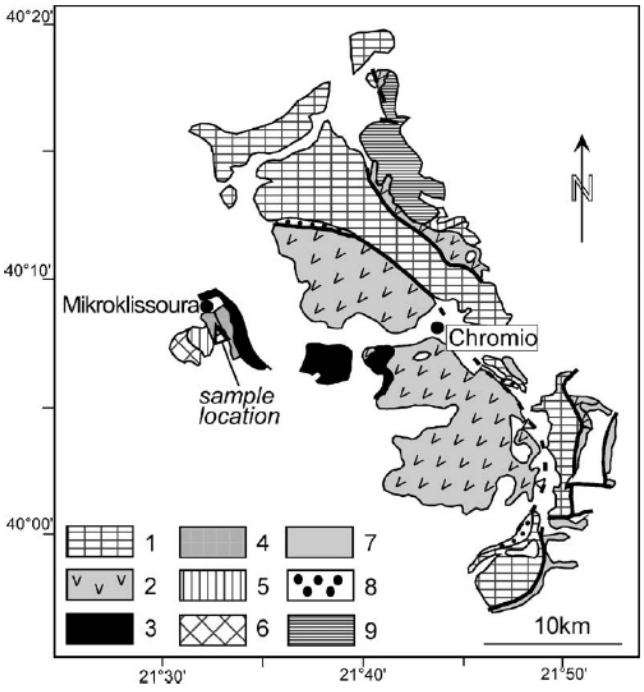

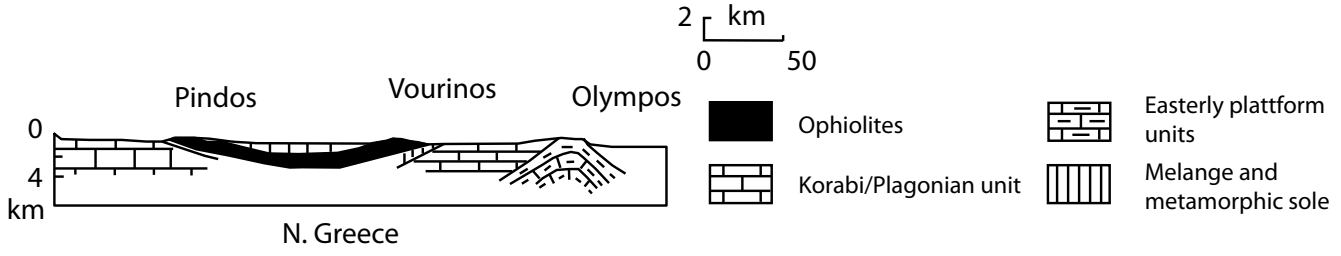

Fig. A.4. Cross section through the Pindos-Vourinos ophiolite body, after Robertson (2000).

Points	Minerals	Li ug/g	sigma (Li)	Be µg/g	sigma (Be)	B ug/g	sigma (B)
Vo41C2cp1	cpx	2.776	3.95%	0.002	105%	0.185	31.82%
Vo41C3cp2	cpx	7.309	2.44%	0.003	87%	0.191	21.86%
Vo43C2cp3	cpx	3.561	2.82%	b.d.l.	-	0.650	18.50%
Vo43C3cp1	cpx	4.316	2.87%	b.d.l.	-	0.606	17.31%
Vo43C3cp2	cpx	3.017	4.41%	0.002	118%	0.066	46.69%
Vo43C4cp4	cpx	4.112	4.73%	b.d.l.	-	0.234	29.35%
Vo43C4cp6	cpx	4.241	5.06%	b.d.l.	-	0.042	45.58%
Vo56C1cp1	cpx	3.385	3.49%	0.001	161%	0.016	97.39%
Vo56C1cp1	cpx	3.663	2.06%	b.d.l.	-	0.024	115.86%
Vo56C4cp2	cpx	3.103	4.06%	b.d.l.	-	0.016	108.79%
Vo56C4cp6	cpx	3.450	3.93%	0.001	162%	0.009	67.31%
Vo57C3cp3	cpx	1.833	4.62%	0.009	55%	0.042	41.97%
Vo57C4cpx1	cpx	1.967	4.37%	0.006	31%	0.325	17.58%
Vo57C5cp3	cpx	1.338	5.45%	0.007	42%	0.178	27.37%
Vo57C5cp4	cpx	1.696	6.83%	0.008	52%	0.137	28.20%
Vo67C1cp5	cpx	0.960	4.08%	b.d.l.	-	0.064	24.57%
Vo41C4cp4	cpx	1.818	5.90%	b.d.l.	-	0.032	45.96%
Vo67C1cp8	cpx	3.546	17.27%	0.002	94%	6.755	10.07%
Vo41C3ol5	ol	0.846	5.22%	b.d.l.	-	0.165	33.29%
Vo41C5ol3	ol	0.850	7.53%	b.d.l.	-	0.207	20.78%
Vo41C5ol5	ol	0.872	6.71%	b.d.l.	-	0.029	36.42%
Vo43C1ol1	ol	0.723	5.23%	0.001	175%	0.043	53.77%
Vo43C1ol3	ol	0.683	6.28%	b.d.l.	-	0.079	44.52%
Vo43C2ol5	ol	0.622	6.12%	b.d.l.	-	0.013	106.30%
Vo43C2op1	ol	0.633	5.23%	b.d.l.	-	0.026	46.02%
Vo43C3op1	ol	0.882	5.73%	b.d.l.	-	0.140	14.59%
Vo43C5ol2	ol	0.750	7.10%	b.d.l.	-	0.024	43.46%
Vo43C5ol3	ol	0.784	3.77%	b.d.l.	-	0.008	81.59%
Vo56C4ol5	ol	1.150	6.80%	b.d.l.	-	0.012	147.74%
Vo57C3ol1	ol	0.471	7.46%	b.d.l.	-	0.030	55.14%
Vo57c4ol1	ol	0.695	6.14%	b.d.l.	-	0.031	41.72%
Vo67C1ol2	ol	0.984	3.04%	b.d.l.	-	0.208	27.22%
Vo67C1ol3	ol	0.795	6.00%	b.d.l.	-	0.054	49.41%
Vo67C1ol4	ol	0.851	2.98%	b.d.l.	-	0.070	19.26%
Vo67C1ol4-2	ol	0.740	5.84%	b.d.l.	-	0.055	55.91%
Vo67C1ol5	ol	0.831	5.27%	b.d.l.	-	0.050	30.46%
Vo67C2ol3	ol	0.840	3.14%	b.d.l.	-	0.047	31.56%
Vo67C1ol1	ol	0.706	4.92%	b.d.l.	-	0.050	22.25%
Vo43C2ol3	ol II	0.568	7.37%	0.001	170%	0.315	23.59%
Vo43C4ol1	ol II	0.693	5.46%	0.001	116%	0.328	30.17%
Vo56C1ol5	ol II	1.031	3.27%	b.d.l.	-	0.005	151.17%
Vo56C1ol7	ol II	0.484	10.39%	b.d.l.	-	0.009	116.59%
Vo56C3ol1	ol II	0.546	7.03%	b.d.l.	-	0.096	28.05%
Vo56C3ol3	ol II	1.314	8.29%	b.d.l.	-	0.000	78.54%
Vo57c4ol1	opx	2.193	27.22%	0.004	47%	0.053	39.59%
Vo43C2op10	opx	1.182	4.04%	b.d.l.	-	0.021	72.48%
Vo43C2op3	opx	0.905	5.79%	b.d.l.	-	0.010	65.58%
Vo43C3op?	opx	0.494	6.79%	b.d.l.	-	0.032	22.60%
Vo43C3op2	opx	1.467	3.05%	b.d.l.	-	0.128	25.03%
Vo43C4op5	opx	0.814	9.21%	b.d.l.	-	0.051	32.73%
Vo56C3op3	opx	0.619	5.45%	b.d.l.	-	0.011	78.98%
Vo56C3oppr1a	opx	0.673	7.36%	b.d.l.	-	0.011	98.14%
Vo56C3oppr1b	opx	0.691	7.45%	b.d.l.	-	0.011	110.26%
Vo56C4op4	opx	0.547	10.86%	b.d.l.	-	0.041	46.67%
Vo56C4op6	opx	0.653	5.06%	0.001	227%	0.016	61.20%

Punkt	Mineral	Li ug/g	sigma (Li)	Be ng/g	sigma (Be)	B ug/g	sigma (B)
Vo56C4op7	opx	0.627	6.68%	b.d.l.	-	0.009	72.63%
Vo57C1op1	opx	0.356	6.88%	0.002	69%	0.037	46.81%
VO57C1OP3	opx	0.660	5.43%	0.002	56%	0.293	20.49%
Vo57C3opp2-1	opx	0.749	5.11%	0.001	140%	0.044	42.74%
Vo57C3opp2-1	opx	0.445	5.55%	0.003	57%	0.024	37.47%
Vo57C5op2	opx	0.834	5.47%	0.004	29%	0.057	33.68%
Vo67C1op6	opx	0.962	5.26%	0.002	89%	0.064	36.40%
Vo67C2op1	opx	1.202	4.43%	b.d.l.	-	0.068	40.64%
Vo67C2opp1-1	opx	12.551	2.78%	0.001	141%	0.047	38.38%
Vo67C2opp1-2	opx	1.349	5.89%	0.002	90%	0.065	19.11%
Vo67C1op2	opx	0.384	7.42%	b.d.l.	-	5.407	3.28%
Vo67C1op3	opx	0.352	4.99%	b.d.l.	-	2.566	5.46%
Vo43C2op7	opx II	0.895	4.53%	0.003	274%	0.038	35.18%
Vo43C4op1	opx II	0.610	8.82%	b.d.l.	-	0.074	36.16%
Vo56C1op5	opx II	0.487	10.08%	0.001	141%	0.007	123.12%
Vo41C3sr7	serp	4.538	3.75%	0.004	67%	4.512	6.18%
Vo41C3sr9	serp	1.662	9.46%	0.002	72%	1.825	22.82%
Vo43C1sr3	serp	2.035	7.13%	b.d.l.	-	1.118	25.72%
Vo43C2sr2	serp	0.190	10.69%	0.004	276%	4.362	11.34%
Vo43C3sr10	serp	0.742	10.27%	b.d.l.	-	0.602	20.11%
Vo43C3sr12	serp	0.743	7.27%	b.d.l.	-	4.842	15.09%
Vo43C3sr2	serp	6.151	2.89%	b.d.l.	-	3.983	4.46%
Vo43C4sr4	serp	1.488	7.79%	b.d.l.	-	11.780	10.67%
Vo43C5sr5	serp	4.437	56.19%	0.000	167%	0.729	50.58%
Vo56C1sr5	serp	1.850	4.70%	b.d.l.	-	0.193	21.12%
Vo56C3sr1	serp	0.333	9.33%	b.d.l.	-	2.359	7.88%
Vo56C3sr3	serp	0.452	8.20%	b.d.l.	-	2.054	6.43%
Vo56C4sr2	serp	0.613	4.39%	b.d.l.	-	1.060	6.27%
Vo56C4sr6	serp	0.618	6.79%	b.d.l.	-	1.342	6.52%
Vo57c1sr1	serp	0.121	18.73%	0.001	91%	25.490	18.30%
Vo57C2sr2	serp	0.121	11.13%	b.d.l.	-	5.392	15.73%
Vo57C3sr2	serp	0.021	15.09%	0.002	94%	25.795	55.87%
Vo57C5sr7	serp	0.151	10.58%	0.002	69%	5.466	12.29%
Vo41C2sr1	serp	2.122	7.81%	0.003	52%	3.325	4.10%
Vo41C4sr2	serp	12.355	1.21%	0.002	60%	2.041	6.76%
Vo41C4sr7	serp	8.157	3.68%	b.d.l.	-	2.102	4.89%
Vo41C5sr6	serp	2.558	6.47%	0.001	81%	4.784	24.20%
Vo41C5sr8	serp	2.239	6.86%	b.d.l.	-	10.728	7.03%
Vo41C5sr9	serp	1.334	6.23%	b.d.l.	-	3.155	5.78%
Vo41C5sr9	serp	1.371	6.21%	b.d.l.	-	2.296	7.52%
Vo57C5Sr3	serp	0.338	46.64%	0.001	100%	26.263	9.60%
Vo57C3sr2	serp	0.058	24.67%	0.001	115%	1.738	18.45%
Vo57C3sr1	serp	0.033	25.93%	b.d.l.	-	7.131	30.38%
Vo41C4sr8	serp	11.150	4.05%	0.002	115%	2.225	19.87%

Cima di Gagnone

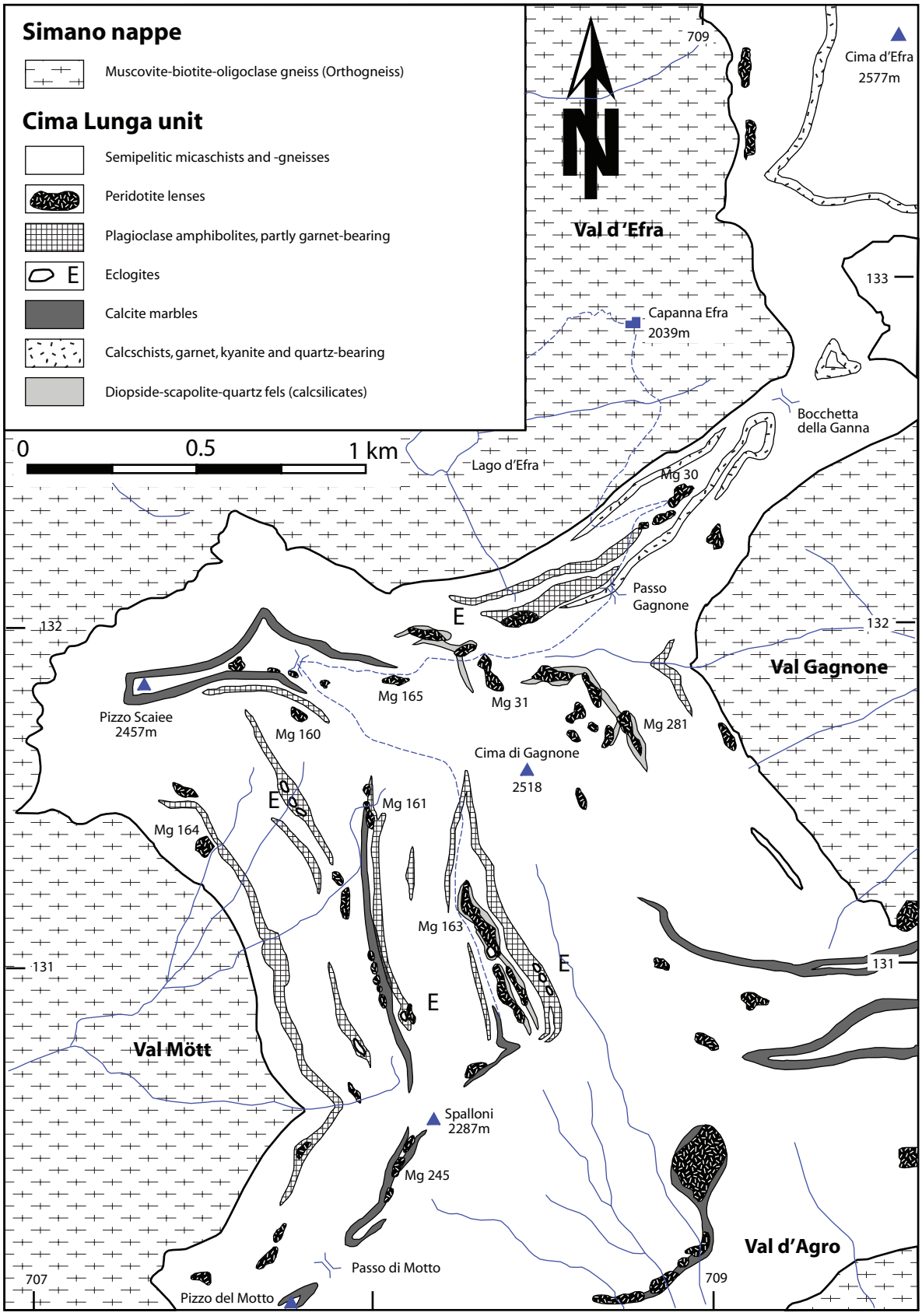

Fig. A.5. Modified after Pfiffner and Trommsdorff (1998). Sample locations are Mg 30 (Cig1); Mg 160 (Cig2); Mg 164 (Cig3)

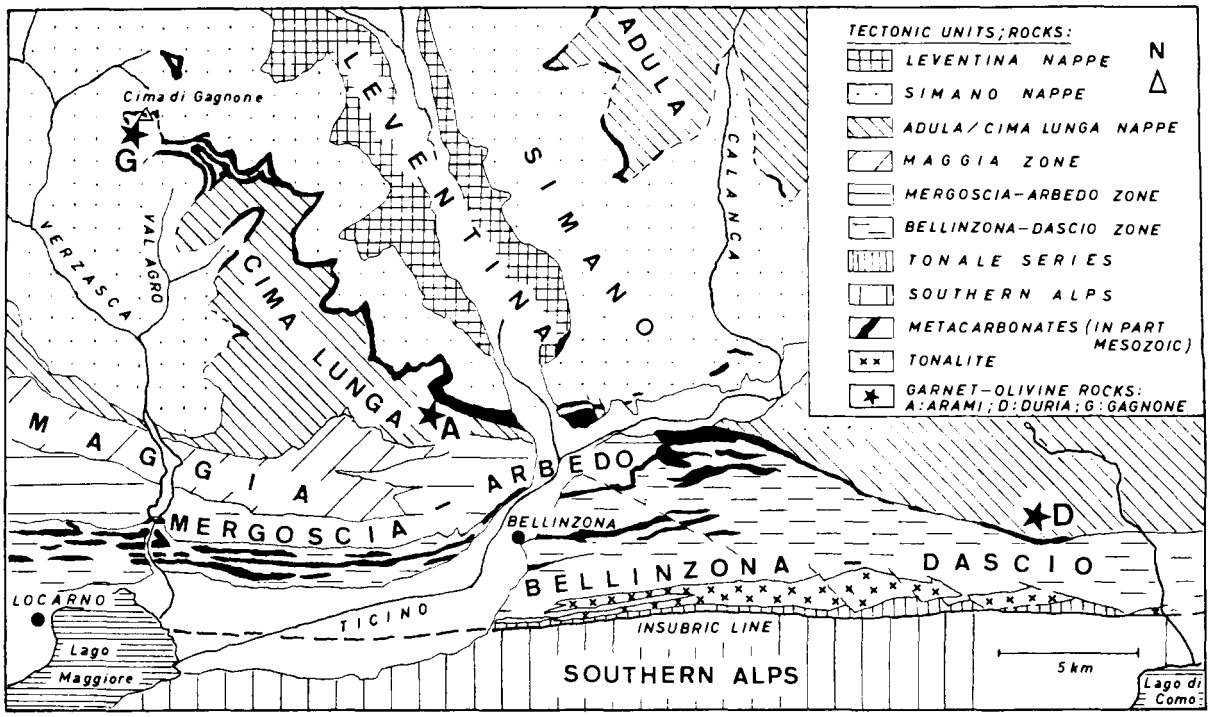

Fig. A.6. Tectonic unit sourrounding the Cima di Gagnone peridotites (after Evans and Trommsdorff, 1978)

Points	Minerals	Li µg/g	sigma (Li)	Be µg/g	sigma (Be)	B µg/g	sigma (B)
cig2c5trem1	amph	2.25	3.69%	0.015	37.26%	6.85	2.49%
cig2c5trem2	amph	2.58	5.60%	0.027	33.31%	7.25	4.04%
cig2c5trem10	amph	26.36	4.57%	0.526	10.06%	23.31	3.16%
cig2c5trem13	amph	8.85	7.31%	0.203	13.75%	12.64	5.75%
cig2c4trem6	amph	2.69	2.91%	0.037	36.46%	9.02	2.67%
cig1c1xx12	amph	1.77	7.62%	0.031	19.32%	1.77	8.47%
cig1c1xx9	amph	1.69	3.76%	0.046	14.39%	2.56	8.98%
cig1c2xx6	amph	2.73	11.51%	0.095	16.13%	4.72	3.67%
cig1c4xx10	amph	0.56	11.00%	0.008	66.12%	1.02	13.53%
cig1c4cp1	amph	4.69	2.69%	0.096	15.50%	0.16	40.38%
cig3c3tc3	cl	1.43	10.85%	0.088	53.19%	9.50	27.23%
cig2c5sr10	cl	0.48	7.03%	2.119	133.89%	2.24	6.22%
cig2c5sr9	cl	0.79	5.13%	5.690	68.83%	2.39	3.22%
cig2c5sr13	cl	0.68	5.48%	3.306	122.65%	0.94	7.72%
cig2c5sr15	cl	0.57	10.23%	4.728	76.07%	1.47	7.61%
cig2c4sr2	cl	0.59	8.16%	4.010	92.09%	0.94	16.73%
cig2c4sr6	cl	0.39	4.39%	3.199	91.45%	1.21	11.41%
cig2c4sr3	cl	1.03	13.19%	11.677	76.42%	1.09	33.64%
cig1c1cp1	cpx	2.96	4.81%	0.089	19.64%	0.21	8.19%
cig1c1cp2	cpx	4.88	3.60%	0.117	15.31%	0.10	23.21%
cig1c1cp9	cpx	3.97	3.83%	0.114	15.87%	0.17	25.77%
cig1c2cp1	cpx	2.99	5.22%	0.104	15.65%	0.14	38.96%
cig1c2cp8	cpx	8.65	3.60%	0.090	20.27%	0.20	31.24%
cig1c4cp2	cpx	3.14	4.36%	0.115	14.10%	0.16	29.38%
cig1c1xx5	ga	0.10	19.73%	0.002	134.14%	0.03	66.12%
cig1c4xx7	ga	3.71	3.57%	0.090	16.16%	0.13	8.82%
cig1c1xx2	ga	1.79	7.91%	0.026	36.97%	2.06	10.94%
cig1c1xx26	ga	1.60	4.74%	0.031	36.65%	1.71	7.08%
cig1c1xx29	ga	0.26	12.33%	0.001	152.80%	0.04	19.10%
cig1c2cp5	ga	0.16	13.91%	0.001	167.03%	0.05	65.36%
cig2c5ol6	ol	3.43	3.02%	3.680	260.98%	0.56	18.30%
cig2c5ol10	ol	3.32	2.92%	0.458	300.00%	0.81	12.12%
cig2c5ol13	ol	3.82	4.44%	0.915	200.02%	0.69	10.13%
cig2c5ol14	ol	2.66	3.57%	0.934	200.00%	0.45	7.30%
cig2c5ol17	ol	3.47	3.79%	b.d.l.	-	0.60	12.40%
cig2c4ol5	ol	4.69	1.79%	0.482	300.00%	0.27	13.93%
cig2c4ol6	ol	3.93	4.32%	1.409	152.76%	0.49	7.79%
cig1c1ol8	ol	1.90	3.92%	b.d.l.	-	0.50	16.48%
cig1c1ol7	ol	1.26	5.12%	b.d.l.	-	0.36	14.48%
cig1c2xx1	ol	1.40	5.63%	0.028	38.42%	1.72	6.10%
cig1c2ol3	ol	1.61	4.40%	0.000	300.01%	0.30	12.59%
cig1c2ol5	ol	1.88	7.62%	0.001	152.77%	0.29	23.72%
cig1c4ol2	ol	1.04	5.76%	b.d.l.	-	0.36	23.97%
cig3c3ol2	ol	42.43	4.46%	0.013	229.39%	7.61	10.44%
cig3c3ol4	ol	66.25	2.34%	0.007	200.01%	36.50	7.53%
cig3c3ol7	ol	34.37	3.83%	0.006	200.01%	9.84	10.81%
cig3c3ol14	ol	69.11	2.56%	0.010	152.80%	26.39	4.08%
cig3c3ol16	ol	47.19	4.40%	0.014	165.39%	44.17	3.57%
cig3c1ol13	ol	59.33	1.74%	0.007	200.01%	29.90	5.53%
cig3c1ol120	ol	53.34	2.43%	0.007	300.01%	23.99	5.69%
cig3c1ol18	ol	29.44	5.09%	0.022	133.64%	9.09	9.96%

Points	Minerals	Li µg/g	sigma (Li)	Be µg/g	sigma (Be)	B µg/g	sigma (B)
cig1c1op6	opx	0.50	7.53%	0.018	38.01%	0.22	19.86%
cig1c1op5	opx	0.41	9.68%	0.017	42.91%	0.21	19.92%
cig1c2op2	opx	0.46	7.15%	0.031	24.38%	0.17	22.58%
cig1c2op4	opx	0.32	13.16%	0.017	40.89%	0.22	27.42%
cig1c4op4	opx	3.01	17.17%	0.194	19.64%	6.47	4.27%
cig1c4op7	opx	0.28	10.34%	0.017	53.19%	0.17	29.92%
cig2c5op8	opx	2.93	3.73%	22.690	25.27%	0.29	13.53%
cig2c5op14	opx	2.10	2.89%	16.209	40.78%	0.25	15.62%
cig2c5op19	opx	2.39	4.03%	19.987	58.62%	0.20	12.72%
cig2c4op1	opx	11.93	2.08%	6.200	111.46%	1.04	5.95%
cig2c4op5	opx	2.85	1.87%	13.995	37.29%	0.21	20.67%
cig3c3tc5	tlc	13.75	3.42%	0.979	18.88%	75.96	5.31%
cig3c1tc12	tlc	0.24	46.26%	0.084	43.42%	15.05	32.67%
cig3c1tc16	tlc	1.05	17.20%	1.096	19.70%	11.44	11.00%
cig3c3tc6	tlc	0.37	40.29%	0.060	88.92%	24.16	25.77%
cig3c3tc9	tlc	0.53	29.09%	0.062	53.63%	16.66	26.78%
cig3c1tcpr1	tlc	0.94	10.91%	0.058	58.22%	33.65	32.00%

amph amphibole; cl chlorite; cpx clinopyroxene; ga garnet; ol olivine; opx orthopyroxene; tlc talc

Appendix C

In-situ $\delta^{11}B$ measurements

On two samples (OD 2 and OD15), in-situ measurements of the B isotopic compositions of serpentine by SIMS were performed. As in-situ B isotope analyses is not yet established for serpentine minerals, the samples were measured in order to quantify the machine fractionation factor. This is important, because as shown in Vils et al. (2008), serpentine minerals control the B budget of serpentinites, thus serpentine should control also the $\delta^{11}B$ whole rock value.

Fig. C.1. In-situ $\delta^{11}B$ versus B concentration of serpentinte in different textures. WR whole rock (WR corrected to SIMS fractionation; added -6 ‰).

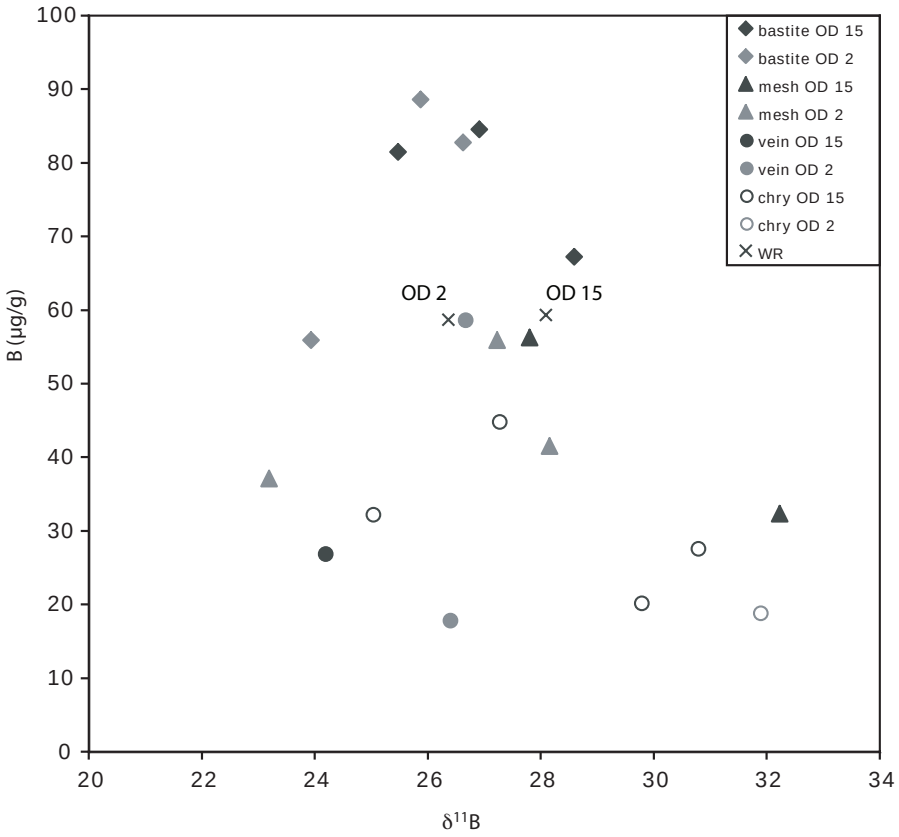

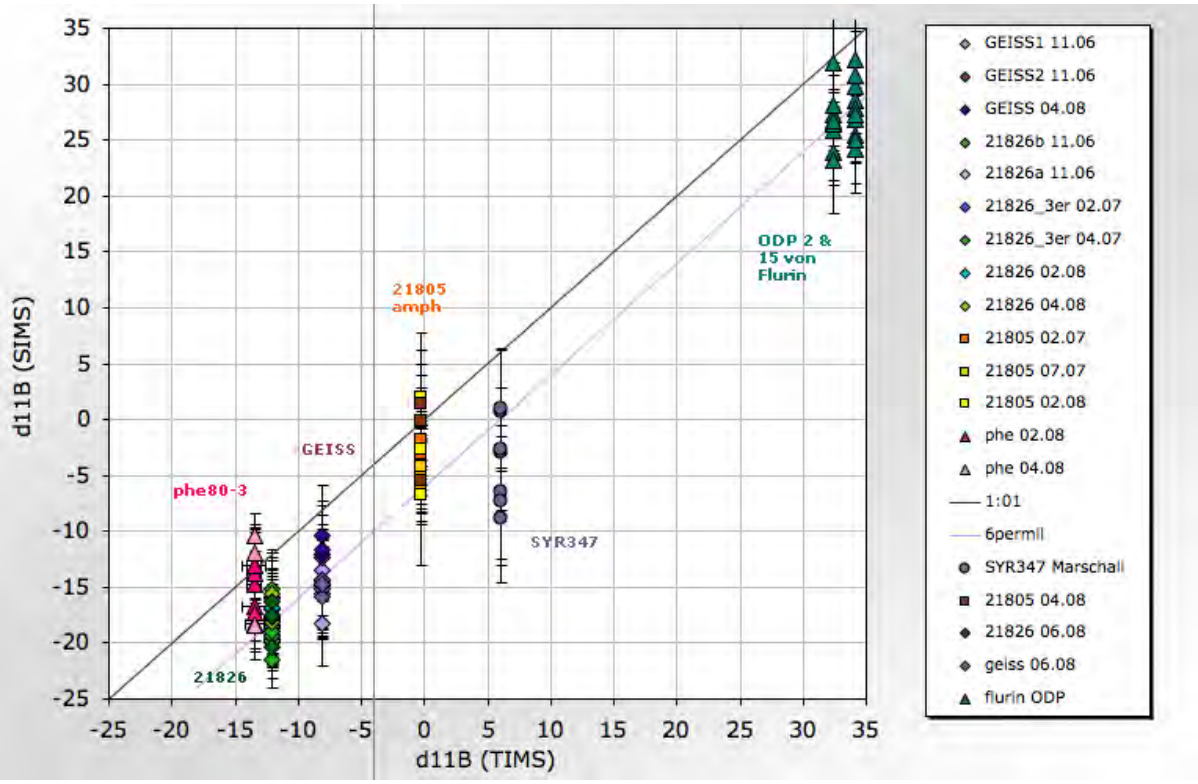

Fig C.2. Diagram showing $\delta^{11}B$ values of whole rock (TIMS) versus in-situ (SIMS) measurements of serpentinites, and phengite and amphibole minerals, used to quantify the fractionation factor of the machine (for the SIMS at the University of Heidelberg).

	In-situ Method	SIMS									
typ serp	Point	Li [µg/g]	*Sigma* (Li)	Be [ng/g]	*Sigma* (Be)	B [µg/g]	*Sigma* (B)	$\delta^{11}B$ [‰]	RSD	1RSD [‰]	R *
	Bastite										
bast	od15c2sr22	0.48	*2.66%*	0.54	*153%*	84.56	*4.49%*	26.92	1.17	2.34%	4.15247
bast	od15c2sr23	0.61	*7.02%*	0.17	*300%*	81.51	*2.50%*	25.47	1.25	2.50%	4.14662
bast	od15c4sr7	0.11	*20.11%*	-	-	67.24	*1.80%*	28.59	1.48	2.96%	4.15923
bast	od2c1sr14	1.19	*4.55%*	0.76	*213%*	55.95	*2.56%*	23.93	1.25	2.50%	4.14040
bast	od2c5sr1	0.28	*10.28%*	0.59	*153%*	82.73	*2.94%*	26.62	1.28	2.56%	4.15129
bast	od2c2sr4	0.97	*17.55%*	1.61	*109%*	88.59	*1.80%*	25.87	1.26	2.52%	4.14825
	Mesh rim										
mesh rim	od15c2sr16	0.01	*58.38%*	0.94	*134%*	32.35	*1.58%*	32.23	1.25	2.50%	4.17394
mesh rim	od15c4sr12	0.11	*25.80%*	0.41	*200%*	56.29	*4.11%*	27.81	1.97	3.94%	4.15607
mesh rim	od2c1sr14	1.19	*4.55%*	0.76	*213%*	55.95	*2.56%*	27.23	1.76	3.52%	4.15372
mesh rim	od2c2sr10	0.03	*27.45%*	0.77	*123%*	37.08	*2.06%*	23.20	2.39	4.77%	4.13742
mesh rim	od2c6sr1	0.03	*36.37%*	0.26	*300%*	41.52	*2.12%*	28.16	1.86	3.72%	4.15749
	Vein										
vein	od15c2sr20	0.04	*30.33%*	0.17	*300%*	27.01	*1.64%*	24.17	1.96	3.91%	4.14137
vein	od2c3sr8	0.09	*23.88%*	0.18	*300%*	17.92	*1.14%*	26.39	2.74	5.48%	4.15032
vein II	od2c3sr19	0.13	*13.57%*	0.24	*300%*	58.77	*1.77%*	26.65	1.45	2.90%	4.15140
	Chrysothile										
chry	od15c2sr19	0.31	*8.63%*	-	-	32.31	*3.38%*	25.02	1.94	3.88%	4.14479
chry	od15c3sr2	0.17	*13.41%*	0.61	*153%*	20.33	*4.43%*	29.77	3.11	6.22%	4.16399
chry	od15c3sr4	0.18	*18.06%*	0.20	*300%*	27.72	*1.11%*	30.78	2.90	5.80%	4.16807
chry	od15c4sr6	0.02	*39.24%*	0.42	*200%*	44.96	*1.80%*	27.26	2.10	4.20%	4.15385
chry	od2c5sr6	0.07	*17.04%*	0.34	*200%*	18.95	*6.45%*	31.87	2.41	4.82%	4.17251

Whole rock Methode	TIMS				PGAA	PGAA	MC-ICP-MS			
Sample	$\delta^{11}B$ [‰]	±2SD	$^{87}Sr/^{86}Sr$ [‰]	±2SD	B* [µg/g]	H_20* [wt%]	Li [µg/g]	±2SD	$\delta^{7}Li$ [‰]	±2SD
OD 2	+32.36	0.41	0.70895	0.00001	58.70	16.1	0.07	*0.00*	-28.46	*0.13*
OD 15	+34.09	0.43	0.70913	3.6E-05	59.30	15.1	0.20	*0.01*	+1.24	*0.89*

R* = Corrected isotope ratio for machine fractionation; sample OD 2 61.76 mbsf and OD 15 99.85 mbsf

Appendix D

Strip heater protocols

In Appendix D, protocols used and developed for work with the Iridium-strip heater are presented. Given that every strip heater has its proper characteristics, the following protocols only refer to the strip heater at the University of Neuchâtel.

Strip cleaning:

While cleaning of the strips, be aware that HF is a very dangerous acid and all necessary precautions should be taken to prevent the smallest accident!!!

Peridotite Protocol for Ir-Strip Heater

Preparation

1. Mix homogenize sample powder with ultrapure-quartz (2:8; 0.02g; 0.08g)
2. Note exact measurements

In the strip heater laboratory:

3. Clean the inside of the strip heater from dust, etc. by wiping out with an ethanol humidified kimwipe
4. Preclean agate mortar with ethanol
5. Mix the powder in the agate mortar, until reaching a homogenous mass
6. Put fresh strip on the machine
7. Add small amount of powder on the strip
8. Set voltage to 32V.
9. Close strip heater with the 3 screws
10. Open argon valve (just a little bit)
11. Close all valves on the machine (including argon valve)
12. Start pumping (the pumping valve has to be open)
13. Fill the chamber with argon (repeat pumping-filling 3-4 times)
14. Stop pumping, close corresponding valve
15. Fill chamber with argon (untill 1 bar)
16. Switch energy on and leave it on for 60s!!!!
17. Measure in the meantime the voltage on the strip (with voltmeter) at transformer 2
18. Switch energy off and open at the same time the argon valve (bottle) to shock the glass
19. Open the valve to let argon out
20. Open the chamber and stop argon flow
21. Extract your glass and use the other side for the next experiment
22. Clean agate mortar and spatulas with ethanol (technical)

At the End:

23. Clean the strip heater lab, so the next person can use it.
24. Inform responsible person if there is still enough strips and cleaning material around

Remarks:

Homogeneizing within a agate mortar can be left out, if one is sure that sample amount used is homogeneous; it is important for ultra-mafic rock, as quartz prevent olivine formation during quenching (spinifex-texture).

Ir-Strip Cleaning Protocol

PLEASE READ IN ADVANCE THE 'HOW TO WORK WITH HF'-RULES

Equipment:

- Wear goggles
- Wear gloves in double layer
- Wear laboratory mantle to protect clothes
- Always inform somebody that you are handling with HF
- Mark working space with HF-work in progress!

In EMERGENCY CASE

- Droplets on clothes or shoes: TAKE them off immediately
- Droplets on skin: wash off immediately with tap water and apply a thick layer of Ca-gluconate paste

1. Precleaning of the strips (getting rid of glass rests)
2. Add the strips into a Teflon screw top beaker (no more than 20) and fill up with 20% HF acid from reservoir bottle (no drops beside!!!)
3. Close the Teflon screw top beaker tightly and put them on a plate (50°C) and leave them overnight (12 hours) to dissolve the rest of glasses on the stripe
4. Intermittently, put the firmly closed beaker in an ultrasonic bath to enhance cleaning (and prevent buildup of jelly coatings on strips)
5. Take the strips out: gently open the beaker, and pour HF-acid into another beaker; repeatedly flush the strips in this beaker with Milli-Q water
6. Repeat steps 2-5 with a clean HF acid
7. Dry them (under Infra-red light or in an oven (50-75°C)
8. Put the stripes for an hour in HNO_3 (concentrated) - again in a Teflon screw top beaker, and firmly close the lid
9. Take the stripes out: gently open the beaker, and pour HNO_3 acid into another beaker; repeatedly flush the strips in this beaker with Milli-Q-water
10. Dry them (under Infra-red light or in an oven (50-75°C)
11. Put them in the clean Ir-strip box
12. Finish the procedure by putting the used HF into the HF-trash bottle and the HNO_3 into the HNO_3-trash bottle
13. Clean working space.

Appendix E

Additional measurements

Additional measurements were conducted on the studied samples, and results are reported in this Appendix. Whole-rock samples from Vourinos (Greece), Pindos (Greece) and ODP Leg 209 Site 1272A and 1274A were analyzed with prompt gamma activation (PGAA) at the Institute of Isotopes at the Hungarian Academy of Sciences (some published in Pelletier, 2008 and Vils et al., 2008). Results are summarized in Table D.1. To identify serpentine polymorphs TEM analyses were performed on one sample from ODP Leg 209 (OD 28). A Philips CM20(0) TEM at the Institute of Microtechnologiy (UNINE) was used. The major findings are presented in the figure captions.

Table D.1: PGAA-whole rock data from ODP Leg 209, Pindos and Vourinos ophiolites.

	B		S		Cl		Sc		Cr		Co		Ni		SiO2		H2O	
	ppm	*unc%*	ppm	*unc%*	ppm	*unc%*	ppm	*unc%*	ppm	*unc%*	ppm	*unc%*	ppm	*unc%*	wt%	*unc%*	wt%	*unc%*
ODP2	58.7	*1.9*			10114	*4.4*			971	*6.9*	110	*6.0*	2416	*3.9*	33.9	*2.7*	16.1	*2.*
ODP6	60.3	*1.8*	1380	*6.1*	7759	*4.4*			1651	*3.8*	92.8	*5.7*	2143	*4.0*	35.7	*2.6*	15.4	*2.*
ODP11	53.9	*1.9*	1353	*7.9*	6389	*4.6*			1832	*4.0*	96.4	*5.4*	1982	*4.5*	35.1	*2.6*	16.4	*2.*
ODP15	59.3	*1.8*	1330	*7.2*	6682	*4.7*			2423	*4.6*	91	*7.9*	1848	*4.2*	35.8	*2.6*	15.1	*2.*
ODP18	59.8	*1.9*	1909	*6.9*	6355	*3.9*			2024	*4.1*	86	*10.3*	1920	*4.9*	35.8	*2.6*	15.3	*2.*
ODP22	65.0	*1.8*	1402	*8.4*	7291	*4.0*			3005	*3.4*	106	*7.1*	1996	*4.2*	36.2	*2.5*	15.2	*2.*
ODP26	61.5	*1.8*	2229	*3.3*	6032	*4.1*			3386	*2.8*	89.8	*4.0*	1822	*2.9*	30.6	*3.4*	13.00	*3.*
ODP29	50.3	*1.8*	1399	*7.8*	6855	*3.6*			2268	*3.8*	94.4	*5.6*	1881	*4.4*	36.5	*2.6*	13.8	*2.*
ODP34	31.2	*1.9*	781	*10.3*	2242	*4.0*			2515	*3.1*	105	*4.3*	2199	*3.1*	36.7	*2.6*	12.7	*2.*
ODP38	17.5	*1.9*	825	*8.0*	2746	*4.7*			1838	*3.3*	105	*3.9*	2104	*3.3*	37.3	*2.5*	13.1	*2.*
ODP42	<0.2		561	*11.7*	1553	*2.1*			1311	*4.0*	124	*4.1*	2255	*3.0*	36.3	*2.5*	13.8	*2.*
ODP45	10.4	*1.9*			1061	*4.2*			1822	*3.9*	103	*4.5*	2384	*3.2*	38.5	*2.6*	10.9	*2.*
ODP48	38.5	*1.9*			1823	*4.2*			3154	*3.4*	89.7	*6.2*	2021	*4.4*	37.5	*2.5*	12.2	*2.*
ODP49	36.6	*1.9*	1056	*7.5*	3566	*4.0*			3252	*3.0*	110	*5.4*	2164	*3.8*	34.6	*2.6*	15.0	*2.*
PI2	<0.05								2897	*2.7*	149	*2.9*	2565	*2.7*	42.6	*2.7*	0.28	*3.*
PI6	0.10	*6.3*			343	*4.0*			3377	*2.7*	103	*3.6*	2415	*2.8*	40.4	*2.6*	6.89	*2.*
PIA44	<0.04				514	*4.6*	12.4	*11.5*	3066	*2.6*	105	*3.3*	2285	*2.4*	40.0	*2.5*	8.50	*2.*
PIA27	1.05	*2.4*			50.1	*7.5*	8.55	*15.1*	2999	*2.8*	122	*3.0*	2524	*2.9*	42.5	*2.6*	3.37	*2.*
PIA109	0.09	*7.6*			129	*5.1*	14	*11.7*	2564	*2.7*	128	*3.2*	2287	*2.7*	43.1	*2.5*	1.69	*2.*
PIA120	0.72	*2.5*			292	*4.0*	21	*13.3*	2603	*2.9*	108	*3.4*	1976	*3.1*	40.9	*2.3*	7.42	*2.*
VOU2	0.15	*5.6*			12	*10.2*			2994	*4.8*	142	*3.5*	2260	*3.8*	41.62	*2.8*	0.37	*3.*
VO41	1.03	*2.4*			45.9	*5.6*	8.2	*14.4*	2958	*2.7*	153	*3.1*	2492	*3.0*	42.8	*2.6*	2.19	*2.*
VO43	0.37	*2.9*			379	*4.5*			2804	*2.7*	113	*3.2*	2389	*2.6*	39.7	*2.5*	9.00	*2.*
VO56	0.17	*6.2*			33.5	*8.3*	15	*11.3*	3211	*2.7*	121	*2.8*	2291	*2.6*	44.6	*2.5*	1.66	*3.*
VO57	0.33	*4.7*			351	*4.3*			2466	*2.7*	111	*3.0*	2313	*2.8*	38.3	*2.5*	11.3	*2.*
VO67	0.05	*5.5*			6.2	*17.6*	6.6	*15.2*	2923	*2.7*	133	*2.7*	2668	*2.6*	44.1	*2.6*	0.29	*3.*

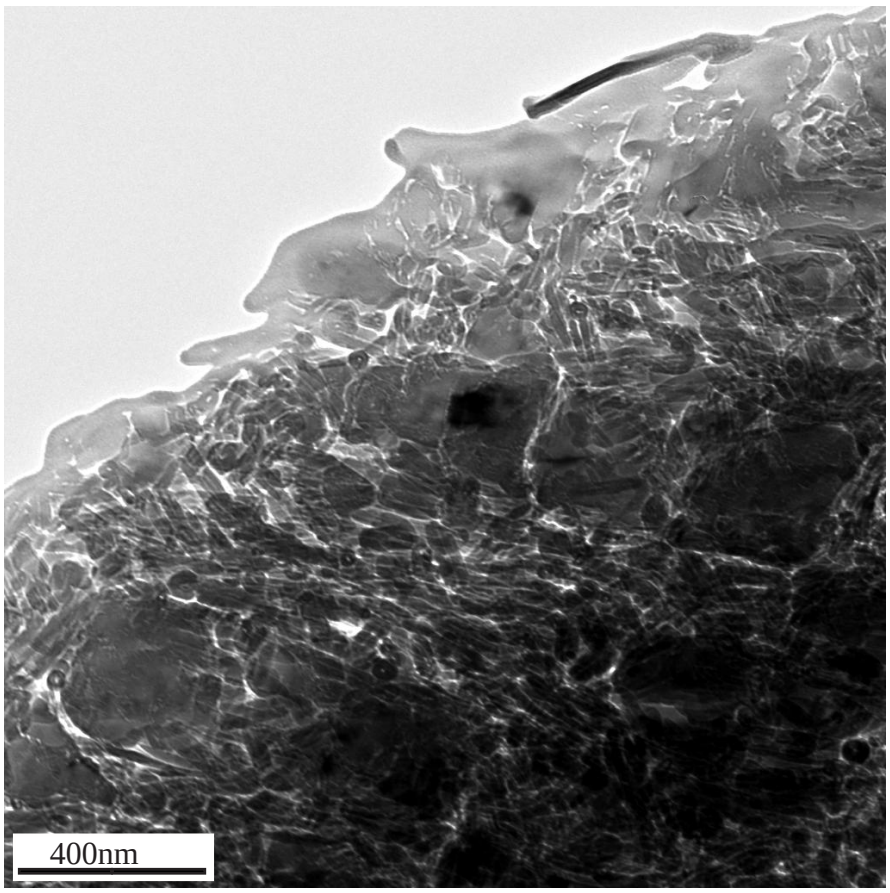

Fig. D.1. TEM image showing chrysotile overgrowing lizardite flakes. In black, an oxide inclusion is visible.

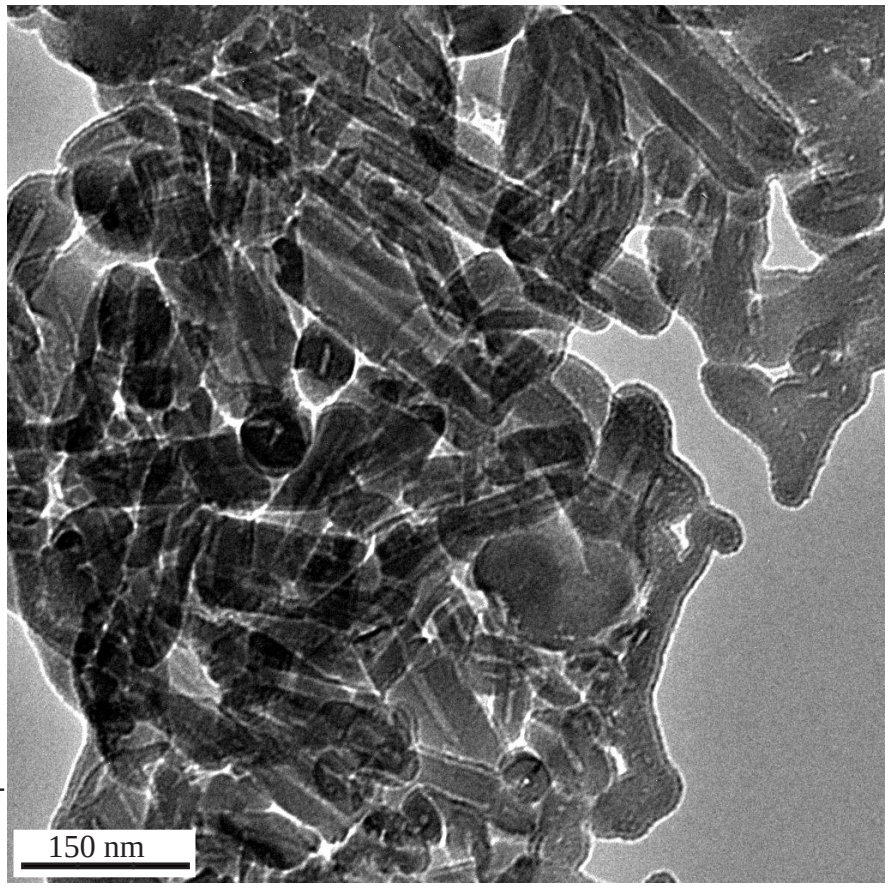

Fig. D.2. Chrysotile grains overgrowing each other. The inner channel of the spiral structures is visible.

REFERENCES Appendix

Evans, B. and Trommsdorff, V., 1978. Petrogenesis of garnet lherzolite, Cima di Gagnone, Lepontine alps. Earth and Planetary Science Letters 40, 333-348.

Liati, A., Gebauer, D., and Fanning, C. M., 2004. The age of ophiolitic rocks of the Hellenides (Vourinos, Pindos, Crete): First U-Pb ion microprobe (SHRIMP) zircon ages. Chemical Geology 207, 171-188.

Pelletier, L., 2008. The oceanic mantle as an important repository for the light elements Li, Be and B, Ph.D thesis, University of Neuchâtel.

Pelletier, L., Vils, F., Kalt, A., and Gméling, K., 2008. Li, B and Be contents of harzburgites from the Dramala Complex (Pindos ophiolite, Greece): Evidence for a MOR-type mantle in a supra-subduction zone environment Journal of Petrology, 49, 2043-2080.

Pfiffner, M. and Trommsdorff, V., 1998. The high-pressure ultramafic-mafic-carbonate suite of Cima Lunga-Adula, Central Alps: Excursions to Cima di Gagnone and Alpe Arami. Schweizerische Mineralogische und Petrographische Mitteilungen 78, 337-354.

Robertson, A. and Shallo, M., 2000. Mesozoic-Tertiary tectonic evolution of Albania in its regional Eastern Mediterranean context. Tectonophysics 316, 197-254.